Royal Holloway
University of London

4D Structural Evolution of the West Niger Delta Deepwater Fold and Thrust Belt

by

Basil Muhammad Tulbah

Supervised by

Ken McClay

Financial Sponsor

Saudi Aramco

A thesis submitted in fulfilment of the requirements of the University of London for the degree of Master of Philosophy

Department of Earth Science

Royal Holloway, University of London

2011

Declaration

I declare that the work contained in this thesis submitted for an MPhil degree at Royal Holloway, University of London is my own, and where work by other authors has been contained, it has been referenced accordingly.

Basil Tulbah

Date

Abstract

The thesis investigates the evolution of fold and thrust structures that occur in the deepwater fold and thrust belt of the Niger Delta. The aim of the research is to construct a 4D evolutionary model for one of the folds at the toe of the Niger Delta to in order to understand the geometries and kinematics of the thrust-related-folding in the toe thrust belt.

Detailed seismic interpretation of 2D and a 3D depth-converted dataset has been used to study the fold structures and growth-stratal geometries. Two main folds occur in the survey area: the Aghar and Bobo folds. The Aghar fold is the main focus of this research. It is 34km long and 6km wide, NW-SE trending fold that creates up to 400m of seabed relief. The fold is highly asymmetric with a steep dipping ~61-72° forelimb and less-steep dipping ~20-40° backlimb. The fold is associated with a SW vergent thrust that cuts the forelimb, but is non-emergent at the seabed. The thrust connects at the decollement in the bottom of the section, and creates a ~40° ramp towards the middle of the section. The detachment is interpreted to be an overpressured shale sequence. The detachment unit thickens under the thrust by ~380m by brittle thrusting mechanisms. In the middle of the forelimb, a mud volcano sits within a scarp face ~16km long. Syn-kinematic units in the hanging wall side show fanning geometries, where as the forelimb growth strata show self similar growth. This departs from classic fault-bend and fault-propagation folds, and is more likely represented by shear fault related fold models.

A ~2000m thick Paleocene to Eocene (?) pre-kinematic section has been preserved. The Oligocene to Present Day (?) syn-kinematic section has fanning geometries that thin from ~2000m to absent at the rest of the Aghar fold. Thinning of the syn kinematic units began in the middle of the Aghar fold, and rapidly progressed laterally, linking up several thrusts along strike. The middle section is characterized to have a fold accommodation thrust the formed in the forelimb at a shallower compared to the main ramp. The northern and southern parts of the fold have a listric fault geometry with a backthrust complex.

The Aghar fold developed as a result of the joining of three faulted detachment folds along strike, where the middle fold developed during the late Lower-Miocene, and the northern and southern segments developed later in the Mid-Miocene. The associated faults linked laterally to form the Present Day fold in the Mid-to Late-Miocene. This evolutionary model probably occurs throughout the Niger Delta and other passive deltas. The model provides insights on brittle detachment development and the evolution of fault related folds in the deepwater fold and thrust belt.


بسم الله الرحمن الرحيم
اللهم انفعني بما علمتني وعلمني ما ينفعني وزدني علماً

Acknowledgements

First I would like to thank Saudi Aramco, who have made my degree and research possible. I would also like to thank CGGVeritas for providing me with the data used in this research.

I must also acknowledge Ken McClay, my supervisor, who has provided many insights in my thesis. Chris Elders is also acknowledged who has provided much needed support and valued opinion throughout the research.

I would also like to thank the Fault Dynamic Research Group, who work together and provide a community of learning and support that was always available. I would like to especially thank, in no particular preference, Ali, Abdulla, Catherine, Diego, Edita, Hanna, James, Jamal, Jonny (Papa) Wu, Lydia, Nicola, Rob and Sukonmeth (Oo).

I would also like to thank the family in room 201, Aji, Alja, Anna, Emiliano (Bob), Hanna, Holly, Igun, Naomi, Ogechi, and the other post grads that have given much support in time of need.

I must also thank my wife for keeping up with me and giving the love and support throughout my research, in good times and bad. I would also like to thank my to be born daughter Lara (Born in 18 February 2011), for giving the inspiration I needed to write this thesis. I would like to also thank my family in Saudi; my mother Faizah, brothers, Faisal and Mahmoud and all my nephews and nieces.

I would also like to thank the staff at Royal Holloway for their continuous support for the student body. I would like to particularly thank all those who taught me during the MSc year and all their efforts.

My colleagues at Saudi Aramco and the Red Sea Team are also acknowledged for their moral and technical support for this research and beyond. I also like to thank the software suppliers Halliburton and Igeoss for providing the applications used in this study.

I shall also thank my brothers and sisters in the ISOC and local community who have helped create a wonderful atmosphere that has inspired me throughout my stay at Royal Holloway.

Last but not least I must show great gratitude to the developers of Adobe Illustrator and InDesign.

Table of Contents

List of Figures

Chapter 1: Introduction

Chapter 2: Regional Geology of the Niger Delta - A Review

Chapter 3: Research Methodology

Chapter 4: Regional Structures and Stratigraphy

Chapter 5: Aghar Fold Geometry and Structural Analysis

Chapter 6: Section Restoration and Forward Numerical Modelling

Chapter 7: Discussion

Chapter 8: Conclusions

List of Figures Page

Appendix A: Structural Maps and Amplitude Extractions

List of Tables

Chapter 1
Introduction

1.1. Introduction

This research analysis the 4D evolution of deepwater delta toe fold and thrust belt of the Niger Delta in West Africa. The Niger Delta undergoes characteristic gravity related deformation known as delta tectonics, where differential loading causes thin-skinned extensional and compressional structures to form in the proximal and distal parts respectively. The large progradational deltas form on a salt detachment such as the Mississippi Delta, Gulf of Mexico (Gonzalez-Mieres & Suppe 2006) and the Angola Basin, West Africa (Morley *et al.* 2010), or detaches on an overpressured shale surface such as the Niger Delta, Gulf of Guinea (Knox & Omatsola 1989; Doust & Omatsola 1990); Baram Delta, South China Sea (Morley 2009); Amazon Delta, Brazilian Atlantic margin (Cobbold *et al.* 2004); Orange Basin, Namibia Atlantic Margin (de Vera *et al.* 2010).

The distal part of deltas is located in deep (500 – 2000 m) to ultra-deep (>2000 m) water that until recently, was beyond seismic imaging and drilling technology. This has opened new opportunities for exploration and production.

The Niger Delta is located in the northeast of the Gulf of Guinea, on the West African Atlantic margin (Fig. 1.1). It has onshore parts and extends into deepwater ~4000m deep (Fig. 1.2). Several works such as Short & Staeuble (1967), Whiteman (1982), Knox & Omatsola (1989) and Doust Omatsula (1990) have detailed investigations of onshore structures and stratigraphy. With the acquisition of high-quality seismic data, recent texts provide detailed analysis of the fold and thrust belts (Morgan 2003; Corredor *et al.* 2005; Bilotti & Shaw 2005; Bilotti *et al.* 2005) ETC.

1.2. Project Area

The focus area of the study is located in the outer fold and thrust belt (Chapter 2.3) of the western Niger Delta lobe (Fig. 1.2). The dataset used for the study is a 2002 3D seismic survey provided by CGGVeritas (Chapter 3.2). Two 2D regional seismic lines are used to provide regional understanding of the Niger

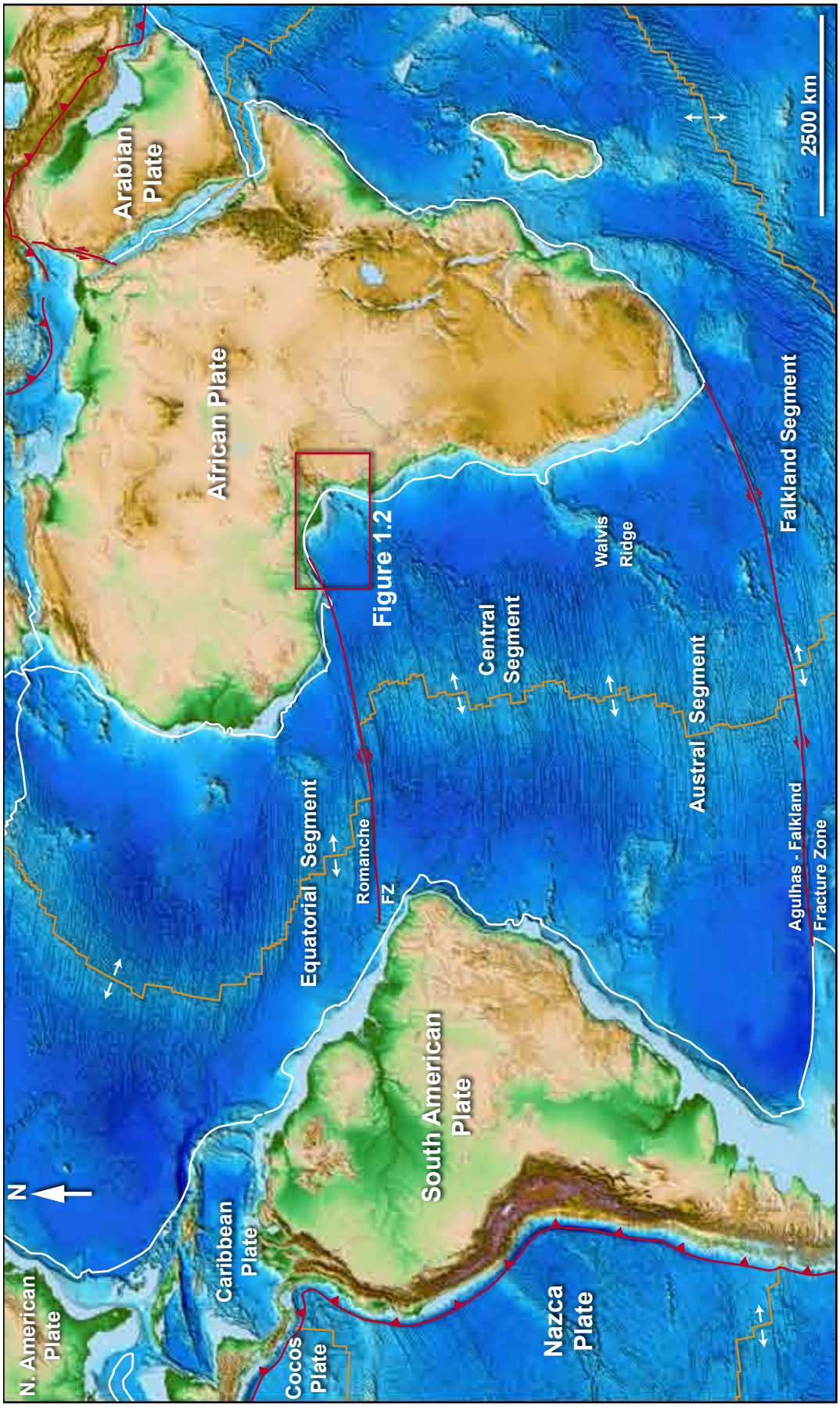

Figure 1.1 Map of the South Atlantic Margins. (Amante & Eakins 2009; Müller *et al.* 2008;)

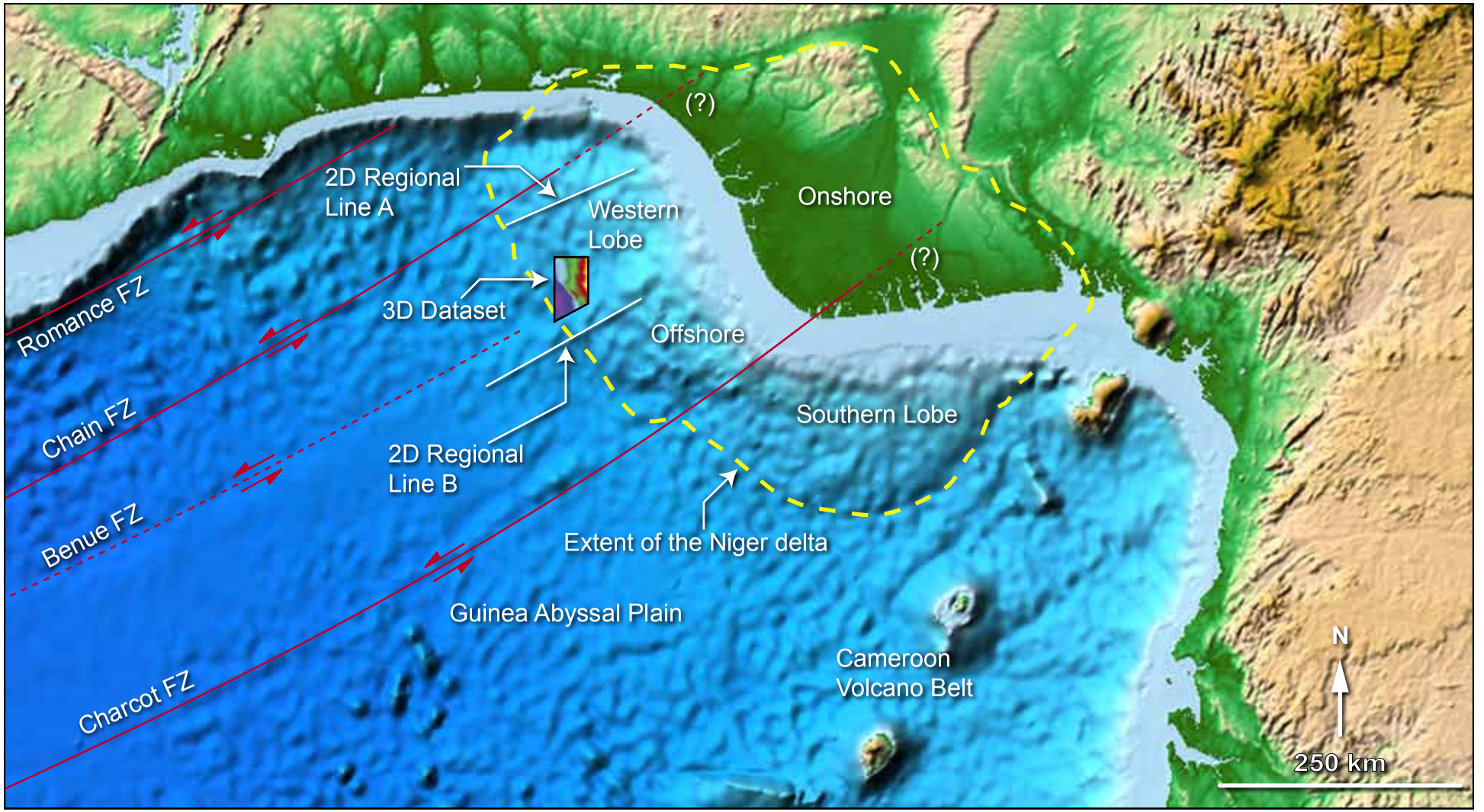

Figure 1.2 Topo-bathymetric map of the Gulf of Guinea. The Niger Delta is highlighted with a yellow border, and the dataset within it (Emery *et al.* 1975; Amante & Eakins, 2009;). FZ: Fracture zone.

Delta deepwater structures.

1.3. Niger Delta

The Niger Delta is an arcuate delta that formed on the western coast of Africa (Fig. 1.1 (Fig. 1.2) on the coast of Benin, Nigeria, and Cameroon. The delta extends from the Benue Trough to the northeast, to the 4000m bathymetic line offshore to the west, and the Cameroon volcanic belt to the south and southwest (Fig. 1.2) (Doust & Omatsola 1990; Corredor *et al.* 2005; Tuttle *et al.* 1999). The Niger Delta is considered one of the worlds largest deltas, covering an area of 300,000km^2 (Tuttle *et al.* 1999) of which 75,000 km^2 is onshore. It has Cenozoic to Present Day sediment upto12km thick (Briggs *et al.* 2006).

The Niger Delta is considered the most prospective basin in Nigeria (Whiteman 1982). The shallow and onshore parts of the delta have been extensively explored since 1952 (Saugy & Eyer 2003). In 1996 deepwater exploration began and lead to the discovery of eight ~1billion barrel discoveries (Cobbold *et al.* 2009). Recent estimates suggest that the delta holds 23 billion barrels oil and 183 trillion cubic feet of gas (Sonibare *et al.* 2008) (Chapter 2.5).

Deposition began in the Niger Delta in the Paleocene/Eocene, during the Atlantic Ocean drift phase and continues to Present Day (Doust & Omatsola 1990). It mainly consists of fluvio-marine clastic sediments overlying extended African continental crust, initially filling in horst-graben structures and then built-out over transitional and oceanic crust (Doust & Omatsola 1990; Tuttle *et al.* 1999; Morgan 2003; Bilotti & Shaw 2005; Briggs *et al.* 2006; Cobbold *et al.* 2009).

The underlying basement is tectonically inactive. The Niger Delta is dominated by gravity driven deformation, making the Niger Delta an excellent location to study shale-detached delta tectonics. The delta is subdivided into three main deformation zones; the proximal extensional zone, the intermediate zone and the distal contractional zone (Chapter 2.3).

1.4. Aims and Objectives

The main aims of this research are

1. To analyse the geometries of fault-related-folds in the deepwater Niger Delta.

2. To analyse the growth-strata on the fold limbs of the folds

3. Develop 4D evolutionary model for folds in the deepwater delta setting

1.5. Thesis Outline

Chapter 1: Introduction: an overview of the research and the geological setting of the Niger Delta.

Chapter 2: Regional Geology of the Niger Delta – A Review: this chapter reviews the structural and stratigraphic elements of the Niger Delta.

Chapter 3: Research Methodology: Discusses the seismic dataset and interpretation methodology, as well as section restoration and numerical modelling methods.

Chapter 4: Regional Structures and Stratigraphy: An analysis of 2D regional lines and general aspects of the 3D dataset.

Chapter 5: Aghar Fold Geometry and Structural Analysis: a detailed description and analysis of the geometry and structure of the Aghar fold.

Chapter 6: Section Restoration and Forward Numerical Modelling: analysis of cross-section restoration and forward numerical models.

Chapter 7: Discussion: an evolutionary history of the Aghar fold is analysed. Compares and contrasts the structures of the study area with similar structures in different deltas around the world. Provides suggested hydrocarbon plays in the Niger Delta.

Chapter 8: Conclusions: Summary of observations and analytical findings as well as a summary of research findings.

Appendix A: Structural Maps and Amplitude Extractions: provides additional interpretation and extraction of the Aghar fold.

Chapter 2
Regional Geology of the Niger Delta - A Review

2.1. Introduction

This chapter reviews the regional stratigraphic and structural setting of the Niger Delta needed to understand its tectonostratigraphic evolution.

The Central Atlantic Ocean began rifting in the Late-Jurassic – Early-Cretaceous and was followed by oceanic spreading that began in the Aptian. Several sedimentary complex were deposited during this period. The onset of Niger Delta deposition came in the Paleo-Eocene when the delta prograded over rifted continental crust as well as oceanic basement (Chapter 2.2). The basement structures were mostly inactive after the onset of Niger Delta deposition and therefore, only thin-skinned delta tectonics affect the delta (discussed further in Chapter 2.4).

Thin-skinned deformation occurs along an overpressured shale detachment (Chapter 2.4.1). Overpressure in the Niger Delta maybe caused by phase changes in clay minerals and hydrocarbon generation, however, the latter is more widely accepted and is more likely to have sustained the overpressure. Differential deposition causes subsidence of listric faults in the proximal parts of the delta, weak detachment translates the movement to the distal parts of which then forms contractional structures (Chapter 2.4). The delta is therefore, split into three zones: the proximal extensional zone, intermediate transitional zone, and the contractional fold and thrust belts. The fold and thrust belt are the focus of this thesis and is discussed in more detail in Chapter 2.3.1.

The delta stratigraphy consists of three main lithological units the Akata, Agbada, and Benin formations that represent pro-delta, pelagic and fluviomarine delta-top depositional environment respectively (discussed in detail in Chapter 2.3). The lowermost formation, the Akata, is considered to be the main hydrocarbon source rock and the Agbada formation is considered the main reservoir and seal unit (for more on hydrocarbon systems see Chapter 2.4)

2.2. Plate Tectonics of Central West Africa

The Niger Delta overlies both continental and oceanic crust. The continental crust is only limited to the proximal parts of the delta and the oceanic crust underlie the rest. The continental part of the delta is located within the Benue Trough, a NE-SW oriented rift basin that formed during the opening of the Atlantic Ocean in the Late Jurassic. The oceanic crust (~100-120Ma) on the other hand dominates the remainder of the delta, including some of the onshore parts of the delta. The following section is an overview of the continental and oceanic crust under the Niger Delta as well as the evolution of the Niger Delta basin.

The development of the Niger Delta basin followed the Triassic breakup of Pangaea and the late-Jurassic Atlantic rifting. The delta began deposition following the later stages of drift and oceanic spreading.

2.2.1. Continental Crust and Deformation

The continental crust in West Africa is divided into two zones: the stable West African Craton (1900-2000Ma) and the mobile zone, which has been heavily deformed and metamorphosed by the Pan-African Orogeny during the Late Proterozoic and Paleozoic (450-680±150 Ma) (Coward *et al.* 1999; McCurry 1971; Benkhelil 1982). Nigeria is located between the West African and Austral Cratons (Fig. 2.1) (McCurry 1971; Moulin *et al.* 2010). These cratons are separated by several shear zones (Fig. 2.1). The continental part of the Niger Delta is located within the Benue Trough; a NE-SW failed rift that formed during the opening of the Atlantic. The basin forms the N70°E arm of the Gulf of Guinea rift-rift-rift (RRR) triple junction system, which ceased extension soon after rifting initiated. The other rift arms were highly oblique (Lawrence *et al.* 2002) and run nearly parallel to the northern Gulf of Guinea boundary.

Some authors (Benkhelil 1982; Guiraud *et al.* 1987; Reijers *et al.* 1997) suggest that the Gulf of Guinea triple junction is a Rift-Transform-Rift type (RTR), where

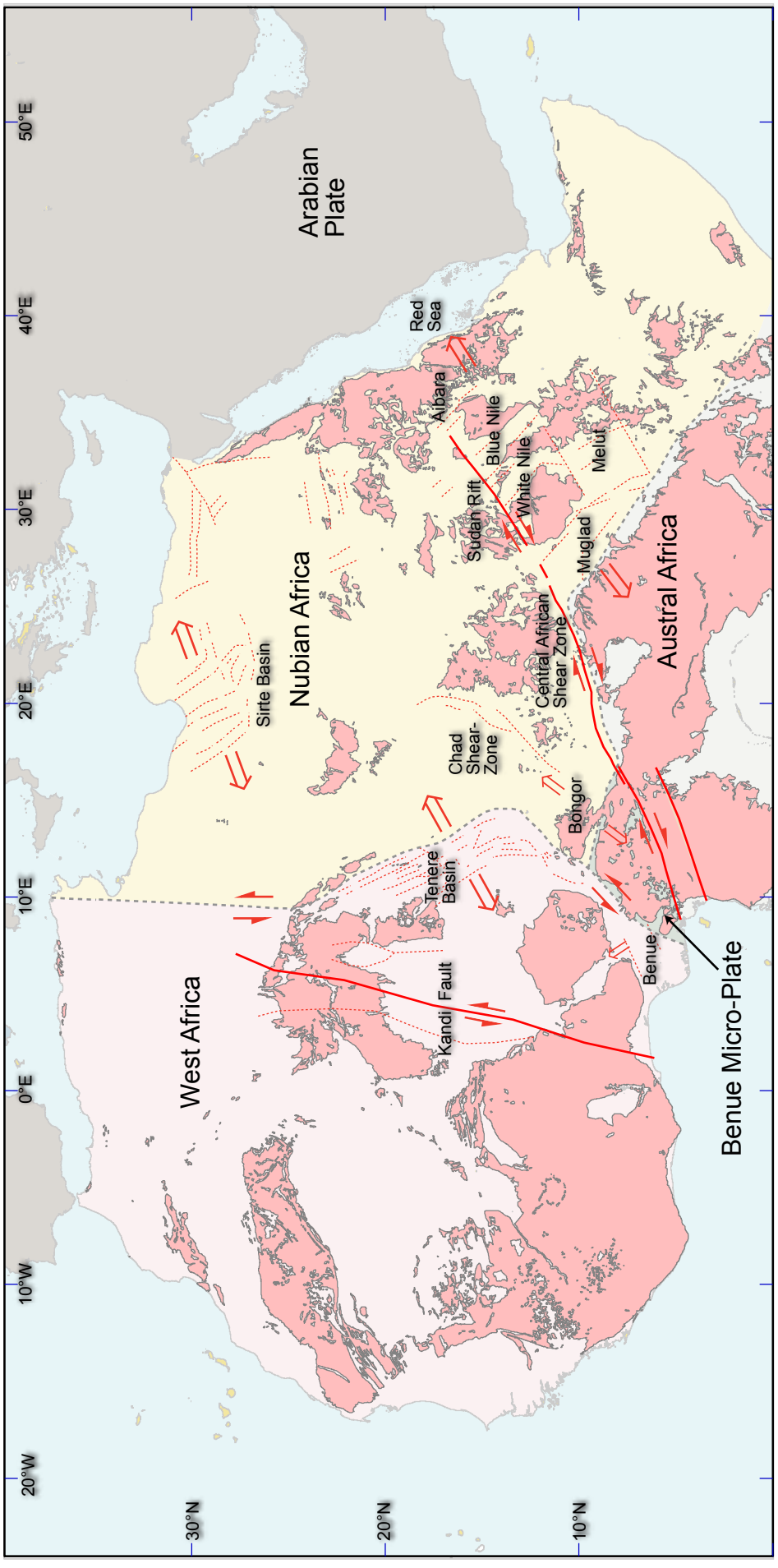

Figure 2.1 Tectonic map of North and Central Africa highlighting the main shear zones and cratons. and basins (Compiled from Konate *et al.* 2003; Guiraud *et al.* 2005; Moulin *et al.*, 2010)

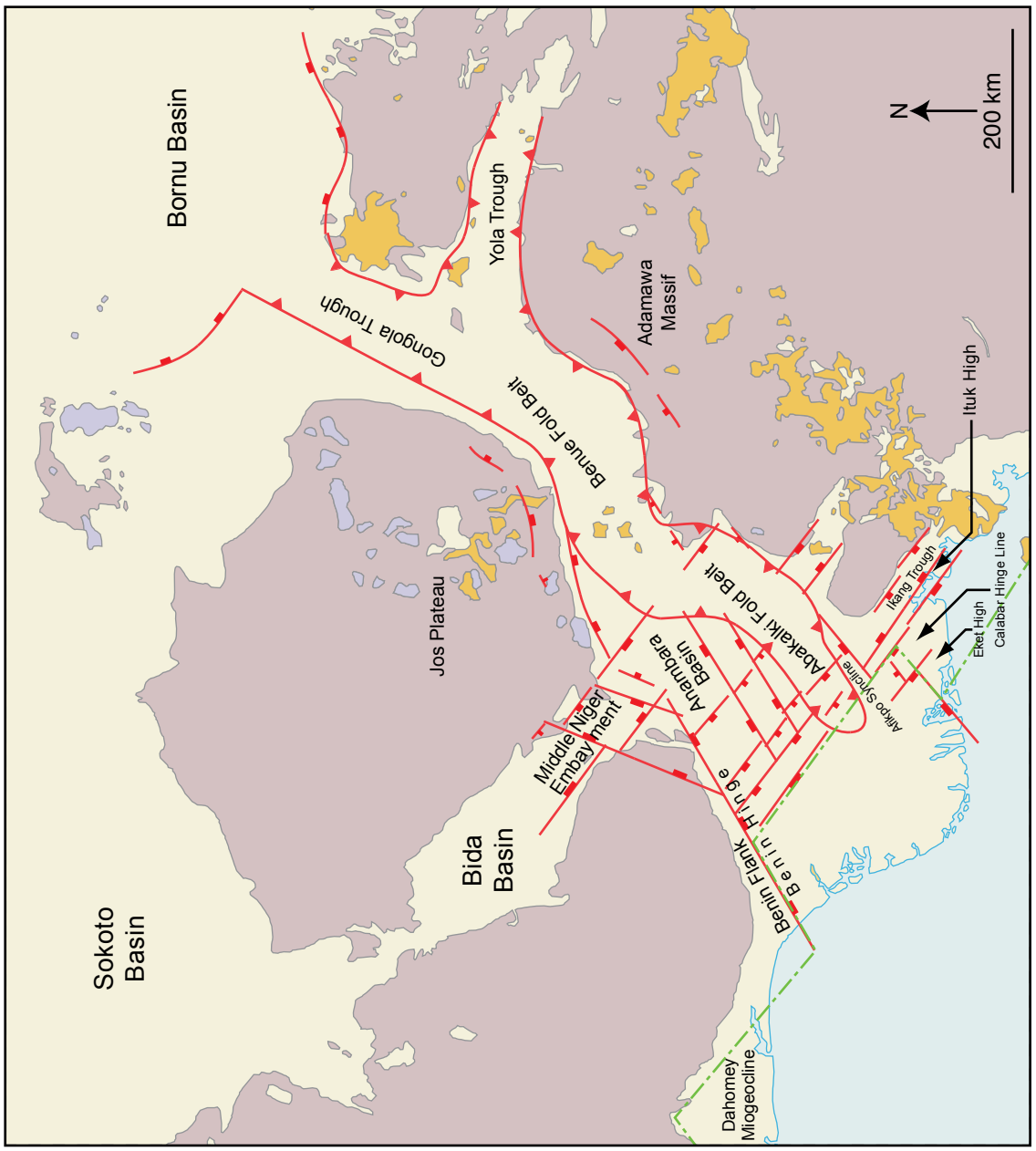

Figure 2.2 Main structural features in the Niger Delta Basin and surrounding area

the Benue Trough acts as a pull apart basin (Daly *et al.* 1989). Daly *et al.* (1989) even suggest a link between oceanic fracture zones and reactivation of continental shear zones. However, even though Atlantic-related deformation needed to be accommodated by intracontinental deformation as well as the oceanic deformation (Eagles 2007), the continental deformation is likely to be decoupled from the oceanic crust transform zone, especially during later stages of oceanic drift (Lawrence *et al.* 2002) since there is no evidence for strike-slip at similar rates to that observed in the oceanic fracture zones.

2.2.2. Oceanic Crust and Deformation

The Niger Delta currently overlies ~95-108 Ma old oceanic crust (approximated from magnetic studies (Müller *et al.* 2008)) (Fig. 2.3). The earliest Niger Delta deposition began during the Paleo-Eocene, when the oceanic crust was ~53-60My old. At this point, the oceanic lithosphere would have been in the later stages of cooling and, as a result, subsidence in the crust is mostly caused by sediment loading (Morley 2003) rather than lithospheric cooling.

The majority of the deformation taking place in the oceanic basement is related to the fracture zones (FZ) that segment the oceanic ridges (Cobbold *et al.* 2009). These dominantly affect the western lobe of the Niger Delta. The three main fracture zones are the Chain, Charcot, and Ascension FZ (Fig. 2.3 & 2.7).

2.2.3. Tectonic Evolution of the Niger Delta Basin

Before the onset of Atlantic rifting, little deformation took place within the Niger Delta basin. The Atlantic Ocean began as a rift basin during the break-up of Pangaea in the Permo-Triassic (Bortolotti & Principi 2005). During this period, E-W trending rifts developed between Africa and Europe, and North and south Americas (Bortolotti & Principi 2005), causing several E-W trending basins to develop between the Americas and Africa and Europe. During the Late Jurassic - Berrisian (Lawrence *et al.* 2002; Bortolotti & Principi 2005; Tuttle *et al.* 1999; Whiteman 1982) central Atlantic rifting initiated in North Gabon, and propagated

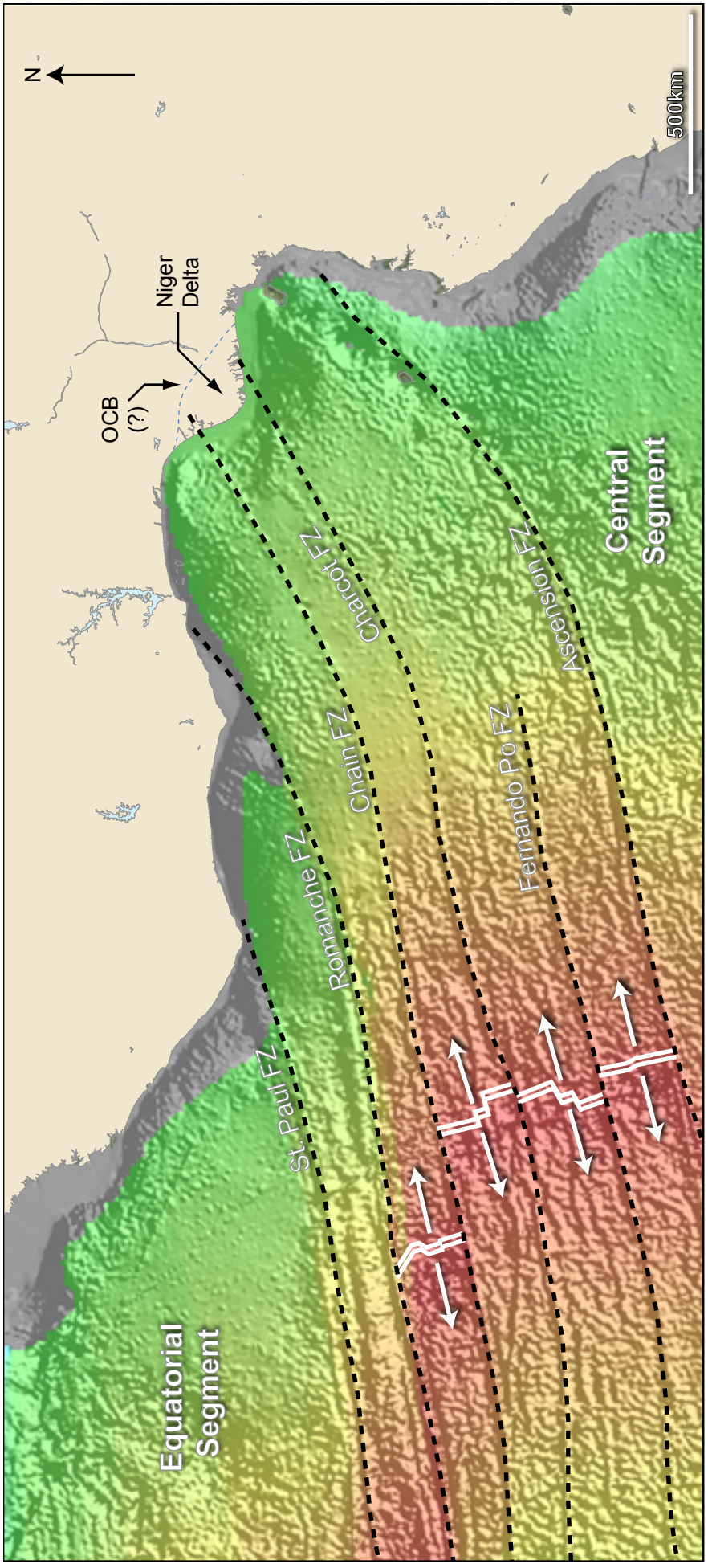

Figure 2.3 Map Showing the Age of oceanic crust in the Gulf of Guinea and near Atlantic (Emery *et al.* 1975; Müller *et al.* 2008; Moulin, 2010)
OCB: Oceanin-Continental Boundary

northwards towards the Niger Delta basin.

Initially the Niger Delta basin formed as part of the Gulf of Guinea Triple Junction. However, soon after rifting began, the NE arm of the triple junction (Benue Trough) failed and rifting ceased (Doust & Omatsola 1990). The other two arms (SW and SE) continued a highly oblique extension until the oceanic spreading initiated between the mid-Aptian (118Ma) (Morgan 2003) to Albian ~105-100 Ma (Lawrence *et al.* 2002; Müller *et al.* 2008) forming a passive margin.

During the Mid-Jurassic to the Santonian (Bortolotti & Principi 2005), the Alpine Tectonic phase began with the inversion the Neo-Tethys, altering the Atlantic opening Euler-pole (Lawrence *et al.* 2002; Doust & Omatsola 1990). This causes a change in the mid-oceanic spreading direction marked by a kink in the Atlantic fracure zones (Eagles 2007; Müller *et al.* 2008).

During the Paleo-Eocene, 53-60 My after oceanic spreading initiated, the Niger Delta began to develop (Doust & Omatsola 1990; Briggs *et al.* 2006). By this time, subsidence due to cooling of the oceanic crust would have been in its later stages, and during the development of the Niger Delta, no notable continental deformation took place, and very little activity took place on the oceanic fracture zones. However, the Adamawa/Cameroon uplift occurred during the Miocene along the Cameroon Volcanic Line, which encourages additional gravitational deformation (Lawrence *et al.* 2002; Meyers *et al.* 1998; van Heijst *et al.* 2002).

2.3. Stratigraphic Setting of the Niger Delta

Sedimentation in the Benue Trough and Niger Delta basin has been active since the initial Atlantic rifts in the Albian and continues to the Present Day (Morgan 2003). The earliest of these sediments were dominantly pelagic marine sediments (Whiteman 1982; Doust & Omatsola 1990) (Fig. 2.4). Following a major Eocene regression (Oboh & Salami 1989), the Niger Delta dominated deposition in the basin as a regressive offlap delta complex (Whiteman 1982;

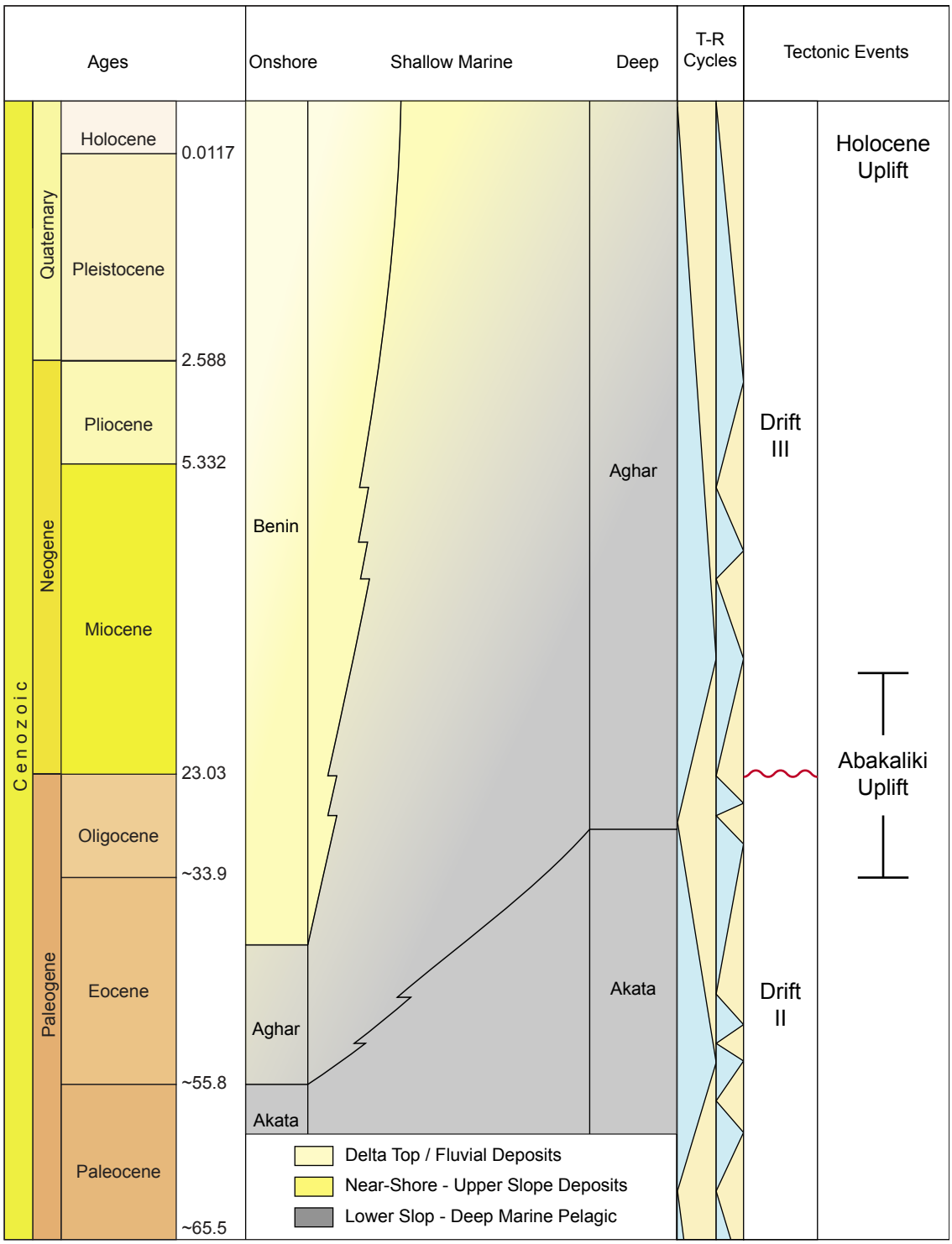

Figure 2.4 Stratigraphic column of the Niger Delta showing a correlation between the onshore and deepmarine parts of the delta. The overall sand content increases towards the onshore and shallow parts of the delta (modified after Doust & Omatsola 1990; Lawrence *et al.* 2002; Krueger & Grant Inpress).

Doust & Omatsola 1990; Corredor *et al.* 2005) (Fig. 2.4). The majority of the delta sediments are derived from crystalline basement complexes and Cretaceous and Cenozoic sediment complexes found along the banks of the Benue-Niger river system (Whiteman 1982).

Deposition in the Niger Delta is both terrigenous and pelagic. The latter takes place in the distal parts of the delta. Terrigenous sedimentation on the other hand mainly occurred in the proximal parts of the delta until the shelf edge. Terrigenous sediments are transported into deeper parts of the basin via turbidity currents and mass transport complexes (MTC) (Damuth 1994). These canyon systems alter the seafloor bathymetry and extend several hundred kilometers depositing submarine fans in the abyssal plain (Damuth 1994).

This section covers the sedimentary sequences of the Niger Delta. It includes a summery of the Pre-Niger Delta sequences and the three main Niger Delta formations: the Akata, Agbada, and Benin formations. The section ends with a discussion about the evolution of the sedimentary systems in the basin.

2.3.1. Basement

The Niger Delta overlies continental and oceanic basement. The latter began to form during the Aptian (~105Ma). The continental basement on the other hand is a crystalline complex that consists of gneisses, Dahomeyan Magmatites and Birrimian (~2000Ma) high-grade metamorphosed sediments (Benkhelil 1982; Ghassemi *et al.* 2010) with igneous intrusions (between Archean and Proterozoic (~2000 ± 250Ma (Doust & Omatsola 1990)) (Coward *et al.* 1999).

2.3.2. Pre-Akata Cretaceous Sediment

Deposition initiated with the early stages of rifting in the Gulf of Guinea. Although these Cretaceous-Paleocene sediments have not been penetrated under the Niger Delta (Tuttle *et al.* 1999; Corredor *et al.* 2005) they have been studied in outcrop by several workers (see Whiteman 1982; Short & Staeuble

1967).

These sediments represent syn- and post-rift sequences. They are preserved in NE-SW and WNW-ESE trending half-grabens that formed as a result of Atlantic rifting (Morgan 2003). The breakup unconformity that followed the deposition of these units erodes through both the post- and syn-rift units.

The syn-rift sediments are Early- to Mid-Aptian in age and vary in thickness between 2500m to 3000m (Morgan 2003), and the post rift sediments are Aptian to Paleocene age (Morgan 2003). Although these sediments have not been penetrated in the delta, several workers have suggested their existence under the distal parts of the delta (Krueger & Grant 2010). These distal sediments are typically deep marine and prodelta sediments (Lawrence *et al.* 2002).

Pre-rift sediment may also be present but limited to the proximal NE part of the delta. These units are Jurassic to lower Cretaceous age, and are estimated to be 5-6 km thick (Dahlen 1990). However, these sequences have been inferred but have not been penetrated under the delta.

2.3.3. Akata Formation

The Akata is the earliest and lowermost Niger Delta formation. Deposition began in Paleo-Eocene and continues to Present Day (Tuttle *et al.* 1999; Whiteman 1982) (Fig. 2.4). This formation does not outcrop in the onshore but occurs throughout the Niger Delta (Whiteman 1982).

The depositional environment extends from the continental shelf to the abyssal plain (Tuttle *et al.* 1999), which is a low-energy oxygen-deficient environment. This produces parallel-laminated pro-delta sequences and pelagic marine muds (Cobbold *et al.* 2009; Whiteman 1982; Morgan 2003). However, during lowstand periods turbidites and mass transport complexes (MTCs) carry terrestrial organic material and clay into the deepwater domain (Tuttle *et al.* 1999; Whiteman 1982; Corredor *et al.* 2005; Heinio & Davies 2006).

The Akata conformably overlies onto the Imo shale in some parts and in other parts it onlaps unconformably on syn- and post-rift sequences as well as continental crust near the Benue Trough and on oceanic crust deeper in the basin (Whiteman 1982).

The anoxic conditions of the pelagic environment allow organic content to be preserved in the Akata. Even during lowstand periods, the Akata remained submerged and was not subareally exposed. Therefore, the Akata is a major hydrocarbon source rock in the Niger Delta (discussed further in Chapter 2.4).

The pressure gradient is normal in the units above the Akata formation, but increases above the normal gradient within the Akata formation, causing overpressure. Consequently, the Akata acts as a main detachment surface in the delta, with thin-skinned tectonics in the overburden and seepage features (Cobbold *et al.* 2009; Whiteman 1982; Bilotti & Shaw 2005). Furthermore, the overpressure reduces the seismic velocity and velocity gradient, which causes the unit to be seismically transparent (Cobbold *et al.* 2009; Morgan 2003; Corredor *et al.* 2005).

The cause for overpressure within the unit is chemical compaction induced by hydrocarbon generation (Cobbold *et al.* 2009). Several authors suggest that the detachment is most active when the Akata is deeper than 4 km depth, which is concurrent with the hydrocarbon generation window (Cobbold *et al.* 2009; Krueger & Grant 2010) (Discussed further in the Chapter 2.4.1 &Chapter 2.4.4).

2.3.4. Agbada Formation

The Agbada formation is an Eocene to Present Day formation that sits conformably beneath the Benin formation and on top of the Akata formation, making it the second of three diachronous Niger Delta complexes (Whiteman 1982) (Fig. 2.4). It is a well-stratified, paralic, siliclastic sequence, which alternates between sand and shale (Cobbold *et al.* 2009; Whiteman 1982; Corredor *et al.* 2005), with a gradually increasing shale-content towards the

base of the unit (Whiteman 1982) producing a gradual transition from the Agbada to Akata (Morgan 2003). The transition becomes more abrupt in the distal parts of the delta where the sand-rich Agbada progrades on top of the Akata (Morgan 2003).

The Agbada is considered to be the main reservoir and seal unit in the Niger Delta, where the sand forms the reservoirs and the shale acts as a seal (Tuttle *et al.* 1999; Whiteman 1982). Organic-rich shale units in the deeper part of the formation may generate hydrocarbons and act as a source rock. Undercompacted shale as well as hydrocarbon generation may produce local overpressure allowing the formation of thrust wedge faults and associated structures.

The Agbada shows repetitive offlaping features, which get younger basinwards (Whiteman 1982). Each para-sequence is characterized by fine marine shales at the base grading into coarser fluviomarine sediments towards the top, at which sedimentation terminates followed by the next marine transgression (Whiteman 1982; Corredor *et al.* 2005). Unlike the Akata the Agbada does not thin towards the basin, maintaining a thickness of ~3000m in water depth of 4500m (Morgan 2003).

2.3.5. Benin Formation

This is the youngest of the diachronous Niger Delta formations, aged Late Eocene to present (Fig. 2.4). It represents the delta top sequence extending from continental to upper coast plain (Whiteman 1982; Corredor *et al.* 2005). Sand dominates the top part of the formation, however, the sequence gradually becomes more marine with depth resulting in increased shale content (Whiteman 1982). The deeper sections also show evidence of brackish water environment and marine fauna (Whiteman 1982). The thickness of this unit varies from 2000 to 3000m, which thins towards the basin due to the greater subsidence of the transitional continental-oceanic crust compared to the

continental crust and the mass movement of the Akata formation. The formation has reservoir potential, however no significant seal was identified and only few oil shows have been identified (Whiteman 1982) and the Benin is generally not targeted for petroleum exploration.

2.3.6. Stratigraphic Evolution

Pre-Niger Delta Deposits

Prior to the development of the Niger Delta, several stratigraphic complexes developed in the Niger Delta and Anambara Basins as regressive offlap sequences (Whiteman 1982) (Table 2.1). These complexes are concurrent with three major transgressive-regressice cycles that took place between the Aptian and Present Day (Tuttle *et al.* 1999; Whiteman 1982) (Fig. 2.4).

From Campanian to Paleocene, deltas were concaved into the Anambara basins (Tuttle *et al.* 1999) (Fig. 2.5). Throughout this period, the delta became tide-dominated during transgression and river-dominated during regression periods (Cobbold *et al.* 2009). Further offshore shallow marine clastics were deposited. However, the distribution of the Late Cretaceous under the Niger Delta is unknown (Tuttle *et al.* 1999).

In the Paleocene, a major transgression (The Sokoto transgression) began with onset of the Imo shale being deposited in the Anambra basin to the northeast of the Present Day Niger Delta (Tuttle *et al.* 1999).

Niger Delta Deposits

Similar to other deltas, the shape of the Niger Delta is controlled by several factors including the wave and tide energy, sediment influx etc. Because of these variations, the shape of the delta has evolved from concave to convex through time (Fig. 2.5).

In the Eocene, the coastline became linear with a slight convex shape and

Cenozoic Niger Delta **Paleogene - Present Day**	Built across the Anambara Basin and extended onto Late Cretaceous contiental margins and cooling oceanic crust High-energy constructive environment dominated the Early Eocene to Early Miocene. During this period three depocenters have been identified with associated lobate-elongated deltas
Anambra Delta Complex: **Late Cretaceous – Paleocene** **(Post-Santonian)**	Anambara Delta Complex: Primarly developed in the Anambra basin situated on the north west flank of the Abakalki fold belt Regressive offlap sequences began to develop during the Campanian, prograding extensively during the Maastrichtian. This delta development ended in the Paleocene when the Imo shale transgression extended into the Anambra basin. The Anambra Delta complex (regressive clastic) can be considered as a Late Cretaceous to Paleocene proto-Niger Delta complex, which extended onto continental crust. This is a smaller sized than the current delta and may have not developed delta tectonics. This is the youngest Cretaceous sediment to be deposited during the drift phase.
Transgresive-regressive complexes **Early Cretaceous (Pre-Santonian)**	Mid-Albian transgression in the Abakalki trough and adjacent flanks Three cycles recognized during the Conician-early Santonian regression Albian-Cenomonian Bima Delta complex developed at the head of the Benue depression about 950km from the current Delta shoreline. Before the Niger Delta, several deltas began to form during regressive period of the early Turonian, Conician-early Santonian,

Table 2.1 Evolution of sedimentary complexes in the Niger Delta Basin (Compiled from Whiteman 1982; Tuttle *et al.* 1999; Cobbold *et al.* 2009).

sedimentation in the basins becomes wave-dominated. The Eocene marked the onset of the Niger Delta, which began to prograde south – southwest and progressively pushed the shoreline to a more convex shape. From the Miocene to Present Day, the Niger Delta remains a high-energy wave-dominated delta with a lobate arcuate structure (Tuttle *et al.* 1999; Whiteman 1982; Doust & Omatsola 1990) that extends into the basin in a series of offlap regressive sequences.

Between the Eocene and Early Miocene three separate depocenters formed three independent elongated lobate deltas (Whiteman 1982). These deltas later joined together during the Miocene, and formed the Niger Delta system (Whiteman 1982). During the Late Eocene, the Niger Delta began to prograde onto oceanic basement (Damuth 1994).

2.4. Structural Setting of the Niger Delta

Structural styles in the Niger Delta are dominated by thin-skinned features. The underlying thick-skinned deformation of the continental crust ceased and was infilled before the deposition Niger Delta (Chapter 2.2.3). Oceanic crust on the other hand shows some deformation near fracture zones (Corredor *et al.* 2005; Cobbold *et al.* 2001). The fracture zones influence the internal structures of the delta and create trenches along the seabed (Fig. 1.2). In particular, the Charcot FZ creates a high that splits the delta into distinct western and southern lobes (Corredor *et al.* 2005) (Fig. 2.6).

To describe the structural setting of the Niger Delta this section begins with a description of the shale detachment system (Chapter 2.4.1). Then a description of the thin-skinned structural system is exhibited in (Chapter 2.4.2). This is followed by a detailed overview of the fold systems of the distal Niger Delta (Chapter 2.3.1). Finally, the section ends with an overview of the structural evolution and escalator regression theory (Chapter 2.3.2).

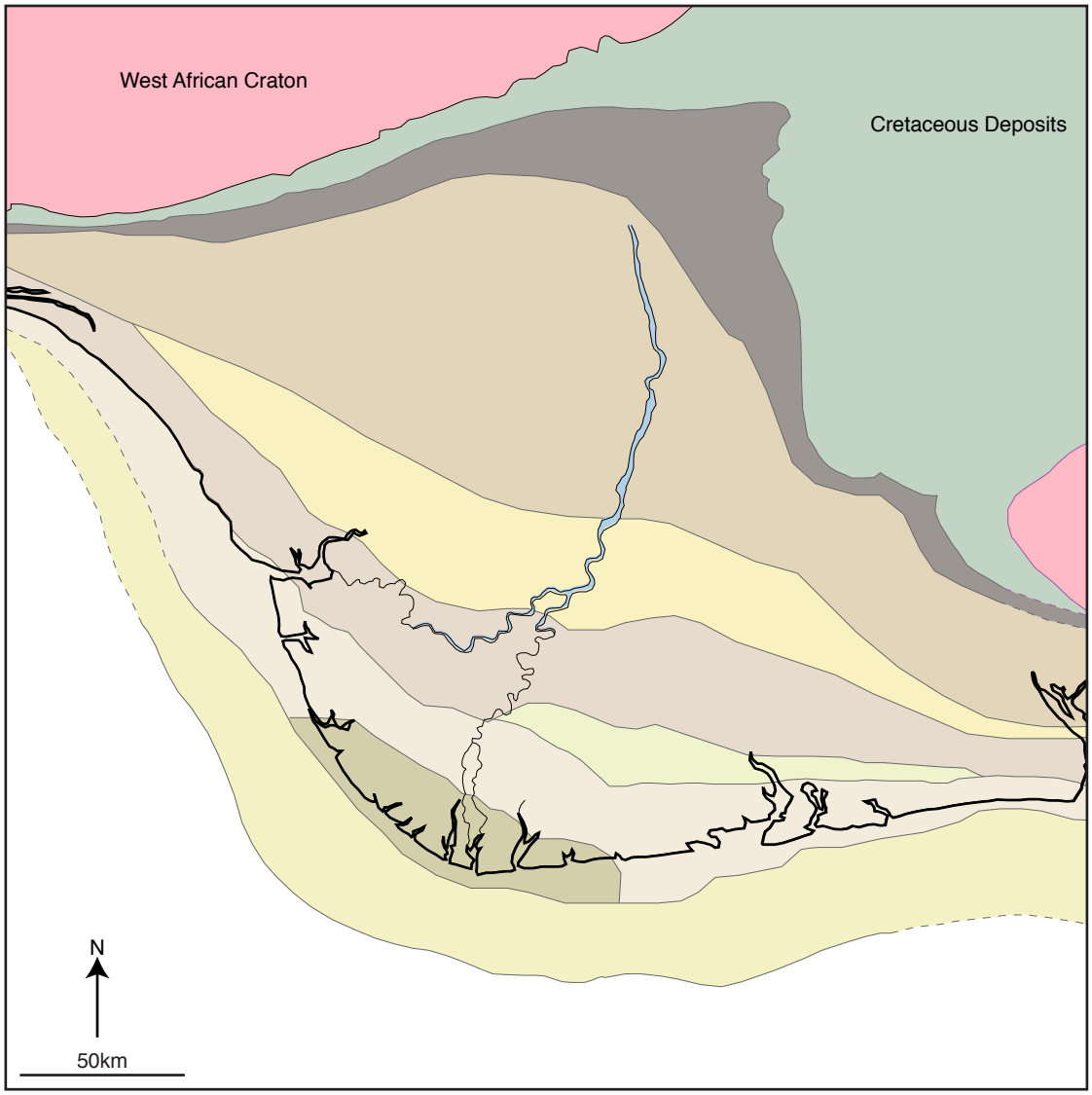

Figure 2.5 Shoreline and depobelt geometry of the Niger Delta shoreline (modified after Magbagbeola & Wilis 2007; Doust & Omatsola 1990).

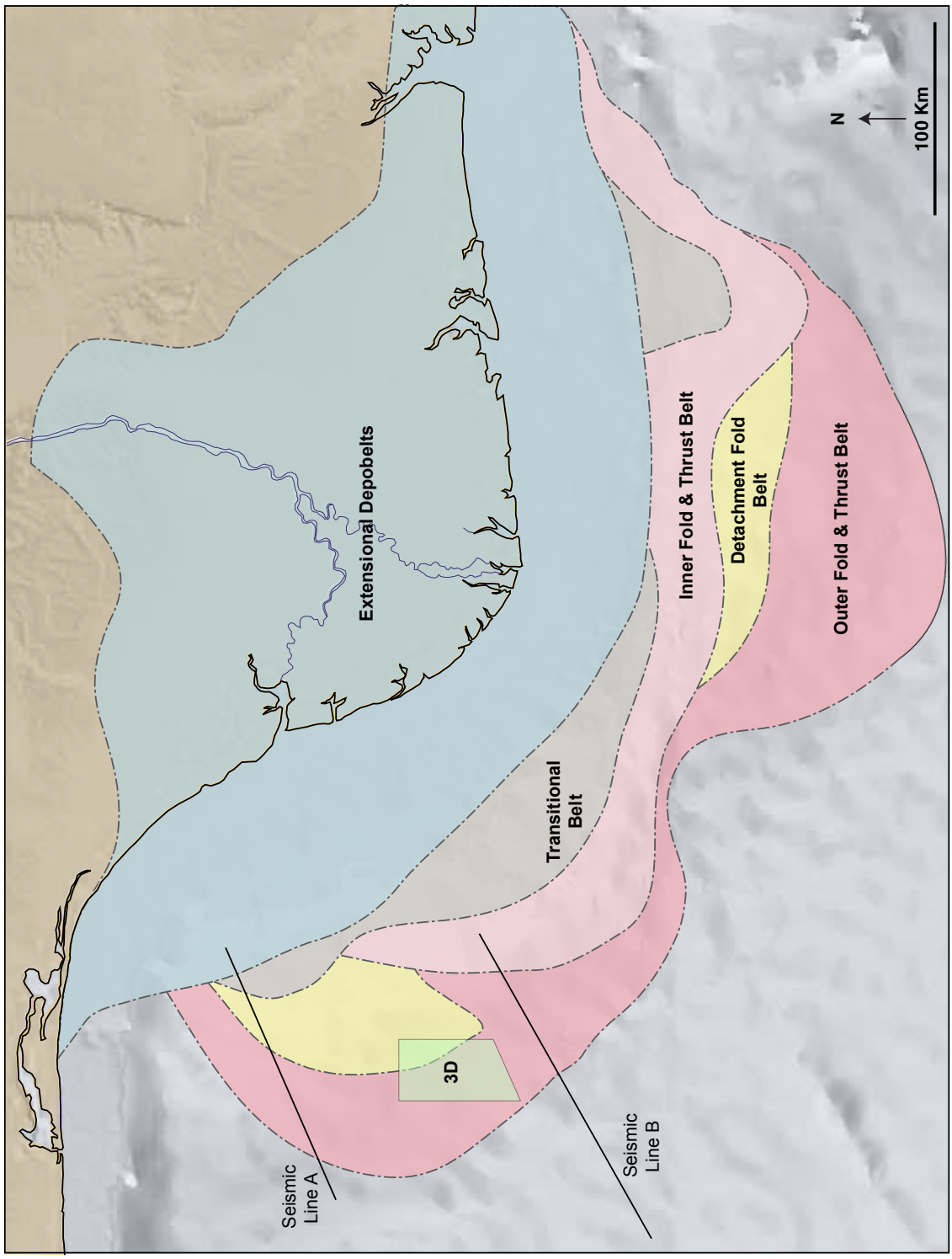

Figure 2.6 Different deformation zones in the Niger Delta. (modified after: Briggs *et al.*, 2006; Corredor *et al.*, 2005; Cohen & McClay, 1996)

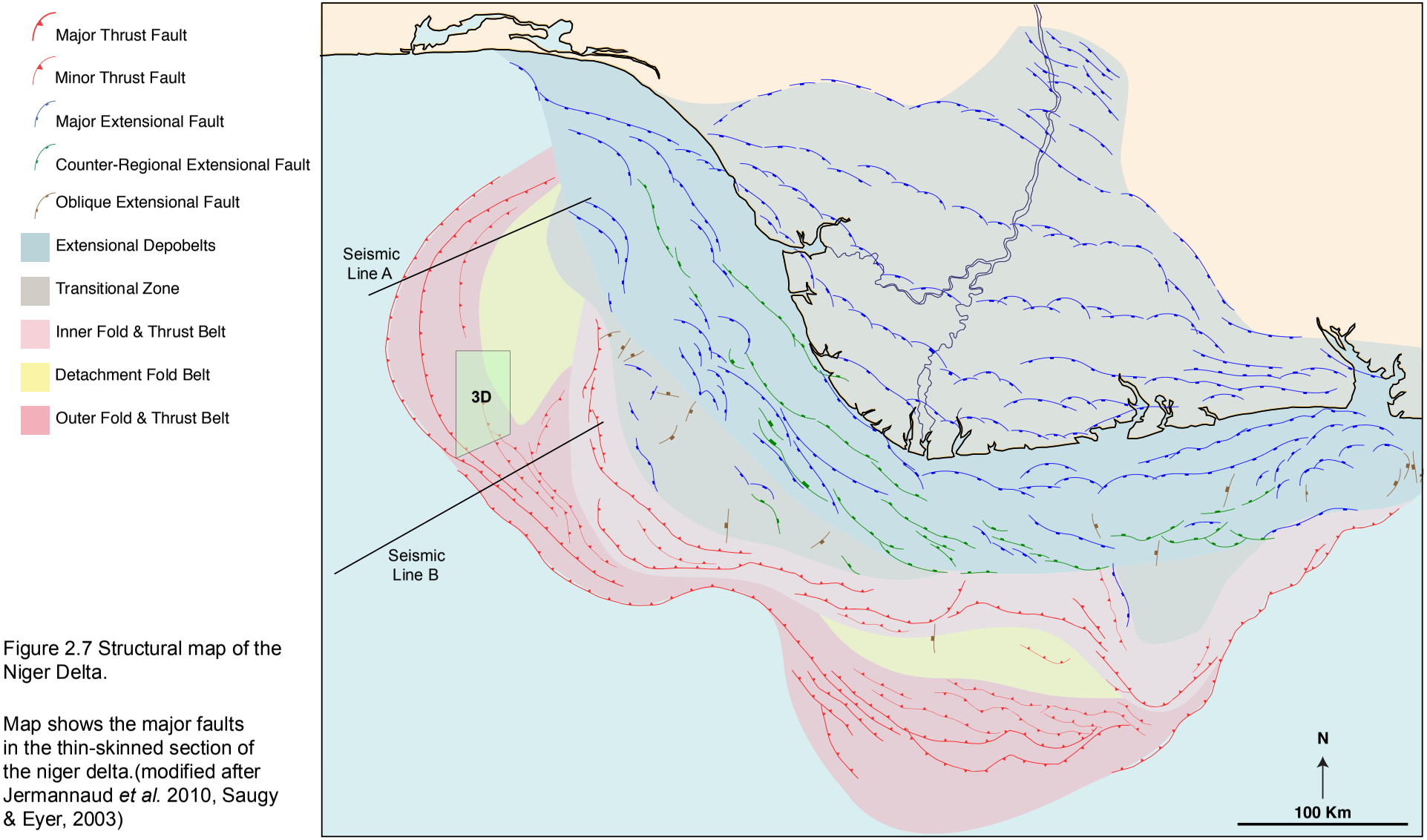

Figure 2.7 Structural map of the Niger Delta.

Map shows the major faults in the thin-skinned section of the niger delta.(modified after Jermannaud *et al.* 2010, Saugy & Eyer, 2003)

2.4.1. Overpressured Shale Detachment Systems

Overpressure occurs when the fluid pressure within a certain rock unit exceeds the hydrostatic pressure gradient. Such a phenomenon is common in rapidly buried sedimentary basins, especially at depth (Cobbold *et al.* 2009). Overpressured pore fluid reduces vertical stress, which in turn reduces the strength of a particular rock unit (Briggs *et al.* 2006) allowing it to behave as a detachment surface.

The Niger Delta thin-skinned system is interpreted to detach along an overpressured shale unit. The detachment system is present under the entire delta, dissipating towards the distal parts that show less extensive deformation. The alternation of forethrusts and backthrusts (Cobbold *et al.* 2009) as well as the very low critical taper angle (critical taper = slope of seabed + slope of detachment) compared to other similar fold belts (Bilotti & Shaw 2005) (Fig. 2.8) indicates that the overpressure is high to near-lithostatic (Cobbold *et al.* 2009; Bilotti & Shaw 2005; Cobbold *et al.* 2001).

Shale detachment is a dynamic systems that constantly change through time and space. The effectiveness of a shale-detached system is controlled by several factors including pore fluid pressure, ductile layer thickness and strain hardening, as well as crustal flexure due to sediment loading (McClay *et al.* 2003). Furthermore, overpressure in the Niger Delta is produced and maintained by hydrocarbon generation (Cobbold *et al.* 2009; Corredor *et al.* 2005). Therefore, factors that control hydrocarbon generation such as burial depth, thermal gradient and source rock richness also affect the nature and extent of the detachment (Cobbold *et al.* 2009; Corredor *et al.* 2005; Cobbold *et al.* 2001). Consequently, the geometry and kinematics of the thin-skinned structures are also affected (Cobbold *et al.* 2009; Briggs *et al.* 2006; Corredor *et al.* 2005). Furthermore, the progradation of the delta further into the basin causes additional burial of the distal parts, which eventually cause hydrocarbon generation to take place further in the basin and progression of the detachment.

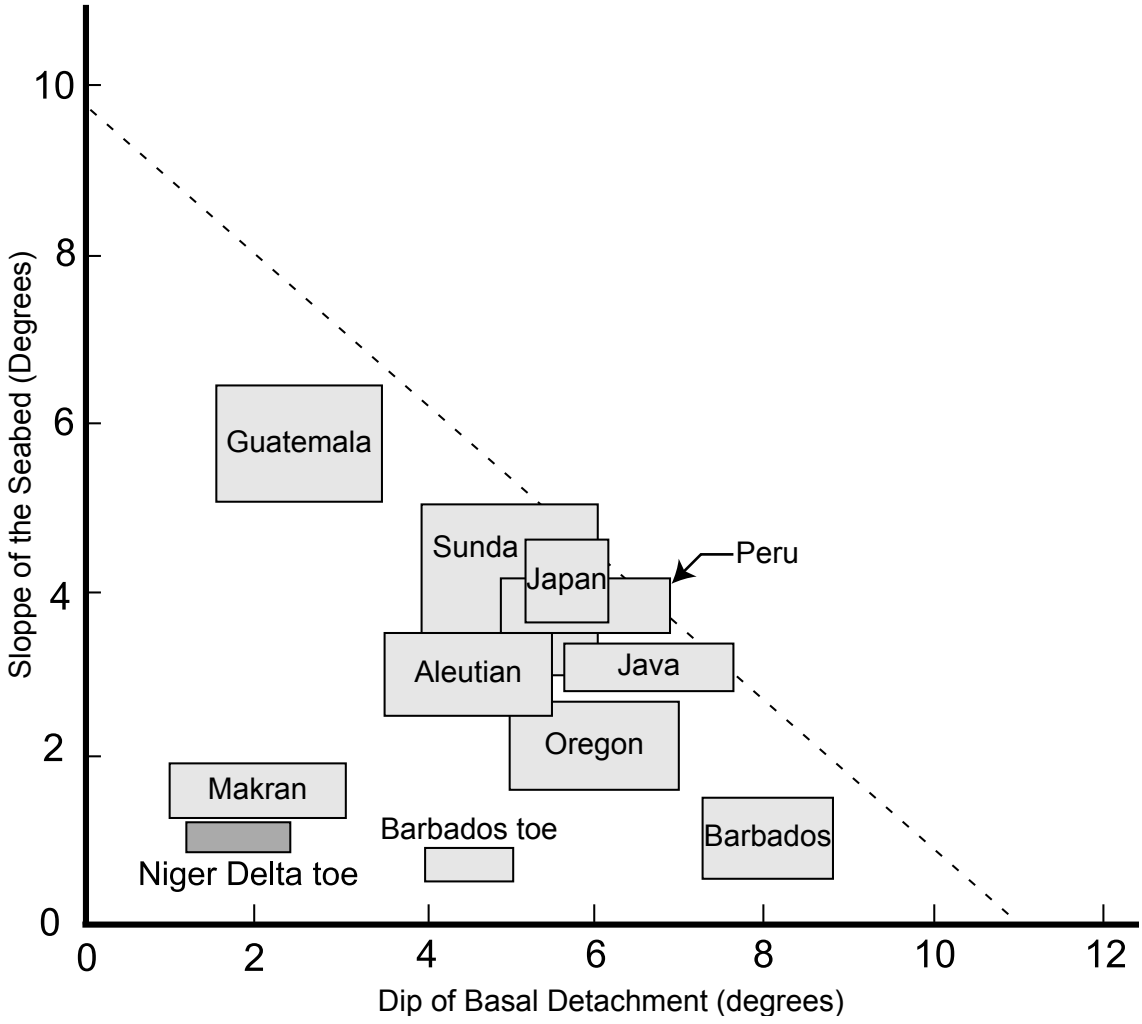

Figure 2.8 Comparison of the slope of the seabed vs. th dip of the basal detachment chart for deepwater submarine fold and thrust complexes. The Niger delta shows lower values than other fold and thrust systems. Makran and Barbados toe are known to have high overpressure values similar to that of the Niger Delta (Modified after Bilotti & Shaw 2005)

Several detachments have been identified in the Niger Delta; the major ones are within the upper parts of the Akata formation (Cobbold *et al.* 2009; Briggs *et al.* 2006; Corredor *et al.* 2005). Three detachment zones are identified within the Akata; the two major detachments are the Dahomy wedge and Top Akata detachments, as well as a third localized detachment, which covers an area of only ~5% (Briggs *et al.* 2006). The first zone is located to the NW of the delta within the detachment fold zone (Fig. 2.6), which creates a zone of deformation located in front of the thrust faults 100-120m thick. Folds in this zone have asymmetric to symmetric geometry with minor thrust faults (Briggs *et al.* 2006). The second zone is located further south and shows more strongly asymmetric to symmetric folds, with tighter interlimb angles and more prominent thrust faults (Briggs *et al.* 2006). The research area is located within the second zone, detaching on the Akata-Agbada interface.

Other observed features associated with overpressured shale include fluid escape features such mud volcanoes (Cobbold *et al.* 2009). These typically occur in fold forelimbs and appear as steep tube like structures that vent at the surface creating a crater or collapse caldera on the seabed (Cobbold *et al.* 2009). The tube itself is poorly imaged and seismically transparent (Cobbold *et al.* 2009).

2.4.2. Thin-Skinned Structures

The Niger Delta exhibits gravity driven deformation controlled by deposition and differential loading. This deformation consists of extension in the proximal part, which is mechanically translated along the detachment and compensated by compression in the distal parts (Cobbold *et al.* 2009; Corredor *et al.* 2005; Bilotti& Shaw. 2005; Briggs *et al.* 2006; Damuth. 1994; (McClay *et al.* 1998)). Such gravity related gliding and spreading is common in continental margin post-rift sediments around the world (Cobbold *et al.* 2001).

Sedimentation is concentrated in the proximal parts of the delta, which receive

the majority of the deposits carried by the delta rivers. This creates a cone shaped delta, which as a result exerts an uneven stress on the proximal part of the delta. As a result, the proximal part of the delta begins to subside by developing basins bounded by listric extensional faults, which are infilled by the incoming sediments. To compensate for the subsidence, the movement from the proximal parts is conveyed along the detachment surface to the distal parts and forms compressional structures (McClay *et al.* 2003) (Fig. 2.10). The compressional features are indicative of a constraint that prevents movement further into the basin. This constraint is likely to be the basinward extent of the detachment syetem (McClay *et al.* 2003; McClay *et al.* 1998).

The delta can therefore be divided into several arcuate zones according to the deformation domain (Fig. 2.6,figure 2.9 & 2.7). The three main domains are (Corredor *et al.* 2005):

1. Extensional zone beneath the outershelf; has both regional and counter-regional listric faults that bound mini-basins called depobelts (Darros de Matos 1999).y

2. Intermediate zone beneath the upper continental slope, containing passive, active and reactive mud diapirs and mud volcanoes (Briggs et al. 2006; Damuth 1994).

3. The compressional zone beneath the lower continental shelf and continental rise, characterized by thrust faulting and associated folding (Briggs et al. 2006) (discussed further in Chapter 2.3.1). This domain is further subdivided into three subdomains (Cobbold et al. 2009; Briggs et al. 2006; Corredor et al. 2005; Bilotti & Shaw 2005):

   1. Inner fold and thrust belt (FTB): highly shortened and imbricated thrust belt forming 1-2 km wide piggy-back basins, with steep structural dips, basinward-vergent, and typically fold associated. Follows an arcuate path across the central part of the delta.

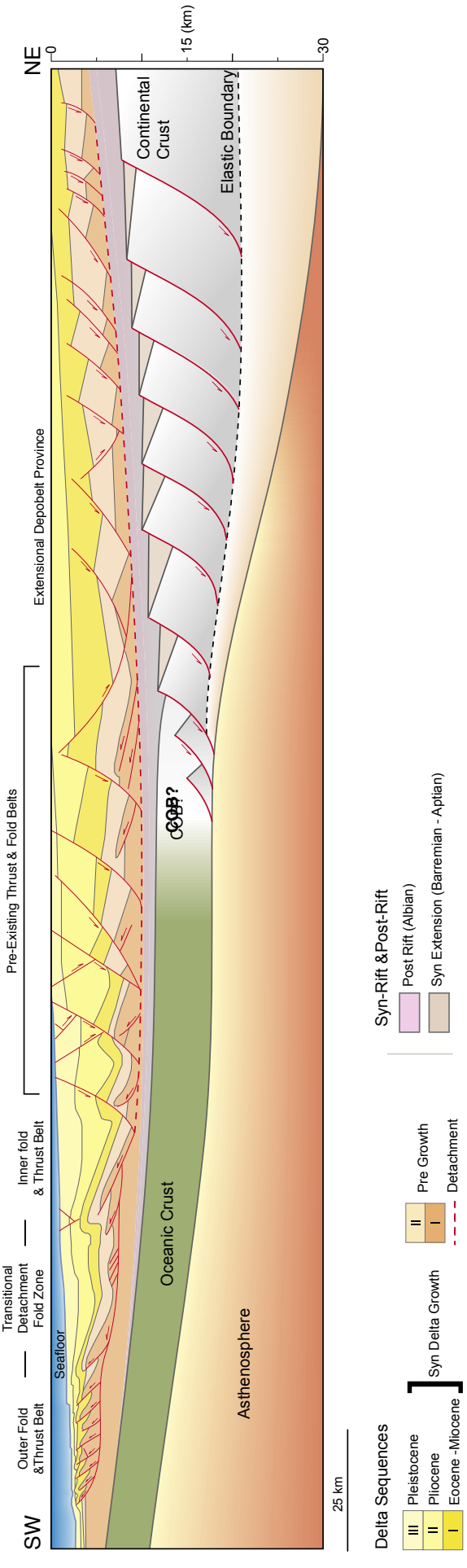

Figure 2.9 Schematic Cross-section of the Niger Delta (modified after Mourgues *et al.* 2009)

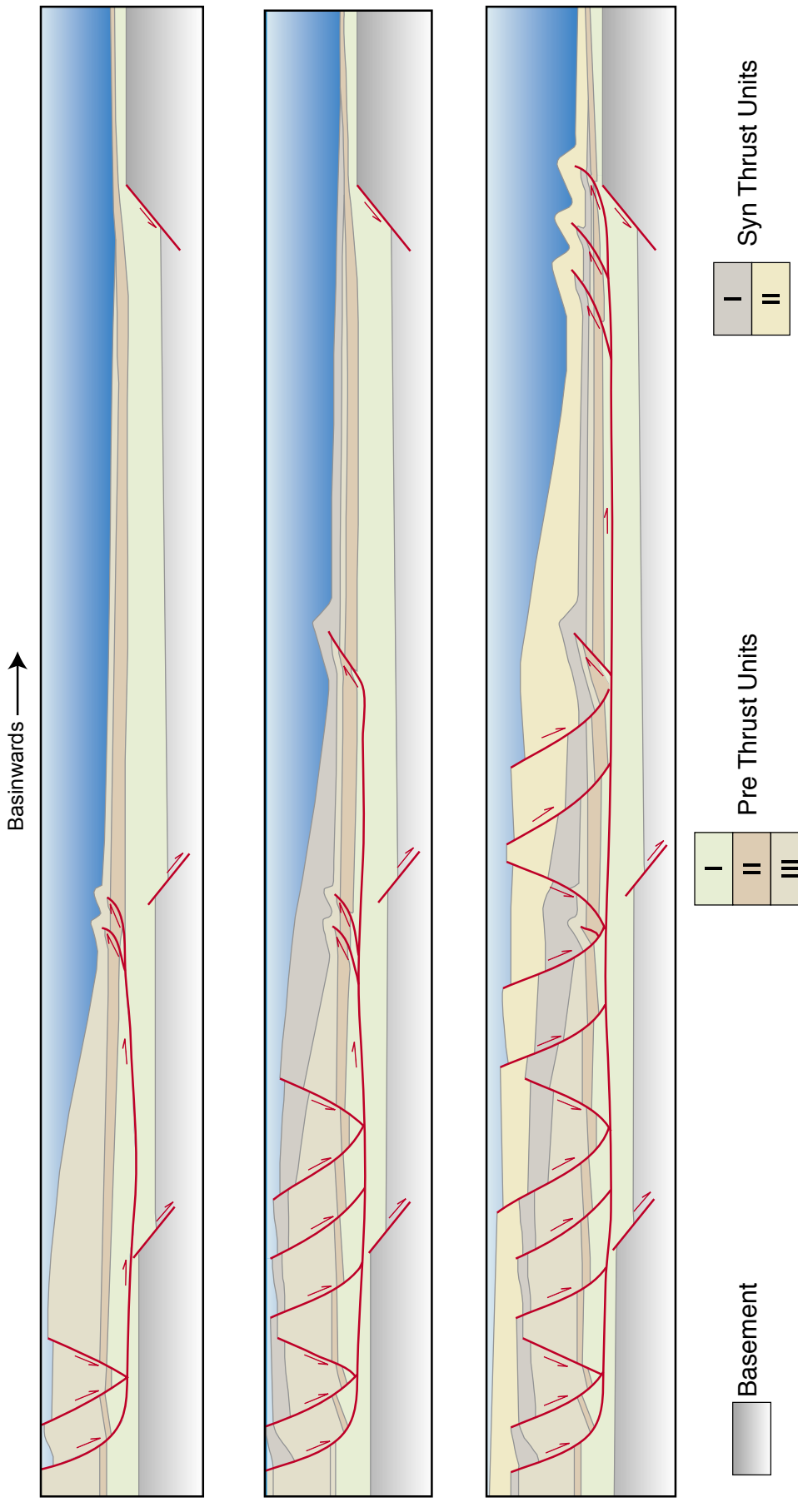

Figure 2.10 Evolution of a shale detached delta (modified after Mourgues *et al.* 2009)

2. Outer FTB: more classic toe-thrust anticlines basinward- and landward-vergent, separated by several kilometers giving a much wider anticline wavelength than the inner FTB and trapping channelized turbidites. The belt is located beneath the lower continental slope.

3. Detachment fold province: located between Inner and Outer FTBs, with little deformation related to thrust and shale induced folding, accommodating less shortening than the other two contractional belts. It is both verging towards the basin and hinterland. Contains northern and southern sections that define the two lobes of the Delta, these two lobes are separated by a basement topographic high related to the Charcot Fracture zone (Corredor *et al.* 2005).

The extensional faults are controlled by the water content and thickness of the detachment (McClay *et al.* 2003). When the extensional faults can no longer accommodate deposition, the sedimentation bypasses the depobelt and carries on to create a new fault-bound depobelt. This type of progradation is known as escalator regression (Knox & Omatsola 1989) (discussed further in Chapter 2.3.2). Seven 30-60 km (Morley 2003; Tuttle *et al.* 1999) wide depobelts have been emplaced since deposition began in the Niger Delta (Fig. 2.5) (Doust & Omatsola 1990; Magbagbeola & Willis 2007). The lifespan of a depobelt may overlap with other depobelts, this is attributed to sedimentation exceeding accommodation which allows deposition to bypass the active depobelt.

Over time, the depobelts have progressed ~240-250 km southwest into the basin (Tuttle *et al.* 1999) as well as the delta thrust front. In some cases, the extensional fault may be superimposed over older thrust faults (Fig. 2.9). Inversion of the thrust faults has not been documented and is unlikely, taking into account the low angle of the thrust faults as well as the weakly lithified stratum.

2.3.1. Thrust Faults and Thrust-Related-Folds

One of the main features of the Niger Delta as well as the focus of this study is the fault-related-folding found in the compressive parts of the delta (Fig. 2.6 & 2.11). These thin-skinned features accommodate for the majority of the shortening (~76%) in the Niger Delta while the remainder is accommodated by sub-seismic deformation (de Vera *et al.* 2010). The folds and especially those in the inner and outer fold belts may create seabed relief, alternating between pop-up structures and flat-bottom synclines (Cobbold *et al.* 2009; Corredor *et al.* 2005).

Some of these folds are associated with thrust faults that follow the decollement, forming detachment folds. Detachment folds dominate the detachment fold belt (Fig. 2.6). The core of these detachment folds is not infilled by flow of shale as previously thought (Bilotti & Shaw 2005; Knox & Omatsola 1989), but is thickened by brittle bourrage deformation, duplex complexes (Spratt *et al.* 2004) and other sub seismic accomodation structures (Maloney et al. 2010).

However, folds in the inner and outer FTBs (Fig. 2.6 & 2.9) are typically associated with listric and sigmoidal thrust faults. These are highly asymmetric fold with a short steep forelimb and longer less steep backlimb (Fig. 2.12) (Corredor *et al.* 2005). The growth strata associated with the forelimb shows a kink-band geometry, which indicates that the forelimb has maintained its dip for most the evolution of the fold. The backlimb, on the other hand, has a significantly shallower dip than the thrust ramp, which is characteristic of limb-rotation. Thus, the fold has evolved with elements of both self-similar and limb rotation (Corredor *et al.* 2005). Therefore, these folds depart from the definitions of fault-propagation-folds and fault-bend-folds (Suppe 1983) since they do not account for shearing and bed slip which commonly occur in the deepwater setting.

Two models were developed to describe the Niger Delta folds, the simple- and

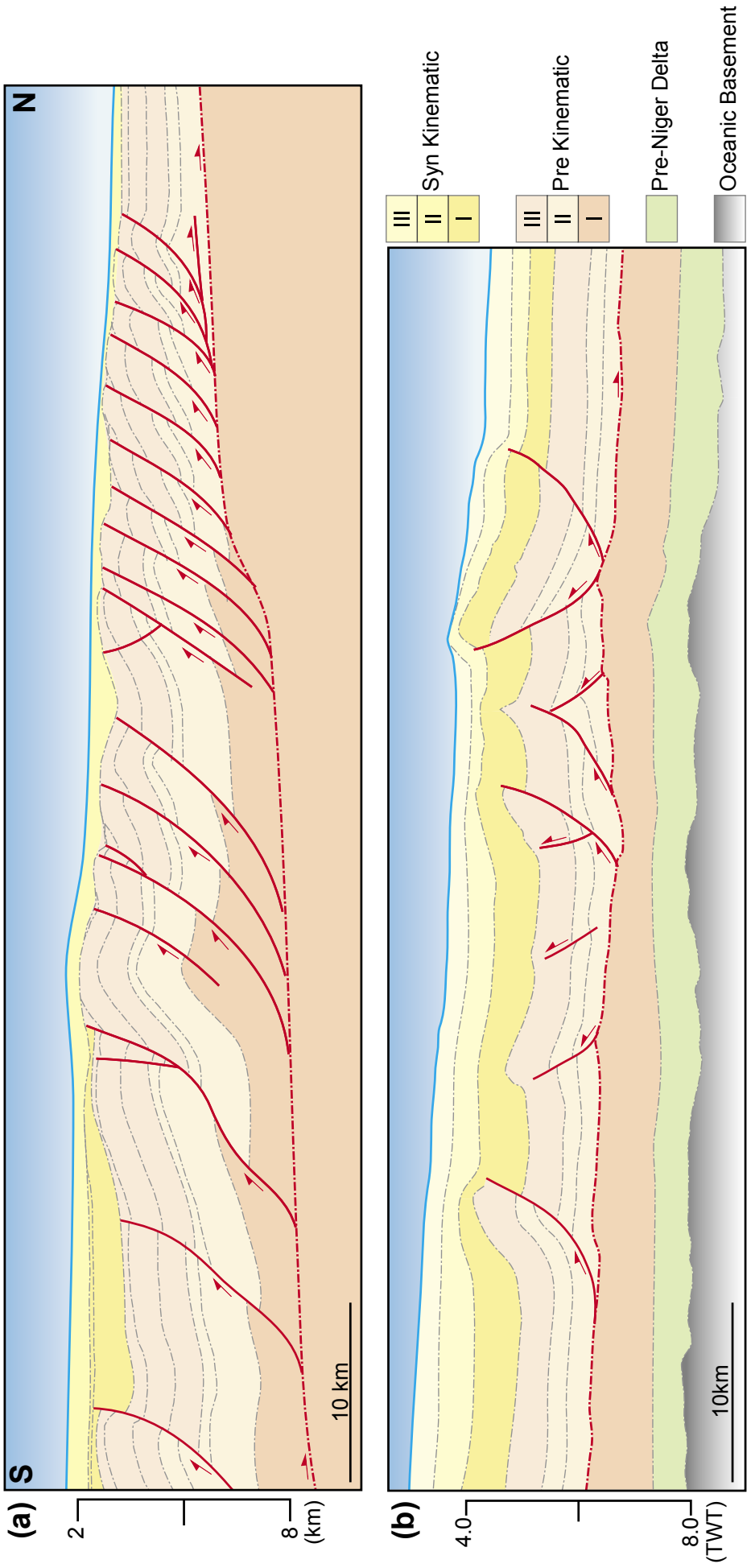

Figure 2.11 Cross section through the fold and thrust belts. (A) in the southern lobe (modified after Hooper *et al.* 2002) and (B) in the western lobe (modified after Briggs *et al.* 2009).

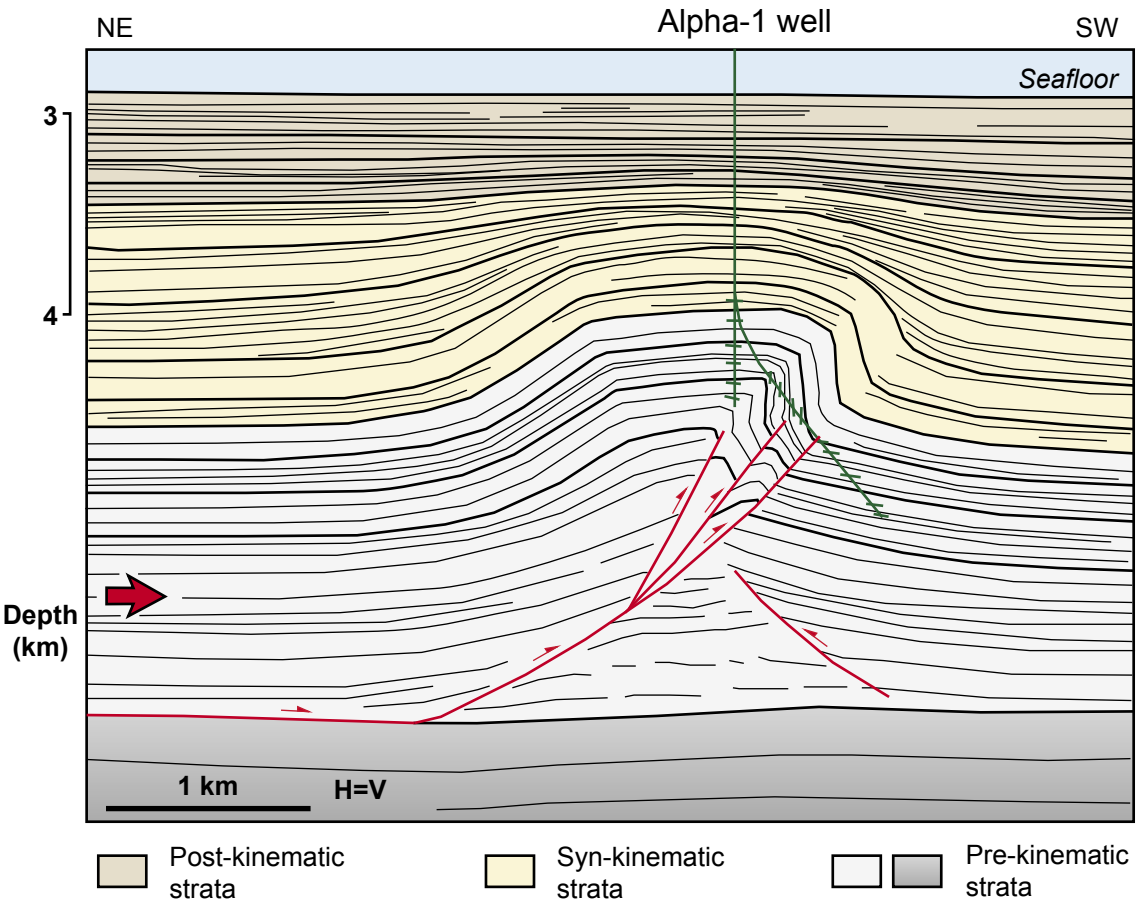

Figure 2.12 cross section through a fault related fold in depth (modified after Kostenko *et al.* 2008).

pure-shear fault-bend-fold (FBF) models (Suppe *et al.* 2004) and thrusted detachment fold model (Briggs *et al.* 2006). The fundamental difference between the two models is the origin of the thrust fault; the shear FBF evolves with a thrust ramp eminating from the decollement where as the thrusted detachment fold forms prior to a thrust that breaches the limb of the fold, and propagates downwards towards the detachment.

The overpressured substrate causes the associated thrust faults to form with horizontal to sub horizontal dips. However, these faults rapidly change to a steep 40° dips towards the upper parts of the sediment sequence (Briggs *et al.* 2006). This not only implies that the overpressure is near lithostatic as mentioned earlier but also indicates that the overpressure is limited to the bottom of the section, and the upper parts of the section become more competent.

The main internal fold structures include forethrusts, backthrusts and associated hanging wall anticlines, they also alternate to form pop-up anticlines and flat-bottom synclines (Cobbold *et al.* 2009). Typically, forethrusts have listric fault planes, whereas the backthrust are planar (McClay *et al.* 2003).

Both typical break-forward and complicated break-backward imbricate systems occur in the Niger Delta (Corredor *et al.* 2005). The later kind is consistent with having multiple detachment surfaces. This also produces antithetic fault linkage, where fore-and back-thrusts link along strike (Higgins *et al.* 2007).

2.3.2. Structural Evolution and Escalator Regression

The extensional faults began to form during the Paleocene before the onset of compressional faults, which also made way for additional local subsidence and accommodation space (Doust & Omatsola 1990) forming a depobelt. This is then translated via the intermediate zone to the fold belts in the deep portion of the delta, forming compressional structures. These thin-skinned compressional faults are evenly spaced (2-5 km and sometimes up to 10 km) and have

dominantly asymmetric folds (Briggs *et al.* 2006).

When the depobelt can no longer accommodate the deposition sedimentation bypasses the fault block, and initiates faulting further into the basin, developing a new depobelt. This is known as escalator regression (Doust & Omatsola 1990; Knox & Omatsola 1989). The Niger Delta has thus far developed seven distinct depobelts (Fig. 2.5). The advance of the depobelt is also associated with a change in the shape of the shoreline (Oboh & Salami 1989; Short & Staeuble 1967).

2.4. Hydrocarbon Systems

Along the South Atlantic passive margins, 93% of discoveries until 1999 were in drift successions and only 6% in the rift and 1% in the pre-rift successions (Coward *et al.* 1999). Of these, 75% is contained within the Niger Delta (Coward *et al.* 1999). A large number of wells have been drilled over the period of four decades; however, a comprehensive understanding of the petroleum system is not yet complete (Samuel *et al.* 2009).

The majority of these exploration efforts have focused on Cenozoic systems within the Niger Delta. Nonetheless, a growing number of worker have (Samuel *et al.* 2009; Haack *et al.* 2000; Katz 2006) suggest petroleum plays sourced from pre-Niger Delta Cretaceous sections. The following is an overview of the petroleum systems concepts in the Niger Delta.

2.4.1. Source Rock and Maturation

The source in the deepwater Niger Delta is proven to be predominantly marine in origin (Schiefelbein et al. 1999), unlike other deltas such as the Mahakam Delta in Indonesia where terrigenous source rock has been emplaced in a deepwater setting by turbidite flows (Samuel et al. 2009). The main controls on the maturity of the source rock are (Samuel et al. 2009):

- Age of the oceanic crust
- Heat-flow through the oceanic crust
- Thermal conductivity
- And thickness of the overburden

Three potential source rocks are found in the deepwater Niger Delta: the Akata (Paleo-Eocene), the Late Cretaceous (Cenomonian to Early Turonian and Maastrictian (Morgan 2003)) and the Lower-Agbada (Oligocene) shales. The latter two are potential source rocks, whereas the Akata is a proven source for many fields throughout the Niger Delta (Matava et al. 2003).

The Late Cretaceous organic shales have petroleum generation potential and occur in offshore West Africa, but are not mature. They are described as lacustrine to marine shales with high algal organic content (Samuel et al. 2009; Haack *et al.* 2000) that produces a marine type I kerogen. Expulsion efficiency of this source rock is controlled by the amount of total organic carbon (TOC) and the thickness of the sequence.

The burial depth of this sequence varies from the proximal to distal regions. In the proximal parts, it may be beyond the petroleum generation window. In distal parts, under the inner and outer FTB, these sequences may still be within the hydrocarbon generation window. Nonetheless, this sequence remains a high risk source.

Similarly, the lower section in the Agbada formation is an organic-rich shale which is potentially a source of hydrocarbons (Sonibare *et al.* 2008). This is especially the case in the proximal inner FTB, which exhibits thickening that would bury the lower part of the Agbada within the oil generation window, but that may not always be the case. This sequence is considered of moderate to high risk because of shallow burial depth.

The Akata (Paleo-Eocene) is the main source rock in the Niger Delta and is underlies the entire delta (Cobbold *et al.* 2009; Sonibare *et al.* 2008). Even in the distal parts of the delta, the thickness of the overburden is in excess of 3.5 km that allows enough burial to produce hydrocarbons. This is considered the lower risk source rock the Niger Delta.

Both the Akata and Agbada delta units contain both terrestrial and marine organic material that is characteristic in deltaic environments (Sonibare *et al.* 2008). The marine kerogen forms in place or can be derived from a submerged nearby location. The terrestrial detritus would have been carried by turbidity and other flow complexes to deeper water. Marine algal content would form Type I kerogen, whereas terrestrial material would form liptinitic Type II kerogen derived from zooplankton and phytoplankton. Some authors suggest that the Agbada formation contains humic Type III kerogen (Matava et al. 2003; Ekweozor & Okoye 1980; Lambert-Aikhionbare et al. 1984; - Ejedawe - 1986; Bustin 1988), however this is likely to be limited to the near-shore area. In the distal deepwater part of the Niger Delta, the oil is sourced from marine algae-rich source rocks with little influence from terrigenous source rock (Samuel *et al.* 2009).

2.4.2. Reservoirs

The main targeted reservoir interval in the Niger Delta is the Agbada sands (Tuttle *et al.* 1999). Characterized as sandstone and unconsolidated sand intervals (Tuttle *et al.* 1999; Akpabio & Ejedawe 2010), the Agbada reservoir quality varies with depositional and burial depth (Tuttle *et al.* 1999) as well as depositional system. The thickness of the sand interval varies between 15m and 45m, where the later is likely to result from stacked channel bodies (Doust & Omatsola 1990).

In the proximal extensional zone of the delta, the thickness of the Agbada interval is controlled by the subsidence of growth faults, thickening in the

hangingwall near the fault surface (Doust & Omatsola 1990; Weber 1987). In the onshore delta, the typical reservoirs are located in Eocene to Paleocene Agbada sands 10 to 20m thick (Sonibare *et al.* 2008; Ejedawe 1986). In the distal offshore contractional fold belts, reservoirs are potentially found within turbidite channels, lowstand sand bodies and submarine fan deposits (Samuel *et al.* 2009; Heiniö & Davies 2007).

2.4.3. Seals and Traps

Most the traps in the Niger Delta are structural traps, however, stratigraphic trap and combinations of both do occur (Tuttle *et al.* 1999). However, the continuous deformation of the delta may cause the trapping style to change with time (Tuttle *et al.* 1999; Doust & Omatsola 1990).

Structural trapping style varies from the proximal extensional part of the delta to the distal contractional fold belts due to variations of trapping mechanism and lithology. Earlier work has focused on the trapping mechanisms in the extensional domain of the delta (eg. Whiteman 1982; Doust & Omatsola 1990). These include listric fault bounded traps, antithetic fault bounded traps as well as roll-over and collapsed rollover traps (Tuttle *et al.* 1999; Doust & Omatsola 1990; Magbagbeola & Willis 2007). More recent research have focused on the contractional fold belts in the deepwater setting (eg. Morgan 2003; Samuel *et al.* 2009).

The interbedded sand and shale in the Agbada increases seal potential. The simplest seal is the vertical seal, which prevents vertical hydrocarbon migration; this is also enhanced by structural folding (Doust & Omatsola 1990). Clay smears create important seals for faults with small displacements (Pochat *et al.* 2004). Furthermore, juxtaposition of shale and sand sequences has trapped hydrocarbons in the reservoir rock.

The continuous structural evolution of the Niger Delta adds additional risk for petroleum trapping. It is common for deformation to breach sealing units,

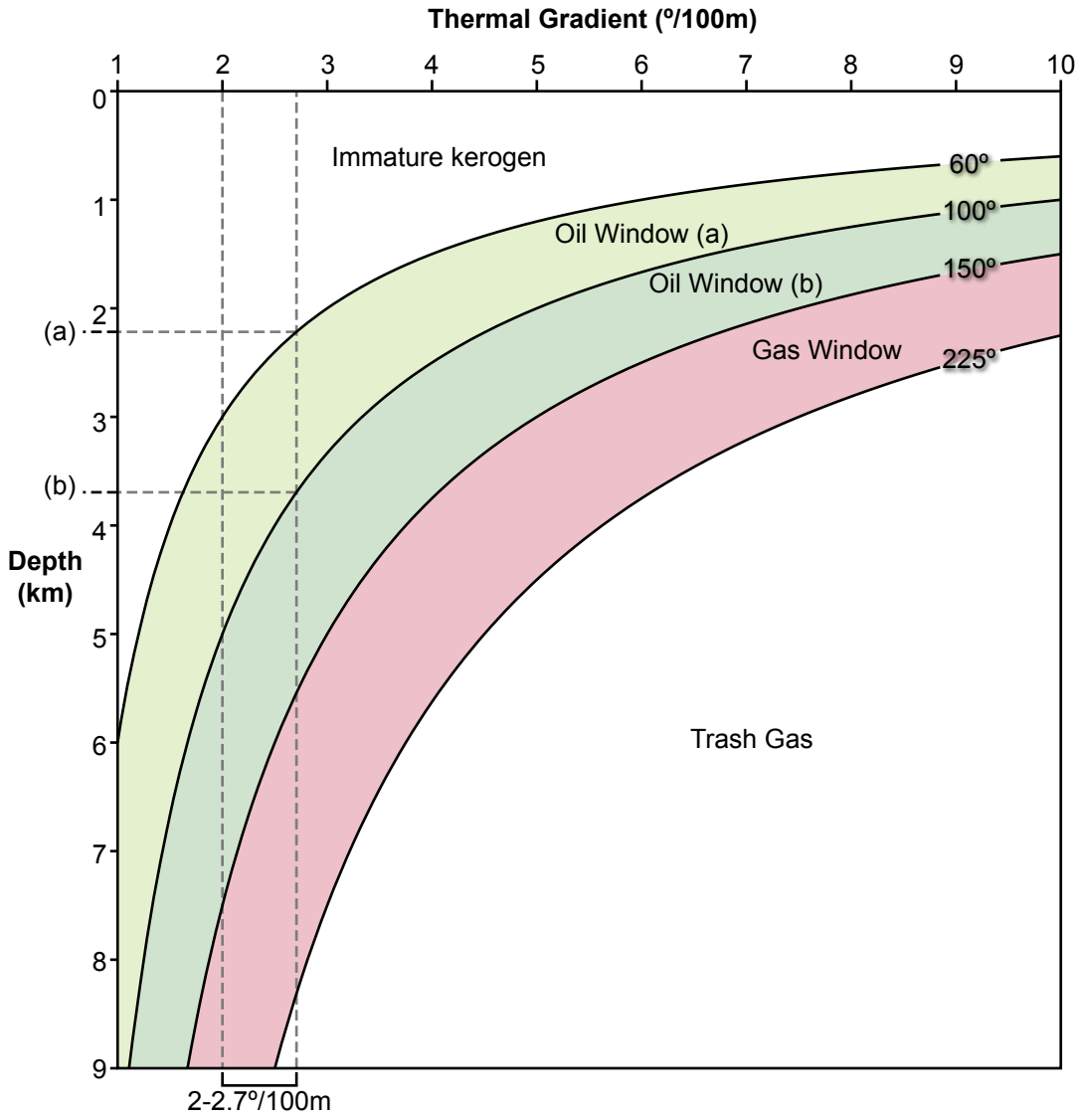

Figure 2.13 Generic depth vs. thermal gradient curve.(Selley 1998; Tuttle *et al.* 1999)

The Niger Delta thermal gradient and associated maturation depth is highlighted. values of (a) are suggested by Cobbold *et al.* (2009) and (b) are suggested by Akpabio & Ejedawe (2010)

either by propagation of major faults through the seal sequence or by creating fractures in folded units, which allows petroleum to escape. Therefore, buried structures that have ceased deformation are more likely to maintain seal integrity (Heiniö & Davies 2007). Furthermore, overpressure may also affect seal integrity since the seals in the deepwater setting are very weak due to the high pore-pressure, and as a result, the fluids may penetrate and breach the seal (Weimer & Slatt 2007).

2.4.4. Petroleum Generation

Deposition has been continuous in the Niger Delta basin since the late Cretaceous. Consequently, even in the distal parts of the Niger Delta, the thickness of the sediment is sufficient for significant hydrocarbon generation to take place within the source unit (up to 4000m thick even in 4000m of water) (Morgan 2003).

The oil generation window in the Niger Delta varies between 100° and 150°C, concurring with a thermal gradient between 20-27°C·km-1 (Cobbold *et al.* 2009; Tuttle *et al.* 1999; Akpabio & Ejedawe 2010). The depth of hydrocarbon generation window varies between ~4-6 km below seabed (Fig. 2.13). The value of the thermal gradient varies throughout the delta, where the minimum thermal gradient is located towards the centre of the delta and within the older sediments and increases towards the edges of the delta (Tuttle *et al.* 1999).

Several workers have suggested that petroleum generation began in the Niger Delta during the Eocene (Tuttle *et al.* 1999; Krueger & Grant 2010). These authors have attributed the activation of structural growth and activation of the basal-detachment to petroleum charge. On the other hand, the lower Agbada entered the oil generation window during the late Oligocene (Tuttle *et al.* 1999).

Hydrocarbon migration is not completely understood (Sonibare *et al.* 2008), although the most significant is likely to be vertical migration (Weimer & Slatt 2007). The main mechanisms for migration are likely to include hydrofracturing

and flow along faults (Weimer & Slatt 2007). But also due to the dynamic nature of the delta setting, the migration pathways are likely to have continuously changed, and may even have caused the petroleum to have migrated several times before being trapped in a reservoir (Weimer & Slatt 2007).

Chapter 3
Research Methodology

3.1. Introduction

This chapter discusses the dataset and the interpretation methodology for this study. The focus is on the evolution of the Aghar fault-related-fold by interpreting and analyzing the growth strata and thrust complexes in the fold. To achieve this, a combination of 2D and 3D data was usd in the research. Detailed seismic interpretation and attribute analysis was carried out on both 2D and 3D datasets and used for structural analyses.

The 2D is used to create a regional overview of Niger Delta structures where as the 3D is used to understand the growth of the Aghar fold structure and construct an evolutionary model (Chapter 3.2). Using the interpreted data, fault displacement and growth strata units are analyzed in cross section and along strike.

The following chapter provides an overview of the datasets used in the study and it limitations (Chapter 3.2). The following section discusses seismic interpretation methodology and amplitude extraction (Chapter 3.3). Chapter 3.4 discusses the methodology used in numerical section restoration and forward modelling.

3.2. Seismic Datasets

Two seismic datasets were used in the study: two 2D lines that go through different structural domains in the delta, and a 3D seismic cube in the distal part of the delta (Fig. 2.6).

3.2.1. 2D Dataset

The 2D lines were acquired and provided by CGGVeritas. The two lines used in the research are the ver99ng200_003 and ver98ng_051 referred to in the thesis as Regional 2D Line A and B respectively. Both lines are located in the western lobe of the Niger Delta.

Sample Interval	4 ms
Record Length	12 s
Cable Length	6000 m
Fold of Coverage	60
Source	18 Airguns 3450 cu. in at 2000 psi
Shotpoint / Group Interval	50 m / 25 m
Main Processing Applied	Anti-alias filter, NMO, AGC, PSTM

Table 3.1 seismic parameters for regional 2D line A. (NMO: Normal moveout correction; AGC: Automoatic Gain Control; PSTM: Pre-stack time migration)

Sample Interval	2 ms resampled to 4ms
Record Length	12 sec
Cable Length	5850 m
Fold of Coverage	58
Source	Airguns 3450 cu. in at 1950 psi
Shotpoint / Group Interval	50 m / 12.5 m
Main Processing Applied	Anti-alias filter, NMO, AGC, PSTM

Table 3.2 seismic parameters for regional 2D line B

Line A is a 150 km NE-SW seismic line acquired in 1999 (Table 3.1). It begins in the offshore extensional depobelt in east, through the detachment fold belt and terminates in the inner and outer fold and thrust belts.

Line B is a 190 km NE-SW seismic line acquired in 1998 (Table 3.2). This line intersects the Inner and outer fold and thrust belt in the eastern half of the line. The western half of the line is beyond the Niger Delta deformation belts.

3.2.2. 3D Dataset

The 3D seismic dataset is provided by CGGVeritas and covers an area of

~2000Km2 (Table 3.3). CGGVeritas also provided migration velocity data for depth conversion. Depth converted datasets were used for structural interpretation and analyses.

3.2.3. Dataset Quality

Although seismic data has provided a great amount of information, it inherently has several shortcomings. The dataset contains several seismic artifacts including bottom-simulating reflector (BSR), migration artifacts, fault shadow zones and velocity pull-ups and pushdowns.

As with many deepwater surveys, the section has a BSR in the upper part of the section. BSR is caused by methane clathrate (also called methane hydrate) found on the seafloor several hundred meters deep. The clathrate has a much lower density than the sediment, and as a result, the BSR appears as a strong event delayed several milliseconds below the seabed (Fig. 3.1-a). However, the BSR curves toward the seabed near mud volcanoes. This is caused by the higher temperature introduced by the volcano's fluids (Fig. 3.1-b), which makes the gas methane unstable, locally reducing the BSR.

Sample Interval	2 ms resampled to 4 ms
Record Length	9216 ms
Band Filter Lowcut / Highcut	3 Hz / 218 Hz
Source	Dual Array airgun sources, 2 x 3090 cu inch at 2500 Psi each
Group Interval / Crossline Spacing	12.5 m
Cable / Inline Spacing	25 m
Main Processing Applied	Anti-alias filter, NMO, AGC, pre-stack time migration (PSTM)

Table 3.3 3D Seismic Dataset parameters

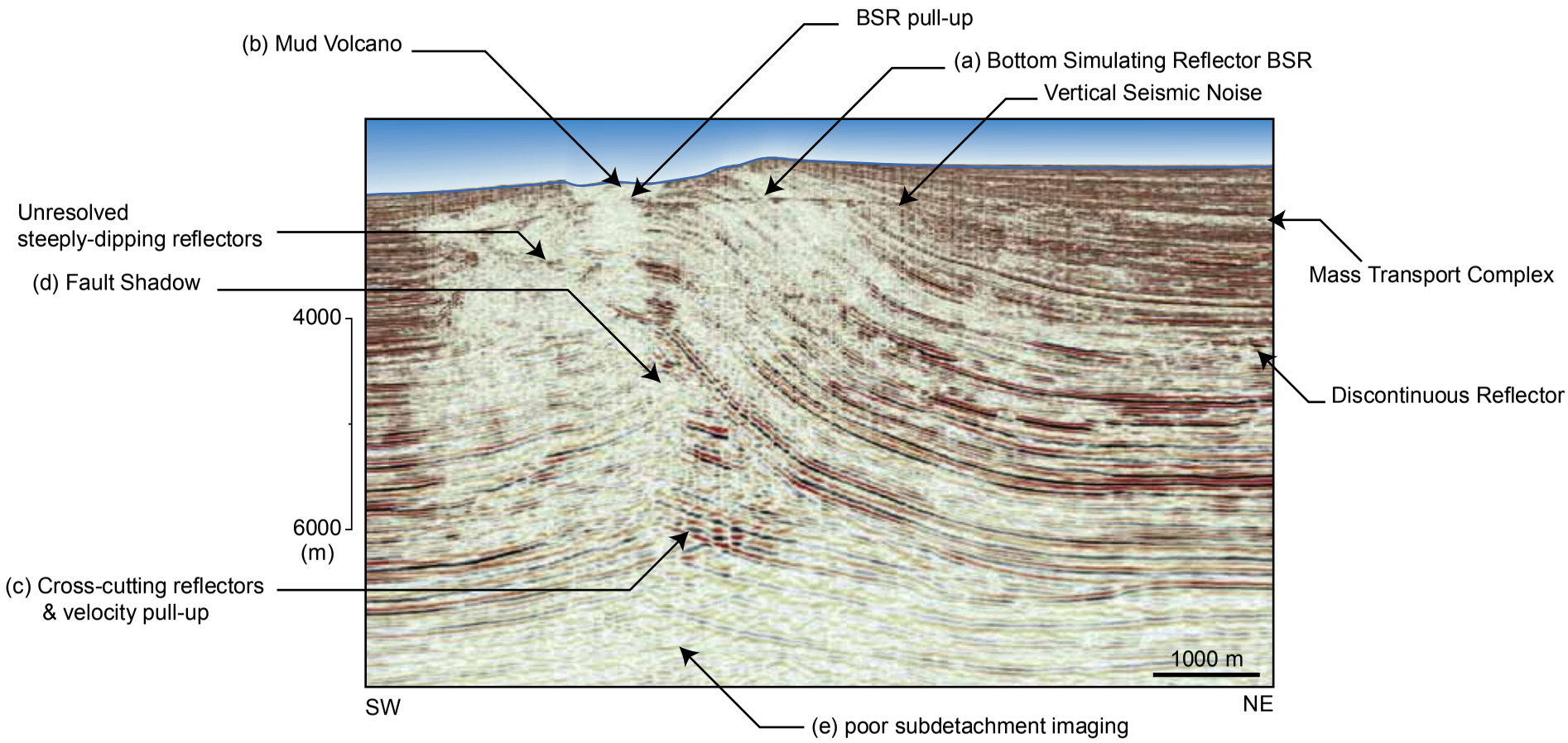

Figure 3.1 Seismic Section V (Fig. 5.11) showing various seismic artifacts.

The diagram shows (a) bottom simulating reflector (BSR) and BSR pull-up at the mud volcano, (b) a Mud Volcano, (c) cross-cutting reflectors, (d) fault shadow zone and (e) poor sub-detachment imaging

Abrupt bed termination and strong lateral velocity variations are not correctly resolved when using pre-stack time migration (PSTM). Migration algorithms would extend the terminating reflector creating a hyperbola curving upwards or downwards. In cases where there is a series of terminating reflectors opposite each other (such as across a fault plane), crosscutting artifact reflectors occur (Fig. 3.1-c). Although this can be used to identify the presence of a fault, the exact placement of the fault and the correct dip of the actual strata are not fully resolved, and needed to be interpolated. Furthermore, at this location under the overthrusted hanging wall, a velocity pull-up occurs. The better compacted overthrusted body has a higher velocity than the surrounding sequences, which poses as a migration problem.

Fault shadow zones occur around the main fault plane and other fault surfaces (Fig. 3.1-d). Poor sub-fault imaging hides reflectors, causing the adjacent reflectors to appear terminated. Consequently, migration algorithms create hyperbolas similar to those mentioned earlier.

Another migration related problem is caused by the low-velocity, detachment surface. Below the detachment, little or no reflectors can be observed, obscuring the sub-detachment structures and reflectors (Fig. 3.1-e).

Several of these problems can be corrected by using pre-stack depth migration (PSDM). With the presence of accurate velocity models, PSDM can resolve bed terminations as well as abrupt velocity variation vertically and laterally. PSDM may also resolve sub fault geometries and steep dipping reflectors, all of which are shortcomings of PSTM. Furthermore, using wider offsets can help image steeply dipping reflectors such as those in the forelimb of the folds, as well as steeply dipping fault planes.

3.3. 3D Seismic Interpretation Methods

The main purpose of the interpretation is to investigate the structural elements and evolutionary history of the Aghar fold and surrounding area. The initial

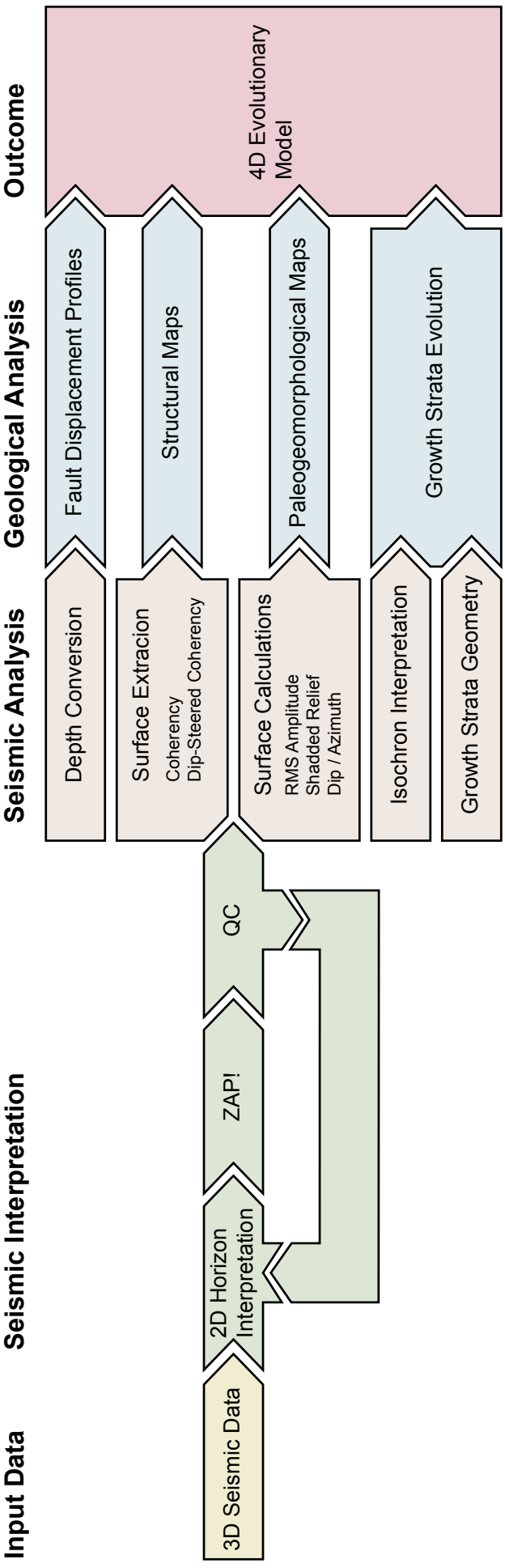

Figure 3.2 Seismic interpretation and analysis methodology. (RMS stands for Root Mean Square)

cross-sectional horizon interpretation is used to create surfaces, and then seismic attribute are extracted along these surfaces. See figure 3.2 for a summary of the research method.

Without well ties, the seismic horizons interpreted were kinematic units only. The units were subdivided to three pre-kinematic, four syn-kinematic units and the seabed (Fig. 4.7 & 4.8; Table 3.4). There are two main formations in the area; Akata and Agbada, which are separated by the detachment surface.

The Pre-kinematic 1 is interpreted as the detachment horizon and lithologically represents the Akata-Agbada formations contact. Thin-skinned tectonics is limited to the layers above this unit. It is characterized by a strong, negative reflection coefficient due to low seismic velocity (~2000ms-1 (Briggs et al. 2006)) of this overpressured unit. Below this unit little can be resolved, and contains several artifact as discussed earilier in the seismic limitations section above.

Two additional pre kinematic horizons were picked, of which Pre-Kinematic 3

Horizon	Age (Ma)	Character	Continuity
Seabed		Strongly Positive	Laterally continuous
SK-4	>1.0	Strongly Negative	Discontinuities caused by MTC and Turbidites
SK-3	1.0	Strongly Positive	Discontinuities caused by MTC and Turbidites
SK-2	1.8	Strongly Positive	Laterally continuous
SK-1	5.3	Strongly Positive	Laterally continuous
PK-3	13	Wealkly Negative	Contiuous with some undulation
PK-2	23	Strongly positive	Low-amplitude beneath thrust in footwall
PK-1	30	Strongly Negative	Low amplitude beneth thrust in footwall

Table 3.4 List of horizons interpreted in the 3D seismic dataset. See figure 4.7 and Fig. 4.8 for seismic stratigraphy

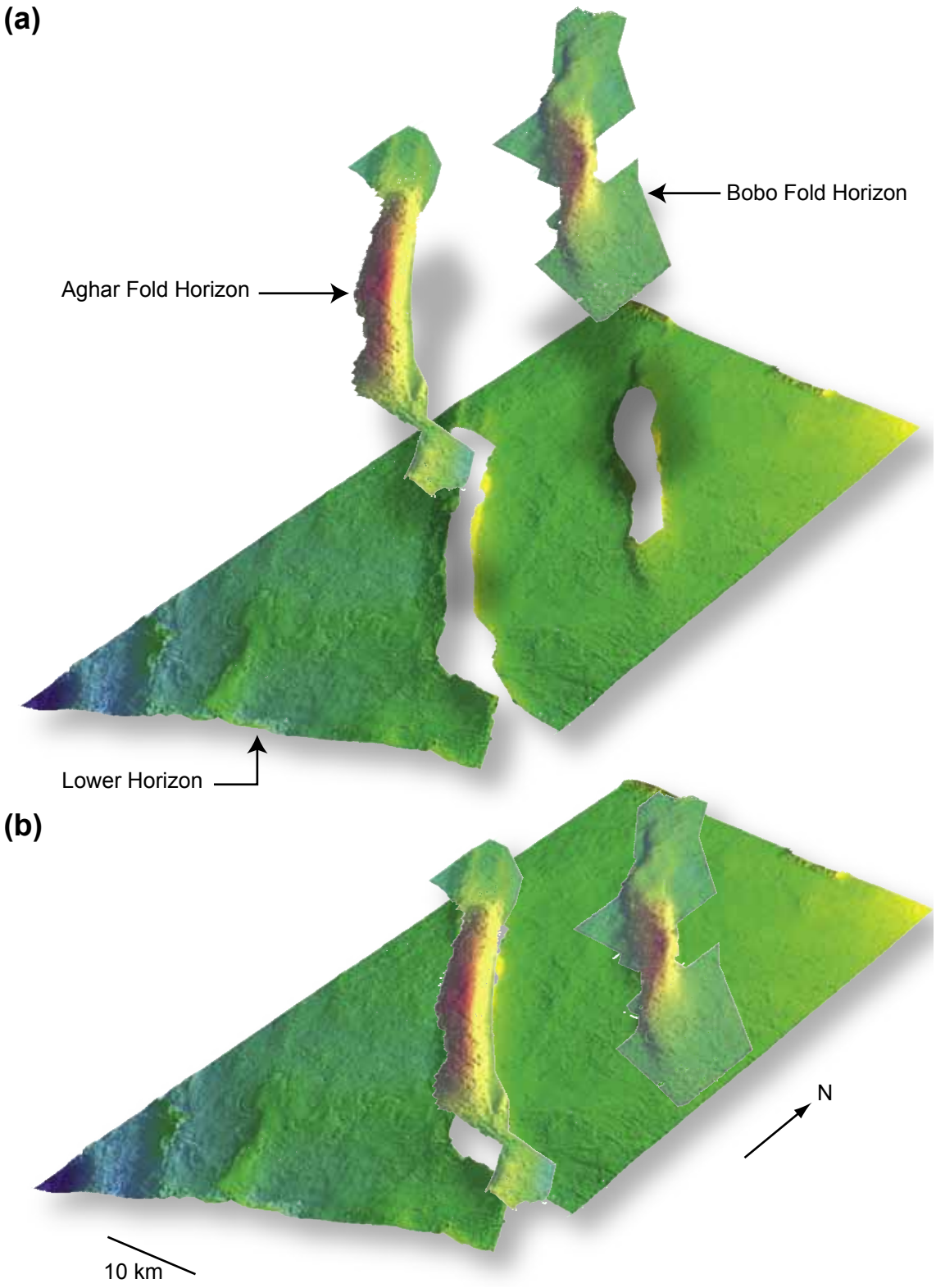

Figure 3.3 Diagram showing Top Pre-Kinematic 3 horizon. Where (a) shows the three different horizons interpreted, and (b) show the surface put together.

is likely to be the top of the pre-kinematic unit. These two horizons were split to three different horizons to be able to superimpose the horizon over the thrust faults (Fig. 3.3). This practice aids in accurately representing the thrust folds in the study are and allow for better assessment of the fault displacement.

Four syn-kinematic units were interpreted, although only the lower three are used in most diagrams. The upper most syn-kinematic layer is used to assess paleogeomorphological features such as turbidite channels and MTC in the upper section.

3.3.1. Seismic Cross-Section Interpretation

This represents the first step of the interpretation process. Horizon interpretation is conducted within a grid, where as the fault interpretation was done in cross section perpendicular to the strike of the structures.

Eight seismic horizons were interpreted in the 3D dataset. The bottom three horizons represent the pre-kinematic sequences, and the upper five sequences, including the seabed represent the syn-kinematic sequences. The interpretation begins with wide spaced grids of 100 line/trace spacing. Then finer intervals of 50, 25 and 5 lines were used to better contrain the data. Wider spacing was adequate for shallower horizons, however, finer spaced interpretation was used for complicated areas and zones of weaker amplitude. The deeper horizons required finer interpretation grids, especially near the major thrusts in the footwall.

Fault interpretation was carried out along the strike of the structures with regular spacing of 25 lines/traces. Faults locations was indirectly determined by discontinuities of beds at the fault surface. However, in the deeper section where the fault planes have shallow dips the fault appears as a reflector intersecting the reflectors.

3.3.2. Mapping Techniques

Maps were used for structural and paleogeomorphlogical interpretation. Furthermore, auto-picking and interpolation is used to assess the interpretation integrity and correlation.

The first step in mapping the area is to auto-pick the horizon over the survey area. Zonal Area Picking (ZAP) cross correlation tracking mode is used to infill the grid that was interpreted in cross section. This stage is repeated several times to check for miss ties in the interpretation. The first iteration was carried out in the early stages, when the interpreted grid was wide. Problematic area or zones with missing sections are infilled with finer interpretation grids. In areas that cannot be resolved by ZAP even with the finer grids are interpolated.

ZAP produces Two-Way-Time (TWT) surface of the interpreted horizon. Multiple amplitude exraction and calculation are carried out along the surface as well as depth conversion. Structural-cube coherency and dip-steered coherency were extracted along all horizon surfaces. This was used for fault and fracture interpretation as well as geomorphological interpretation. Shaded relief, dip, azimuth were calculated for all the surfaces and were used for structural evaluation. Root mean square (RMS) amplitude was used to interpret sedimentological features such as turbidite channels and overbank deposits, terminal fans as well as mass transport complexes (MTCs). The Attribute extractions are discussed further in the following section.

The horizon surfaces and fault planes were also depth converted. They were used for fault displacement profiles and various dip measurements. In this thesis, detailed seismic cross sections were interpreted and presented by 1:1 ratio depth converted section.

Time and depth thickness maps or isochron and isopach maps respectively, where calculated for the growth sequences. The StratThickness algorithm was used to calculate the isopachs and isochron. This algorithm accounts for

dipping strata such as that observed on the fold flanks where simple subtraction algorithms would measure thickened sections for the dipping strata.

3.3.3. Attribute Extractions and Analyses

Attributes have been extracted for the entire cube as well as along a specific horizon. Attribute were used in this study to provide additional information on the faults that surround the folds as well as to visualize turbidite channels and mass transport complexes. Coherency cube (Structural cube) and dip-steered semblance were extracted for the whole cube. Dip, azimuth and RMS where calculated along the surfaces.

The coherency calculation was used to emphasize incoherent or discontinuous reflectors such as those in turbidite channels, mass transport complexes (MTC), faults and heavily fractured strata. Small coherency values are indicative of coherent reflectors that do not vary in amplitude from one trace to another and vice-versa. Coherency was calculated for the entire cube and investigated in cross-section, time-slice and extracted along interpreted horizons. It was calculated within a ±15ms window over a 5 trace/line spacing interval.

Coherency, however, cannot correctly resolve steeply dipping data and creates artificial discontinuities. To correct for this, dip-steered semblance was used as a substitute. The dip-steered algorithm follows individual reflectors, which can significantly reduce aliasing caused by steep dipping strata. Semblance itself can be thought of as the opposite of coherency where the higher values indicate coherent waveforms in adjacent traces. The cube was calculated on 80ms (±40ms) windows and using the recommended parameters by the software developers.

Dip and Azimuth calculations were calculated for all the horizon surfaces. They are used to highlight structural trends and abnormalities in the surface. Shaded relief, which is a derivative of both dip and azimuth, was extensively used to assess bed dips and structural orientation and integrated into the geological

maps.

Root-Mean-Squared or RMS amplitudes were also used in the research. The algorithm calculates the average amplitude of a wavelet within a certain vertical window. Lateral amplitude variation in the horizon such as those caused by sedimentological element will appear as anomalies along the horizon surface. The windows varied from one surface to the other and multiple calculation were conducted along each horizon, however, a typical window is ±25ms.

3.3.4. Software Used

Landmark OpenWorks® package was used to for all seismic-related interpretaion and analyses conducted. The following modules were used:

- SeisWorks: used to interpret the horizons and faults as well as surface gridding amplitude extraction and computation along surfaces.
- TDQ: used for converting horizons and fault from time- to depth-domain.
- PostStack / PAL / ESP: used for 3D attribute extractions in the 3D seismic cube.
- GeoProbe: used for 3D visualization and fault interpretation as well as additional volume and surface attribute extractions and calculations.
- PowerCalculator: calculating dip-corrected isochrons and isopachs.
- dGB Earth Science OpendTect was used for extracting dip-corrected coherency of the 3D seismic volume.

3.4. Section Restoration and Forward Numerical Modelling

3.4.1. Introduction

Igeos Dynel2D is a 2D finite element method (FEM) program used for section restoration and forward numerical modelling that integrates geological and

		Sandstone	Shale
Elastic Properties	Youngs Modulus (Pa)	2.20E+10	2.80E+10
	Poissoisn's Ratio	0.24	0.14
	Bulk Modulus (Pa)	1.41E+10	1.30E+10
	Shear Modulus (Pa)	8.87E+09	1.23E+10
Rheology	Density (Kg/m3)	2480	2530
	Porosity	0.49	0.63
	Compaction Constant (1/m)	0.274787	0.51739
	Friction Angle (º)	27.8	14.4
	Compressive Strength (Pa)	9.60E+07	9.50E+07
	Tensile Strength (Pa)	5.00E+06	3.00E+06
	Cohesion (Pa)	3.84E+07	2.72E+07

Table 3.5 Elastic and rheological properties of sandstone and shale used in the section restoration and forward models.

petrophysical attributes into the experimental models. Unlike kinematic modelling software, this program obeys conservation laws of mass, momentum and energy. Dynel2D algorithms are based on equations of motion for linear continuum, which can incorporate a wide range of rheological properties such as ductility and viscousity of strata. It can also account for strain-based decompaction and change in porosity.

For the deepwater Niger Delta, the lithology is shale dominated with some sand bodies transported by mass transport mechanisms. This was incorporated into the models using the default parameters provided in the software (Table 3.5). The pre-kinematic units in all models were shale. The syn-kinematic units were interbedded sandstone and shale lithologies.

3.4.2. Background

Dynel2D utilizes finite element method (FEM) for modelling the mechanical behaviour of geological features due to structural deformation. To achieve this, Dynel2D applies physical principles of linear elasticity, which accounts

for the conservation of mass, momentum and energy but assumes isothermal and isochemical equilibrium throughout the model. Nonetheless, this departs form the old kinematic description of faulted bodies where rigid blocks slide against each other. Faulted and folded rheologies undergo a significant amount of deformation during faulting and folding events. Geometric and kinematic models, such as those that rely on conservation of area, do not account for such deformation.

Therefore, to account for these mechanical properties, one must use the equation of continuity to honour the conservation of mass and the equations of motion for material continuum to honour conservation of momentum. This can be achieved by using linear elasticity, which honours such physical laws that control deformation.

The equation of motion and equation of continuity do not rely on the mechanical behaviour of the object (brittle, ductile, fast or slow deforming). To simulate without bias, these equations require that the velocity of movement is not too great to cause relativity to be a factor and rock body to be adequately modelled as a continuum. To numerically describe this, constitutive equations are used to negate the need for the stress component in the equation of motion, which reduces the number of variables.

For brittle faulting and fracturing, elastic laws are accepted since strain deformation is either small or restricted to a narrow part of the deformed body. This is an approximation, where in reality there would be damage zones surrounding the fault/fractures, with larger strains and inelastic deformation than the assumption made above. To reduce the effect of this simplification by making sure the area of inelastic deformation is much smaller than in-planer length and the total offset of the fault needs to be small compared to the in-plane length.

The equations of motion that accounts for the motion of an elastic body are

a form of Navier's equations. These equations have 25 physical variables: acceleration, velocity, displacement, and body all in 3 components (x,y,z), as well as the 6 components of each of stress and strain (xx, yy, zz, xy, xz, yz), and the density (ρ). However, for tectonic deformation, the acceleration is negligible and can be ignored. For more information on the derivation of the equations, please refer to the Igeoss Dynel2DUser Manual (version 1.6.5).

FEM is used to provide quick and approximated solution for complicated partial differential equations including the equation of motion for linear elastic continuum, which has 22 physical terms. The method discretises the model into smaller elements each of which abide by a simplified version of the original equation of motions. The simplification here would be a linear function for each element.

To create the finite elements Dynl2D subdivides the geological model in to triangular elements, which adjust shape with deformation. Each of these elements have their own material properties and behave in accordance with the linear elastic law, allowing the model to be constraint by internal forces, displacements and interference interactions.

FEM places particular influence on the boundary conditions. The three main boundary effects that may occur in a model: a lower, an upper, and a lateral boundary effects. Typically, models are initialised with a lower depth, which is obviously not applicable to nature. This would create a free space below the model without restraining it, and therefore, the model needs to be significantly deep to avoid this problem. The upper part of the model is a free surface, similar to nature, however, any undulation or truncated beds are not accounted for and would cause aliasing particularly in restoration. The final boundary is the lateral boundary, which creates edge effects in the model, and similar to the lower boundary, it needs to be extended beyond the area of interest to avoid aliasing.

3.4.3. Methodology

The procedures for section restoration and forward numerical modelling in Dynel2D are similar. The following is a summary of the methodology used to construct the models (Fig. 3.4):

1. Input model geometry: The initial model is drafted in this stage; for section restoration, the Present Day cross section is imported, and for forward models the initial pre-deformed section is imported.

2. A mesh is created within the model. In Dynel2D, a triangle-element mesh is used.

3. In the simulation setup the geological and lithological parameters of the sequences and surfaces as well as the boundary conditions are incorporated. This includes the lithology of the sequences, bed-contact type (sliding or locked) and fault parameters.

4. Also during the simulation setup the deformation parameters are added; whether shortening is applied for the forward models or stretching for section restoration.

5. Running the simulation

6. Introduce syn-kinematic erosion or sedimentation to the model and repeat steps 2 – 5.

3.4.4. Section Restoration

Section V (Fig.figure 5.12) was used as a representative section for the middle of the Aghar fold. In this cross-section the Aghar fold shows a sigmoidal flat-ramp-flat thrust fault geometry with a forelimb breakthrough thrust (Fig. 3.5).

One of the issues encountered while restoring the section was the detachment geometry. Further interpretation shows the detachment is more like to follow a

Figure 3.4 Dynel2D section restoration and forward numerical modelling methodology. The procedure is an iterative process, where after each iteration the model requires to be re-meshed and the simulation parameters, including the lithological parameters need to be added anew.

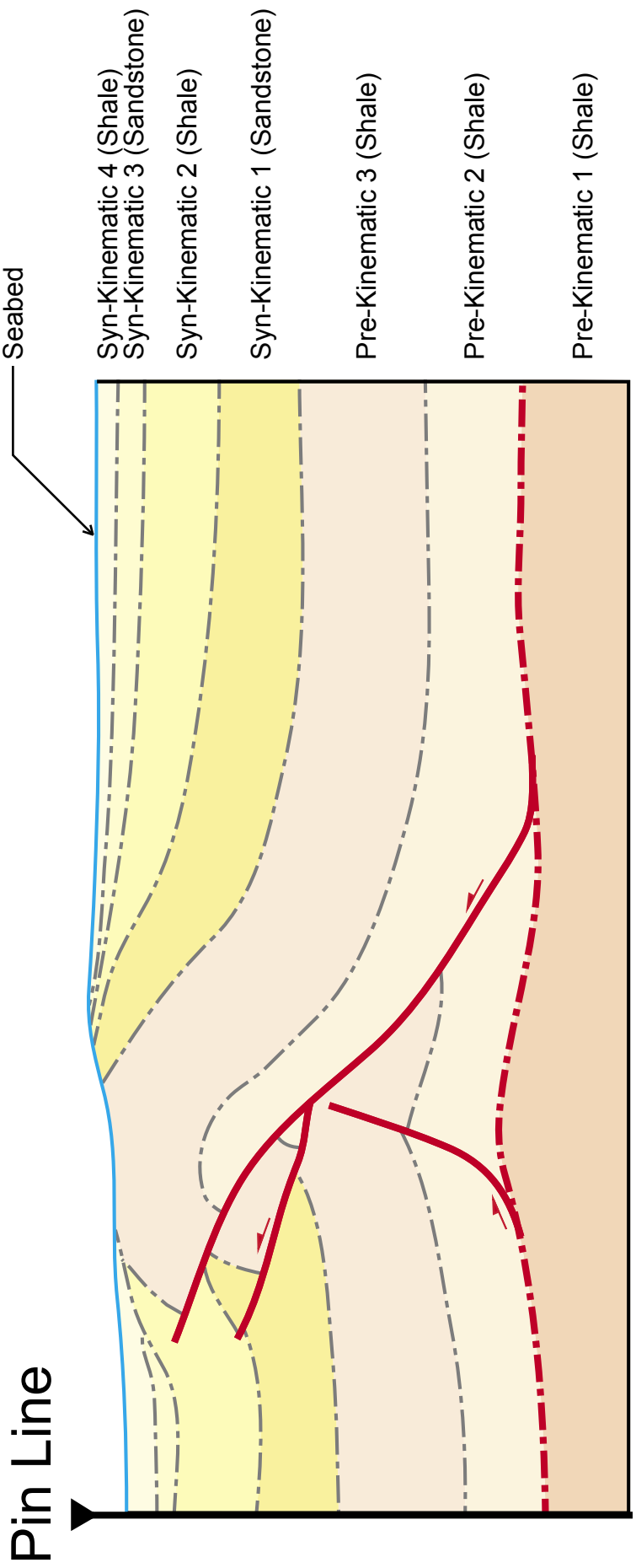

Figure 3.5 Initial setup for the section restoration model. The detachment geometry is an element of high uncertainty and probably causes some aliasing in the results of the restoration.

flat geometry with brittle thickening mechanisms discussed in Chapter 2.

3.4.5. Forward Numerical Models

Two models are simulated (Chapter 6.3); a listric flat-ramp thrust model with a a backthrust (Fig. 3.6-a) and a sigmoidal flat-ramp-flat thrust model with a froward breakthrough thrust (FBT) (Fig. 3.6-b). These simulate geometries observed in the Present Day Aghar fold.

3.4.6. Limitations of Method

- Initial model in the restored section needs refinements and added complexity compromises the results integrity and accuracy.
- Lithological properties used in the restoration and forward models were based on lithified rheologies as opposed to poorly lithified sediments that occur in the deepwater settings. This would have played an important role, in particular during the early stages of shortening.
- The package does not allow dynamic syn-kinematic sedimentation, where the sediments are added while the model deforms.
- The 2D algorithm is not sufficient for modelling complex 3D geometries such as along strike linkage of folds and faults.
- With each iteration, the modelling settings are reset and therefore, the package does not correctly address strain hardening/softening.
- Complex geometries do not behave like ideal elastic solids, and requires non-linear, non-recoverable stress-strain model parameters.
- FEM analysis creates boundary effects. The lower boundary is not realistic and is only to constrain the lower extent of the model. Lateral boundaries are also arbitrary and if too close to the area of interest, would cause undesirable boundary effects.

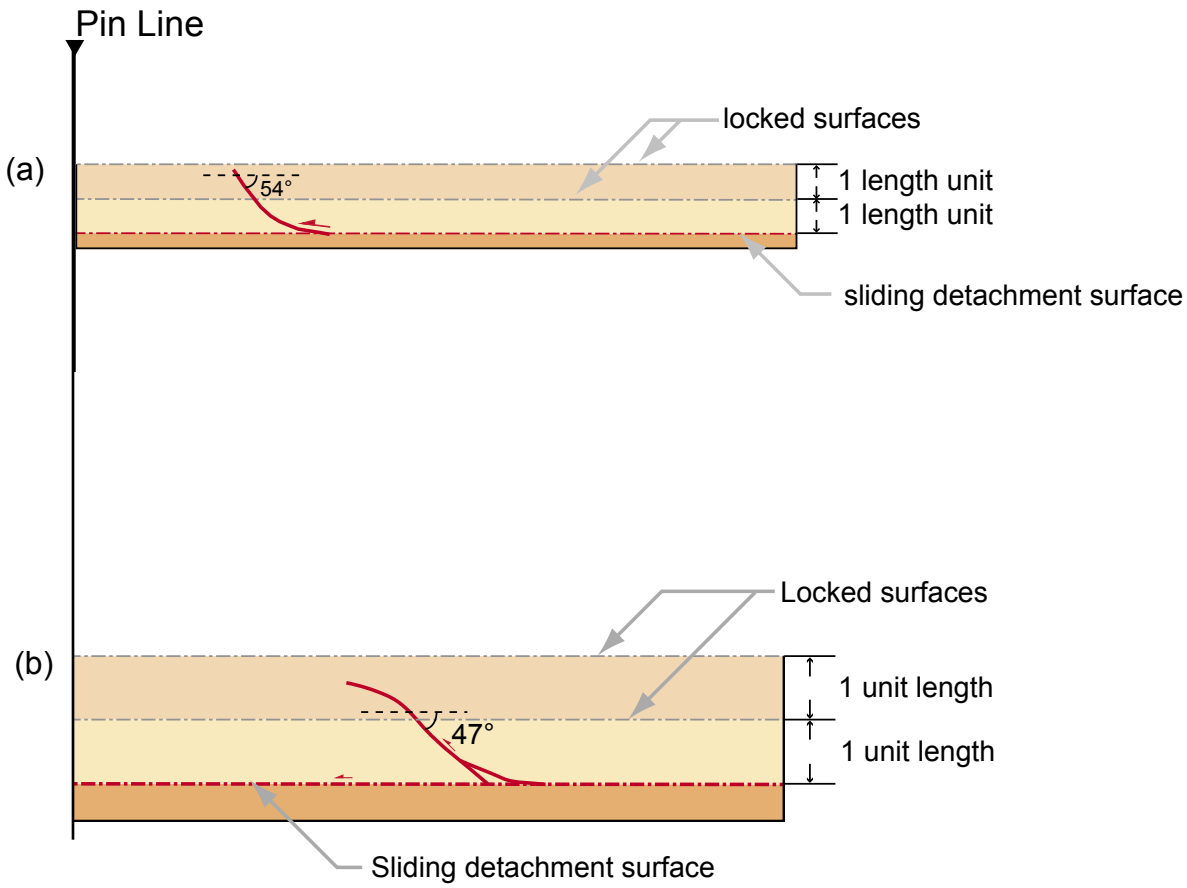

Figure 3.6 Initial setup of the forward numerical models. (a) is for the sigmoidal flat-ramp-flat geometry, (b) is for the listric fault geometry.

- The program does not account for thermal effects on rock behaviour.

- The package assumes isothermal and isochemical equilibrium which does not account for mineral changes and temperature effects on rheology.

Chapter 4

Regional Structures and Stratigraphy

4.1. Introduction

The Niger Delta is a Cenozoic delta that formed in the Gulf of Guinea on the West African margin (Fig. 1.2). It exhibits thin-skinned extensional and contractional tectonics over an overpressured shale decollement surface. Deformation was induced by differential sedimentary loading on the proximal part of the delta. Parts of the onshore delta and the entire offshore Niger Delta formed over oceanic crust that is typically deformed by small extensional faults (Fig. 4.4 & 4.5).

Seismic interpretation of 2D seismic data was used to construct a regional understanding of the Niger Delta. A detailed structural and stratigraphic interpretation and analysis was carried out on the 3D seismic dataset in order to study the fault-related-folds (FRFs) in the western lobe of the Niger Delta.

This chapter starts with a regional overview of the Niger Delta study area, using the regional 2D lines (Chapter 4.2). The remainder of the chapter focus on the 3D seismic study, with a description of the seismic stratigraphy (Chapter 4.3), an analysis of the structure in the study area (Chapter 4.4) and a description of the syn-kinematic sequences (Chapter 4.5). The chapter concludes with a summary and discussion of the results (Chapter 4.6).

4.2. 2D Regional Seismic Lines

Two 2D regional seismic lines A and B were interpreted to understand the regional structure and stratigraphy of this part of the Niger Delta (Fig. 1.2). Regional Line A extends from the extensional zone to the contractional toe of the delta, whereas Regional Line B extends from the inner-fold and thrust belt (FTB) to the outer-FTB.

4.2.1. Seismic Line A

This line shows both extensional and compressional structures of the Niger Delta (Fig. 4.1 & 4.2). It extends from the offshore depobelt in the east, through

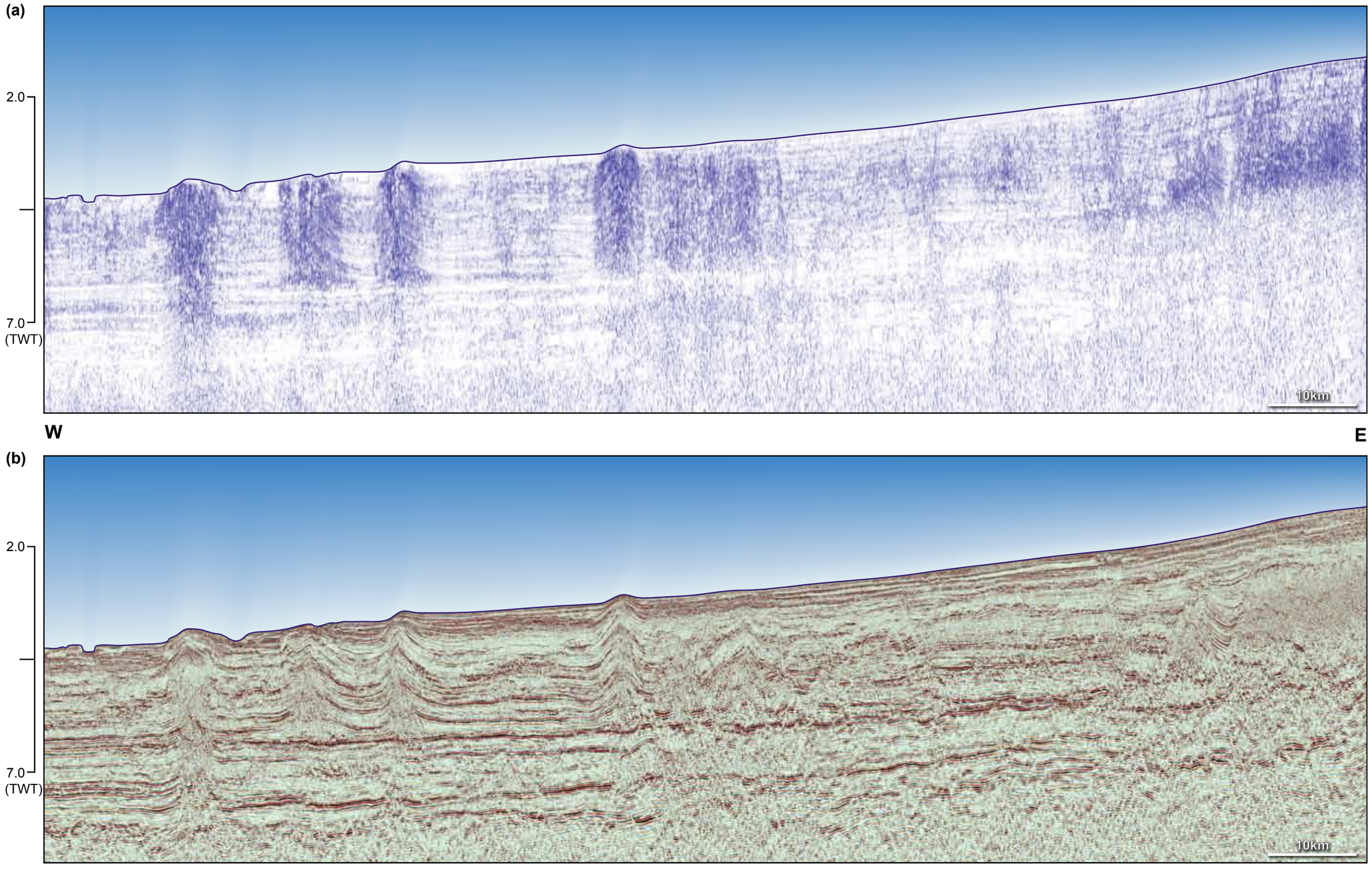

Figure 4.1 : 2D Regional Seismic Line A, Showing the seismic amplitude (a) and coherency (b) sections.

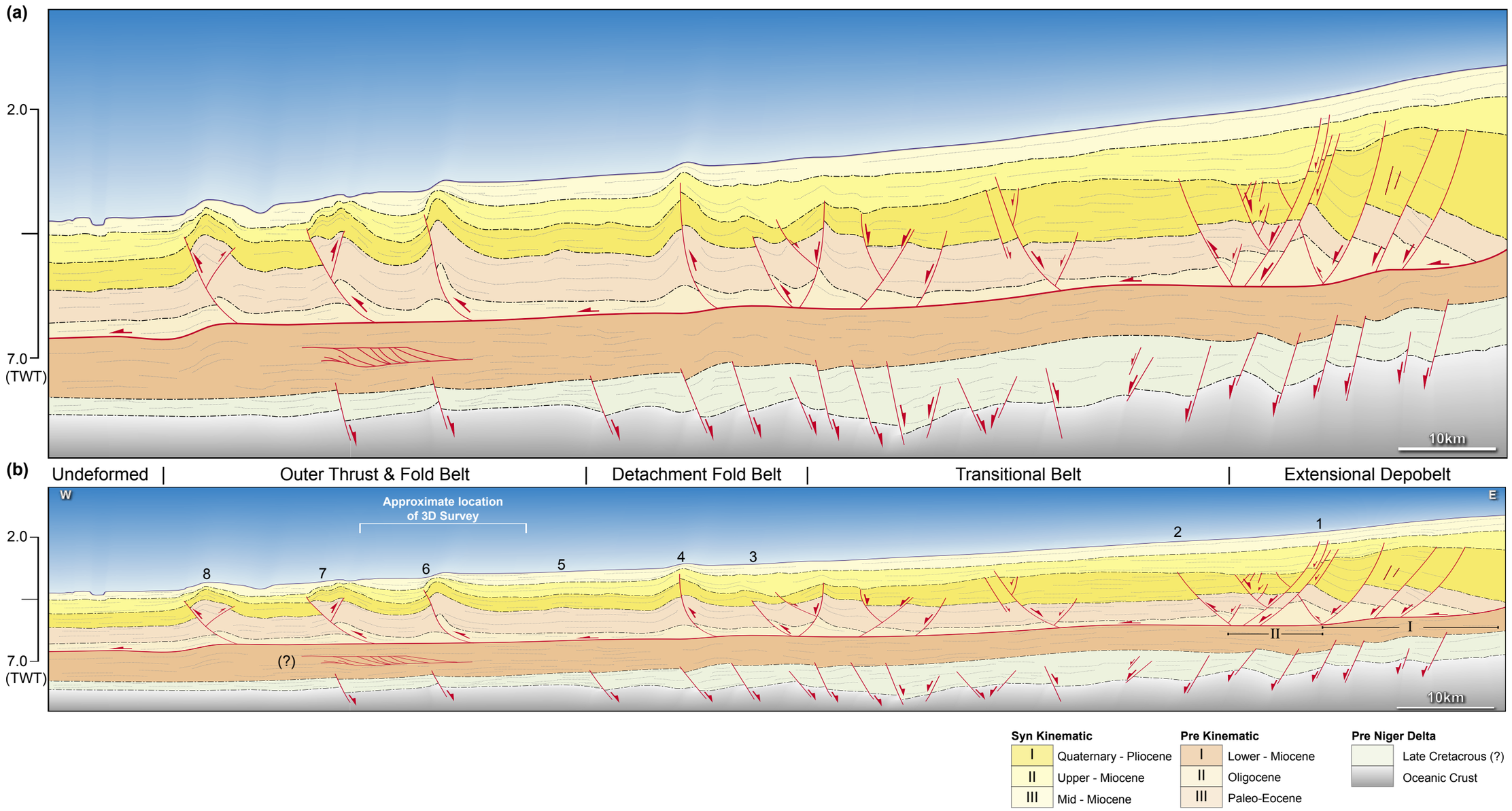

Figure 4.2 : Interpreted 2D Regional Line A with large (a) and halfed (b) vertical exaggeration. Numbers 1 to 8 highlight thrust related faulting and roman numeral I and II highlight the extensional systems. See fFigure 4.3 for a detailed view of small scale imbricate in the west of the regional line..

the transitional zone, detachment fold belt, to the outer FTB in the west of the section (Fig. 2.7). Beyond the outer FTB, the sequences are undeformed. Basement structures are also identified, however, have not influenced the structure of the delta.

Extension dominates the eastern 70 km of the section. The dominant fault orientation is regional dipping towards the basin with some counter-regional antithetic faults. The eastern most of the extensional faults have the largest displacement, with highly rotated beds that cannot be fully resolved from seismic. However, the extensional faults have little influence on seabed bathymetry.

The extension is subdivided into two extensional phases; phase I predated phase II (Fig. 4.2). There is also superposition of extensional faults over thrust faults, as is the case with thrust faults 1 and 2 (Fig. 4.2).

To the west of the section, four major folds (folds 4, 6, 7 & 8) and two minor fold (fold 3 & 5) are identified (Fig. 4.2), each associated with a thrust fault. Two smaller thrust faults are identified towards the east of the section, but have been superimposed by younger extensional features. Fold 4 and 5 are semi-symmetric structures where the first developed a thrust ramp. Folds 6 to 8 are asymmetric FRFs that accommodate the majority of shortening in the section. These are described to have steep forelimbs, and less steep backlimb geometry.

The syn kinematic sedimentation shows that folds 1, 2 and 3 (Fig. 4.2) were the earliest fault activated in the area during the early Mid-Miocene, but ceased movement soon after, and were superimposed by extensional faults soon after. Folds 6, 7, and 8 were began to shorten during the Mid Miocene and continue to Present Day. These fold structures account for the majority of the shortening taking place in the section. Fold 5 is a short lived detachment fold that initiated in the Mid-Miocene and ceased in the Late-Miocene, but did not develop a

thrust ramp. Fold 4 is interpreted as the youngest fold, probably initiating in the Late-Miocene and continues to deform at Present Day.

The detachment is a continuous basinward dipping reflector that extends through most of the section and terminates at the outer FTB boundary. Furthermore, the detachment has a shallower dip than the seabed. This is common in delta settings causing the differential loading required to drive deltaic deformation. Within the detachment unit, a 17.5km duplex system is observed (Fig. 4.3), however there is no evidence for deformation occurring within the deltaic units as a result.

The basement is dominated by a series of regional dipping faults to the east, and counter-regional faults further towards the basin. The area where the regional and counter-regional faults converge is deeper than the surrounding areas, and as a result, it has a thicker syn-extensional interval.

The pre-Niger Delta sedimentary section thins towards the basin. Basement faults deform this section but terminate prior to Niger Delta deposition. Furthermore, within the pre-Niger Delta section, a small-scale (~10km) duplex system is present under folds 2 and 3; however, these duplexes do not affect Niger Delta structures.

4.2.2. Seismic Line B

This line is located further south than the previous line, oriented NNE – SSW. It intersects the inner and outer FTBs, and continues into the undeformed domain to the furthest stratigraphic extent of the Niger Delta (~4000m depth) (Fig. 4.4 & 4.5).

The inner FTB is dominated by a basinward-vergent imbricate fan. The fan is characterized by highly rotated rear folds that have been carried over and rotated by the younger forward-breaching thrust faults. Within the detachment unit ahead of the inner FTB, a series of imbricated basinward and landward

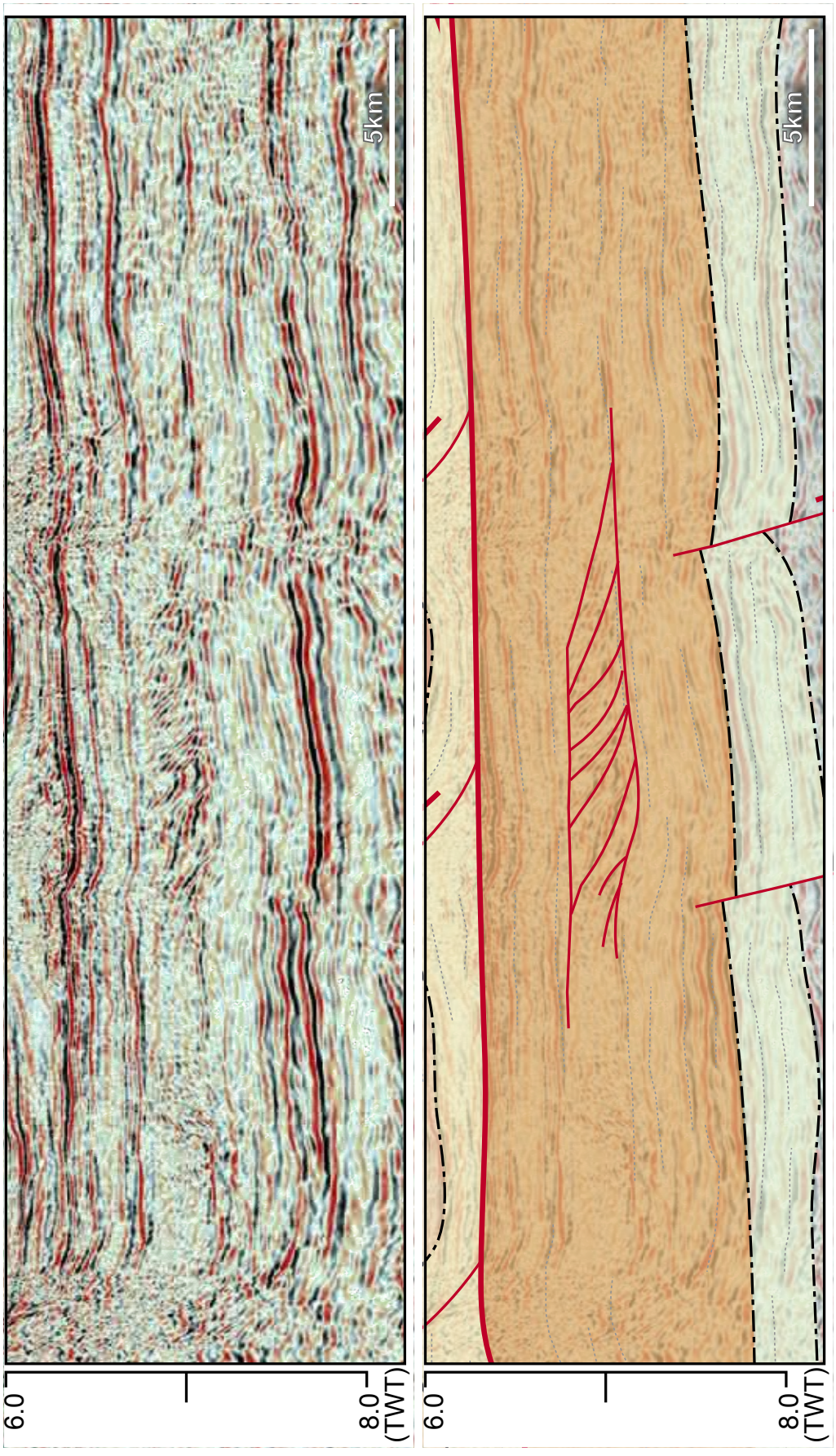

Figure 4.3 Close up of the duplex system in regional seismic line A (Fig. 4.1 & 4.2). (a) shows the seismic amplitude display and (b) shows the interpreted section. The duplex complex is interpreted to span ~17.5 km with a basinward direction of transport.

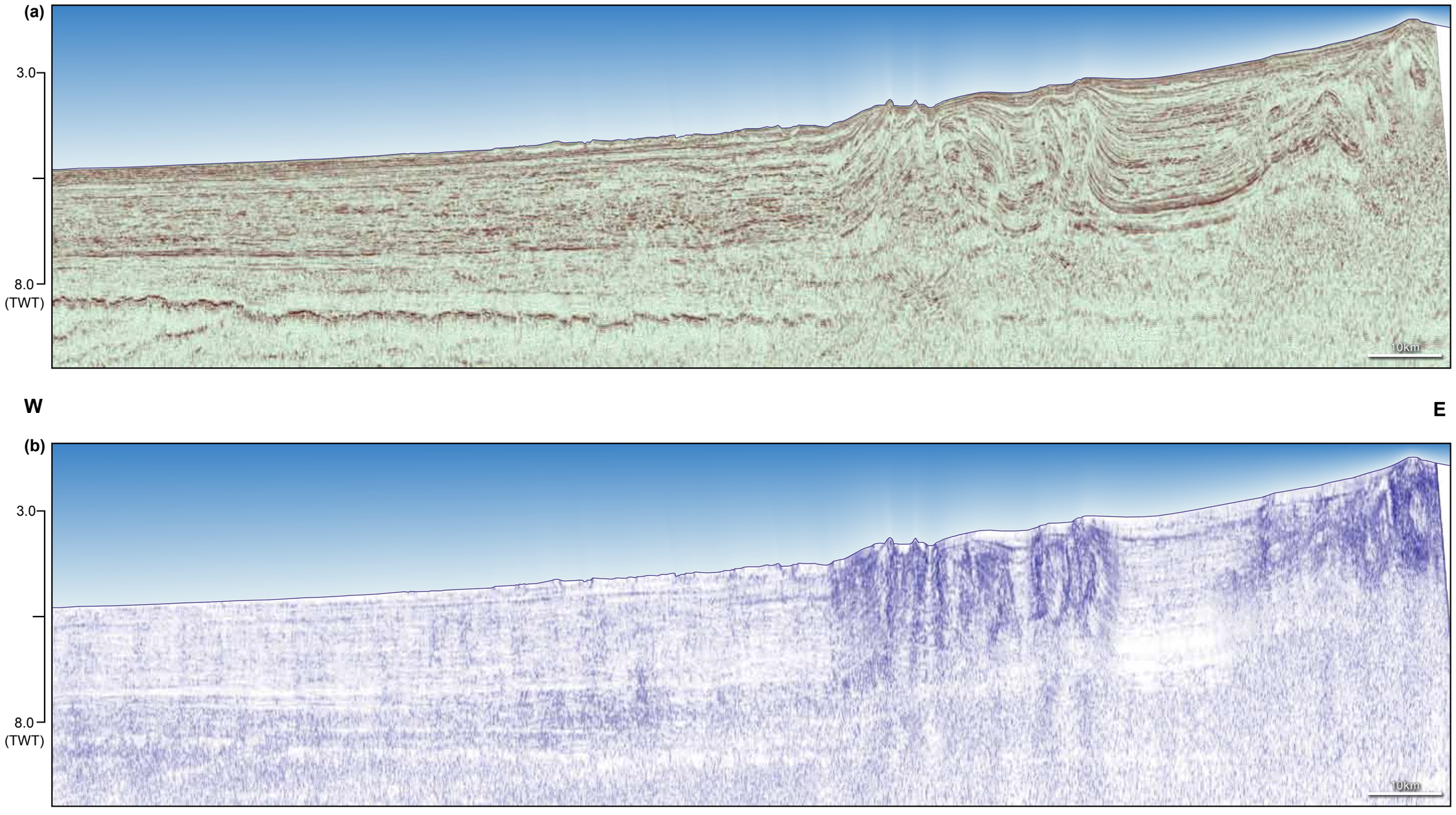

Figure 4.4 : 2D Regional Seismic Line B. Seismic amplitude (a) and Coherency (b) sections. The section shows both the outer and inner thrust and fold belts. The inner thrust and fold belt shows a highly shortened section compared to the outer FTB. This indicates that the inner belt developed earlier than the outer belt.

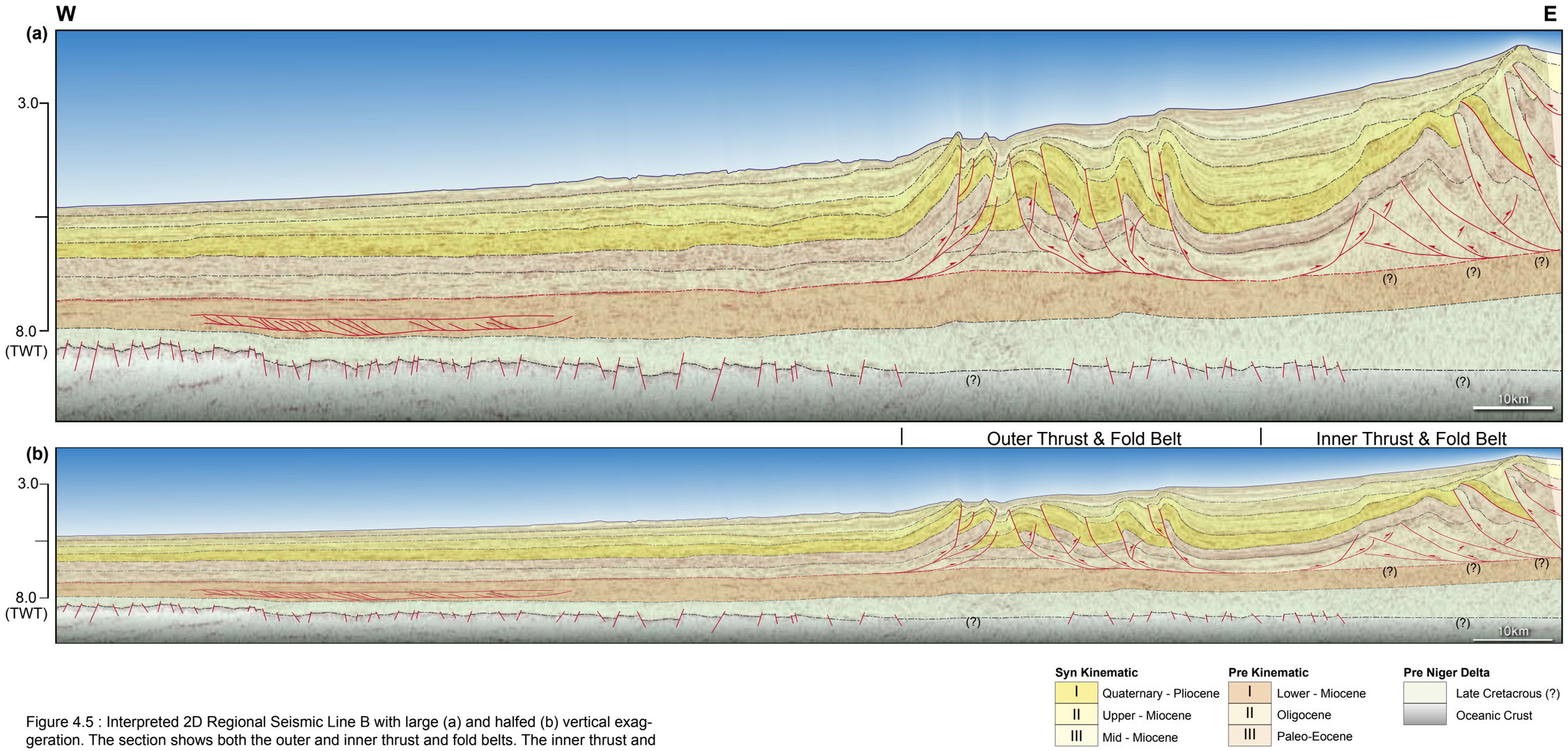

Figure 4.5 : Interpreted 2D Regional Seismic Line B with large (a) and halfed (b) vertical exaggeration. The section shows both the outer and inner thrust and fold belts. The inner thrust and fold belt shows a highly shortened section compared the outer FTB. This indicates that the inner belt developed earlier than the outer belt. See Figure 4.6 for a detailed view of the duplex at the western part of the line.

thrusts occur, creating a thickened detachment unit with a triangle zone between the opposite verging thrusts. These faults are typically limited to the detachment unit and rarely penetrate into the overlying strata. They create a significantly thicken detachment unit that is poorly imaged, and is commonly mistaken to be thickened by viscous flow of shale.

The outer FTB is characterized by a series of asymmetric thrust related folds. It consists of four basinward-vergent folds to the east and two landward-vergent folds to the west. A poorly imaged triangle zone (Type I) was formed between the opposing thrust faults. The pre-kinematic section of the wedge is likely to be a series of horizontal to semi-horizontal reflectors, whereas the growth strata form a syncline. Between the inner and outer FTBs are parallel to semi-parallel reflectors that dip gently towards the basin. Slumps in the inner fold and thrust belt thicken this intermediate section slightly, but have no structural implications.

The undeformed delta domain extends across the western half of the section and marks the transition into the abyssal plain. It is characterized by structural quiescence and sub-horizontal reflectors in the delta sequences that gently dip towards the basin with the exception of a duplex complex that is limited to the detachment unit. Some undulation is observed in the reflectors related to stratigraphic features such as turbidite channels, deepwater fans and mass transport complexes (MTCs). The seabed in this segment has a dip shallower than the deformed eastern segment. This is caused not only by the deformation of the eastern segment, but also because sedimentation is ponded behind the delta toe folding, preventing sediment transport into the basin.

The duplex system observed within the detachment unit is a local system that extends a distance of 50 km (Fig. 4.6). Even though length is comparable to that of inner or outer FTB, this duplex is only limited to the detachment unit, and shows no influence on the delta units. The duplex is interpreted to have a bottom or floor thrust fault as well as a roof thrust with more than 20 thrust horses associated with it. The detachment is interpreted to be a localized

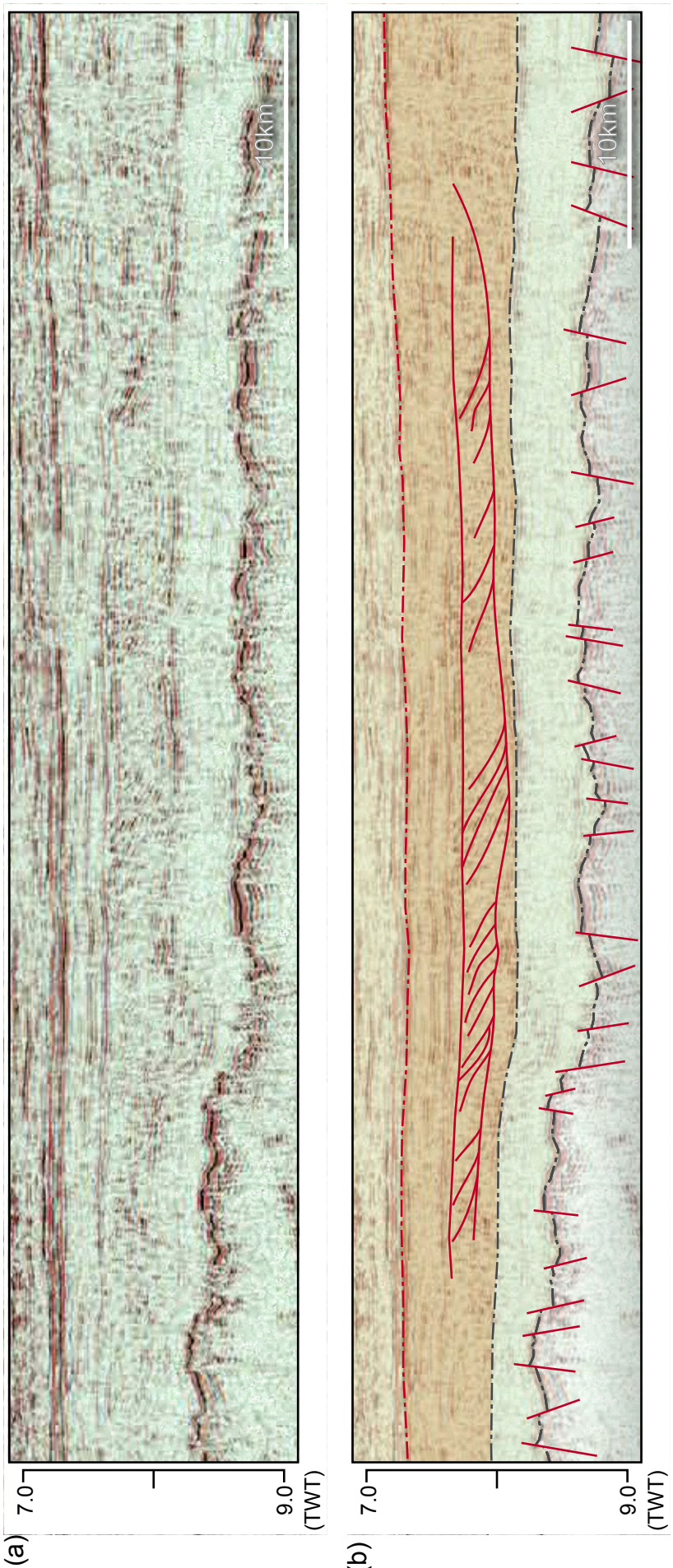

Figure 4.6 Close up of regional seismic line B (Fig. 4.4 & 4.5) that highlighting the duplex complex. (a) shows an amplitude display and (b) shows the suggested interpretation. The Duplex extends a distance of 50 km.

overpressured feature but the out-of-plane extent of this feature is not known. The source of the overpressure is caused either by a short-lived dewatering event such as those associated with clay diagenesis or by hydrocarbon generation.

The active detachment associated with the deltaic deformation only occurs in the eastern part of the section and terminates at the outer fold and thrust belt. Reflectors are poorly resolved under the detachment but beyond the detachment the lack of low-velocity overpressured shale marks an improvement in seismic imaging of the basement and sub Niger Delta intervals.

The oceanic crust is a heavily fractured basement that is infilled by a thin sequence of syn-kinematic sediment. The extensional fractures ceased activity before the deposition of the Niger Delta `and did not influence its structures.

4.3. Seismic Stratigraphy of 3D Dataset

4.3.1. Introduction

The study area has ~2000m of Oligocene to Early Lower-Miocene pre-kinematic strata and a similar thickness of late Lower-Miocene to Present growth strata. However, in the absence of well data, the stratigraphy is divided into tectonostratigraphic sequences based on seismic interpretation only. Seven key sequences were interpreted; three pre-kinematic and four syn-kinematic sequences were mapped across the 3D study area.

figure 4.7 and Fig. 4.8 show the seismic stratigraphy charts for TWT and depth sections respectively. Top of Pre-Kinematic 1, the two lowermost horizons, represents the top of the Akata formation. The Agbada extends from the Top Akata to the seabed. Top of Pre-Kinematic 3 horizon (PK-3) were chosen because of their lateral continuity and high-amplitude character.

The syn-kinematic horizons have been chosen for interpretation because each

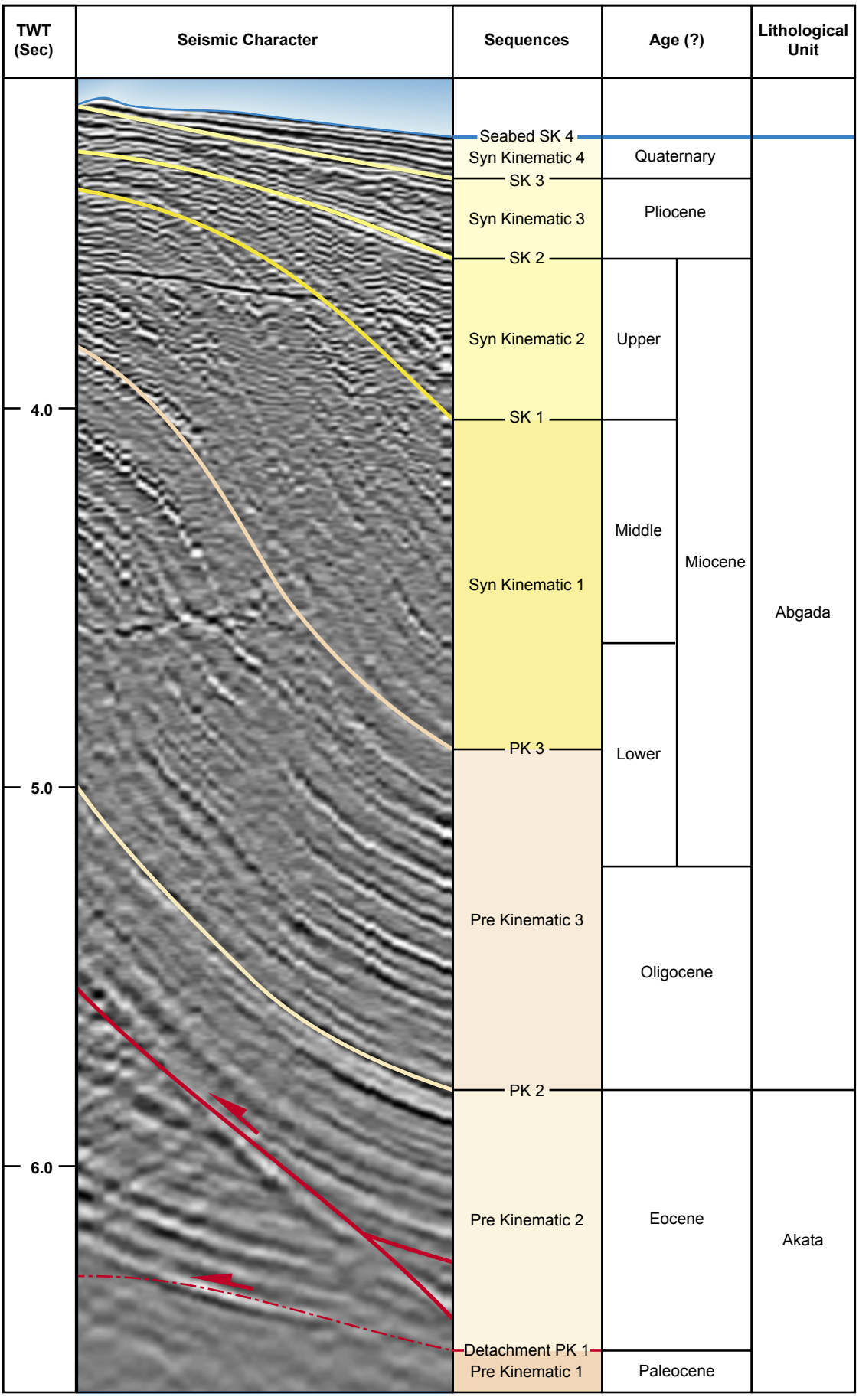

Figure 4.7 3D Seismic Stratigraphy chart in TWT (Sec), age estimates from Krueger & Grant (2010).

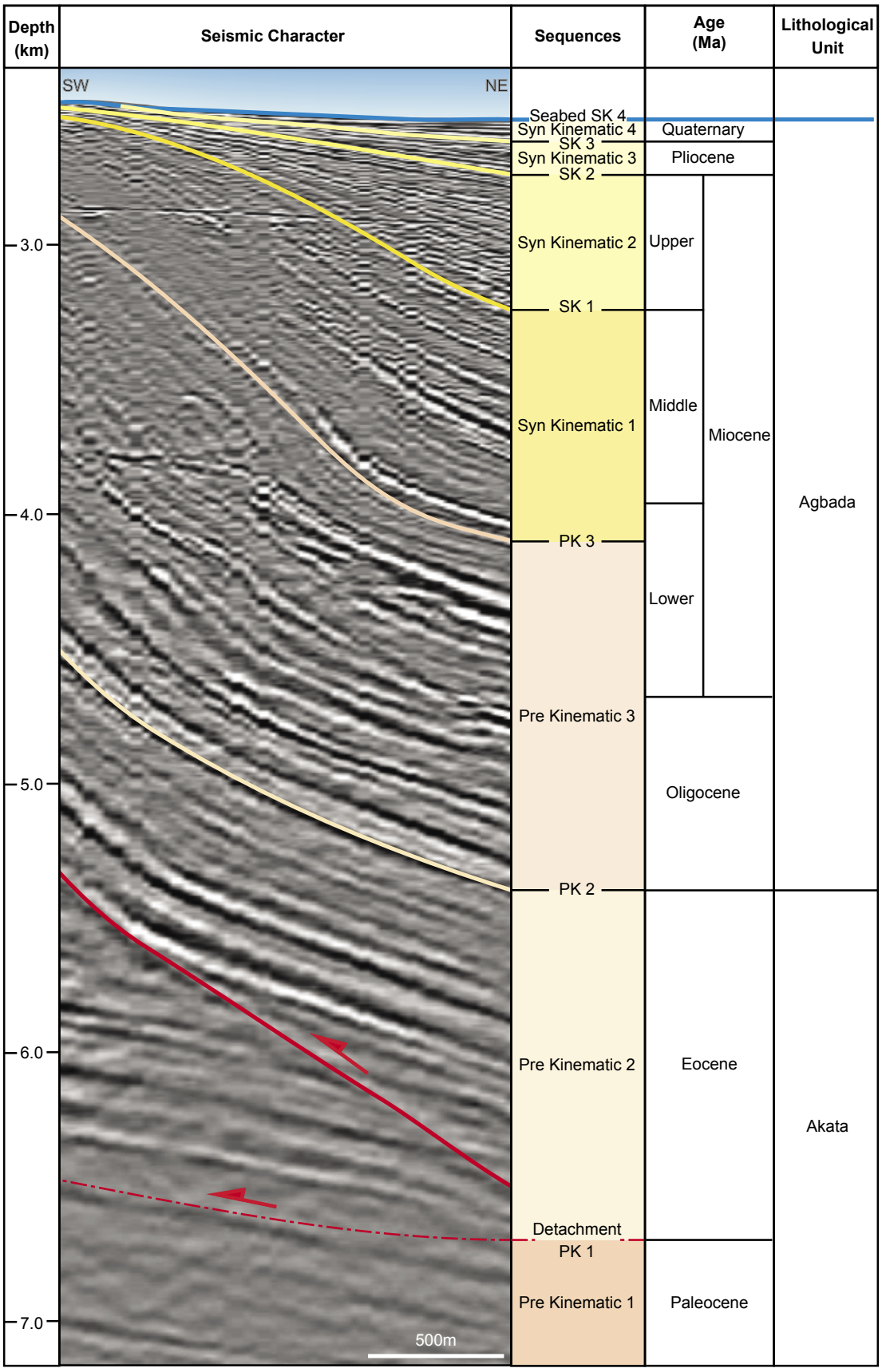

Figure 4.8 3D Seismic Stratigraphy chart in depth converted (km), age estimated from Krueger & Grant (2010)

horizon marks the top and bottom of reflector packages with consistent fanning geometries. The interpreted syn-kinematic horizons mark abrupt changes in the angle of younger beds, which causes the reflectors to onlap onto older horizon. This is indicative of either periods of sedimentary quiescence or periods of rapid folding which exceeded the sedimentation rate.

The key seismic horizons are the Pre-Kinematic 1 (Paleocene), Pre-Kinematic 2 (Eocene), Pre-Kinematic 3 (Oligocene to Lower-Miocene), Syn-Kinematic 1 (Lower- to Mid-Miocene), Syn-Kinematic 2 (Upper-Miocene), Syn-Kinematic 3 (Pliocene), and the Seabed (Quaternary) (Fig. 4.7 & 4.8). The ages used in the study are estimate from Krueger & Grant (2010).

4.3.2. Seabed Horizon (SK-4)

Depth: 3163 - 4533ms (2320 – 3105 m)

The Seabed creates a high-amplitude positive reflector with little or no amplitude variation. The high-reflective coefficient also affects reflectors up to 15 to 20 ms under the seabed.

4.3.3. Pre-Kinematic 1 (PK-1)

Depth: 6067 – 6881 ms (~5805 – 7032 m)

This sub-detachment sequence is shale-dominated prodelta and pelagic unit. It is characterized by a high-amplitude reflector with a negative reflective index (RI), which is attributed to the overpressure that occurs near this surface. The reflector quality degrades under the folded areas, in particular beneath the thrust faults.

4.3.4. Pre-Kinematic 2 (PK-2)

Depth: 3440 – 6584 ms (~3328 – 6607 m)

This unit represent the upper Akata formation. This unit is dominated by deep-

marine shale and few turbidite deposits. It mostly consists of a series of flat lying reflectors with some undulation interrupted by turbidite features. The top of the sequence is defined by a high-amplitude reflector with a positive RI value. However, the reflector becomes less apparent beneath the thrust faults. The amplitude is also affected by steep dips in the fold forelimb.

4.3.5. Pre-Kinematic 3 (PK-3)

Depth: 3440 – 6376 ms (~2578 – 6308 m)

This represents the first horizon within the Agbada formation. This sequence is similar to Pre-Kinematic 2 but shows more turbidite features. It is defined by a weak reflector with a negative RI. The reflector is mostly continuous but turbidity and MTCs cause irregularities and discontinuities to occur in the deeper parts of the section. Near the crestal part of the Aghar Fold, the sequence has been uplifted and removed by erosion or fold degradation and create truncational features.

4.3.6. Syn-Kinematic 1 (SK-1)

Depth: 3203 – 5097 ms (~2400 – 4267 m)

Thickness: 0 – 1000 ms (~0 – 1701 m)

This is the lowermost of the syn-kinematic sequences. It is defined as a laterally continuous reflector with few turbidite related discontinuities. The reflector has a strong positive signature. Reflectors within this sequence create onlap features onto the Pre-Kinematic 3 on fold structures in the area. The SK-1 has also been upliftd and eroded from the fold crest, creating truncation features with the seabed and Syn-Kinematic 2 sequence.

4.3.7. Syn-Kinematic 2 (SK-2)

Depth: 3163 – 4533 ms (~2371 – 3548 m)

Thickness: 0 – 750 ms (~0 – 1221 m)

This sequence has stronger reflector signatures than the previous sequence. However, the reflectors are heavily disrupted by turbidites and MTCs.

MTC bodies appear throughout the unit. These MTCs are low-amplitude to transparent bodies with erosional bases that lack internal structure. However, poor imaging may hinder definition of their internal structures.

The sequence varies in thickness between 0-750ms (~0-1221m) (Fig. 4.35) and greatly thins near the crest of the folds especially the Aghar Fold. The later is a consequence of fold growth as well as fold crest degradation and slumping. This is evident from the truncated beds toward the top of the unit.

4.3.8. Syn-Kinematic 3 (SK-3)

Depth: 3211 – 4284 ms (~2407 – 3304 m)

0 – 410 ms (~0 – 467 m) thick.

This sequence has a similar character to the SK-2 sequence, varying between moderate to strong positive amplitudes. The sequence is heavily eroded by a series of MTC complexes and turbidite channels. As with the previous sequence, the MTC are chaotic sequences, but high amplitude, discontinuous events occur within the MTC bodies.

4.3.9. Syn-Kinematic 4 (between seabed and SK-3)

Depth: 3163 - 4533ms (2320 – 3105 m)

Thickness: 0 – 396 ms (~0 – 362 m) thick.

The seabed defines the top of this sequences. The sequence contains some MTC bodies, but dominantly consists of a series of laterally continuous high-amplitude reflectors. Turbidite channel complexes are also present, disrupting the continuity of the reflectors. However, turbidite and MTCs are less common

than in a deeper sequences.

4.4. Structures of the 3D Seismic Data

The 3D survey is located between the detachment and outer fold and thrust belt (Fig. 2.6). Within the study area, there are two main fold structures, the Aghar and Bobo folds that are separated by 12.5 km. Additionally, three imbricates fold occur in the southwestern part of the survey and will be referred to as the Southern imbricates. These imbricates are located ~11.5 km to the southwest of the Aghar Fold. However only a small segment of these folds was present in the study area and therefore were not described comprehensively.

4.4.1. 3D Transect Structural Features

To understand the features in the 3D survey, five NE-SW regional lines perpendicularly dissect the major structures (Fig. 4.19). The three northern lines, Lines A – C show the Aghar Fold and Bobo structures (Fig. 4.9 - 4.14). Line D shows the Aghar, southern extent of the Bobo fold, and the Southern imbricates (Fig. 4.15 & 4.16). Line E shows only the southern part of the Aghar Fold (Fig. 4.17 & 4.18).

The structures in the study area are NW-SE (~N140°E) trending structures that are parallel to the edge of the Niger Delta. The deformation occurring within the survey area has characteristics of both the detachment and outer FTB. The Aghar and Bobo structures are separated by ~12.5 km and deform independently, which is characteristic of the detachment fold belt. On the other hand, the Southern imbricates are chracterised by a tight imbricate system where the displacement is dominated by the foremost fold, which is characteristic of the outer fold and thrust belt (Chapter 2.4).

All the folds within the 3D survey have buried faults that do not emerge to the surface. Generally, the faults are curved at the base of the section near the detachment surface and some become planer in the upper parts. Backthrusts

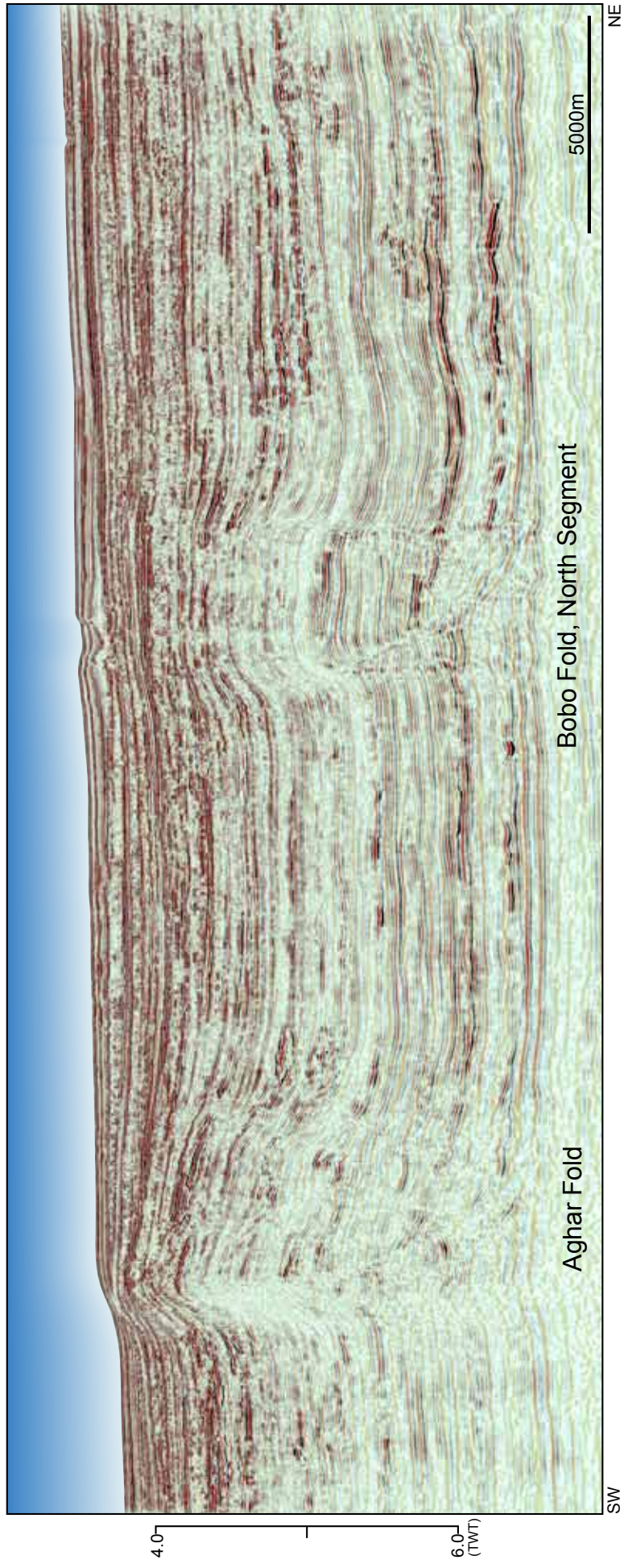

Figure 4.9 Cross-section A - TWT Seismic amplitude display. (Location shown in figure 4.19)

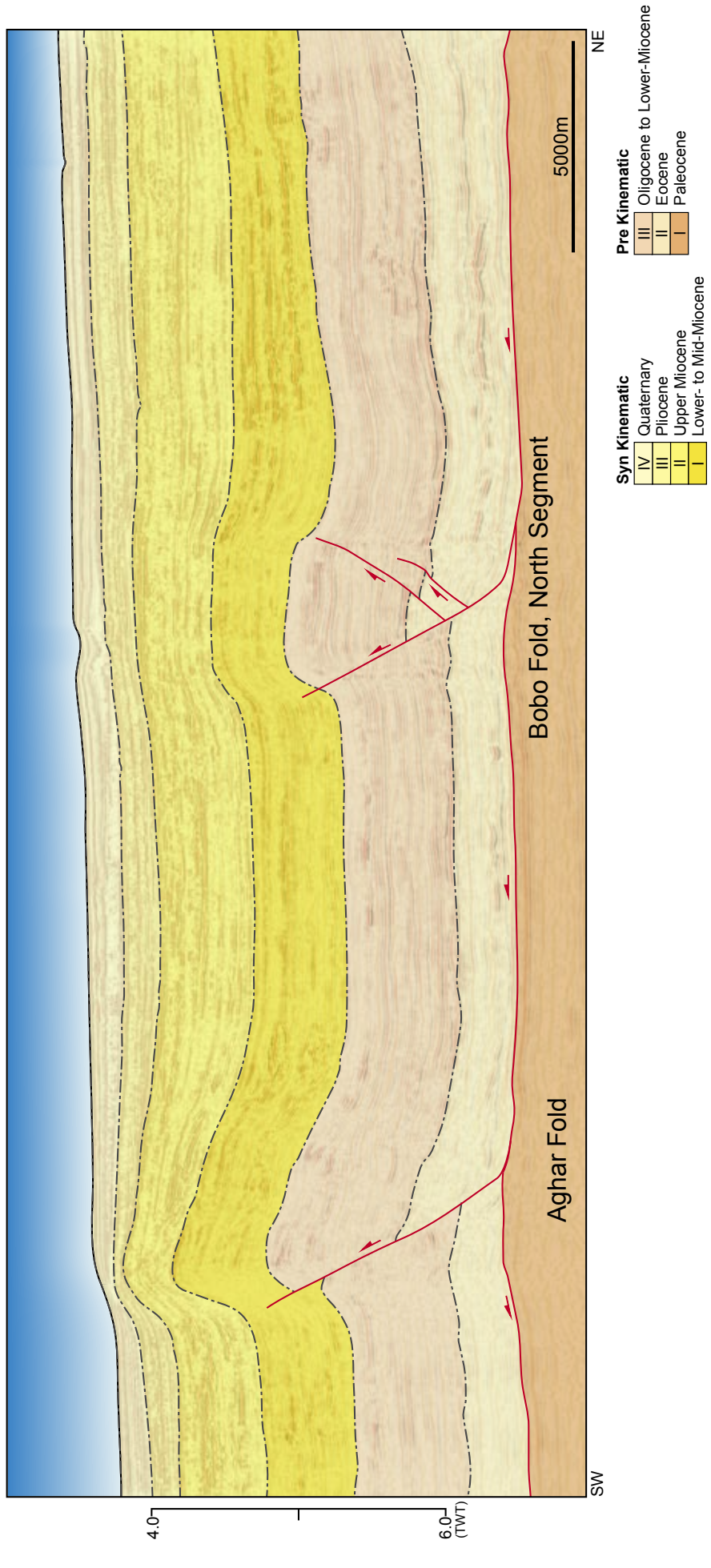

Figure 4.10 Cross-section A - Interpreted TWT section (Location shown in figure 4.19) Interpreted shortening of ~1800m.

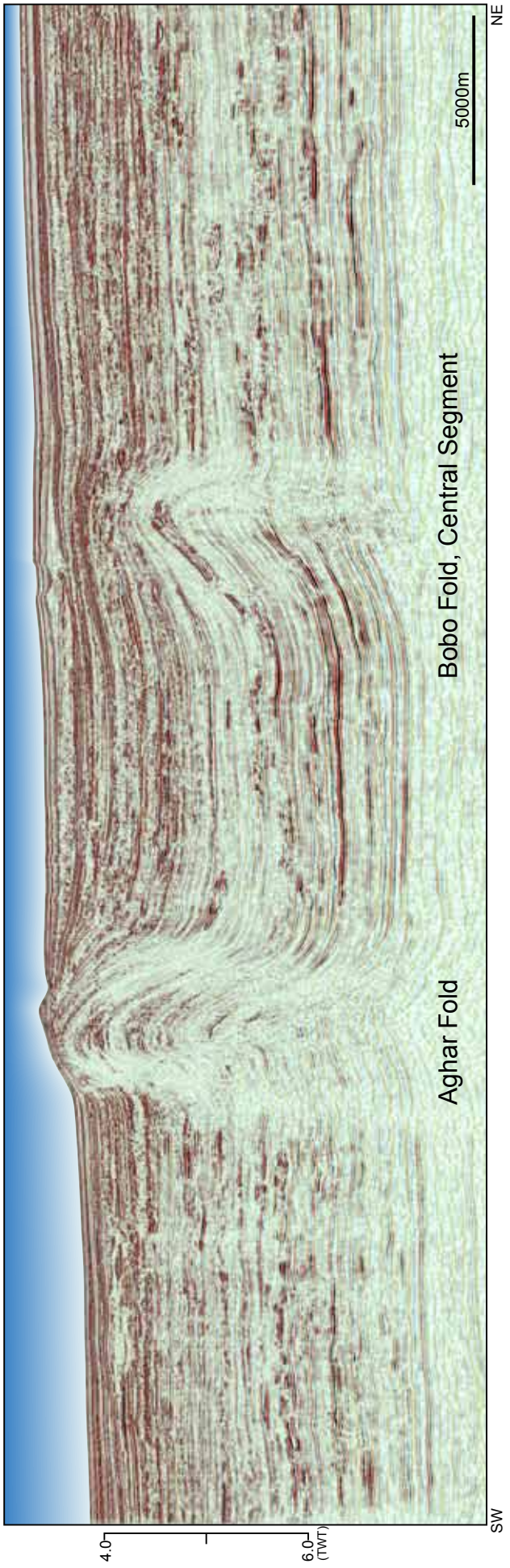

Figure 4.11 Cross-section B - Seismic amplitude display (Location shown in figure 4.19)

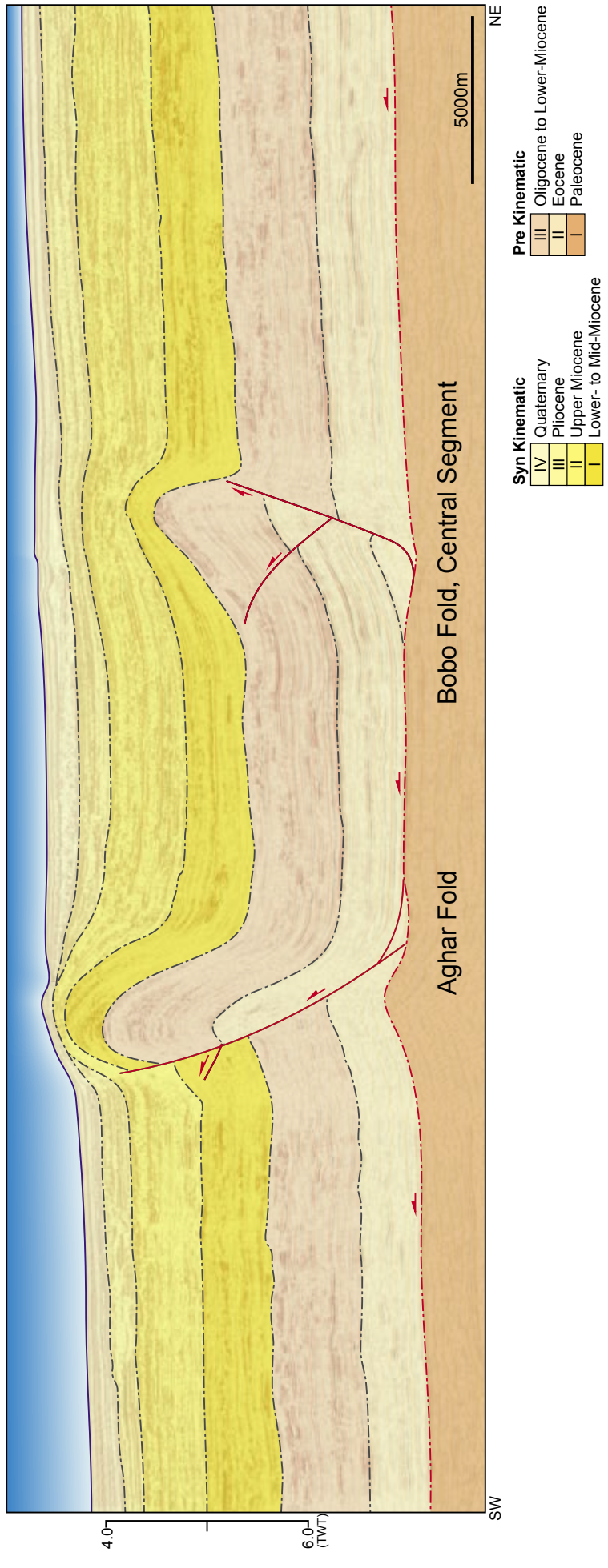

Figure 4.12 Cross-section B - Interpreted section (location shown in figure 4.19) Interpreted shortening of ~2450m.

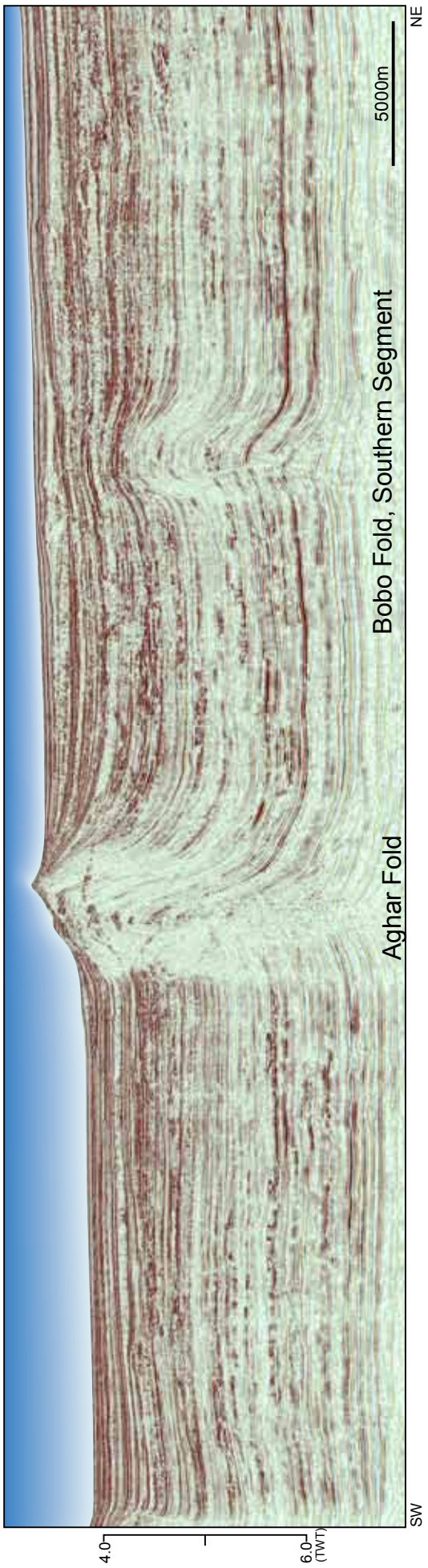

Figure 4.13 Cross-section C - Seismic amplitude display (Location shown in figure 4.19)

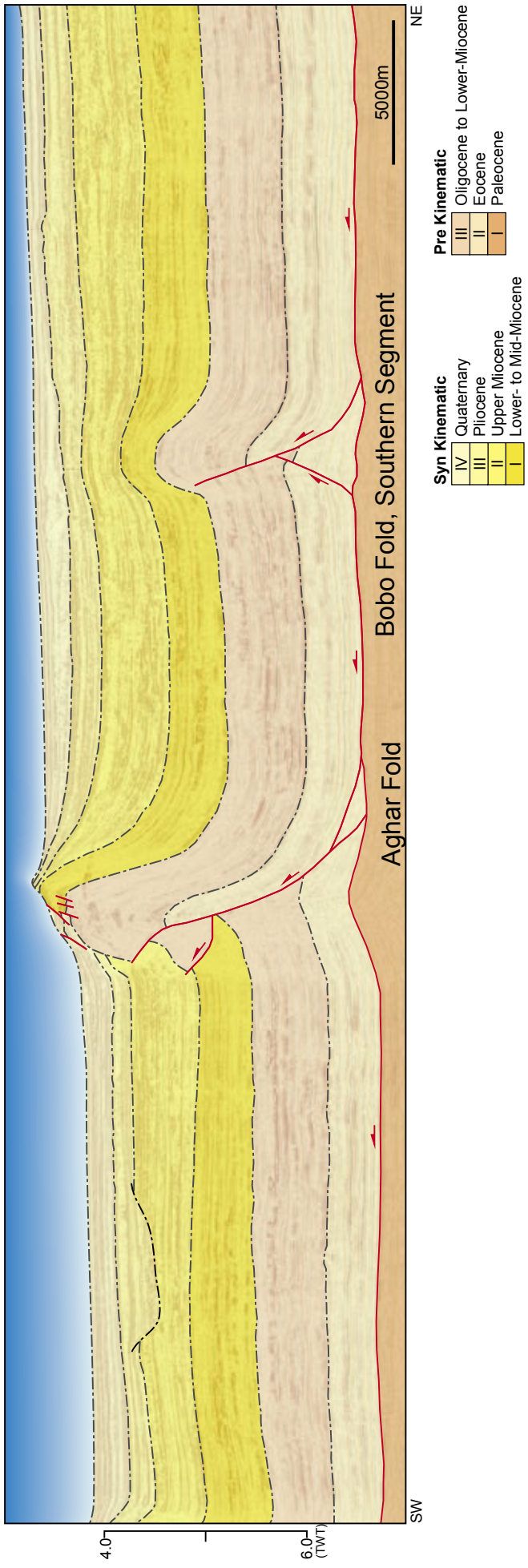

Figure 4.14 Cross-section C - Interpreted section (Location shown in figure 4.19) Interpreted total shortening of 2550m.

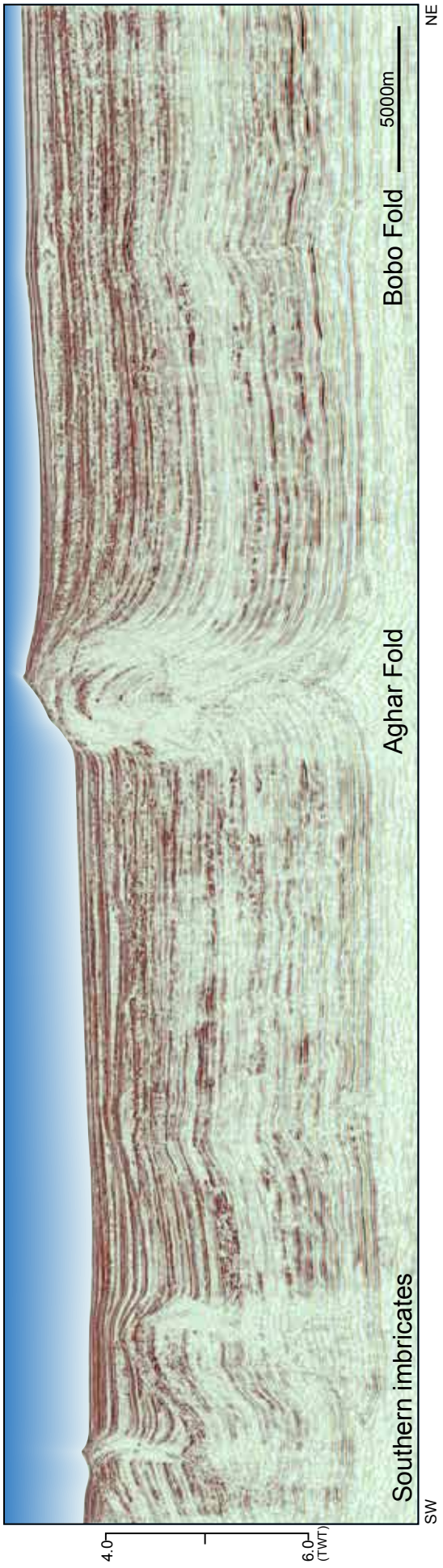

Figure 4.15 Cross-section D - Seismic amplitude display (Location shown in figure 4.19)

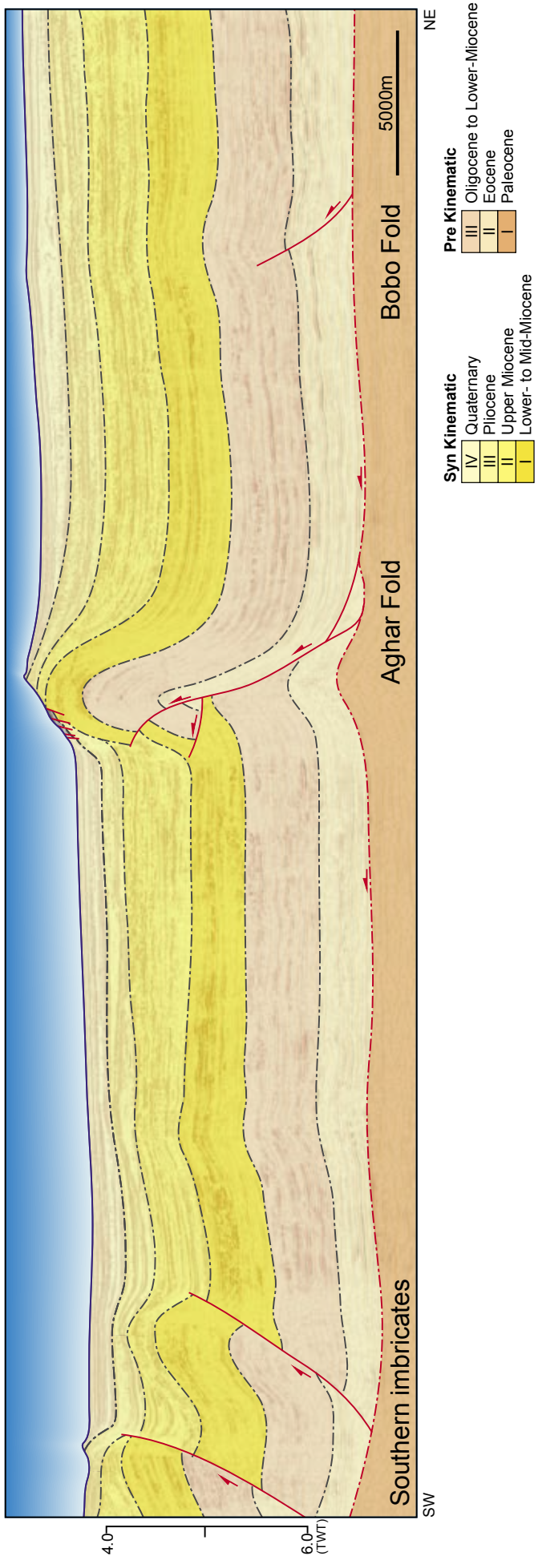

Figure 4.16 Cross-section D -Interpreted section (Location shown in figure 4.19) total interpreted shortening of 4100m.

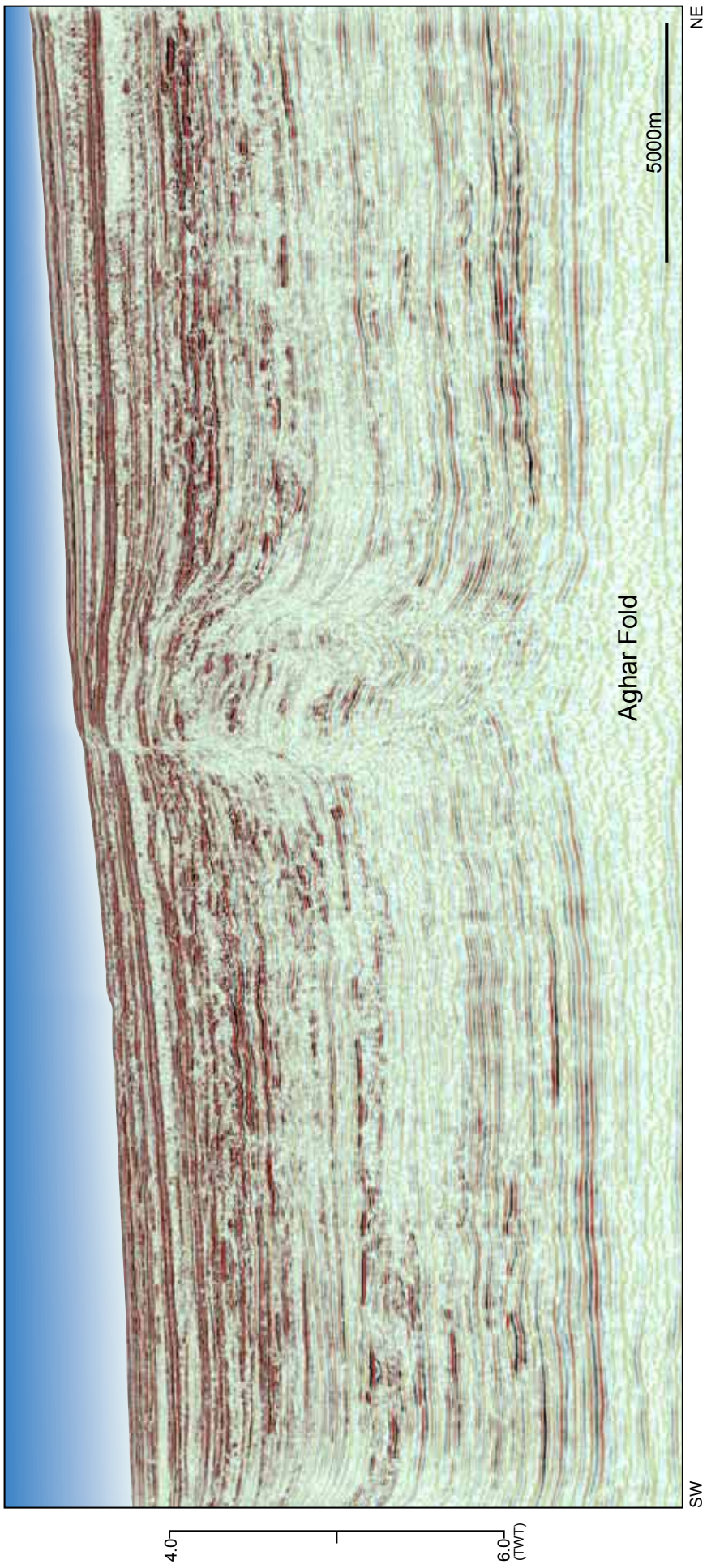

Figure 4.17 Cross-section E - Seismic amplitude display (Location shown in figure 4.19)

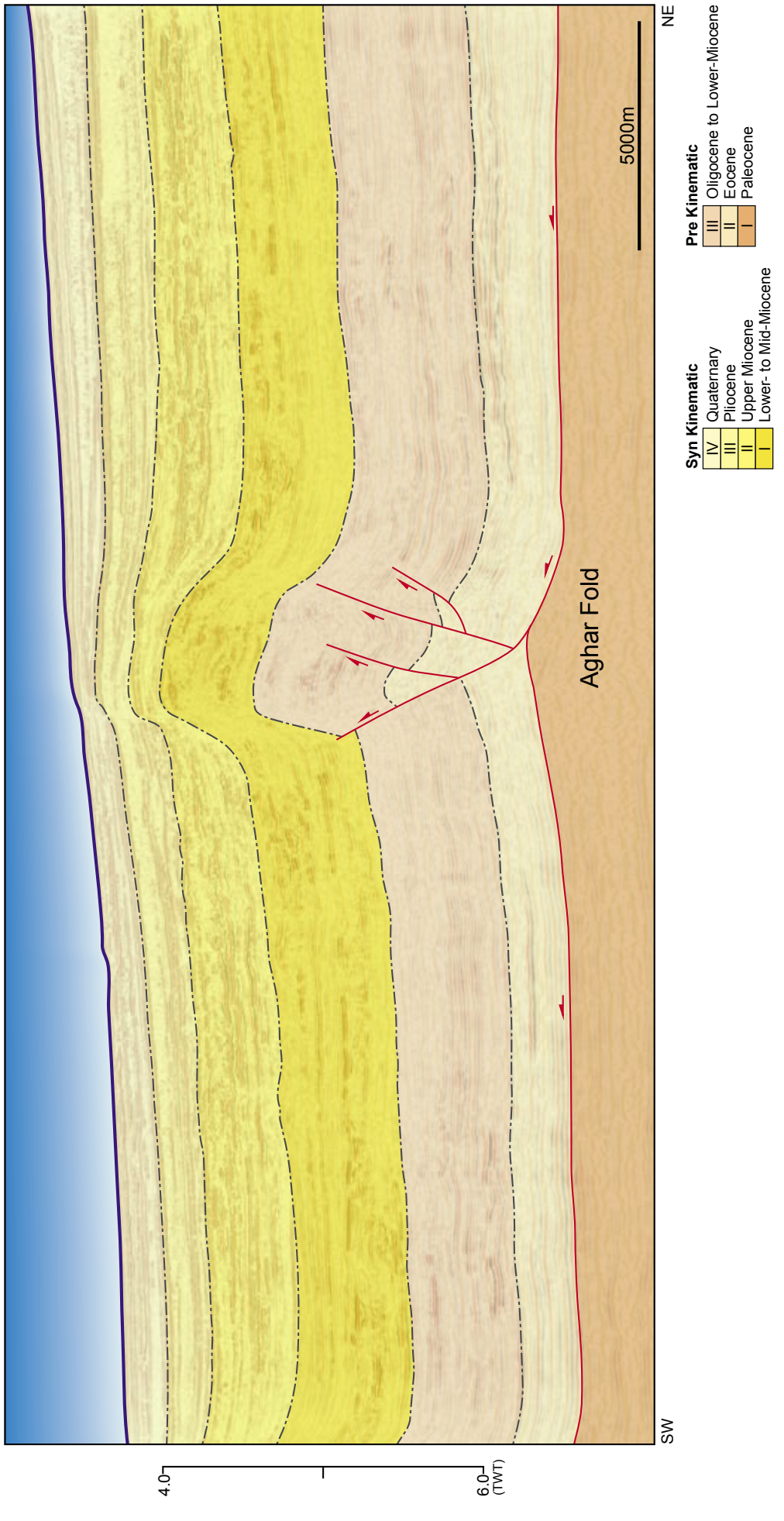

Figure 4.18 Cross-section E - Interpreted section (Location shown in figure 4.19) total interpreted shortening ~950m

also occur along the section, however, these fault tend have a planer geometry.

The Aghar is a basinward-vergent asymmetric FRF. It lies within a series of similar trending folds that extend to the west and south beyond the 3D survey (Fig. 4.25), these are referred to as the Aghar North, Aghar Main and Aghar South folds.

Bobo fold is an independent structure that amalgamated from three opposite verging folds referred to as the Bobo North, Bobo Central and Bobo South. The Bobo North and Bobo South are basinward vergent folds (Fig. 4.9 - 4.10 and Fig. 4.13 - 4.14) while the middle structure is a landwards vergent fold (Fig. 4.11 - 4.12). The thrust faults associated with the fold create complex interactions that have been discussed in several works (Heinio & Davies 2006; Higgins *et al.* 2007; Higgins *et al.* 2009).

4.4.2. Horizon map interpretation

Seven of the eight interpreted horizons are described in this section using the TWT structural maps, coherency maps and Root Mean Square (RMS) amplitude extractions.

Seabed (Quaternary)

The seafloor has a gentle dip (~1°) towards the SW (Fig. 4.19). This almost flat-lying surface is interrupted by several structural and stratigraphic features. The dip of the seabed is even shallower beyond the Aghar Fold which traps the incoming sediments resulting in a dip of ~0.5°.

One of the main features of the seafloor in the study area is the Aghar Fold (Fig. 4.19), which creates up to 400m relief above the seafloor and has a backlimb dip of ~3.5° and a forelimb dip of ~10-12°. Extending over the majority of the fold is a large slump feature caused by forelimb degradation. This creates chaotic sequences (Fig. 4.20) and shallow low-angle extensional faults that form near the seabed (Chapter 5.2.3).

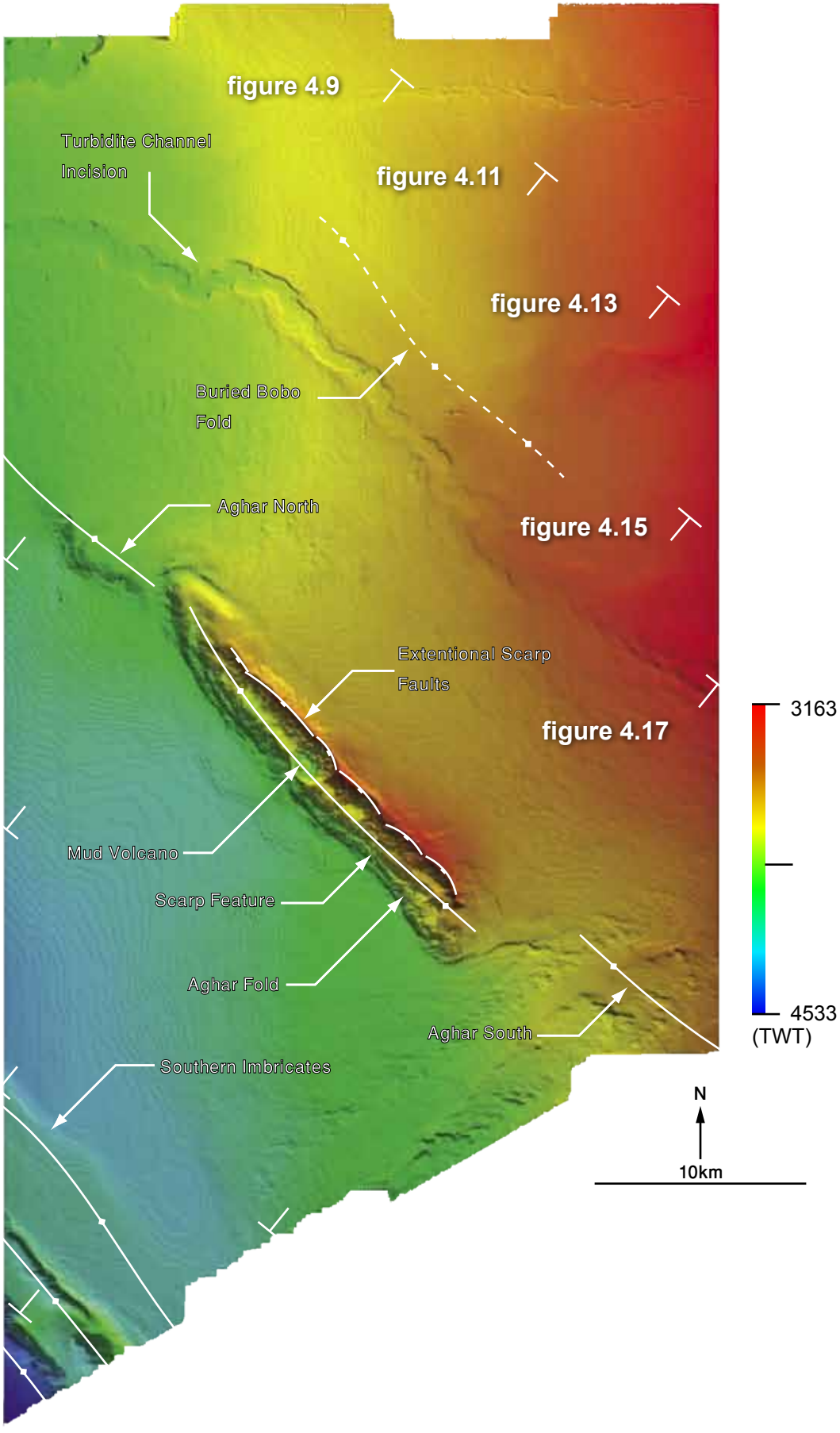

Figure 4.19 Seabed TWT structure map. The map shows the location of the main structural features in the 3D study area.

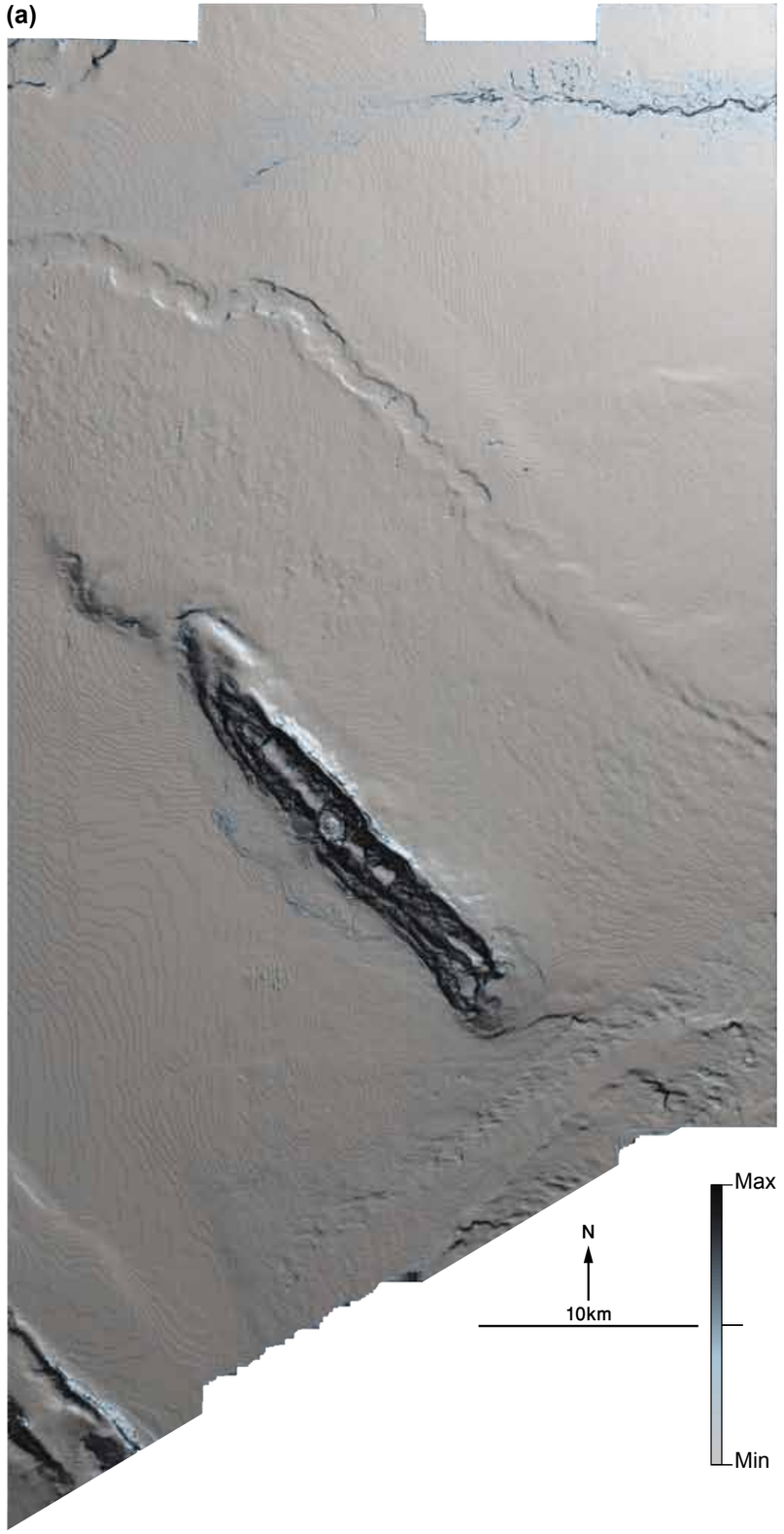

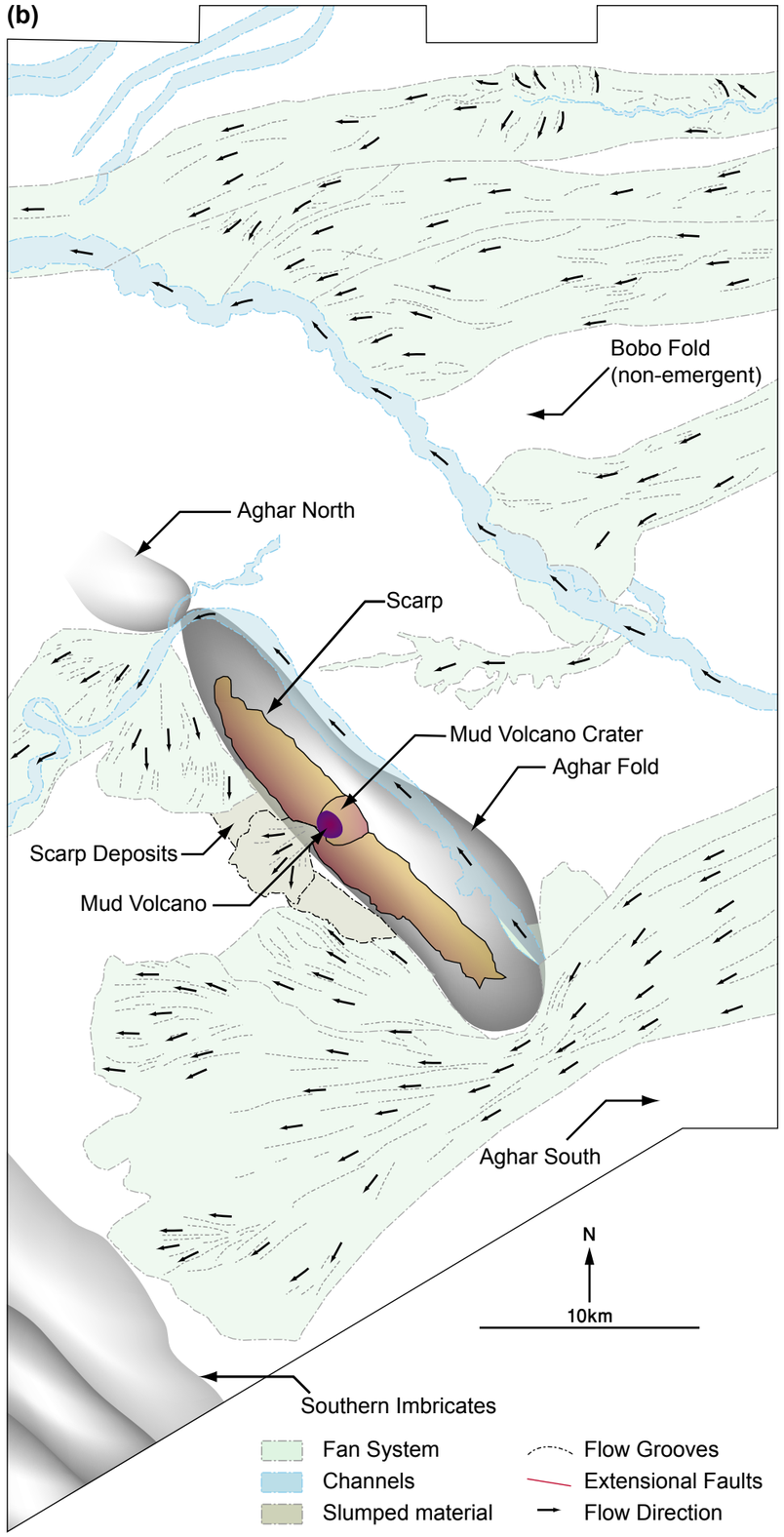

Figure 4.20 : Seabed dip-corrected coherency map and interpreted map section.

This section has been interpreted incorporating the TWT structure map (Figure 4.19), Dip-corrected coherency map and RMS amplitude maps (Figure A.2 &Figure A.3).

Aghar North fold creates a subtle relief, which decreases northwards. The shape of this structure is less regular compared to the well-developed Aghar Fold but is only offset a few kilometers west of the Aghar Fold. The spacing between the Aghar and its southern extension, Aghar South, is much greater; this causes the development of en-echelon extensional faults. However, the en-echelon faults are not immediately apparent, they only create a subtle relief on the seafloor that has been overcome by incoming NE – SW turbidity flows.

The Bobo structure on the other hand does not influence Present Day bathymetry. Furthermore, the thrust faults associated with both major folds do not immerge at the seabed. However, the en-echelon fault system that occurs to the south of the Aghar Fold may influence the shape of the turbidite related features.

In the middle of the Aghar Fold a mud volcano created a radial collapse crater ~2.1km in diameter (Fig. 4.19 & Chapter 5.2.4). The location of the crater allows it to be larger than typical mud volcanoes, which typically do not exceed ~1km in diameter. The steep unstable forelimb of the anticline causes a larger area surrounding the mud volcano to collapse. Flow lines stretch away to the south and southwest of the mud volcano. RMS extraction of the seabed shows that the mud volcano contributed to the slump deposits ahead of the Aghar Fold (Fig. figure A.2 & A.3).

Three main channel systems are identified on the Present Day seabed (Fig. A.2); a northern E – W channel, a central SE – NW channel, and a southern NE – SE channel. The three channels vary in energy; the highest energy of the three is the central channel, which is ~1km wide meandering channel that transects the 3D survey without losing flow. The two other channel systems have less energy and terminate within the survey area. The northern and southern channels diminish gradually into elongated submarine terminal fans. A minor splay from the central channel is observed at the northern tip of the Aghar Fold. This channel is located in the saddle point between the Aghar Fold and

the the Aghar North fold (Fig. A.2) following the bathymetric low in the area.

The Aghar and Aghar North structures create relief on the seabed but their associated thrust faults are non-emerge. The relief causes the various flows to go around the main structure, then breach the saddle point between the Aghar North and the main Aghar structures as well as the area south of the main Aghar structure (breaching the saddle point and the Aghar South structure itself). Therefore, the mean flow direction follows the structural strike (SE to NW) rather than following the regional dip direction (NE-SW). The Aghar forelimb has a large scarp that dominates the majority of the structure (~18×2 km), which creates a fan to the SW of the Aghar structures, which also includes the mud volcano collapse crater.

The Bobo and Aghar South structures do not divert submarine flows and have no relief on the seabed. The Bobo and Aghar South were overridden by submarine flows and creates no relief on the seabed.

Pre-Kinematic 1 (Paleocene)

TWT: 6067 – 6881 ms Depth: 5805 – 7320 m

The Pre-Kinematic 1 (Fig. 4.21), which is also the top of the detachment unit, is a gently SW dipping surface (0-1°) with few perturbations under the Aghar and Bobo folds. The uplift beneath the folds can either be attributed to velocity pull-ups, which are seismic artifacts, or can be interpreted as a thickened core of a detachment fold.

The amplitude of the reflector is coherent through most of the horizon (Fig. 4.22), with some anomalies at the uplifted areas beneath the Aghar and Bobo folds as well as the Southern imbricates. Although turbidite channels are probably present, the coherency extraction cannot resolve sedimentological features. This is an imaging problem due to both the depth of the horizons and its low seismic velocity.

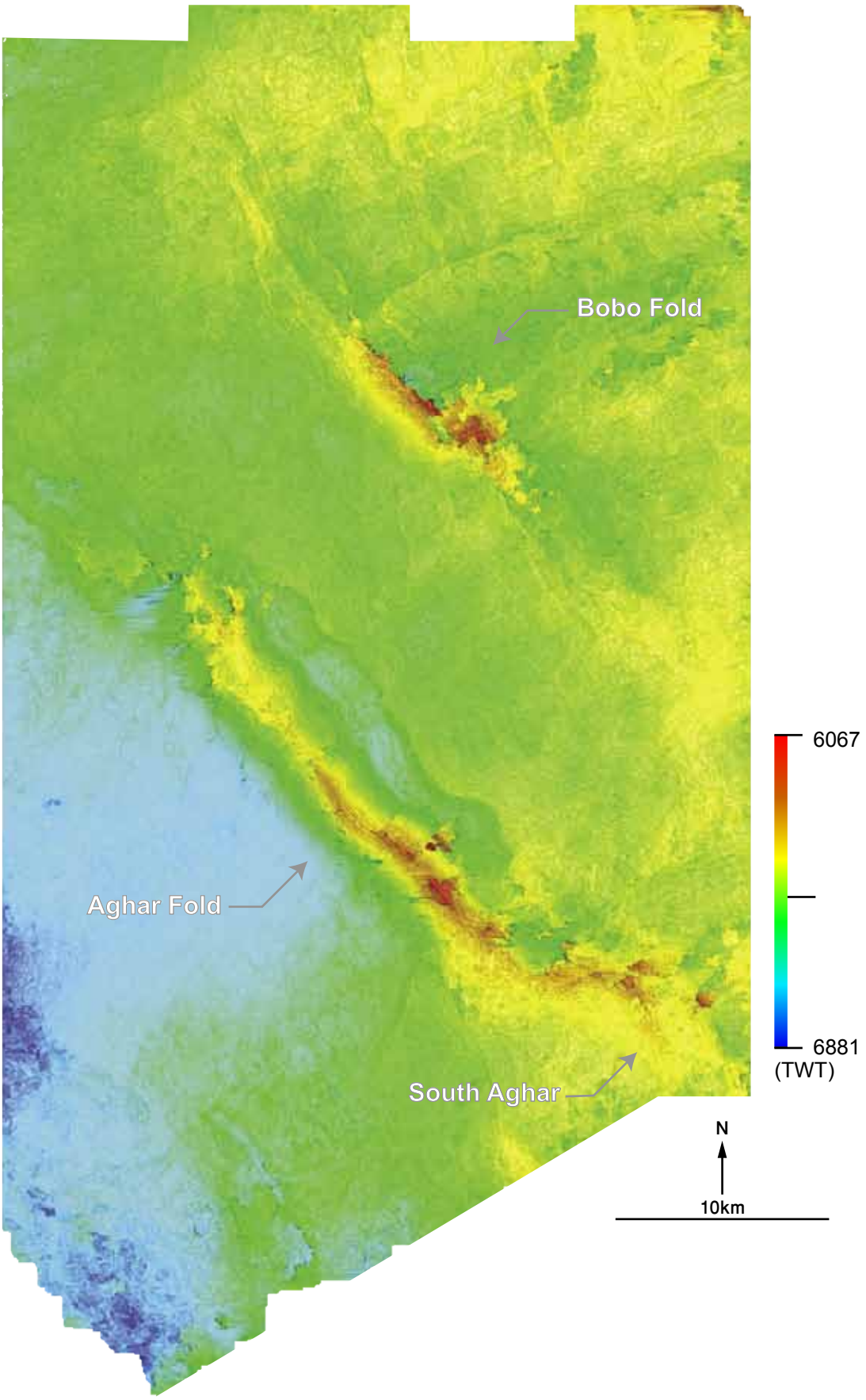

Figure 4.21 Top Pre-Kinematic 1 (Akata) and detachement TWT structure map

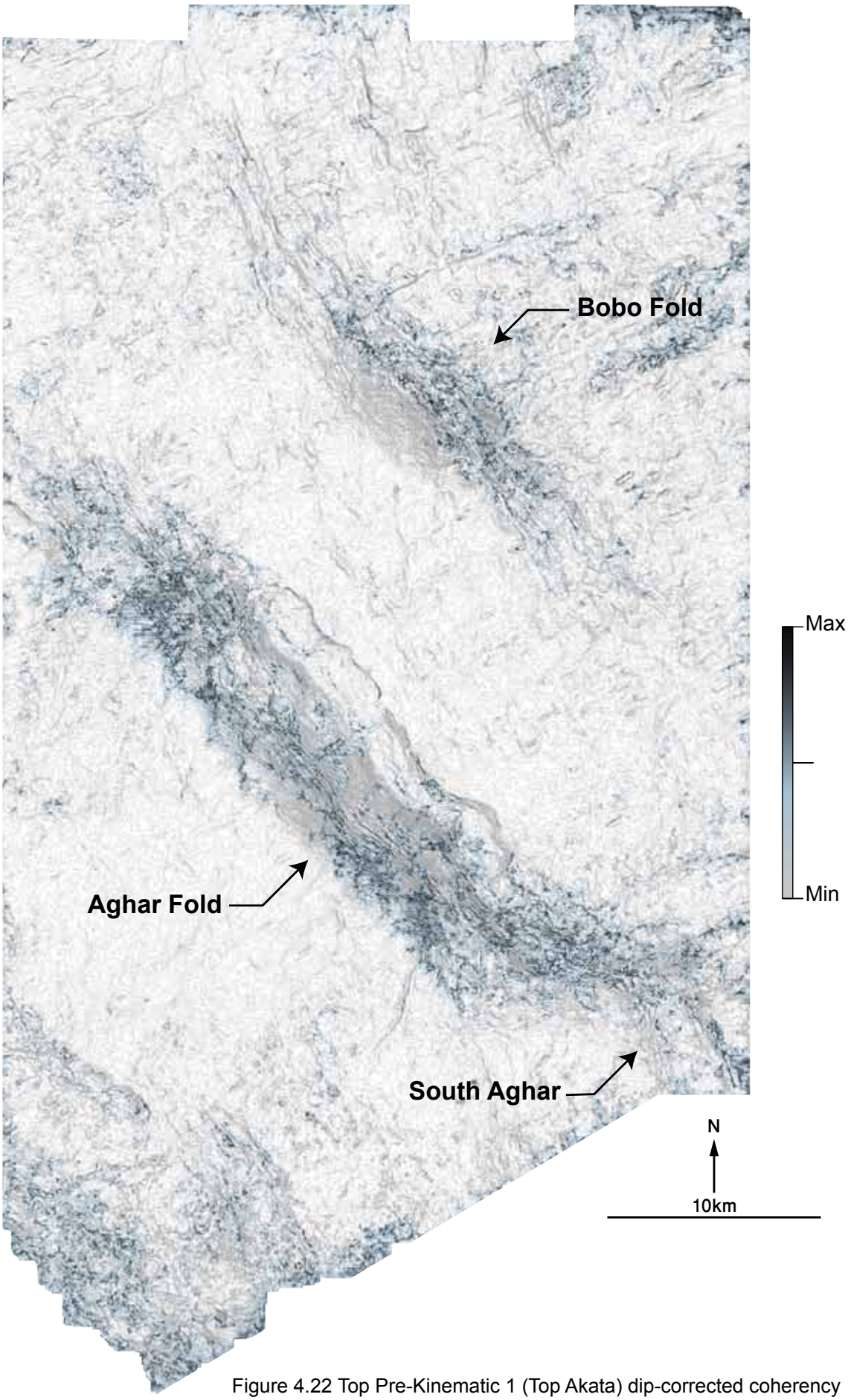

Figure 4.22 Top Pre-Kinematic 1 (Top Akata) dip-corrected coherency map.

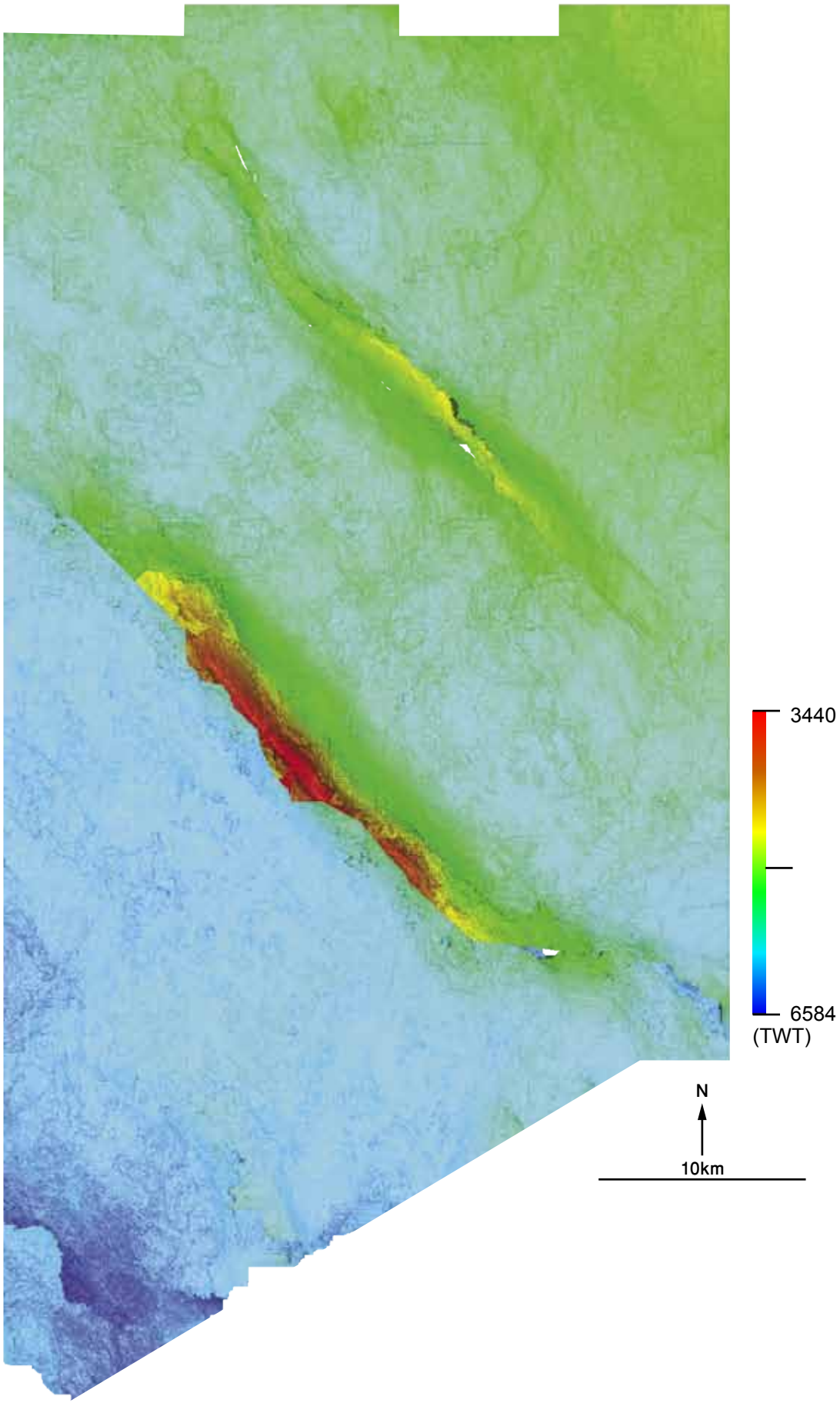

Figure 4.23 Top Pre-Kinematic 2 TWT structure map.

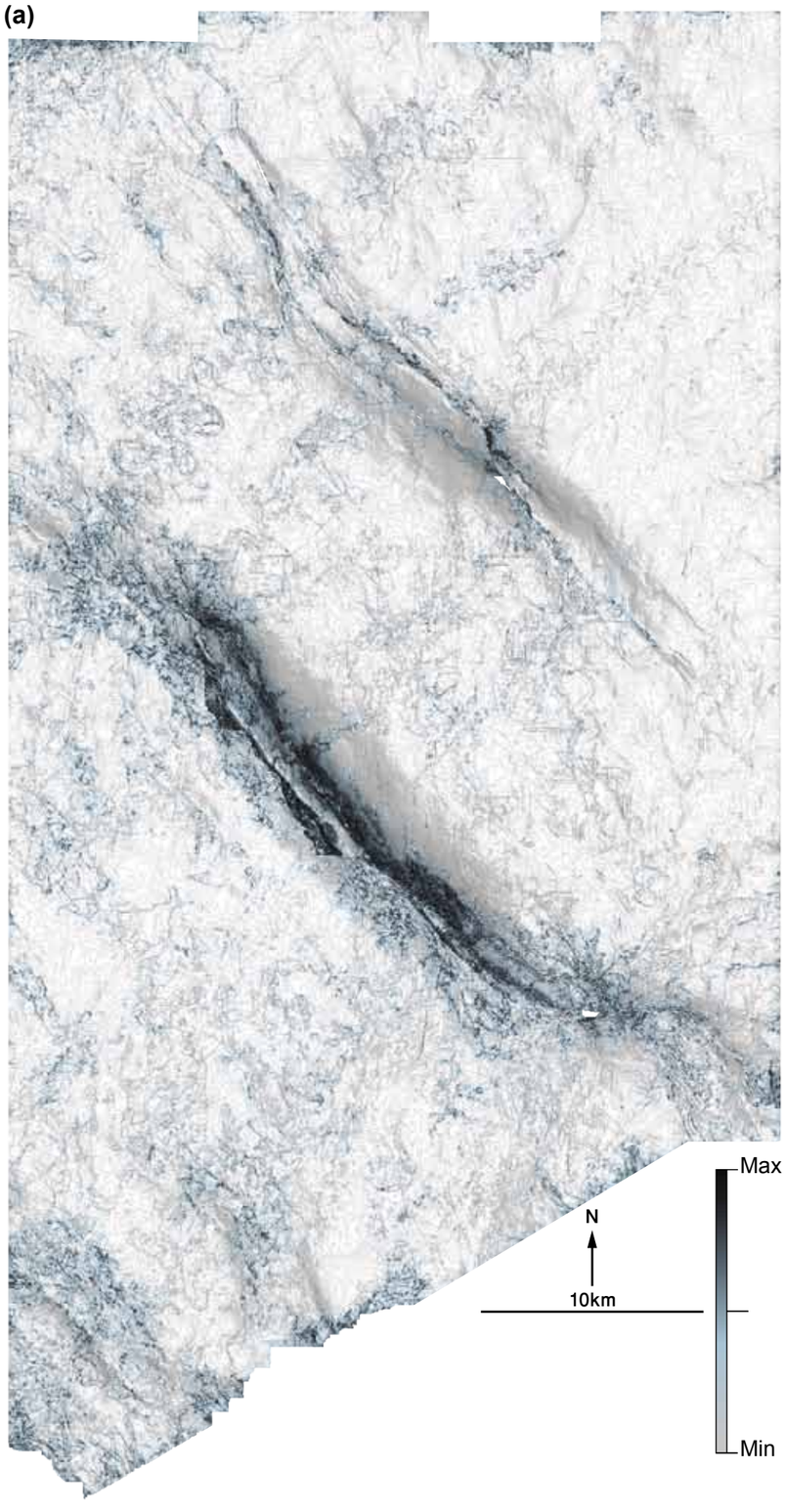

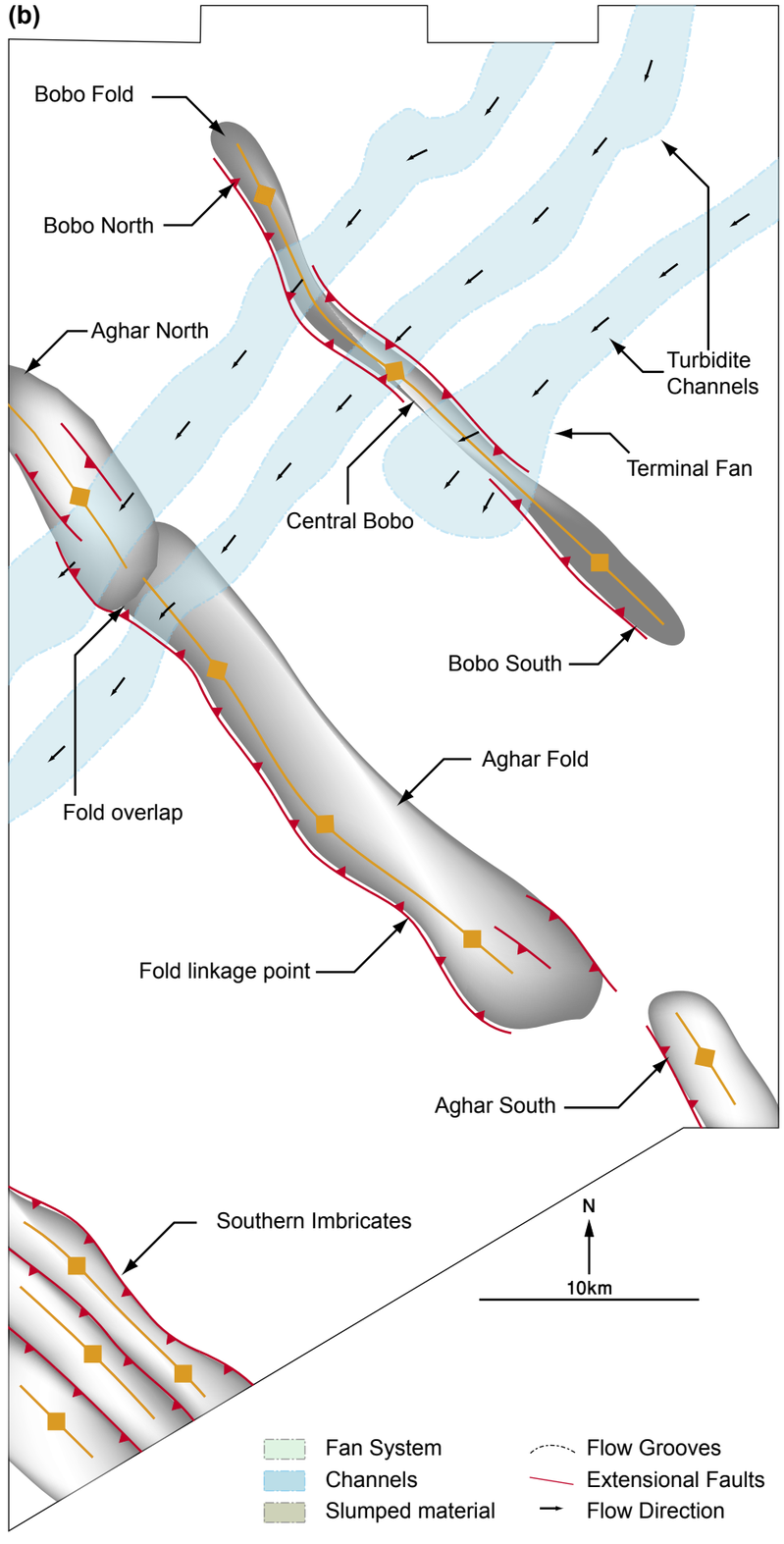

Figure 4.24 : Top Pre-Kinematic 2 dip-corrected coherency map and interpreted map section.

Interpreted by intergratin the Dip-corrected coherency map and the TWT structure map (Figure 4.23).

Pre-Kinematic 2 (Eocene)

TWT: 3440 – 6584 ms Depth: 3328 – 6607 m

This pre-kinematic surface is the lowermost of the supra-detachment horizons. It shows the Bobo and Aghar Folds with their associated structures as well as the Southern imbricates (Fig. 4.23). Kinks and bends in the fault and fold structures highlight the linkage points between structures that previously were independent and subsequently have laterally joined with the increased shortening.

The Aghar structure at this level shows two kink points; one near the overlap with the Aghar North and in the southern part of the fold (Fig. 4.24). The fold linkage point highlighted in the diagram shows a hard link of thrust faults that were initially three separate thrust faults. The kinks in the structure show that the Aghar Fold is part of a series of left-stepping en-echelon structures that extend beyond the dataset to the west and south. The area between the Aghar Main and Aghar South shows amplitude anomalies that may be caused by interaction between the two structures.

The Bobo fold on the other hand shows three main structural elements with two distinctive kinks; the Northern and Southern Bobo (basinward vergent) and the central Bobo (landward vergent). The Bobo North and central have a long overlap section of ~8 km compared to the southern and Central Bobo overlap of ~2 km both of which are associated with kinks.

At this depth, only the channel systems were resolved by the seismic data. These channels show a dominant NE to SW flow trend. The channels have tight meandering geometries, similar to gentle gradient riffle type channels.

Pre-Kinematic 3 (Oligocene to Lower-Miocene)

TWT: 3440 – 6376 ms Depth: 2578 – 6308 m

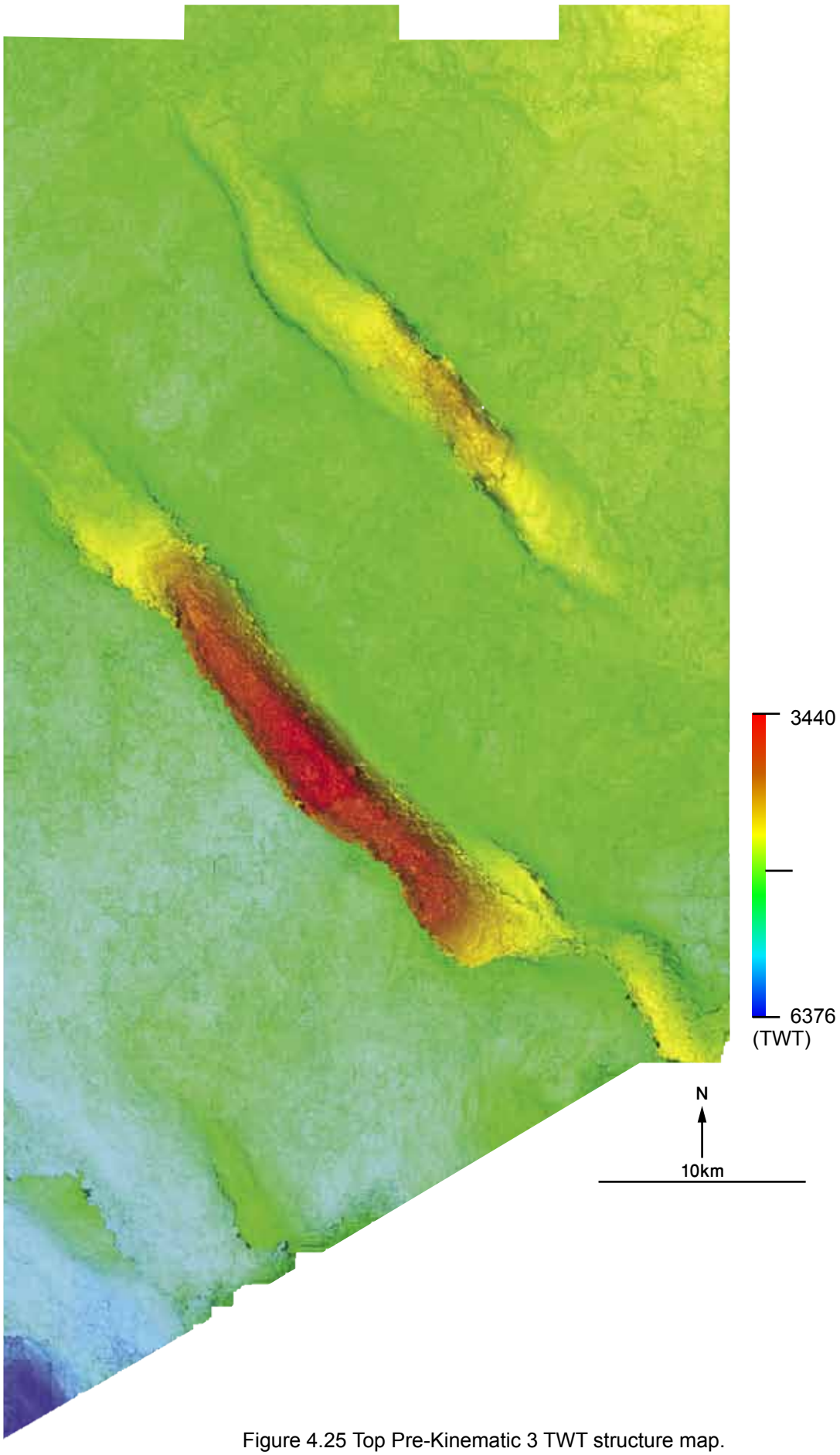

Figure 4.25 Top Pre-Kinematic 3 TWT structure map.

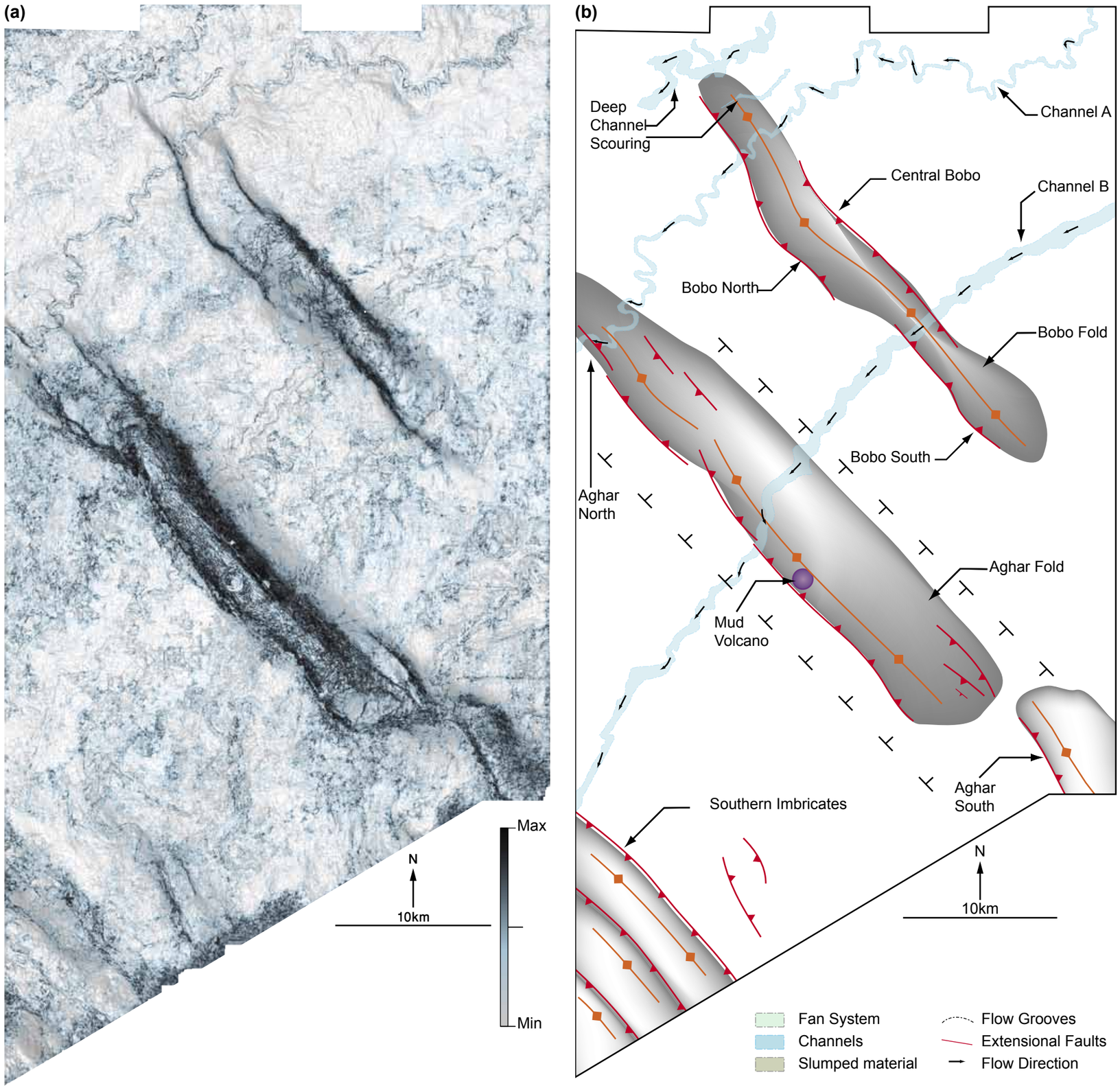

Figure 4.26 : Top Pre-Kinematic 3 dip-corrected coherency map and interpreted map section.

interpreted by integrating the dip-corrected coherency with the TWT structure map (Figure 4.25).

The top of Pre-Kinematic 3 (Fig. 4.25) map shows the top of the pre-kinematic horizons. The surface shows similar structural trends to the Pre-Kinematic 2 horizon, however, the fault linkage points are less pronounced. The saddle separating the Aghar Main and Aghar North is indistinguishable, making the two folds appear as a single structure. The separation between the Aghar and Aghar South narrows compared to the PK-2 surface, causing more interaction to occur between the structures that are visible on the dip-corrected coherency map (Fig. 4.26). Backthrusts form in the northern and southern parts of the Aghar Fold, these correspond to wider, subtler anticline structures. The Aghar Fold has the greatest relief at the middle of the structure.

The three Bobo thrust faults are emergent at this level, each associated with a fold. However, the overlap between the thrusts increases to ~9 km in the North and ~4.5 km in the South. The highest point of the Bobo is located in the middle of the central Bobo thrust, which should account for the majority of the shortening in the structure.

The channel systems enter the area from the NE, and follow a meandering path to the SW. The meandering in Channel A to the north of the area (Fig. 4.26) is similar to the PK-2 channels but with wider meander spacing. Channel B (Fig. 4.26), on the other hand, is a wider channel with less meandering. A subtle channel diversion takes place to the north of Central Bobo, indicating that the central part of the Bobo fold created a relief at the time of channel activity. Otherwise, the channels are not disturbed by folding.

Syn-Kinematic 1 (Lower- to Mid-Miocene)

TWT: 3203 – 5097 ms Depth: 2400 – 4267 m

The Aghar and Bobo folds as well as one of the Southern imbricates create a relief on Top Syn-Kinematic 1 surface (Fig. 4.27). The main Aghar Fold remains breached by a thrust fault in the forelimb; however, the remaining structures have lower amplitudes with non-emergent thrust faults (Fig. 4.28). The main

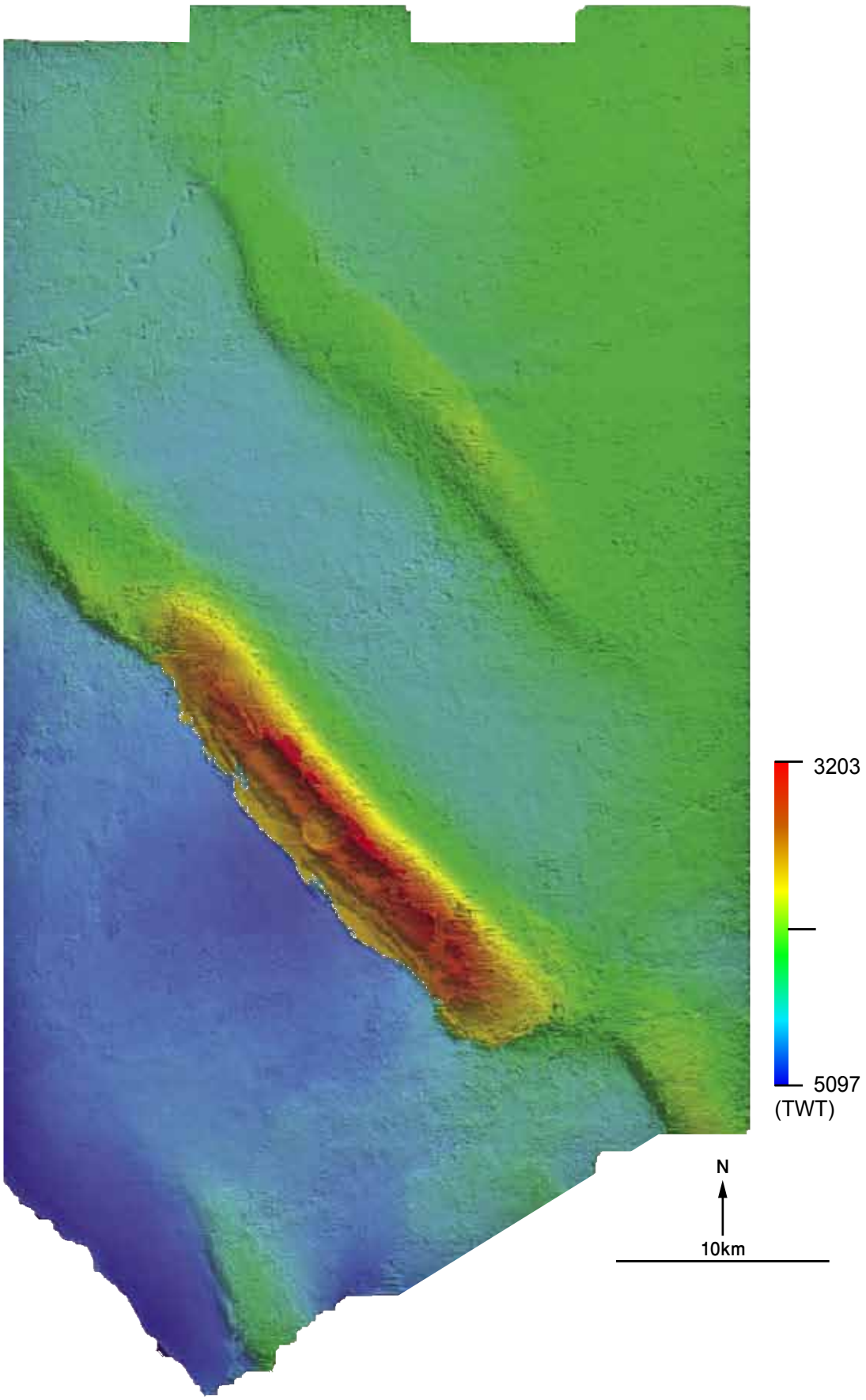

Figure 4.27 Top Syn-Kinematic 1 time structure map.

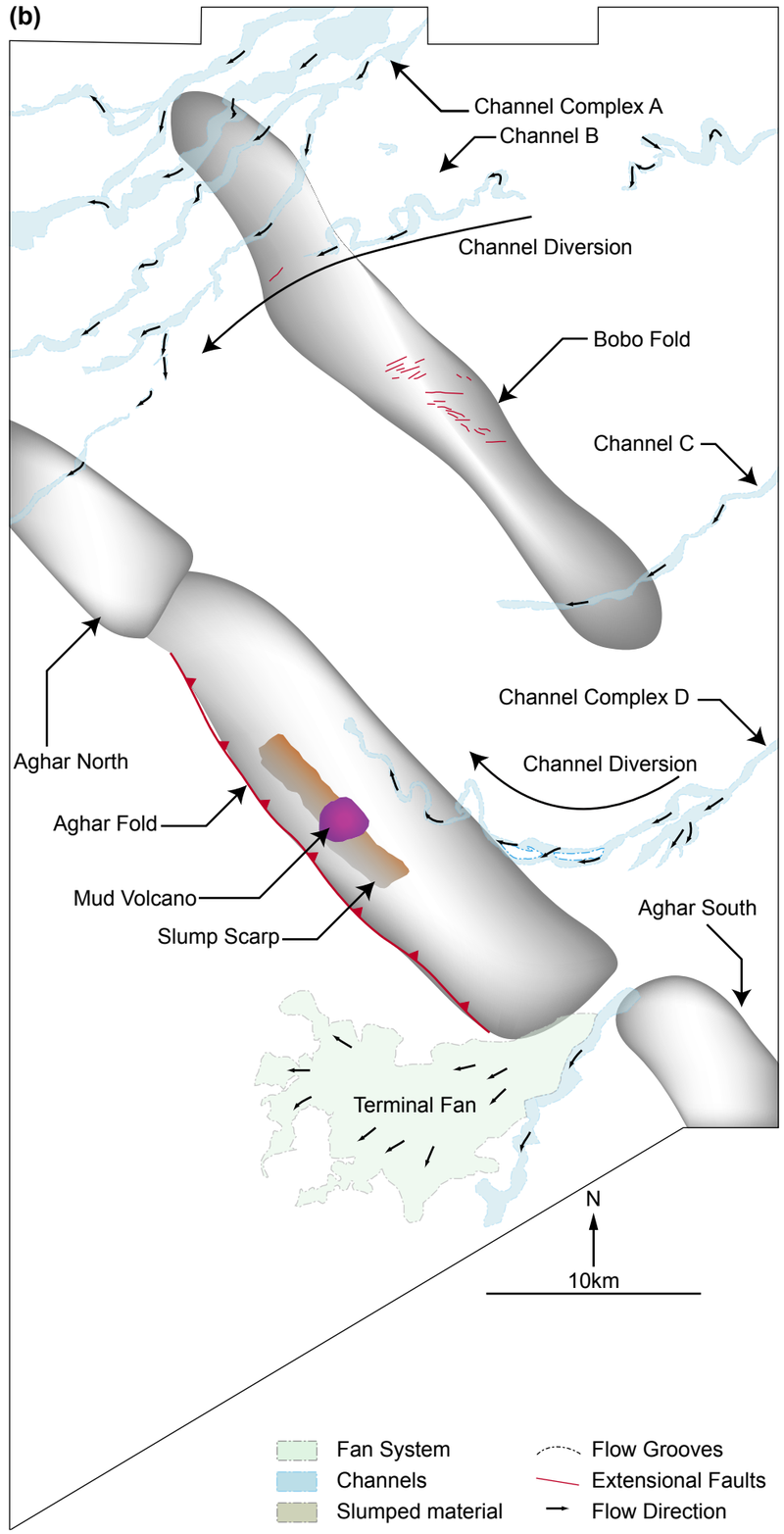

Figure 4.28 : Top Syn-Kinematic 1 coherency map and interpreted map section (b).

Interpreted by integrating the coherency map with the time strucutre map (Figure 4.27) and RMS amplitude maps (Figure A.7 &Figure A.8)

Aghar thrust fault shows no evidence for fault linkage at this level. A section of the Aghar mud volcano is located in the middle of a ~17.5 km paleoscarp on the Aghar forelimb.

The Aghar North and South have gently dipping backlimbs with a flat, less curved crestal area when compared with the main Aghar Fold. Similarly, the Bobo fold creates a subtle relief on this horizon. The crestal area is dominantly flat with rounded edges above the thrust faults.

Multiple channels are present on this surface. Channel Complex A (Fig. 4.28) (NE to SW flow direction) consists of a series of channels that enter the survey area from a narrow point to the north and fan out over the Bobo North. Similarly, Channel B enters the survey area from the NE (flow ENE to SW) and cuts across the Bobo North with a slight curvature. Channel C enters the survey area from the middle of the eastern border of the section (flowing NE to SW) and is slightly diverted south at the Bobo South. Channel Complex D also enters from the middle of the eastern border of the survey flowing in a NE to SW direction and diverts to SE to NW at the backlimb of the Aghar Fold. A terminal fan with an irregular-shaped toe nucleates between the Aghar Main and Aghar South and extends over a ~15km radius.

Syn-Kinematic 2 (Upper-Miocene)

TWT: 3163 – 4533 ms Depth: 2371 – 3548 m

Both the Aghar and Bobo folds as well as the Southern imbricates show relief on this surface, however, the Bobo fold shows a subtler relief compared previous sections (Fig. 4.29). The thrust faults of the Aghar Fold are emergent, especially in the middle part of the Aghar Fold. Whereas the Aghar North and South as well as the Bobo fold thrust faults are non-emergent. The NE fold of the Southern imbricates creates less relief compared to the other two folds. This fold also shows a saddle point, which may have been breached by turbidity flows.

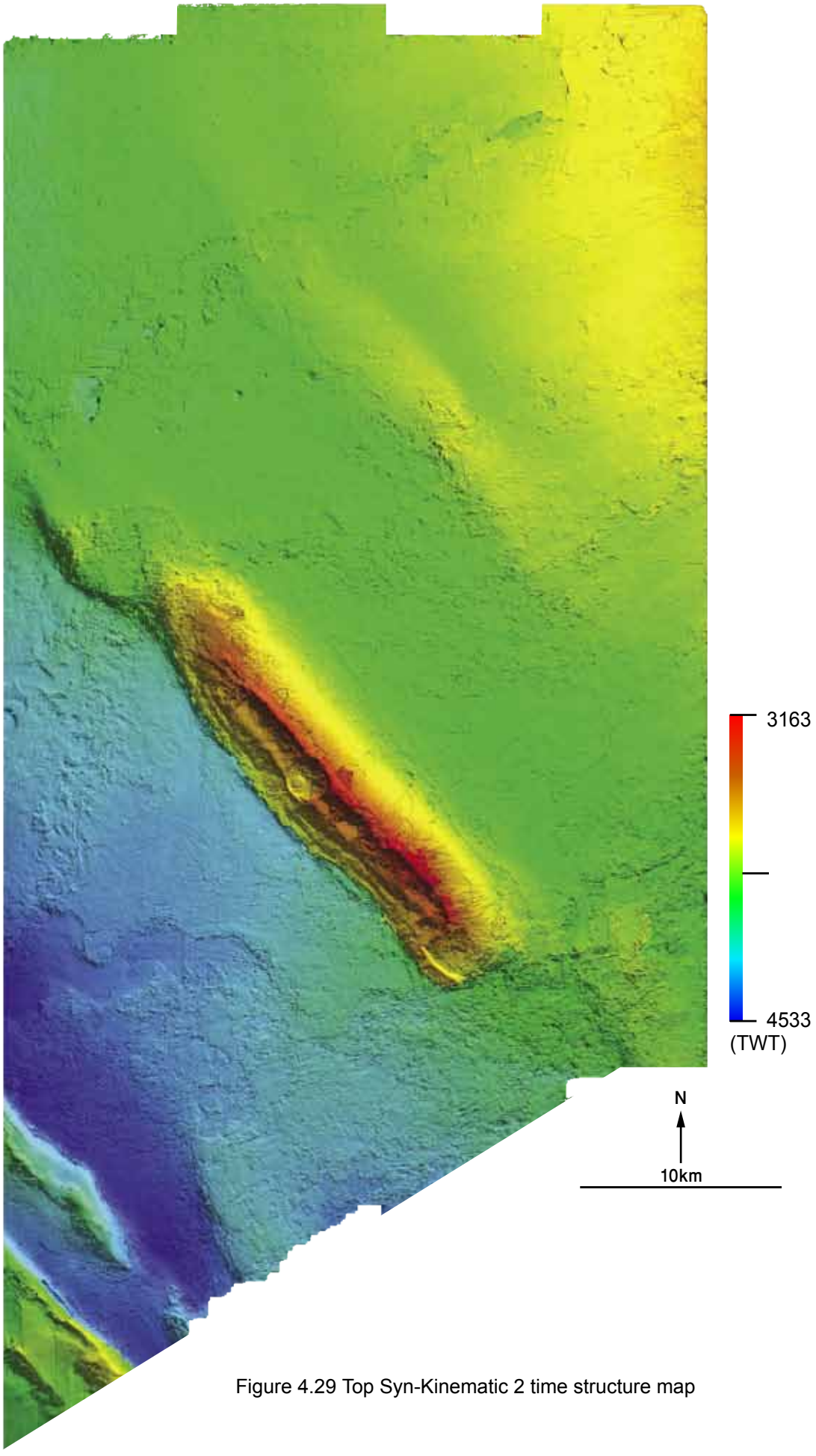

Figure 4.29 Top Syn-Kinematic 2 time structure map

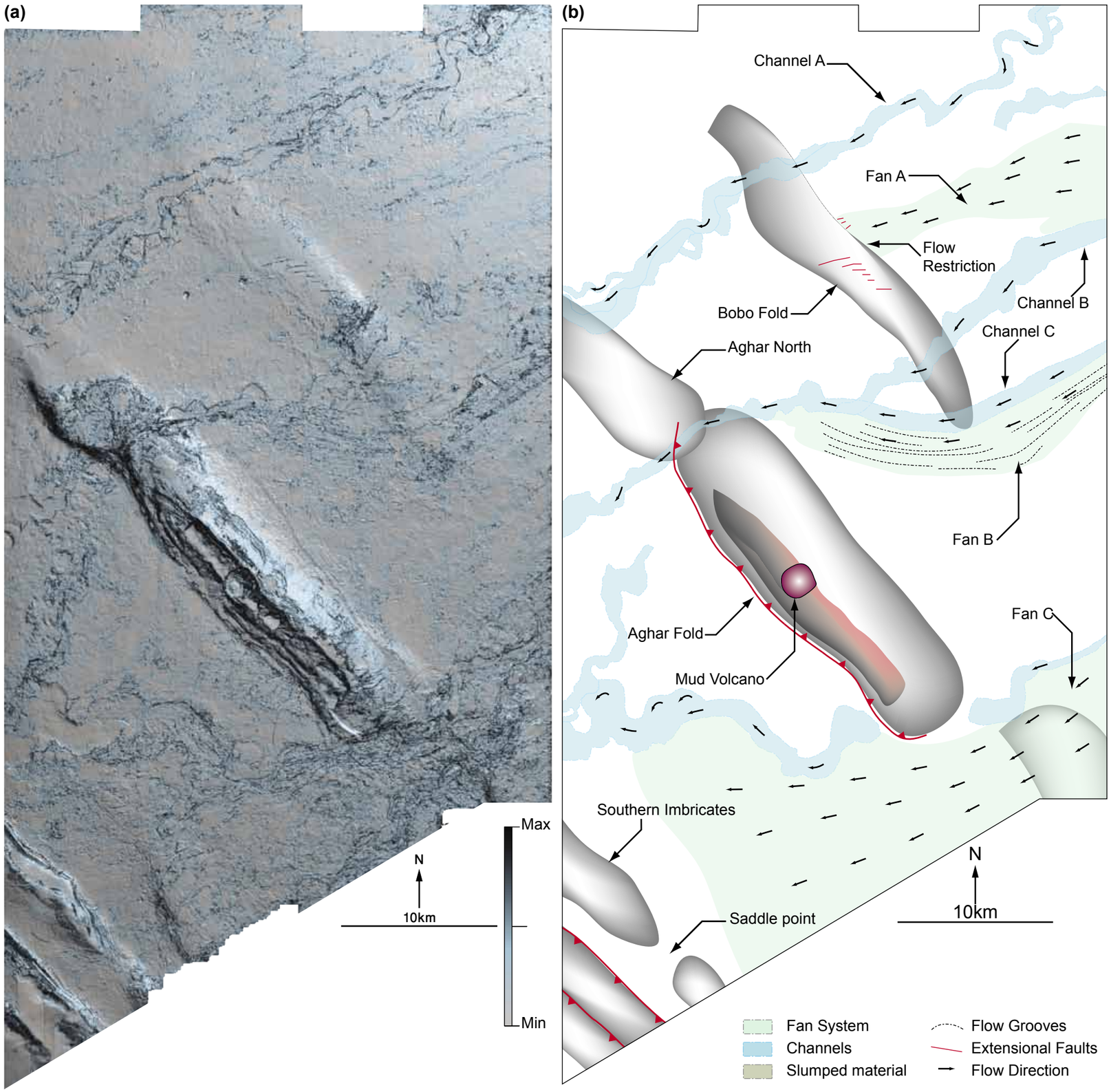

Figure 4.30 : Top Syn-Kinematic 2 dip-corrected coherency map and interpreted map section.

Interpreted by integrating dip-corrected coherency, TWT structure map (Figure 4.29), and RMS maps (Figure A.10)

The paleoscarp is also present in this horizon as well as the mud volcano pipe (Fig. 4.30). The scarp is ~35 km long by ~4.7 km wide, and the mud volcano pipe (~2km in diameter) creates a crater ~4km in diameter. Furthermore, within the central part of the scarp, coherent bodies 5.4 – 7.7 km long by ~2km wide occur.

The area to the SW of the Aghar Fold is significantly lower than the area to the NE. The two areas also have different slope gradients, where the higher NE part has >1° dip and the SW part ~1° dip.

Turbidite flows enter the area at two points; one from the NE and the other from the SE The flows then follow the overall SW dip. The northern Channel A has a series of abandoned channels (similar to ox-bow lakes) that have been intersected by younger channels. Channels B and C have similar geometries. Channel B, however, is diverted away from the middle of the Bobo fold and joins channel C midway between the Aghar and Bobo structure. The emergent channel then breaches the saddle point between the Aghar Main and Aghar North structures.

To the North, Fan A enters the section in a ENE to WSW direction, but the Bobo fold restricts the flow, preventing further progression. Fan B is a sheet-flow complex that creates groove features several kilometers long. These grooves are interpreted as flow direction indicators. Both Channel C and Fan B are diverted from a NE – SW direction to an ESE – WNW at the backlimb of the Aghar Fold. Another large fan complex enters the survey area from the SE, flowing over the Aghar South, and terminates to the NE of the Southern imbricates.

Syn-Kinematic 3 (Pliocene)

TWT: 3211 – 4284 ms Depth: 2407 – 3304 m

This horizon shows a large relief on the Aghar Fold and a less pronounced relief

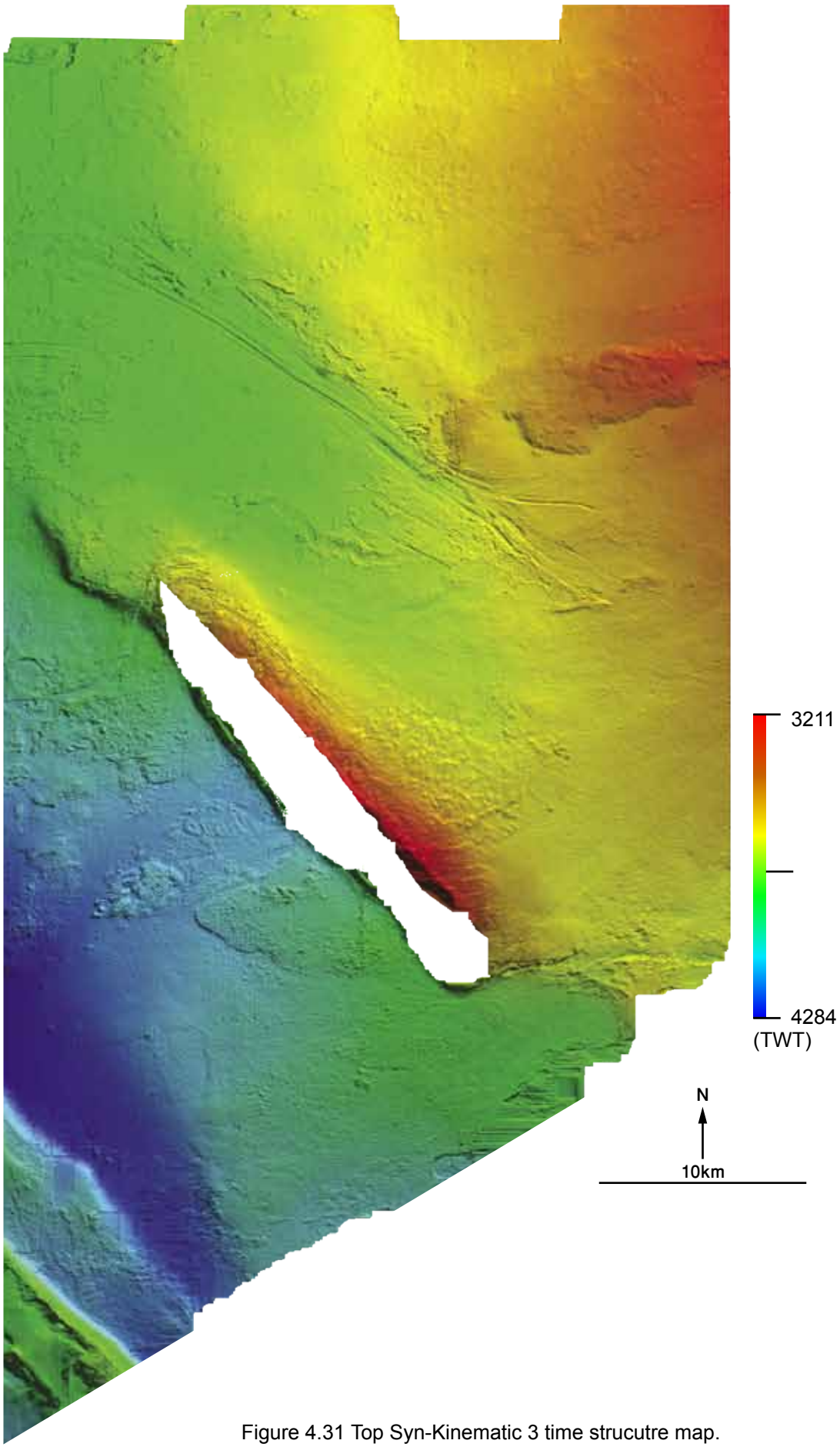

Figure 4.31 Top Syn-Kinematic 3 time strucutre map.

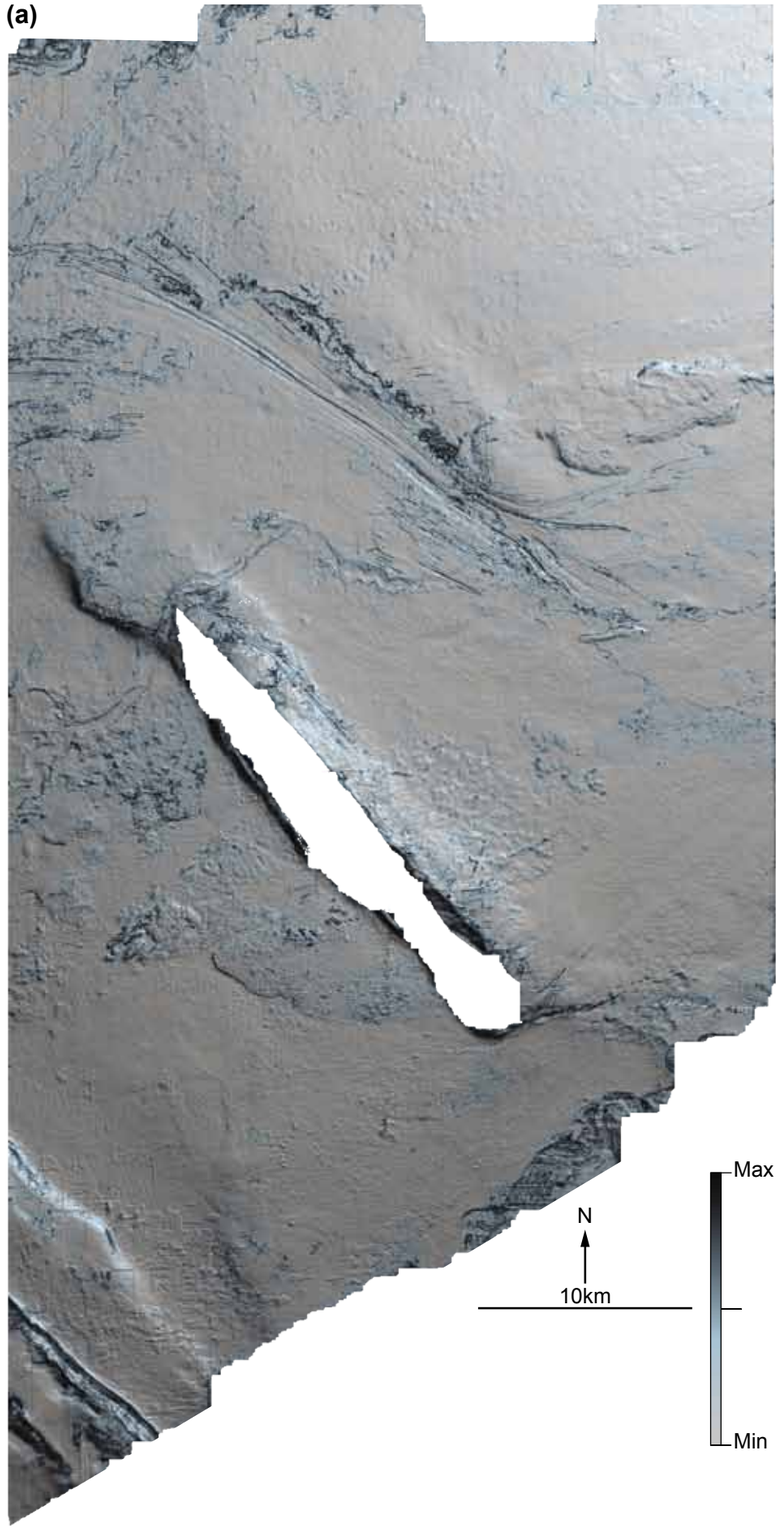

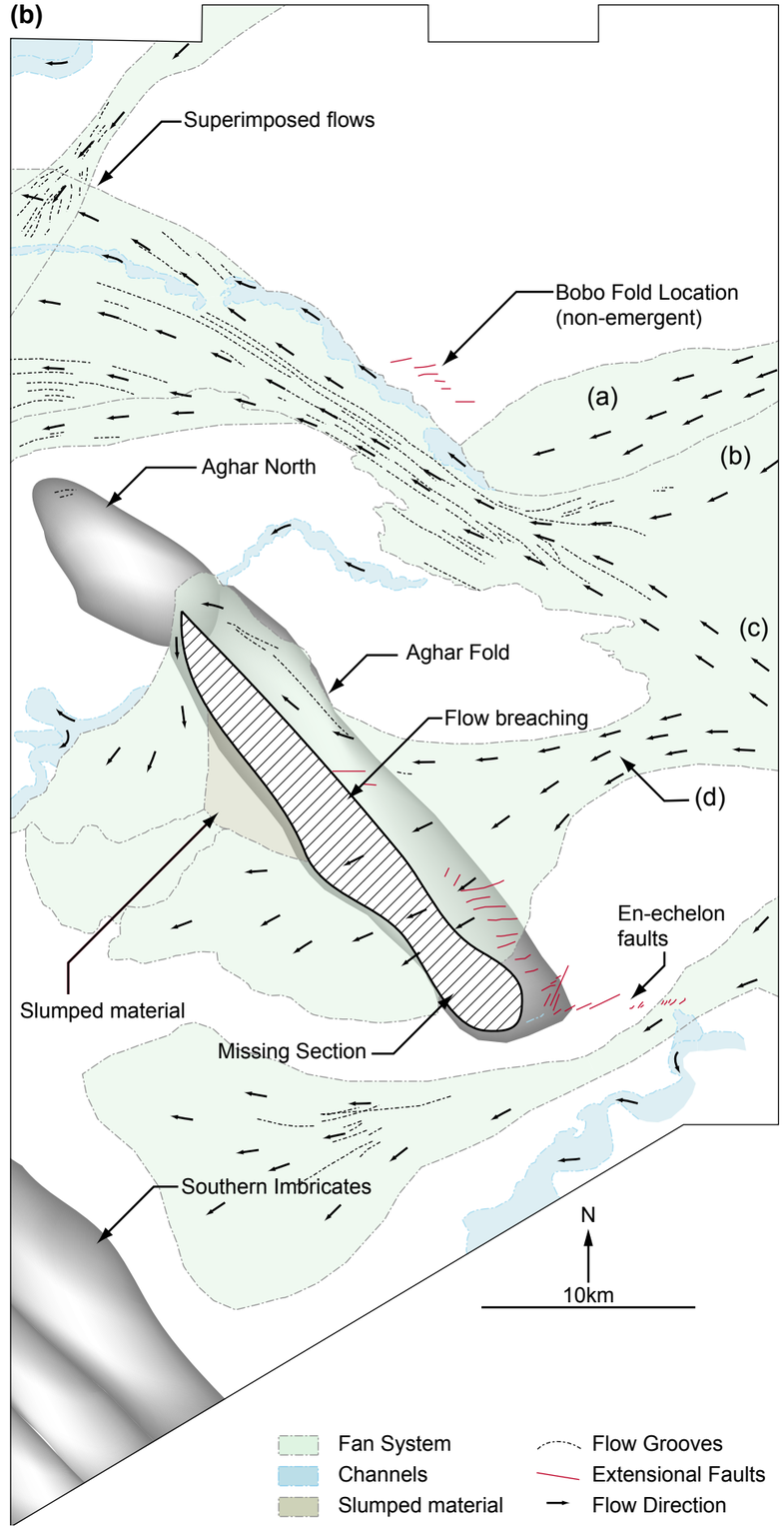

Figure 4.32 : Top Syn-Kinematic 3 dip-corrected coherency map and interpreted map section.

Interpreted by integrating dip-corrected coherency, TWT structure map (Figure 4.31), and RMS maps (Figure A.12 &Figure A.13).

on the Bobo fold (Fig. 4.31). The Southern imbricates also create some relief, especially the two SW folds (Fig. 4.31). The Aghar South is not emergent on this surface and does not create any relief. The horizon also has a missing section at the forelimb of the Aghar Fold associated with the scarp face ~24 km long and ~2.5 km wide. The scarp produces slumped complexes along the scarp face (Fig. 4.32).

On the backlimb of the Aghar Fold, a set of conjugate fractures trend N75°E – N94°E and N60°E – N70°E and vary in length from 0.5 – 7 km in length. Additionally, several fractures are developed above the non-emergent Bobo fold, trending N87°E – N90°E. To the south, a series of ~N30°E – N65°E en-echelon faults (0.5 – 3.2 km long) developed between the Aghar Main and Aghar North structures.

This horizon is dominated by fan and unconfined sheet flows and shows some evidence of channel development, although the latter has probably occurred at a higher level and only deeply eroded channels appear on this surface. The two main flow entry points are identified; one to the mid-east of the survey area and another to the SE. The mid-east fans have a wide entry point ~19.5 km wide. The fan consists of at least four separate turbidite flows (Fig. 4.32); two northern flows (a) and (b) flowed in a NE to SW direction, the SE to NW flow (c) and the E to W flow (d). Flows (a), (b) and (c) all converge over Bobo South, flow in a SE to NW direction following the structural strike and create multiple fan complexes north of Aghar North fold. Multiple groove features up to 23 km long are associated with these flows. Turbidite flow (d) enters the survey area and spreads across the Aghar Fold. Some of the flow goes to the NW and is confined between the Aghar and Aghar North saddle point. However, the majority of the flow overcomes the Aghar Fold, and deposits a fan to the SW of the Aghar Fold.

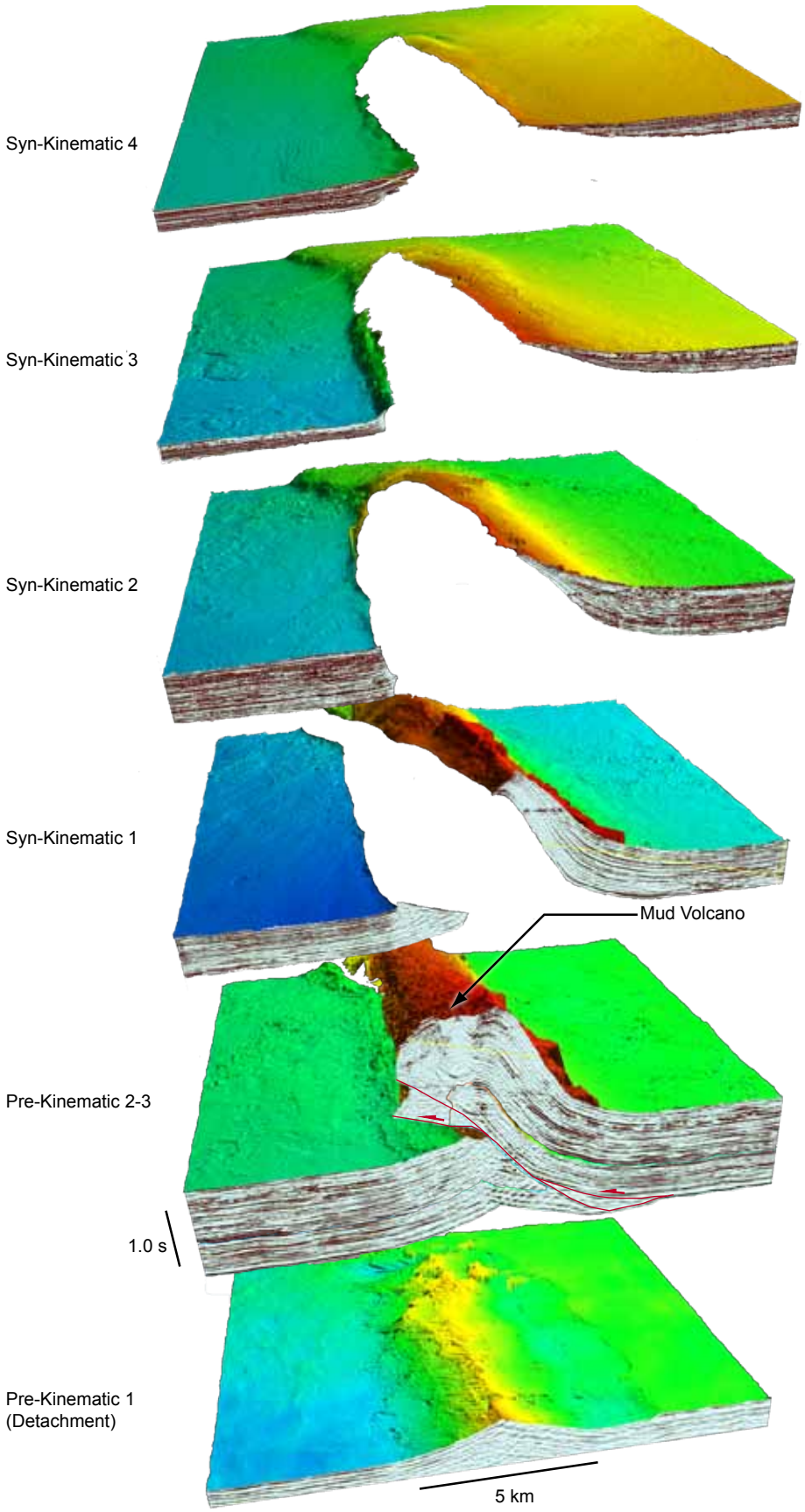

Figure 4.33 3D Visualisation of a section from the Aghar Fold showing the different geometries of the syn-kinematic megasequence. The bottom section shows the Top of the Pre-Kinematic 1 (PK1), which is also Top detachment surface.

4.5. Syn-Kinematic Sequences

The syn-kinematic units are used to determine the growth history of the folds within the 3D seismic survey (Fig. 4.33). Incorporating syn-kinematic geometries in the detailed seismic section with the regional lines, provides an understanding of how these structures evolve with time as well as the kind of deformation taking place.

The syn-kinematic sequences show a backlimb fanning geometry, indicative of fold growth with en-echlon limb rotation. Each mega sequence consists of smaller sequences that onlap on a condensed section. These onlapping reflectors are described as either parallel to semi parallel.

The main factors that determine the geometry of the syn-kinematic units are the sedimentation and growth rates as well as post-depositional erosion. Missing section and gaps in the syn-kinematic units are attributed to uplift and erosion or have not been emplaced due to a topographic high. Both apply to the Aghar Fold; fold degradation and erosion (Fig. 4.13 - 4.16) as well as thinning on topographic highs (Fig. 4.11 - 4.12 and Fig. 4.34 - 4.37). The Bobo fold on the other hand does not show thinning of syn-kinematic units, which indicates either high sedimentation rates or weak fold growth.

4.5.1. Thickness map interpretation

Time and depth thickness maps or isochron and isopach maps respectively are derived for the four growth sequences. These isochron/isopach maps are used for interpreting thinning caused by structural growth of the fold. The final results are used to create the evolutionary model in the discussion chapter.

Syn-Kinematic 1 Sequence

TWT: 0 – 1000 ms Depth: 0 – 1701 m

This is the lowermost syn-kinematic sequence and shows evidence of the initial

stages of fold growth in the area. This syn-kinematic unit shows indication of the growth of the central part of the Aghar, Central Bobo, and Bobo South folds. The North Bobo and Southern imbricates remain dormant. The isochron has two main minima that occur at the centre of the Aghar and Bobo fold crests (Fig. 4.34).

The Aghar Fold has a thinned area ~14.6 km long and ~3.3km wide located within the northern segment of the fold. The ~6.7 km section that corresponds to the centre of the Present Day Aghar Fold is thinnest. Some thinning occurs in the hanging wall of the Aghar North and South.

The Bobo fold also has a thinned segment that dominates the Central Bobo (~15km long and up to 4km wide). However, Bobo North and South show no evidence for thickness variation in this isochron, even though the latter shows some indication in cross-section.

Syn-Kinematic 2 Sequence

TWT: 0 – 750 ms Depth: 0 – 1221 m

The second syn-kinematic unit shows growth on all folds; thinning of the section is observed above the Aghar and Bobo folds as well as the one of the Southern Imbricates (Fig. 4.35). Sedimentary features such as channels cause some thickening of the sequence.

The Aghar Fold has a thinned segment that extends for the majority of the present extent of the fold. In the crestal area, a missing section extends ~20 km long by ~3.2 km wide. The Aghar South also shows some thinning, and similarly the Aghar southern part of the Aghar North.

The Bobo fold shows a thinning sequence that extends over the entire length of the Bobo North, Central and South. In particular in the overlap area between the Central Bobo and Bobo South, which shows a subtle thinning compared to the

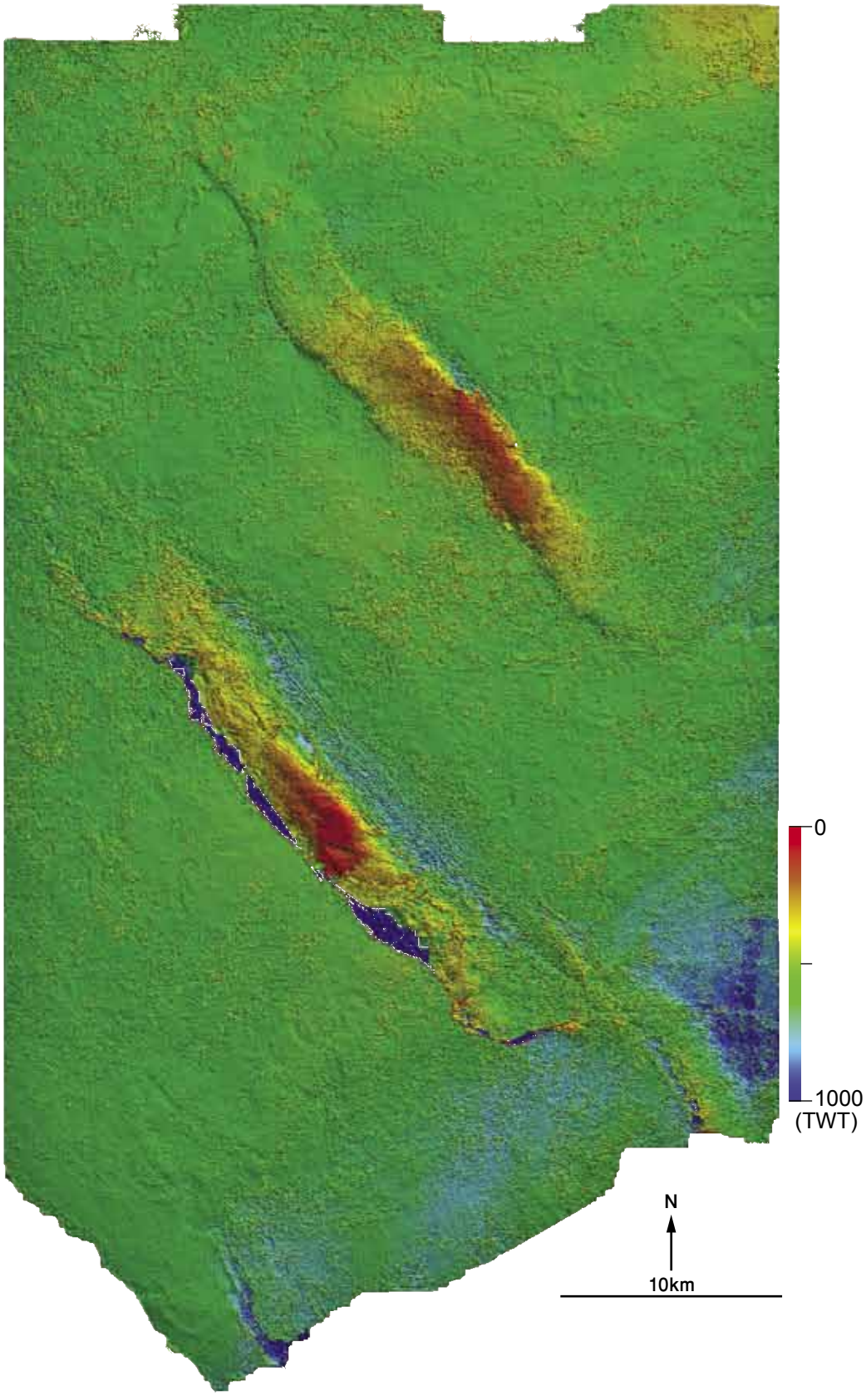

Figure 4.34 Syn Kinematic 1 time thickness map (Isochron)

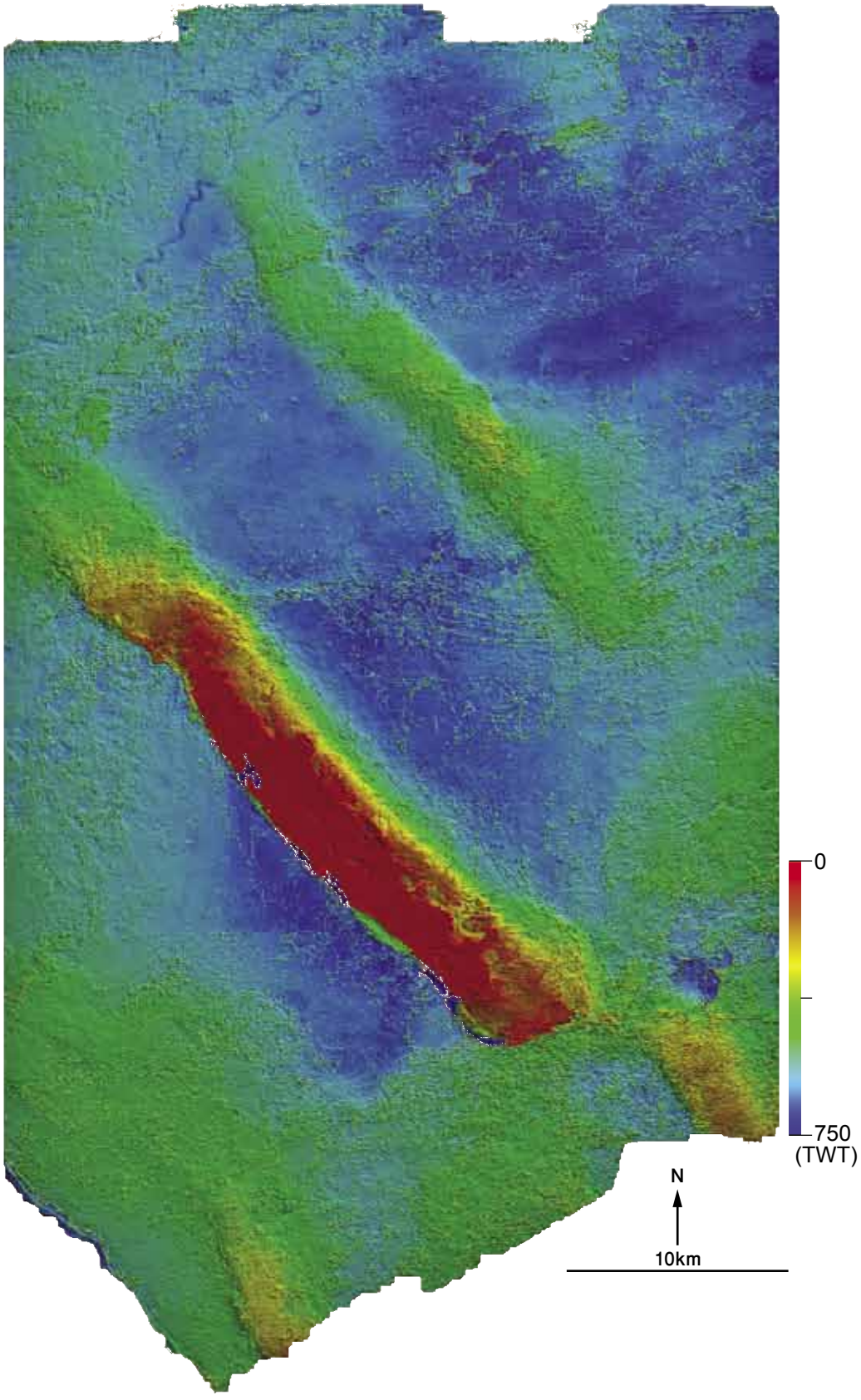

Figure 4.35 Syn Kinematic 2 time thickness map (Isochron)

rest of the Bobo fold.

Syn-Kinematic 3 Sequence

TWT: 0 – 410 ms Depth: 0 – 467 m

The Aghar Fold continues to grow during the Syn-Kinematic 3 period, while the Bobo fold shows a reduction in growth rate and becomes inactive in the south. The Aghar Fold creates a 26.4 km long by 5 km wide thinning sequences that is dominated by a 24.6 km by 3 km missing section (Fig. 4.36). The Bobo fold is associated with a subtler thinning (12.6 km long by 3.5 km wide) within the Bobo North and Central segments of the fold. The Southern imbricates are also associated with thinning in all three folds. Some thickening related to sedimentary features such as grooves SW of the Bobo Fold and submarine fans also occur in this sequence.

Syn-Kinematic 4 Sequence

TWT: 0 – 396 ms Depth: 0 – 362 m

This sequence shows a thinning towards the Aghar Main, and North Aghar Folds. The thinning is also accompanied by a missing section 24.5 km long and 2.8 km wide. In general, the Aghar North and Main fold follow a similar thinning trend. The Bobo fold becomes dormant with little or no indication of growth along the fold segments.

The Southern imbricates also have a thinned section. However, to the NE of the imbricates is a thickened area that may be related to the sedimentation being blocked by growth of the imbricates. The NE fold of the Southern imbricates is likely to have ceased growth during this period, whereas the two folds to the SW are active to the Present Day.

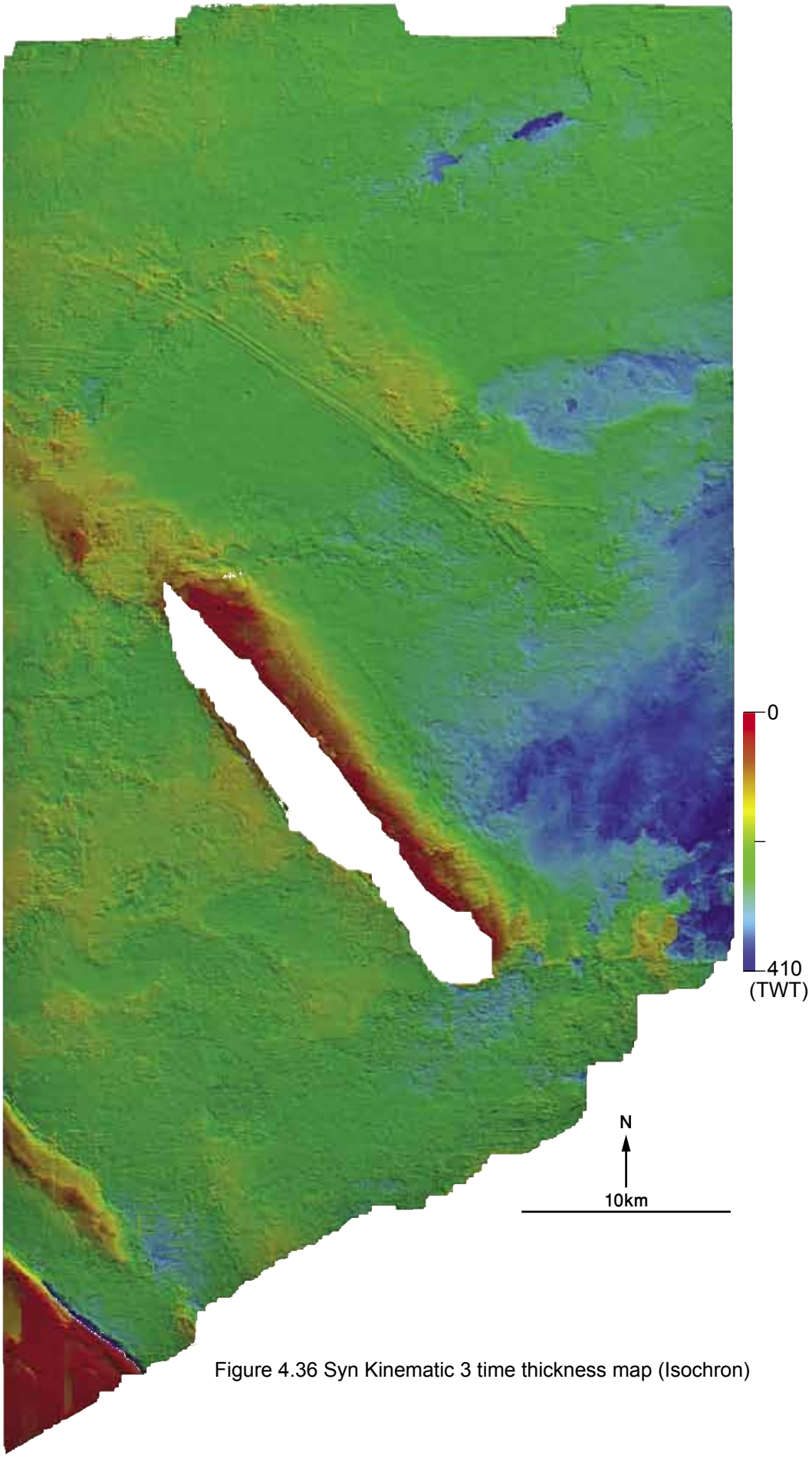

Figure 4.36 Syn Kinematic 3 time thickness map (Isochron)

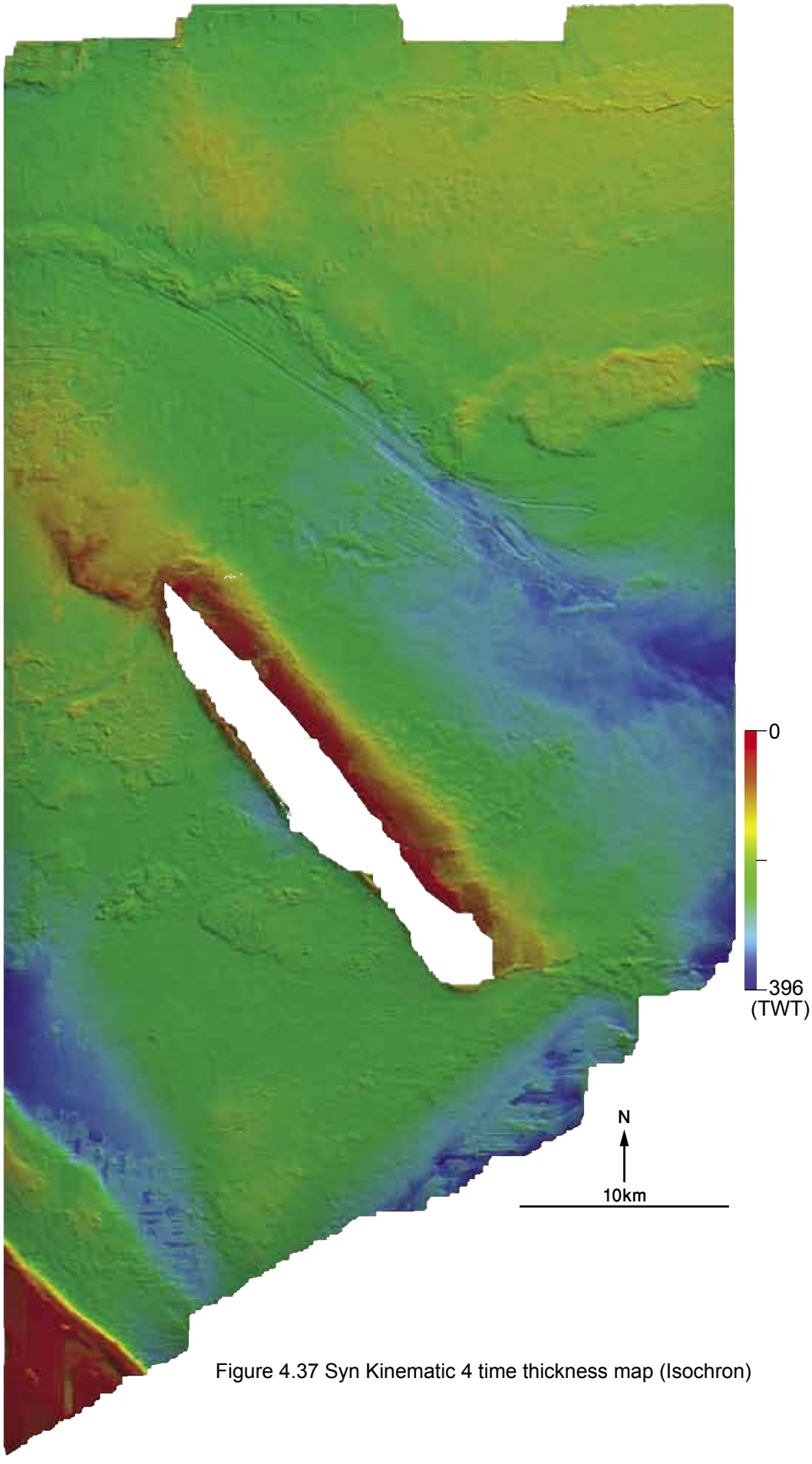

Figure 4.37 Syn Kinematic 4 time thickness map (Isochron)

4.5.2. Implications of the Regional Syn-Kinematic Geometries

This section compares the different growth stratal geometries associated with the structures within the 3D area.

Oligocene to Lower-Miocene

This is the pre-kinematic period. There is no movement occurred on any of the structures.

Lower- to Mid-Miocene

At this time, movement initiated in the Aghar and Bobo Folds. For the Bobo fold, this a phase of maximum shortening, while the Aghar fold was amplifying at a slower rate. The Southern Imbricates have not yet began growth.

Upper Miocene

During this period, the Aghar fold begins to amplify and shorten at higher rate, while the growth of the Bobo fold begins to decelerate. This period also marks the most rapid growth of the Southern imbricates.

Pliocene to Present Day

Rapid growth continues on the Aghar Fold and Southern Imbricates. The Bobo Fold continues to decelerate during the Pliocene, and ceases completely during the Quaternary.

4.6. Summary and Discussion

4.6.1. Regional structure of the Western Lobe in the Niger Delta

- Pre-Niger Delta sediments may have undergone thick-skinned deformation over the oceanic basement; however, this is not observed in the Niger Delta sequences.

- The direction of thin-skinned tectonic transport is towards the basin.

- Basinward-vergent extensional faults dominate the proximal parts of the delta and may have overprinted previous compressive structures. The largest displacements occur on the eastern faults (landward vergent) and are likely to be older than the younger more distal fault that show smaller displacements.

- Syn kinematic sequences show that the deformation migrates basinwards.

- The inner FTB is dominated by basinward-vergent imbricate thrust system that is highly shortened. The Outer FTB has both basinward and landward-vergent FRFs, which develop a thrust triangle.

4.6.2. Structures of the 3D Seismic Survey

- Deformation began within the survey area in the mid-Miocene and continues to Present Day, which is probably the case for other parts of the outer FTB.

- The Aghar and Bobo are fold structures oriented N140°E and separated by 12.5 km. The Bobo formed from three opposite vergent fault-related folds and was only active between the mid-Miocene and early-Pleistocene.

- The Aghar Fold is located within a left-stepping en-echelon series of fault-related folds. The main Aghar and Aghar North overlap and creates a complex thrust fault geometry, whereas the main Aghar and Aghar South are laterally spaced by ~5.4 km and create a series of near-surface extensional en-echelon faults.

- RMS and coherency extraction shows sedimentary feature interaction with structural growth. Turbidite channels and MTCs flows are diverted by folds or ponded between them. In some cases, the flow overflow above structures or are limited to flow at saddle point between structures.

- The decollement is interpreted as an overpressured shale detachment that dips to the SW 0° - 1°.

4.6.3. Syn-Kinematic Sequences

- The growth units show fanning geometries that are caused by the continuous rotation of the hanging wall with increased shortening.

- The Aghar Fold evolved from a ~14.6 km long by ~3.3 km wide structure in the mid-Miocene to the Present Day size in the Pliocene. This indicates that the fold rapidly translates along strike with small displacement.

- Growth stratal geometries in cross section and thickness maps show that initially in the Lower- to Mid-Miocene, growth took place on the Aghar and Bobo Folds. In the Upper-Miocene, growth initiated in the Southern imbricates, and accelerated in the Aghar fold but began to slow down in the Bobo fold. In the Pliocene the Bobo Fold decelerated growth and ceased, while the Aghar fold and Southern Imbricates continue to grow to Present Day.

Chapter 5

Aghar Fold Geometry and Structural Analysis

5.1. Introduction

Chapter 4 provided a general overview of structural and sedimentological features of the western Niger Delta. This chapter focuses on the structural elements of the Aghar fold. It integrates detailed seismic interpretation with quantitative analysis to provide the understanding required to produce the evolutionary model.

This chapter starts with a detailed description of the geometries of the Aghar fold (Chapter 5.2) in terms of entire fold geometry, detachment system, thrust fault geometry, fold degradation and mud volcano. Chapter 5.3 analyses the faults that occur within the fold. The growth strata is analyzed in Chapter 5.4. The chapter ends with a summary and discussion in Chapter 5.5.

5.2. Structural Geometry of the Aghar Fold

The Aghar fold is located between the detachment belt and the outer fold and thrust belt (FTB), at a water depth of ~1400 m. The Aghar fold is a basinward (SW) vergent Fault-related-fold (FRF) associated with a landward-dipping thrust fault complex. The folded structure spans a length of ~34 km and ~6km wide.

The Aghar fold is part of an en-echelon FRFs series oriented ~N140°E. It overlaps with the Aghar North to the north of the fold, and interacts with the Aghar South that is located ~5.4 km to the east of the southern tip of the Aghar Main (Fig. 5.1). The latter causes the development of extensional en-echelon faults in the growth strata.

This section is a detailed description of the Aghar fold based on nine depth-converted (1:1 lateral to vertical ratio) cross-sections spaced 3.5 km (Fig. 5.2) that dissect the Aghar fold.

5.2.1. Fold geometry

The Aghar fold is a ~34 km long and ~4.3 – 7.2 km wide structure that creates

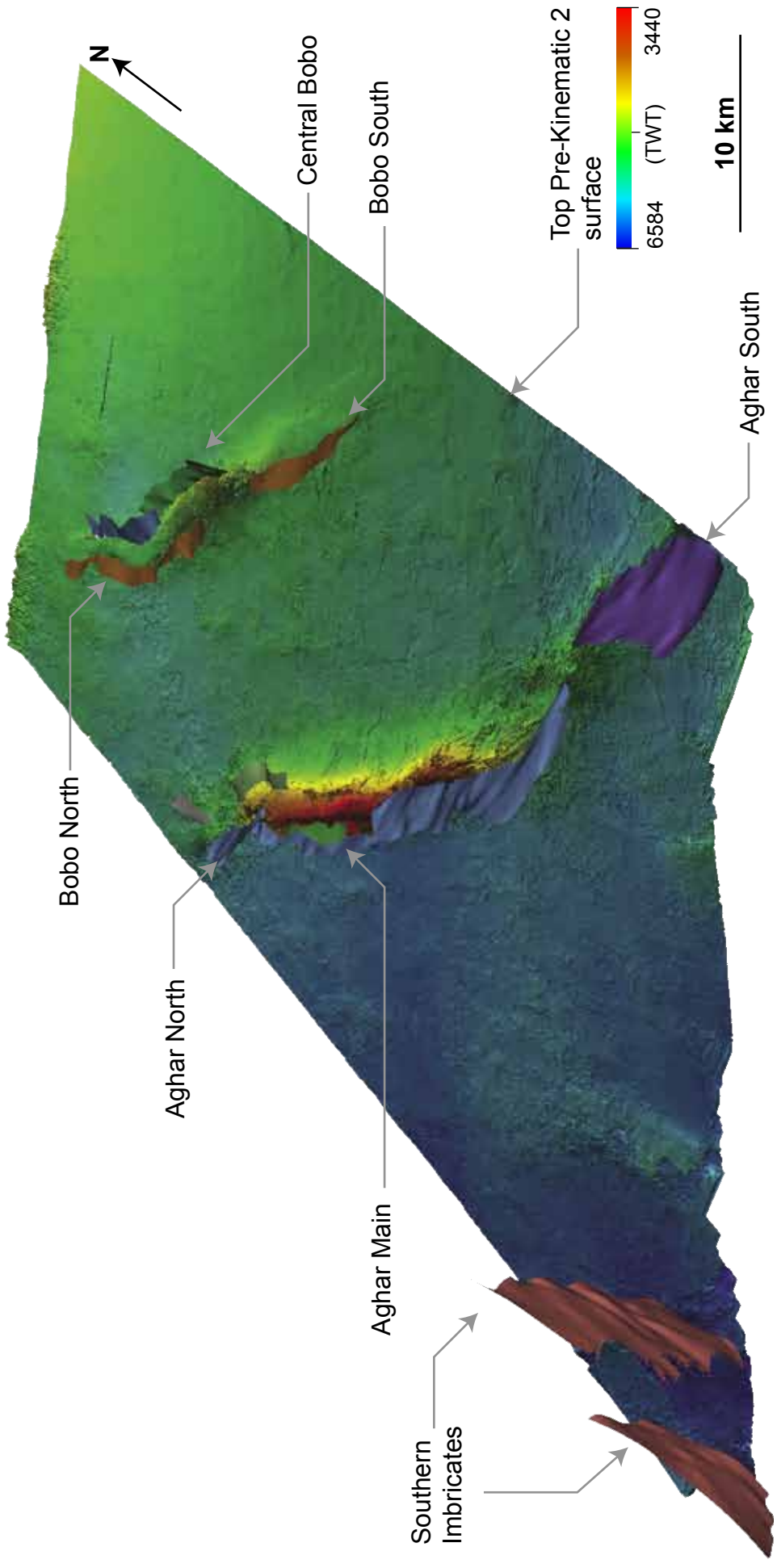

Figure 5.1 3D perspective view of the Top Pre-Kinematic 2 surface and major fault systems. For a detailed view of the faults see figure 5.22

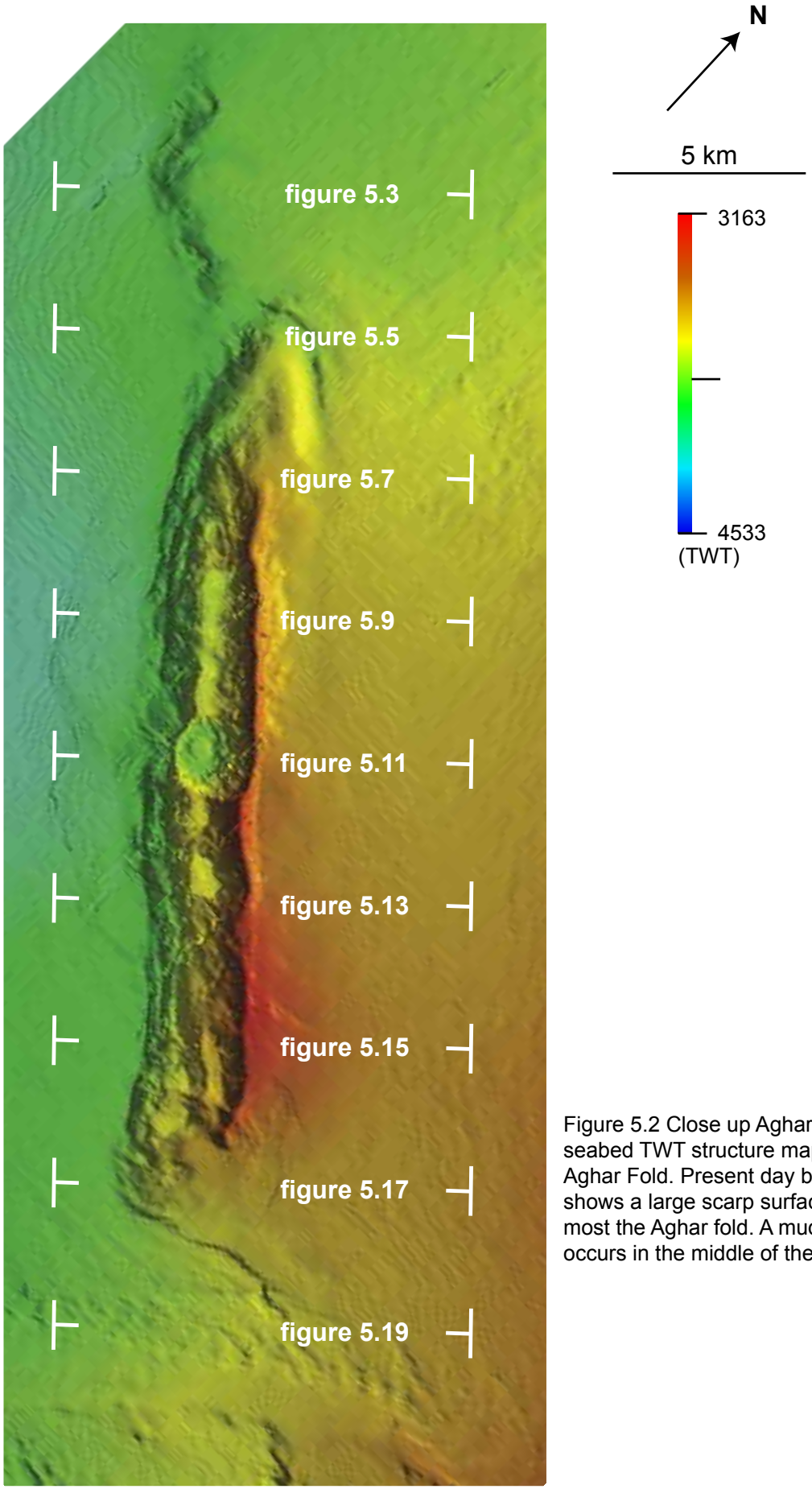

Figure 5.2 Close up Aghar Fold seabed TWT structure map of the Aghar Fold. Present day bathymetry shows a large scarp surface along most the Aghar fold. A mud volcano occurs in the middle of the fold.

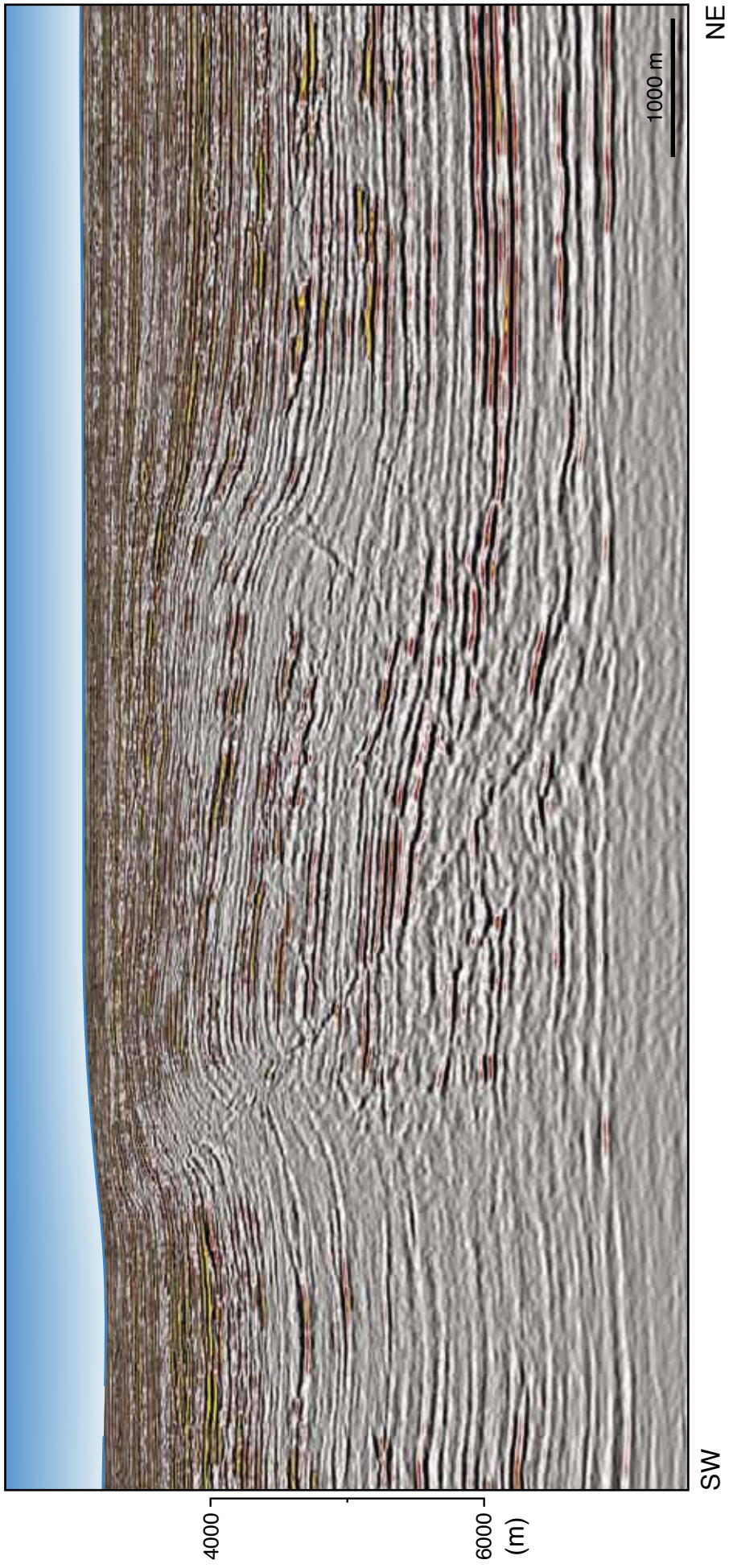

Figure 5.3 Aghar Cross section I - amplitude display

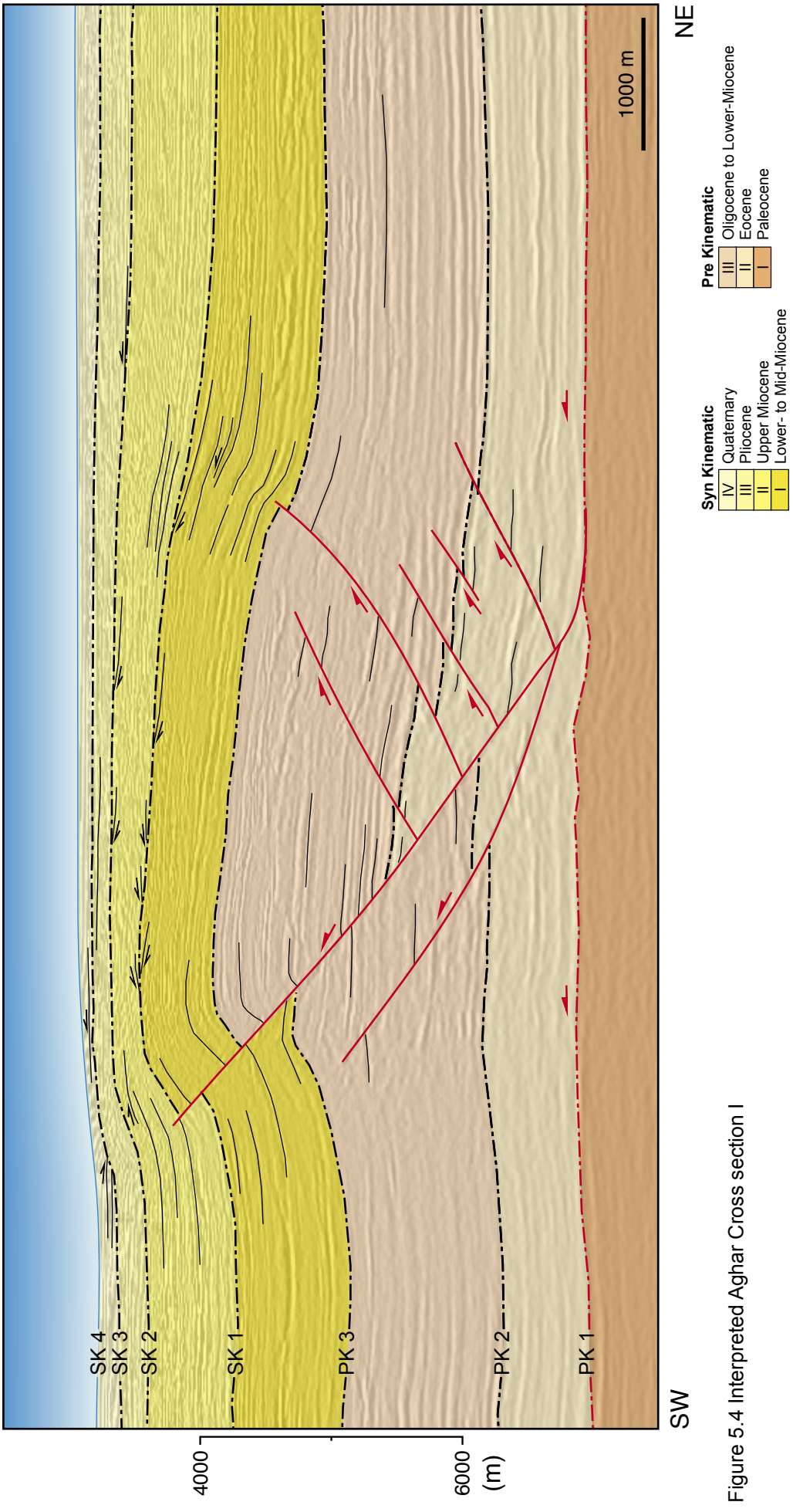

Figure 5.4 Interpreted Aghar Cross section I

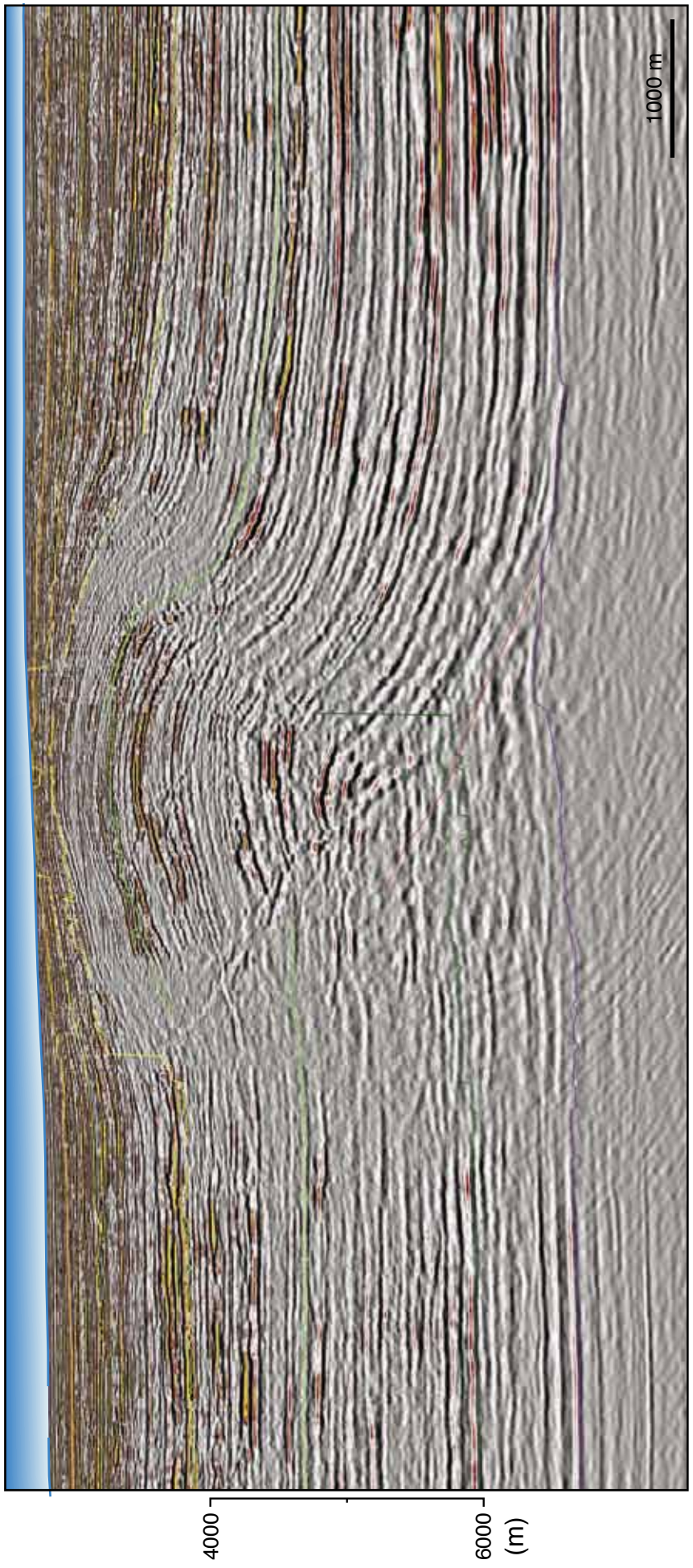

Figure 5.5 Aghar Cross section II - amplitude display

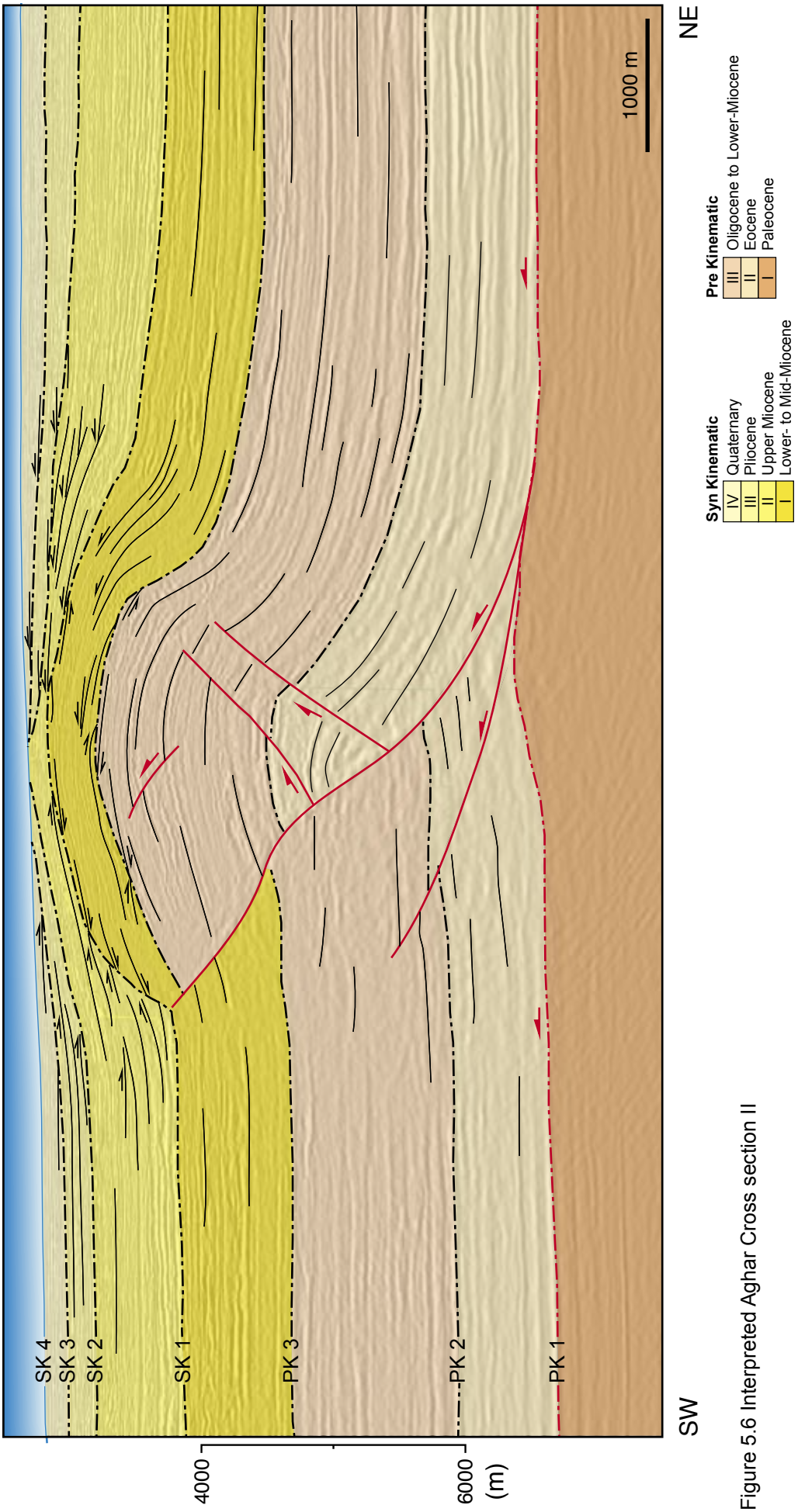

Figure 5.6 Interpreted Aghar Cross section II

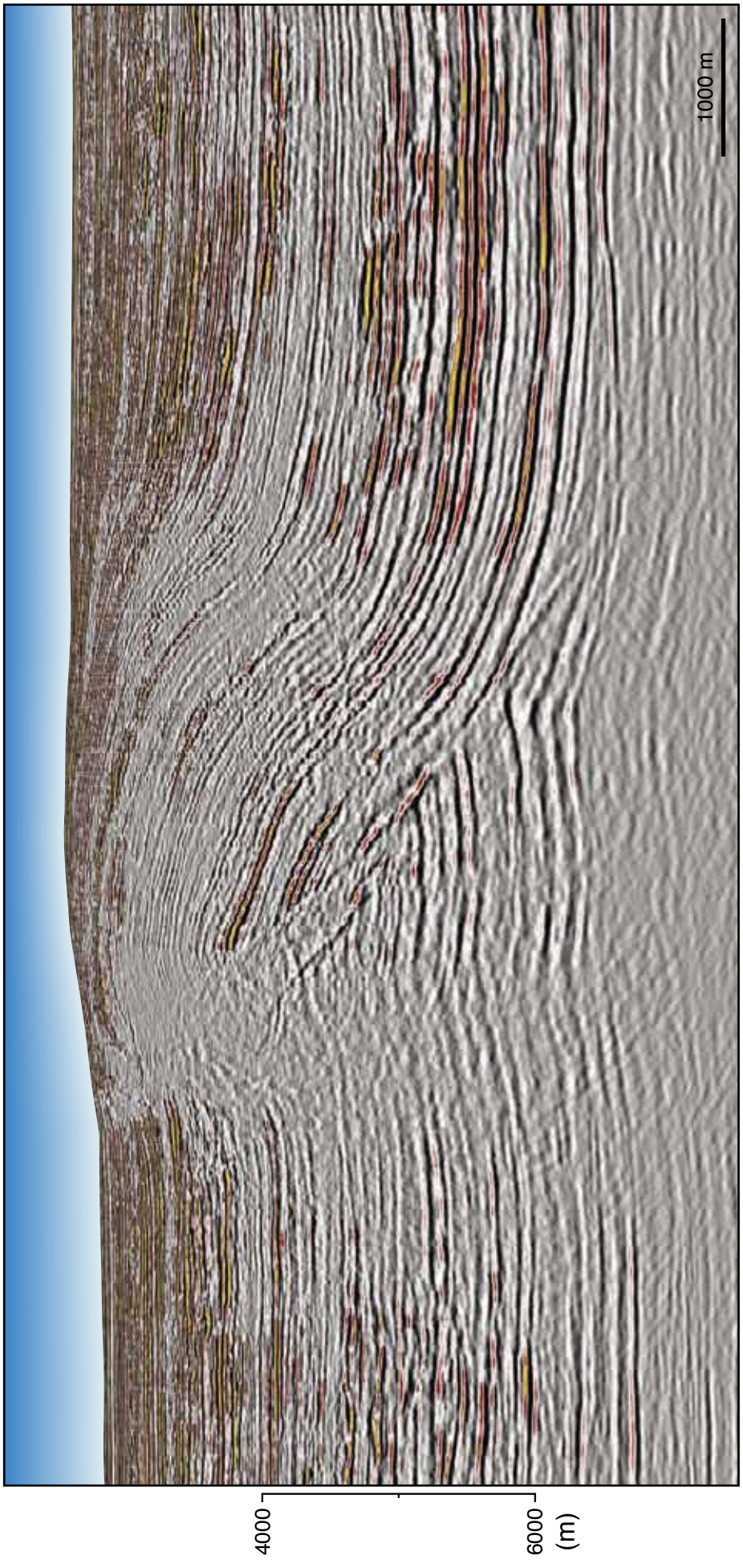

Figure 5.7 Aghar Cross section III - amplitude display

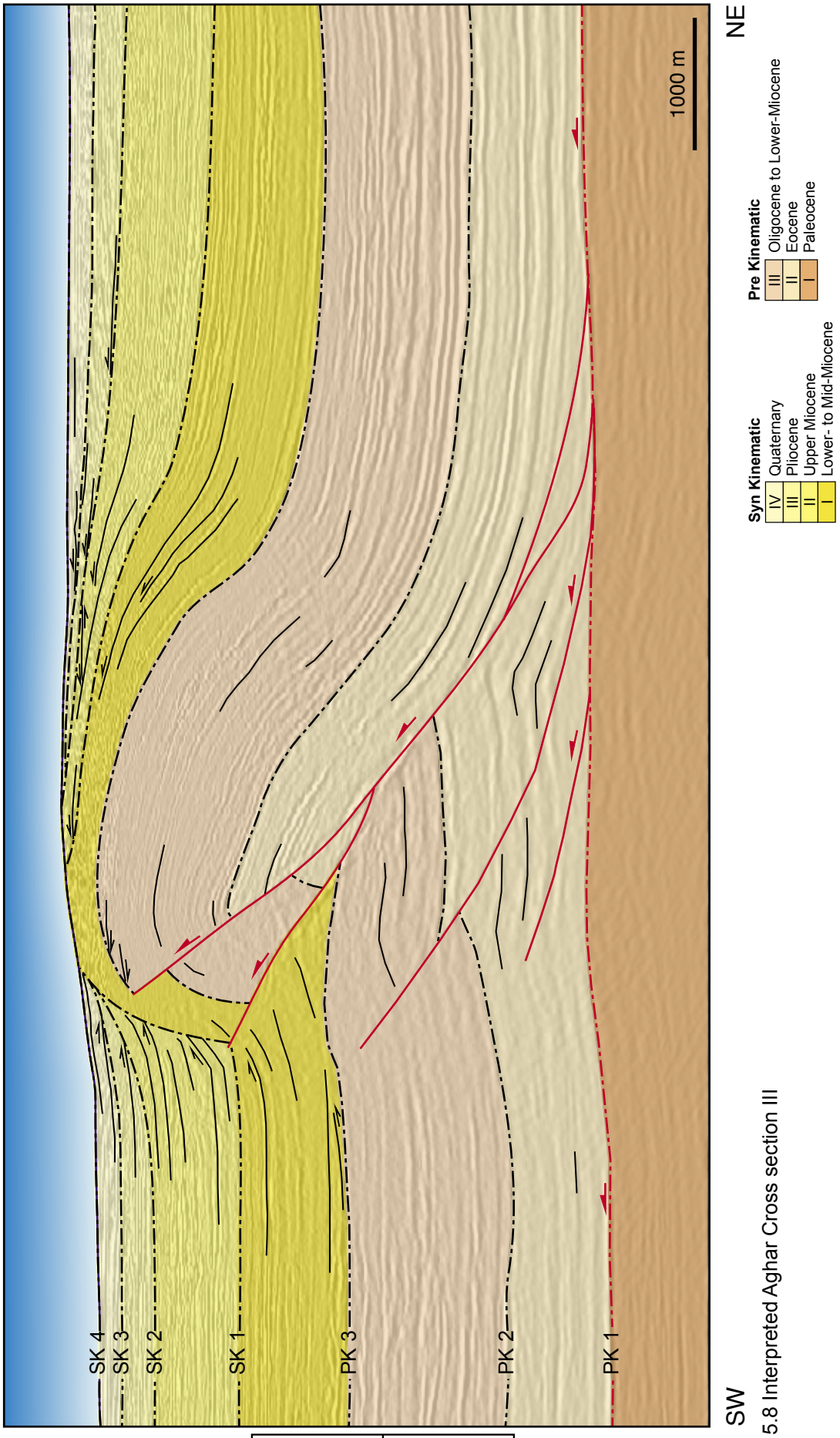

Figure 5.8 Interpreted Aghar Cross section III

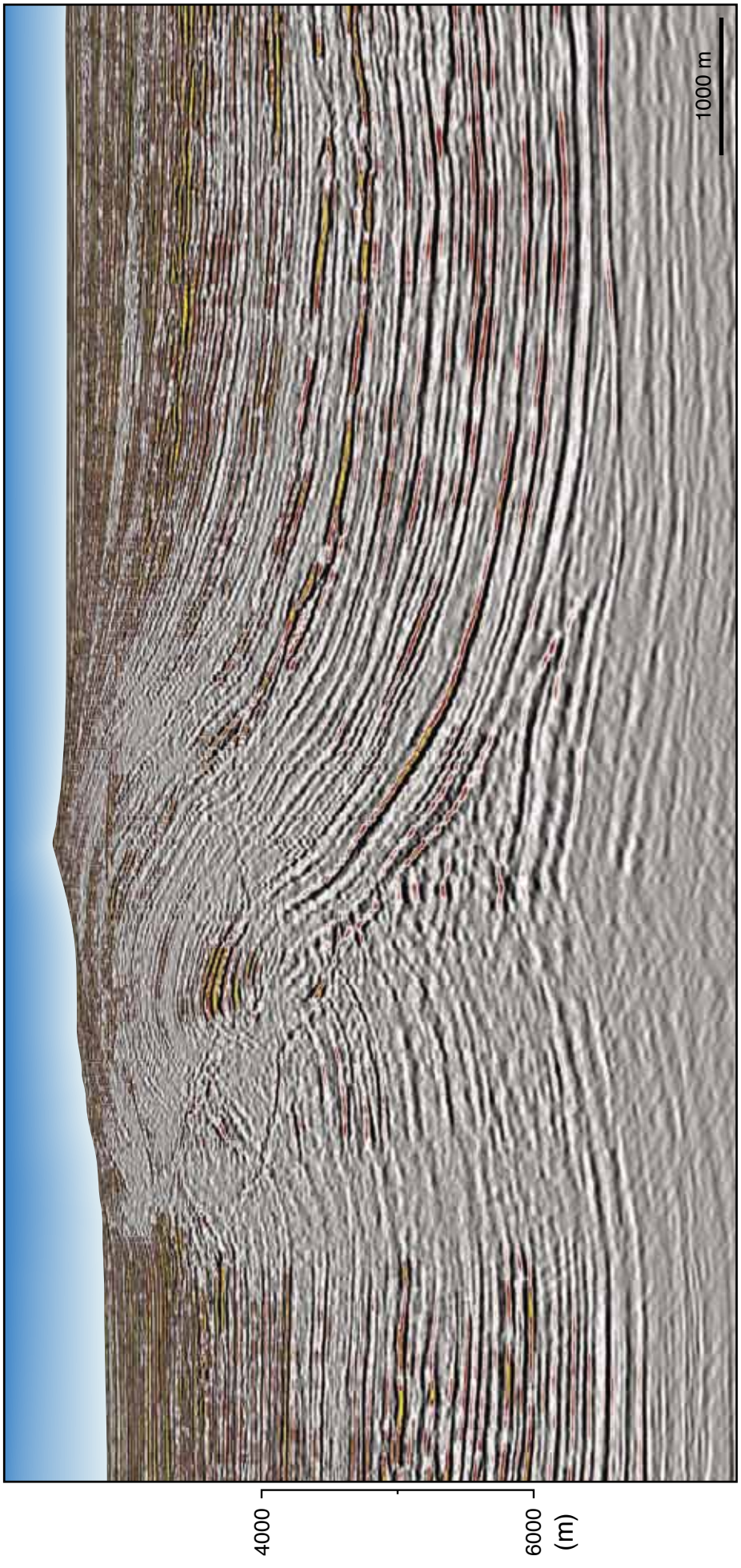

Figure 5.9 Aghar Cross section IV amplitude display

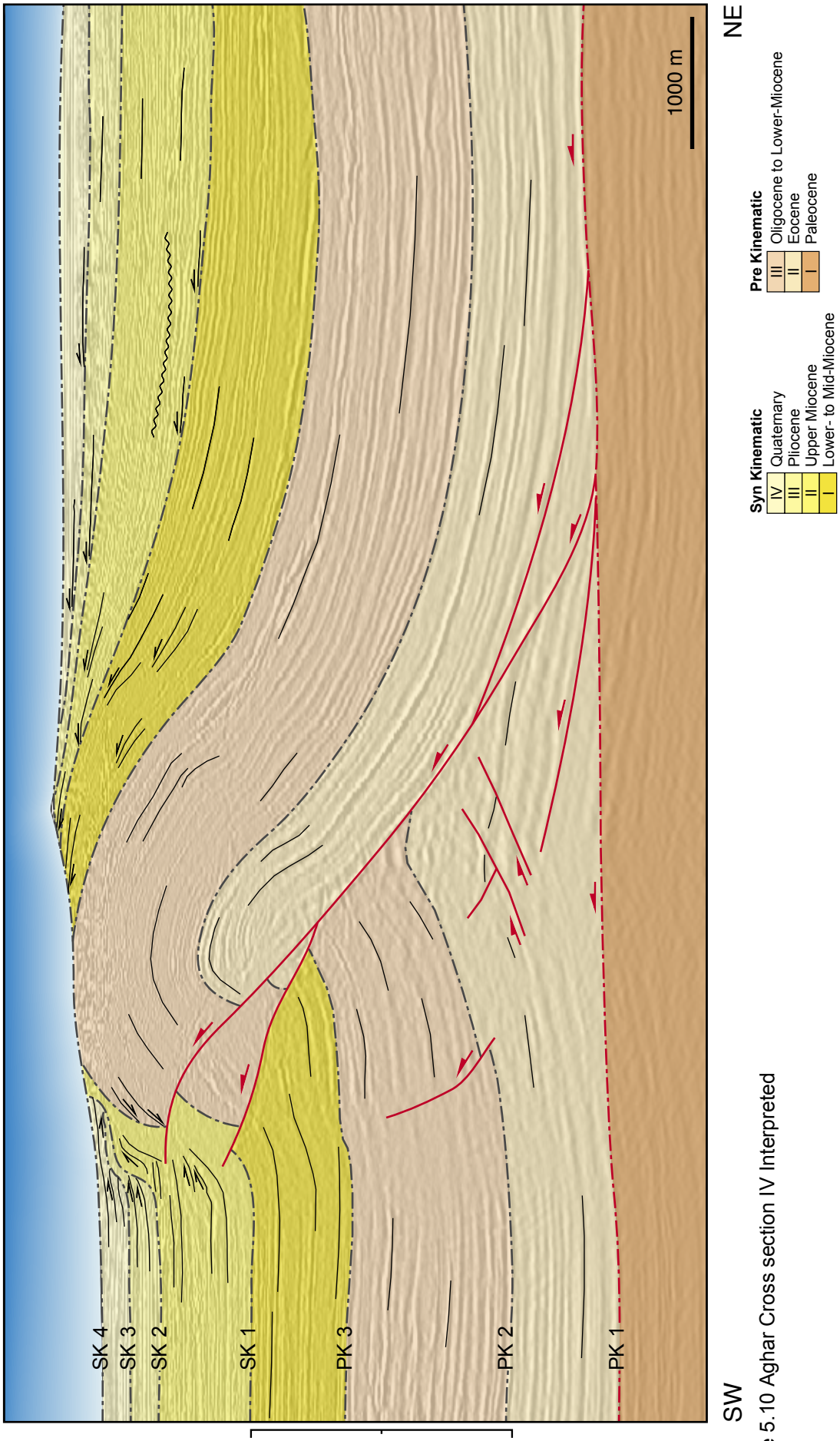

Figure 5.10 Aghar Cross section IV Interpreted

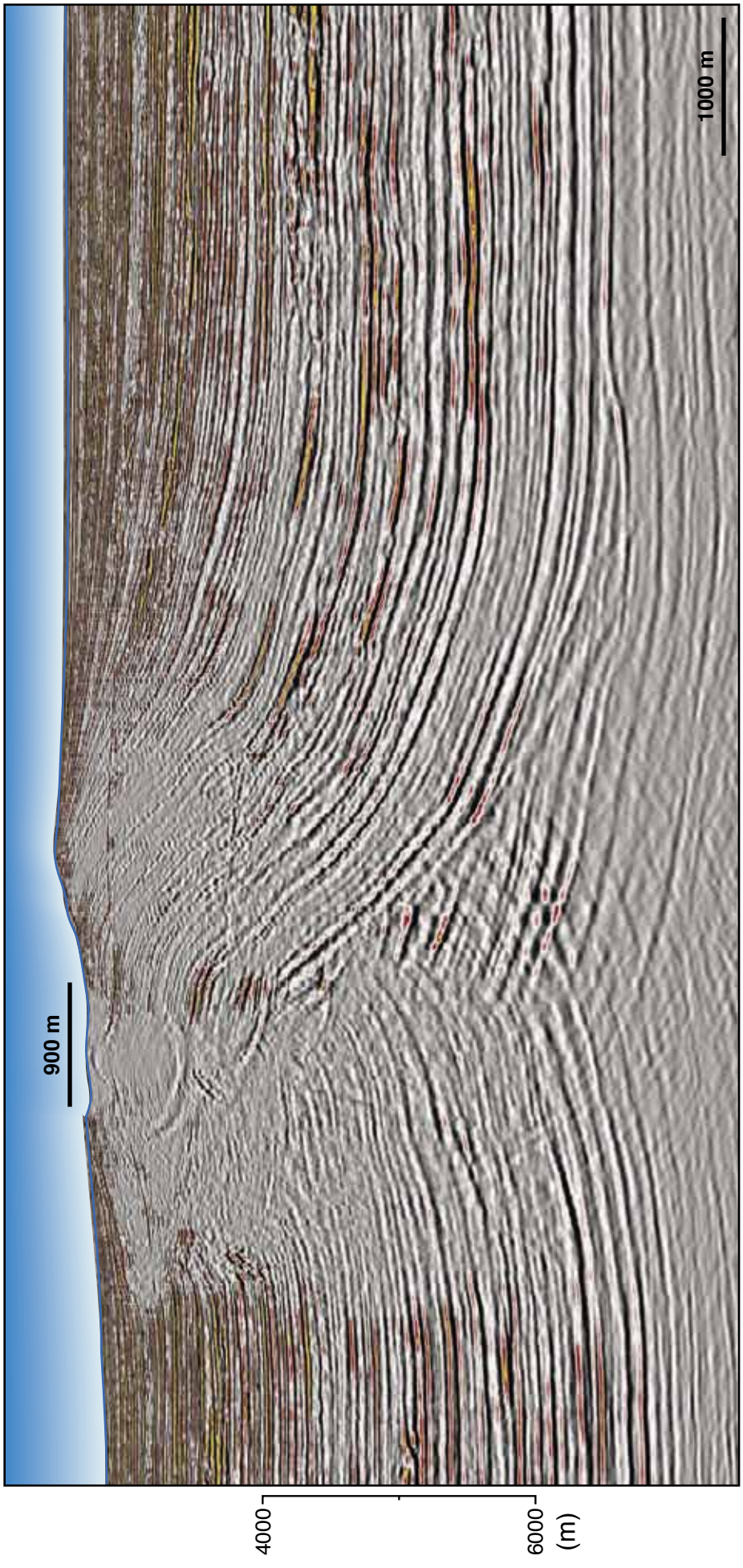

Figure 5.11 Aghar cross section V amplitude display. The discordance near the seabed at the forelimb highlights the location of the mud volcano ~900m wide.

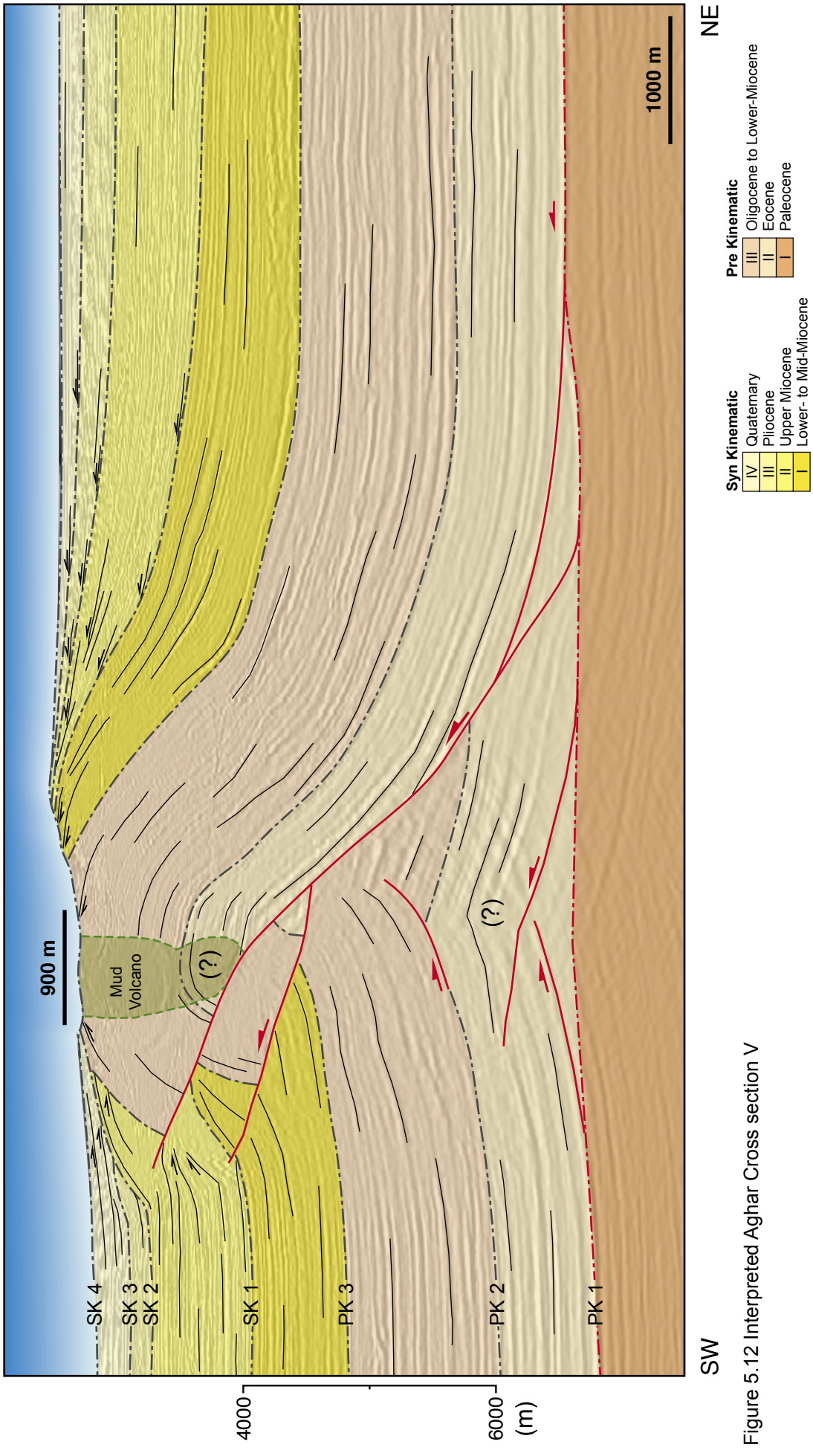

Figure 5.12 Interpreted Aghar Cross section V

Figure 5.13 Aghar cross section VI amplitude display

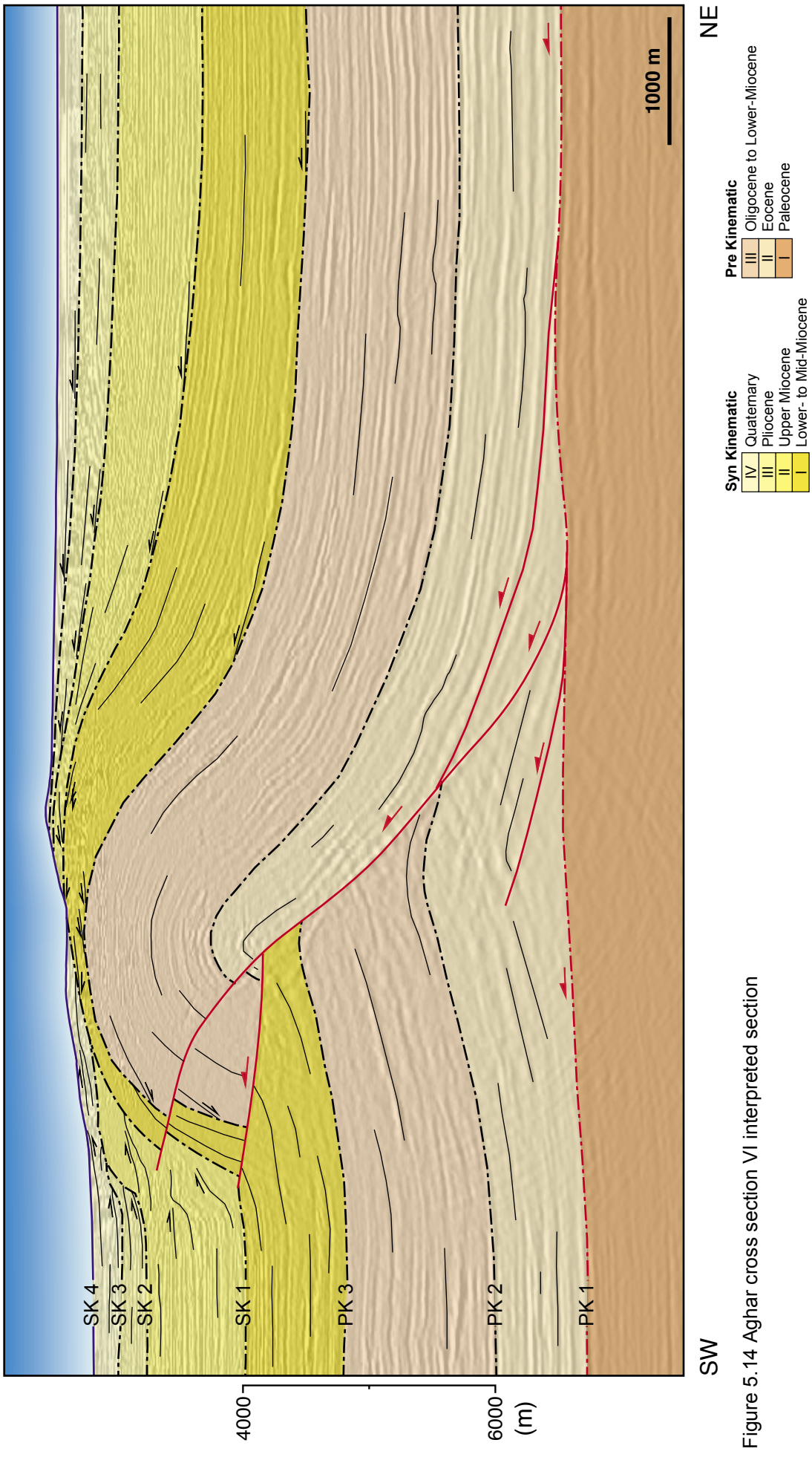

Figure 5.14 Aghar cross section VI interpreted section

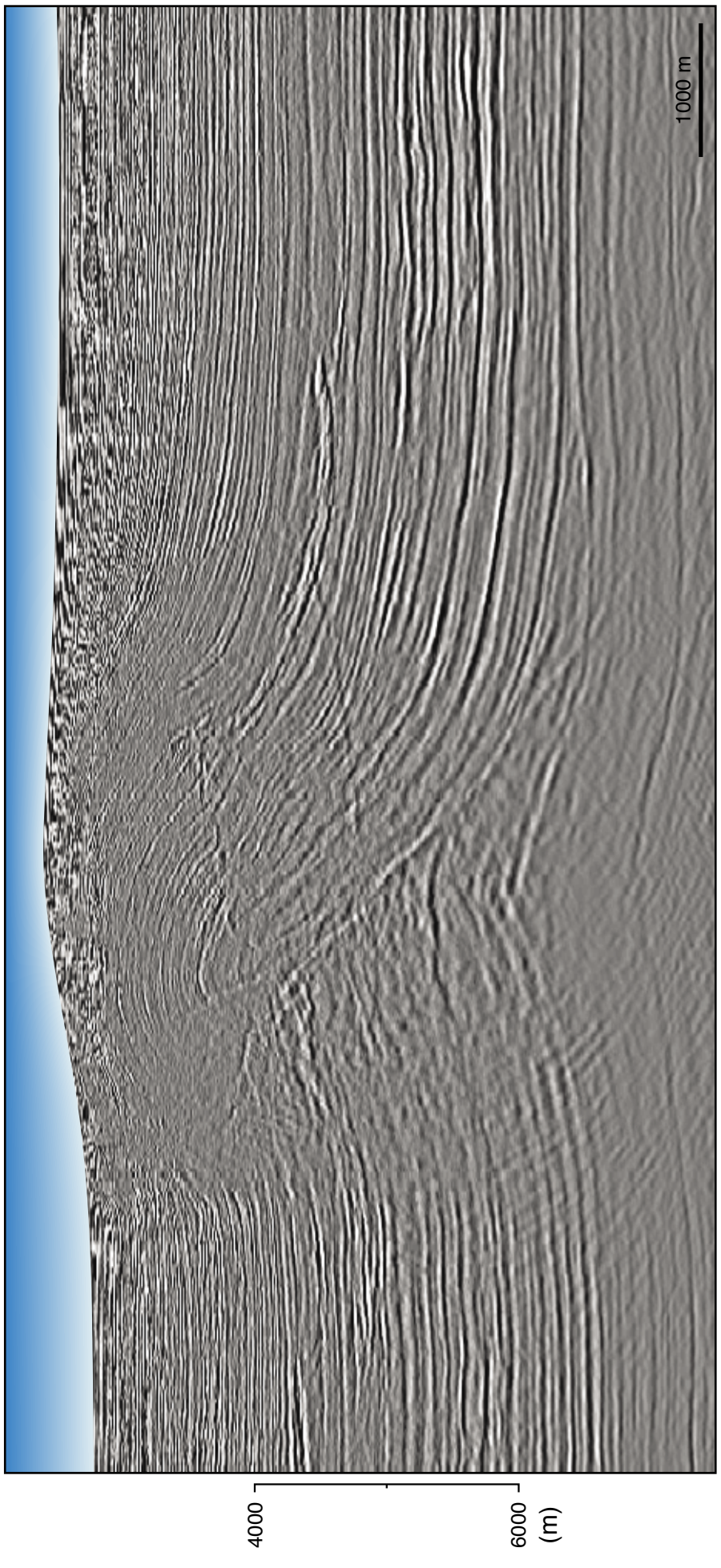

Figure 5.15 Aghar cross section VII amplitude display

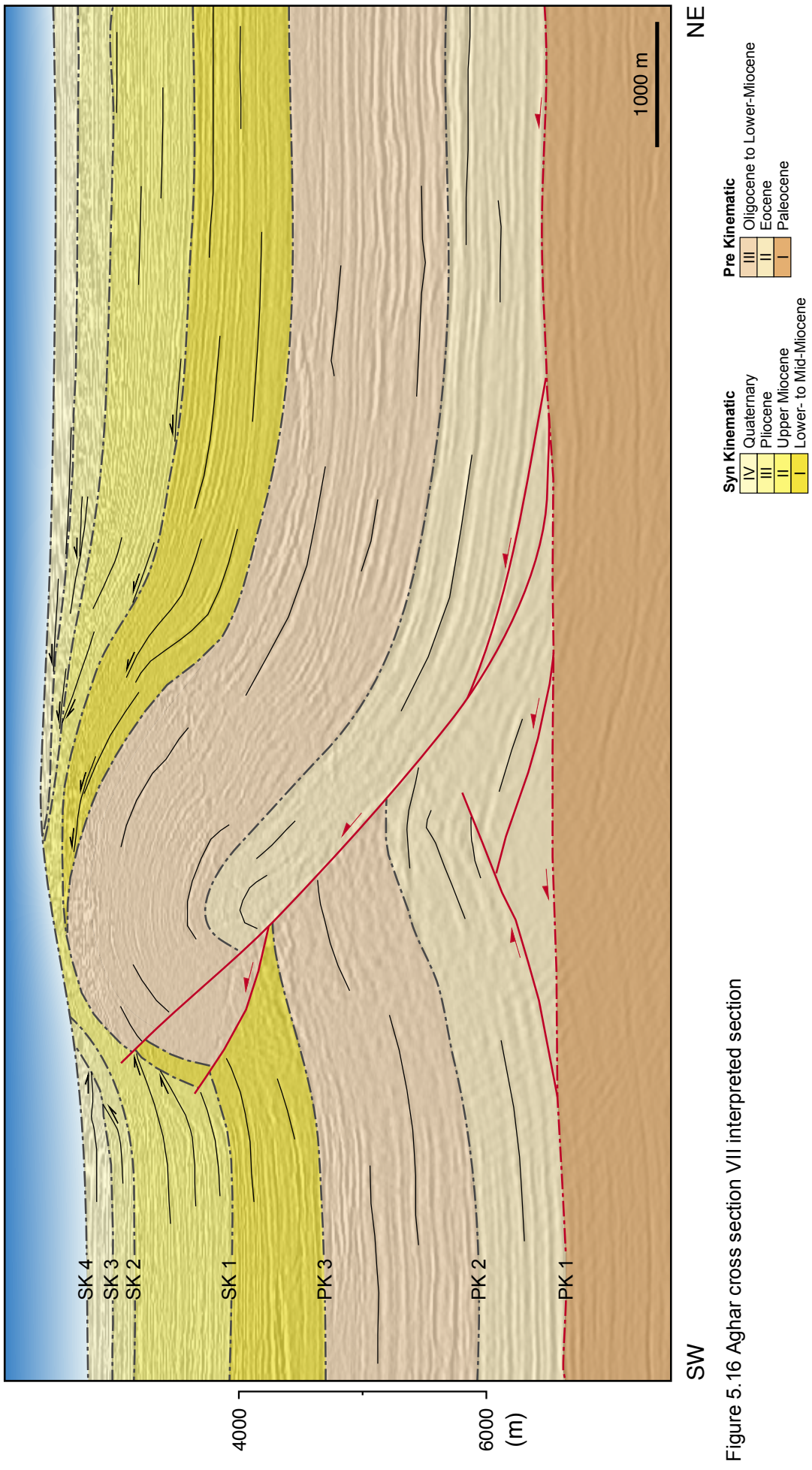

Figure 5.16 Aghar cross section VII interpreted section

Figure 5.17 Aghar Cross section VIII amplitude display

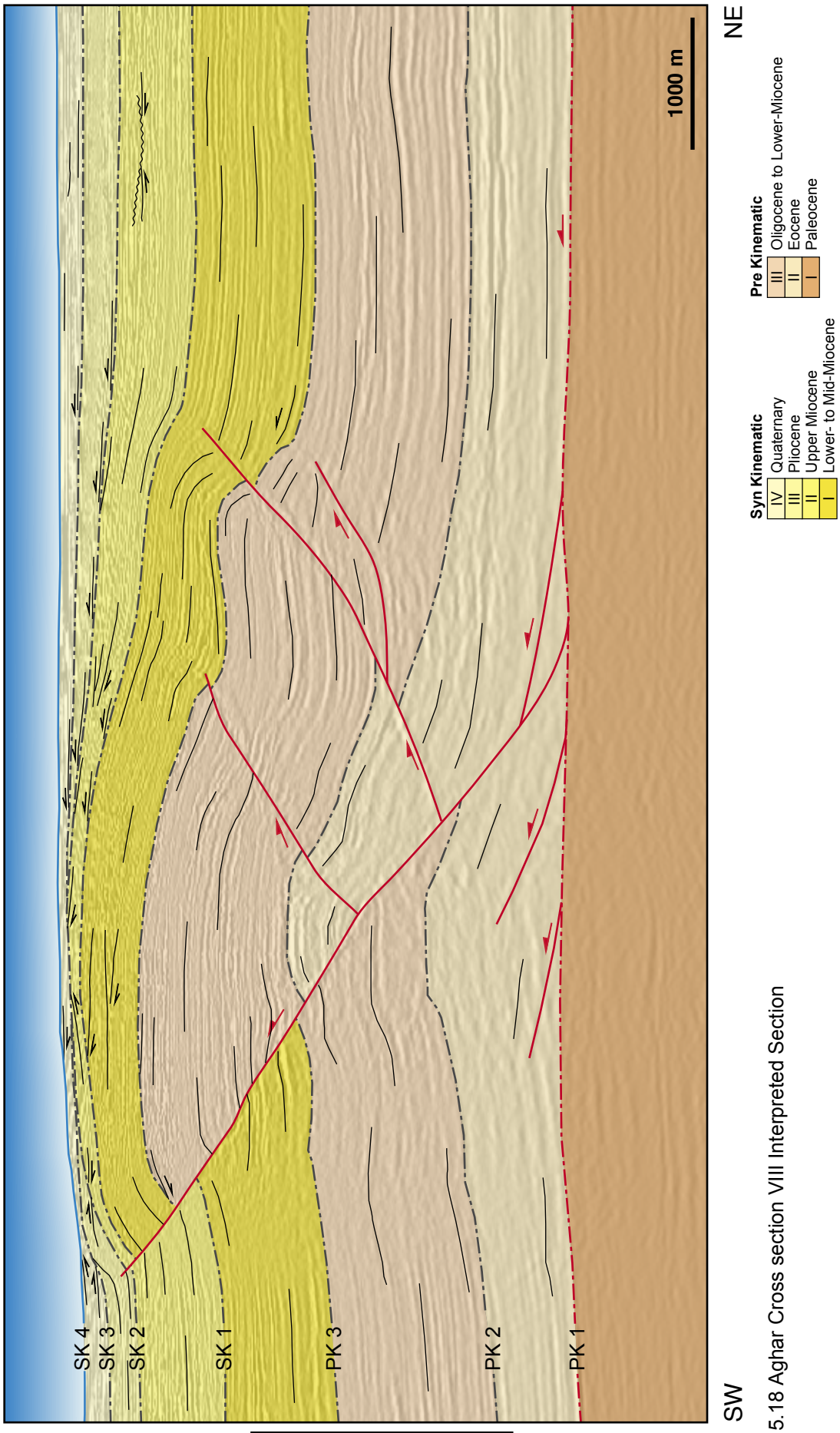

Figure 5.18 Aghar Cross section VIII Interpreted Section

Figure 5.19 Aghar Cross section IX amplitude display

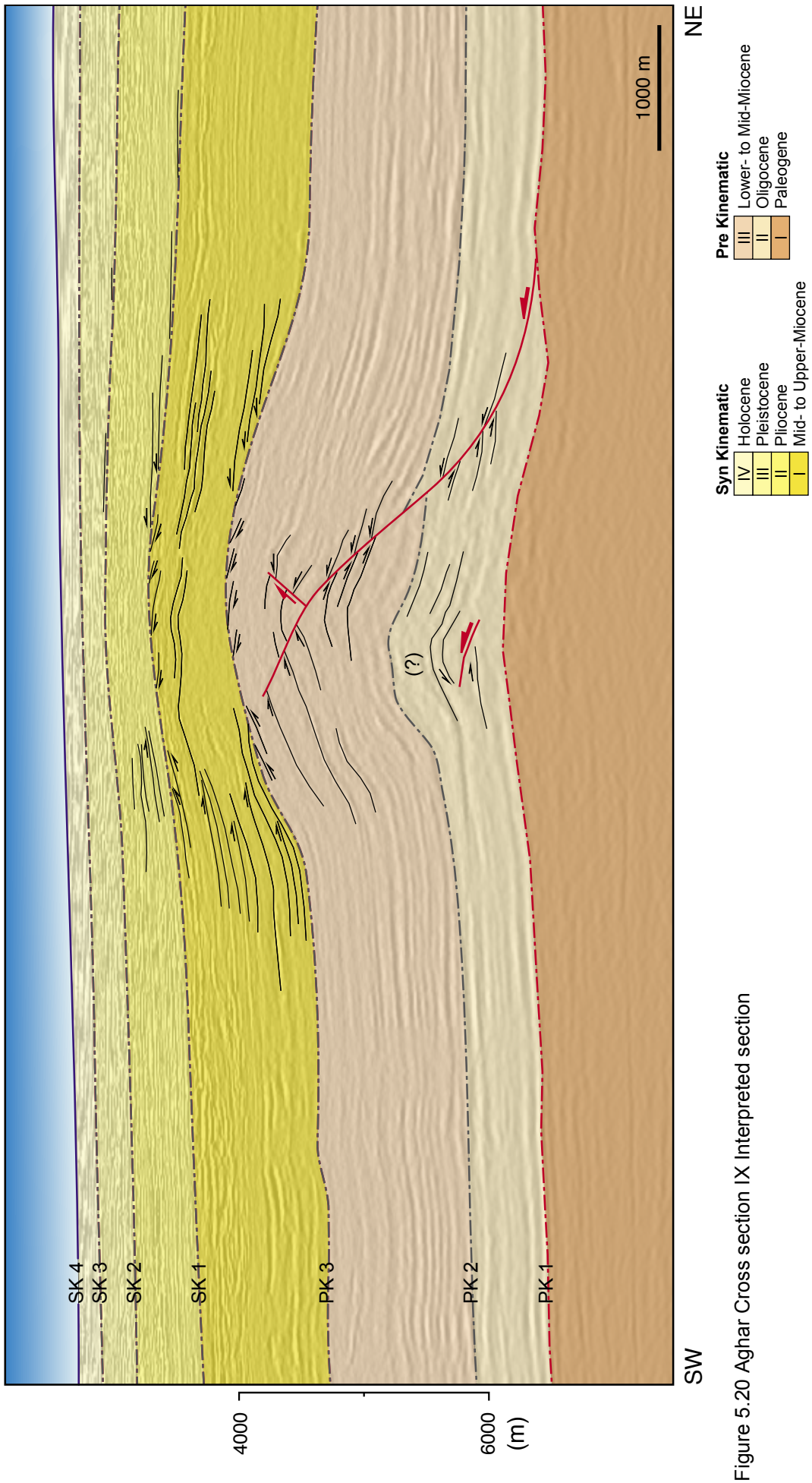

Figure 5.20 Aghar Cross section IX Interpreted section

a seabed relief of 400m. It is an asymmetric fold with a steep ~61° - 72° dipping forelimb and a less steep ~20° - 40° dipping backlimb. The forelimb is also considerably shorter than the backlimb.

The shape of the fold varies with the variations in the associated fault complexity. In parts of the fold where the thrust fault is limited to SW vergent faults, the fold backlimb follows geometry similar to the fault plane, which occurs in the centre of the fold (Sections IV - VI; figure 5.9 - 5.14). However, back-thrusts complicate the backlimb geometry. Landward-vergent back-thrusts create kinks in the backlimb and reduce the hanging wall cut off angle (Chapter 5.3.1) (Sections II, III and VII; figure 5.5 - 5.8 and Fig. 5.15 - 5.16) as well as extending the forelimb and shortening the backlimb observed in Sections I and VIII (Fig. 5.3 - 5.4 and Fig. 5.17 - 5.18).

The degree of interaction between the fold and the neighbouring Aghar North and South fold varies, which causes different amounts of deformation to occur on the fold termination. In the north, the nose of the fold is not apparent, and highly deformed by the Aghar North fault system (Sections I & II; figure 5.3 - 5.6). Aghar South caused little or no deformation to the nose of the Aghar Main fold (Section IX; figure 5.19 - 5.20).

Detachment

Within the Akata (Top of the Pre-Kinematic 1) is interpreted to be an overpressured shale detachment. The decollement dips vary from 0.3° – 0.4° in the tips of the fold (Sections I, II, VIII & IX; figure 5.3 - 5.6 & 5.17 - 5.20) to 1.1° – 1.5° in the centre of the fold (Sections IV – VII; figure 5.9 - 5.16).

5.2.2. Thrust Fault Geometries

There are two fault systems influencing the Aghar fold structure. The main thrust fault complex is responsible for the majority of the shortening, and extends through the section form the detachment into the Syn kinematic sequences. The

other set of faults are minor faults the occur ahead (basinwards) of the main fault complex. The minor faults typically are limited to the Pre-Kinemtic 2 in the central and southern parts (Secion IV - IX; figure 5.9 - 5.20) and Pre-Kinematic 3 in the North part (Secion I - III; figure 5.3 - 5.8).

The Minor faults occur both as basinward vergent (in all sections), and landward vergent faults (central sections IV to VII; figure 5.9 - 5.16). These fault complexes occur as wedge thrust complexes beneath the main fault. In some cases the faults are either terminate against the main thrust (Secion I and II; figure 5.3 - 5.6). In other parts the fault is interpreted to sole along the detachment.

The Aghar main thrust ramp is a SW vergent, NE dipping fault complex, with a geometry that varies both in cross section and along strike of the fold. Furthermore, several backthrusts and forelimb breakthrough thrust (FBT) form in the upper parts of the fault (Fig. 5.21). The northern and southern tips of the fold also show evidence of interaction and crosscutting between Aghar main and the neighboring folds, especially in the north.

A time slice at 5000ms (Fig. 5.21) shows that the active main thrust fault has two main kink-points (also appears on the Pre-Kinematic 3 surface figure 4.24). These kinks divide the fold into a northern, central and southern segments. Each of these segments is between ~6.5 – 13.6 km in length and are arranged in an left-stepping en-echelon configuration. The inactive upper flat, on the other hand show a much more segmented complex, with at least 6 different segments along strike.

The northern and southern segments are characterized to have listric flat-ramp geometry (Sections I & VIII; figure 5.3 - 5.4 and Fig. 5.17 - 5.18) that has been back-thrusted. Two adjacent backthrusts developed in the northern part of the Aghar Main fold, one extending 6 km (Section I; figure 5.3 - 5.4) and another ~5 km. The southern segment has three back-to-back backthrusts; two main back-

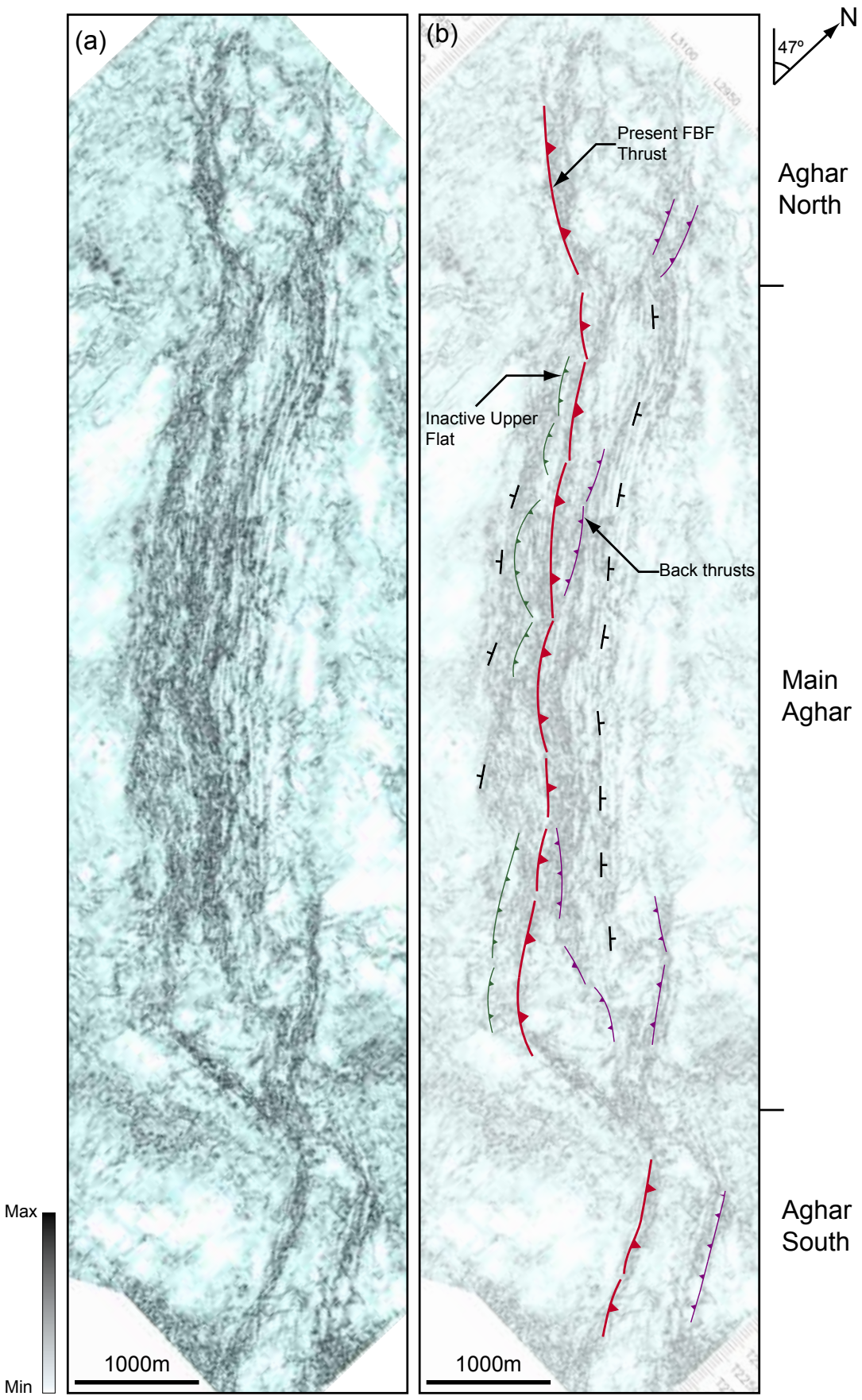

Figure 5.21 Map of the main faults in the Aghar fold. (a) is a coherency cube time slice through at 5.0 seconds and (b) is the interpretation of this section.

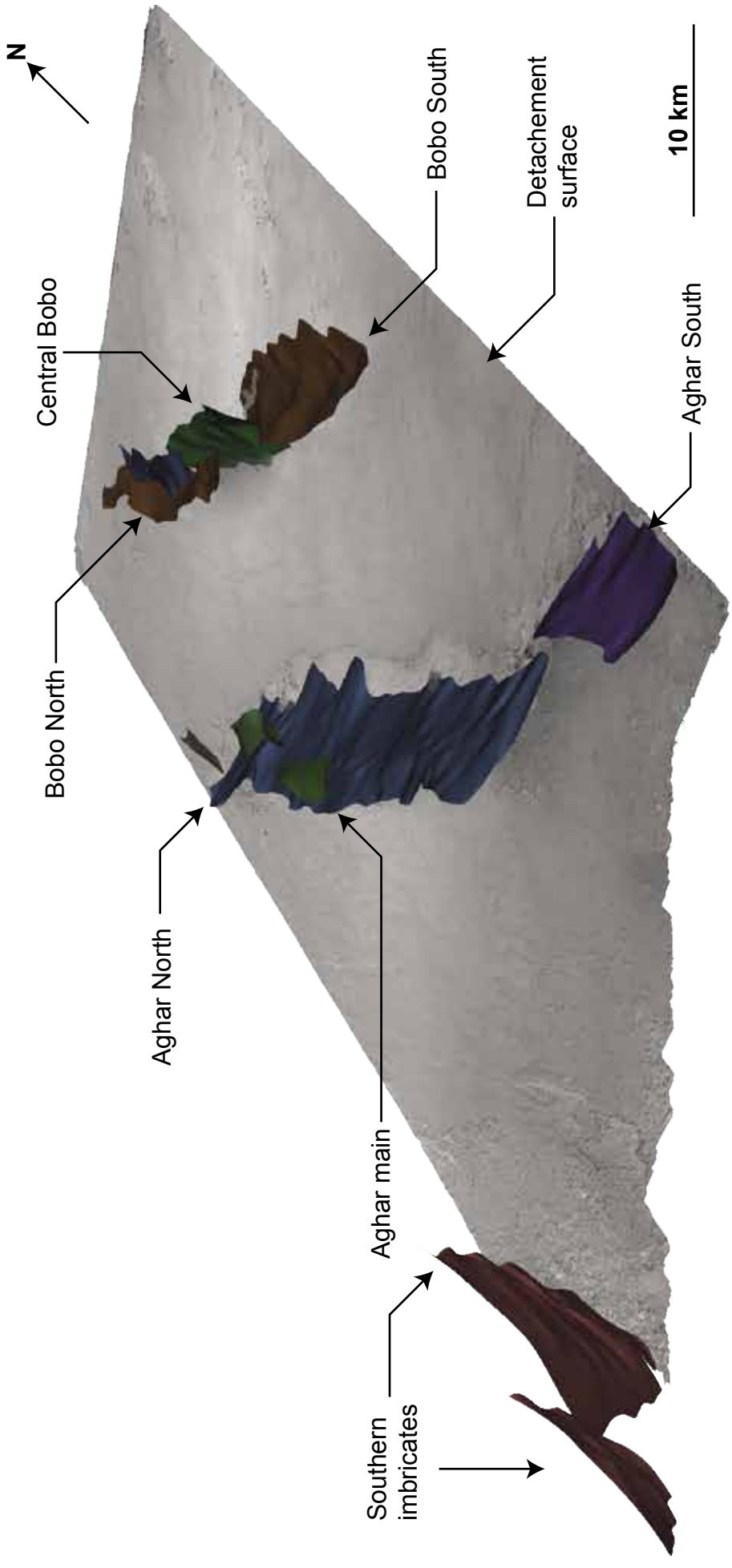

Figure 5.22 3D visualization of the fault in the study area.

thrusts (6 km and 3.5 km) and one minor back-thrust (~1 km). The fault are oriented N128° - 141°E and all terminate against the main thrust fault.

The central segment is located between Section III and VI (Fig. 5.7 - 5.14). In cross-section the thrust fault has a flat-ramp-flat geometry where the upper are nearly horizontal and lower parts of thrust fault are flat to near flat (~8° - 19°), whereas in the middle section of the fault is significantly steeper (~40°). The shape of the fault plane may also vary; it may have a planar ramp (ex. Sections I & III; figure 5.3 - 5.4 and Fig. 5.7 - 5.8) or it may have some irregularities (ex Section II; figure 5.5 - 5.6).

A FBT developed along the central segment extending ~15 km. It intersects the main thrust fault at a depth of ~160 – 900 m. This thrust fault has a dip of ~40°, similar to the middle part of main thrust fault.

The minor faults on the other hand are

5.2.3. Fold-Degradational Features

Fault scarps develop in the forelimb of the fold. This feature dominates the Present Day seafloor, but has also occurred since the late-Miocene.

These scarp faults only occur in the upper parts of the fold, and differ from the crestal collapse faults that are generally steeper and penetrate deeper into the fold structure (Fig. 5.13). Within the slump scarp, several homogeneous blocks are present (Fig. 4.24). These blocks are likely to have originated in the upper parts of the fold, and later moved down slope during the degradation process.

5.2.4. Mud Volcano

The mud volcano is one of the prominent features of the Aghar fold. The volcano creates a circular vent ~990 m in diameter that reaches the surface and creates a crater ~2000 m in diameter (Fig. 5.23-a). The vent has a strong negative seismic amplitude, which is indicative of a low seismic velocity relative

(a)

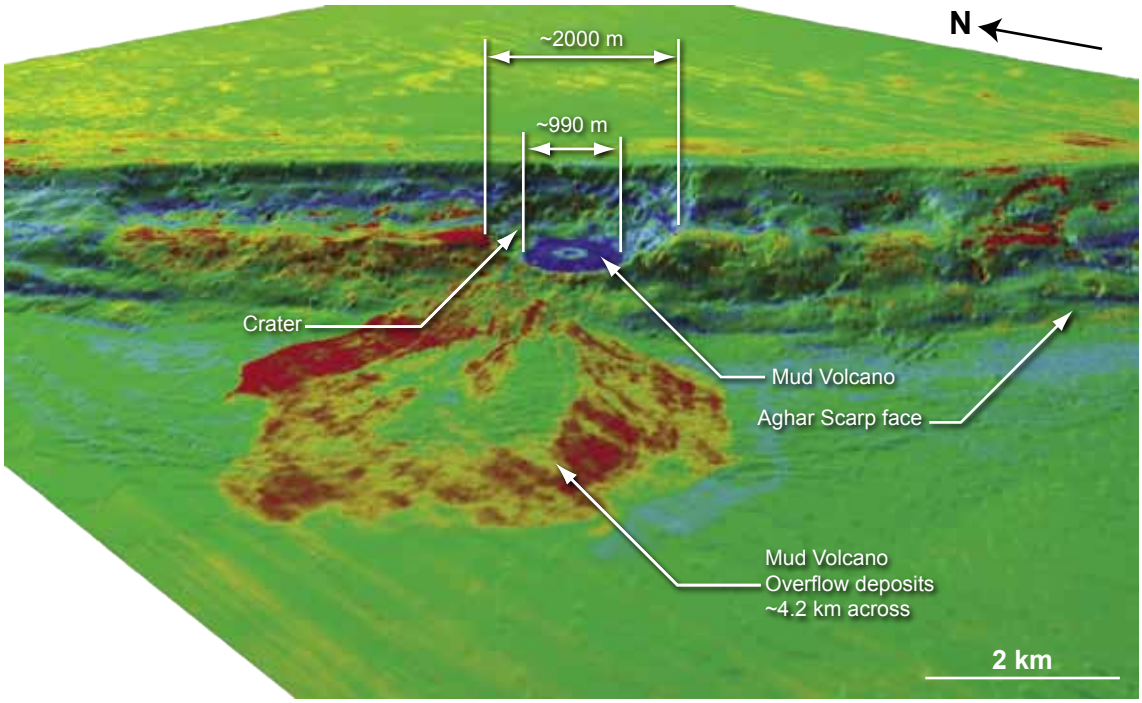

(b)

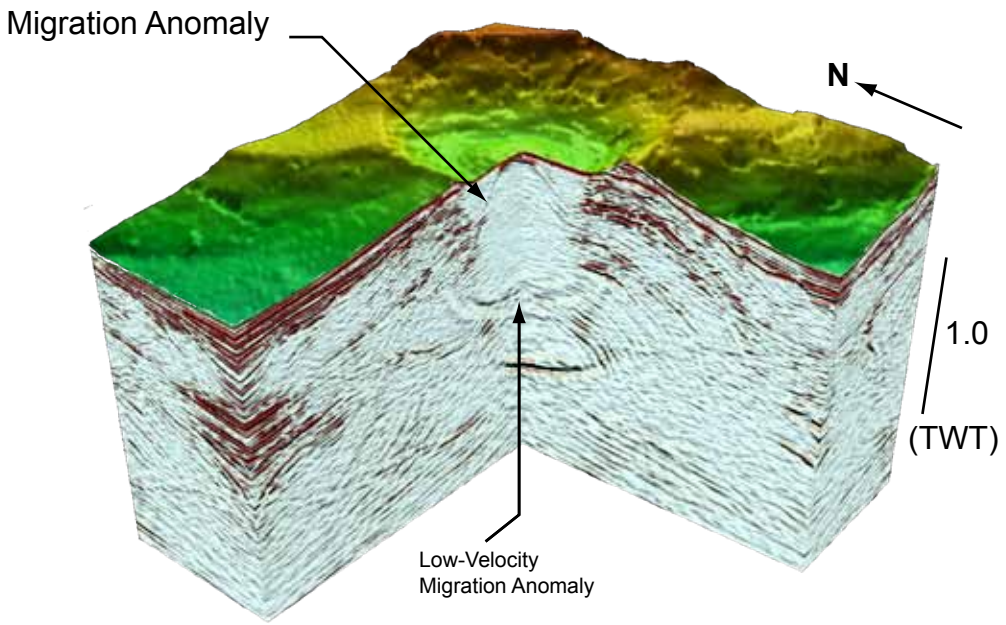

Figure 5.23 Geometry and characteristics of the mud volcano. (a) shows the over all geometry and associated overflow fan on the seabed, (b) shows the cross-section of the volcano and associated seismic anomalies.

to the surrounding seabed (Fig. 5.23-b). In cross-section, the vent creates two sets of parabolic artefacts, one near the seabed and the other ~1-1.5 s below. The upper artefact is a downward parabola, and the lower artefact is an upward parabola. These parabolas are migration artefact caused by the abrupt lateral velocity variation. Furthermore, the mud volcano is associated with a reduction of the BSR, which deflects and pull upwards.

5.3. Fault Analyses

The geometry of the fold requires a complete geometric understanding of the fault plane. In this section, the cutoff angles of the Pre-Kinematic 2 and 3 sequences are investigated for Sections I – VIII (Fig. 5.4 - 5.18) in figure 5.24 to have a better understanding of the fault geometry and behaviour.

The second set of analyses is related to the fault displacement. The first analysis compares the total displacement of all the faults along strike. A total displacement profile (Fig. 5.25) was used to compare the displacement of the Pre-Kinematic 2 and 3 along strike of the Aghar Fold. A more detailed individual fault displacement analysis was done separately for each of the Pre-Kinematic 2 and 3 sequences (Fig. 5.28 & 5.29 respectively).

5.3.1. Cutoff Angle Analysis

The hanging-wall cutoff angles of the Pre-Kinematic 2 and 3 have been measured along the fold in Sections I – VIII (Fig. 5.3 - 5.18). The measurements show a near consistent value between 0 and 1750 ± 250 m height above the decollement with a cutoff angle of 0 – 20°. Beyond this height, the cutoff angles begin to deviate. This coincides with the upper inflection point between the ramp and flat of the fault plane.

Cutoff angles of Section I and II (Fig. 5.3 - 5.6) diverge closer to the detachment than the other sections. Both, and in particular Section II (Fig. 5.5 - 5.6), have significantly steeper cutoff angles than the other sections. Both these sections

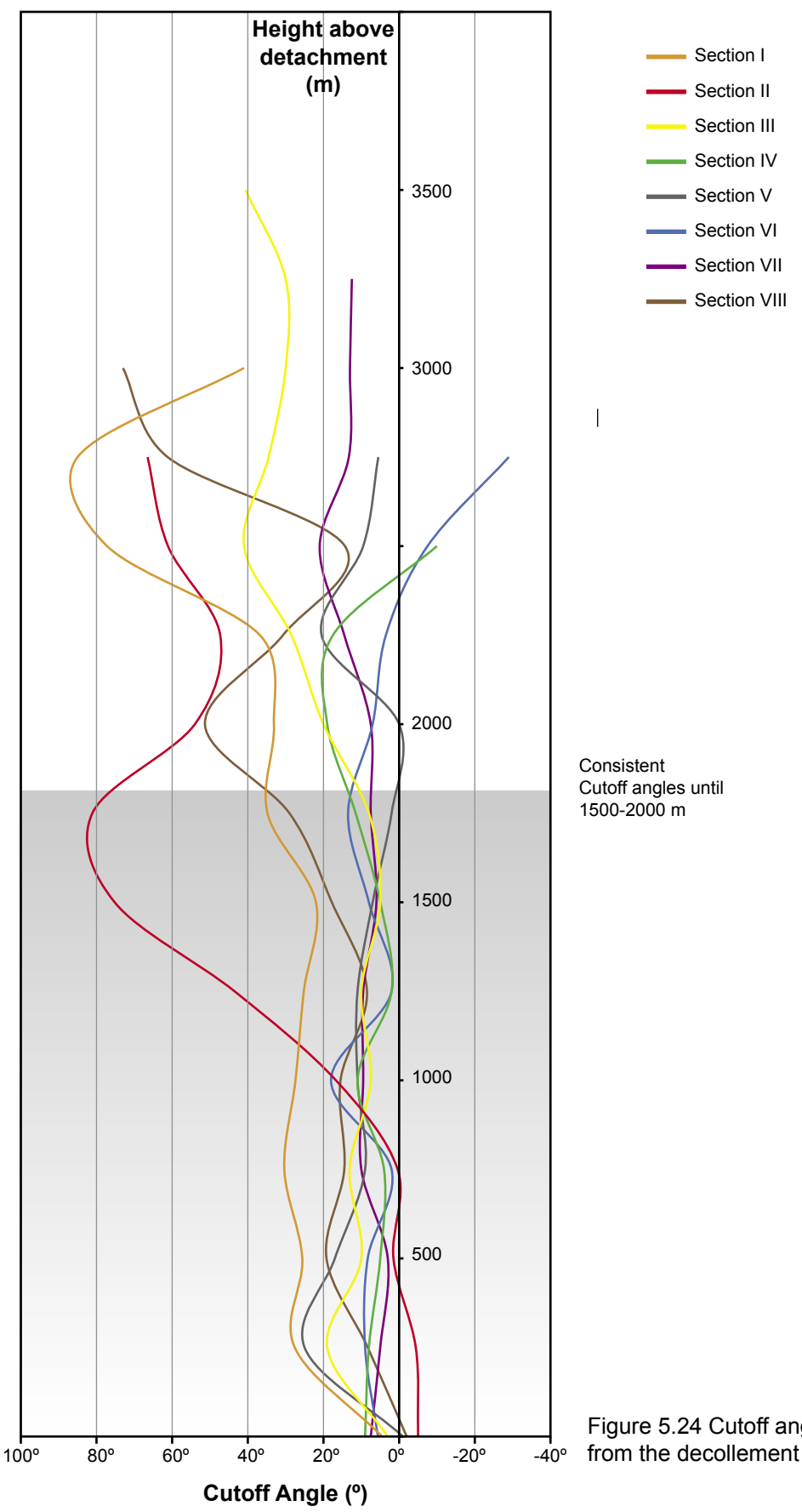

Figure 5.24 Cutoff angle vs. height from the decollement chart

have a fault plane geometry that is nearly planar in the upper parts.

5.3.2. Fault Displacement Analyses

Fault displacements have been measured along strike and plotted for the Aghar fold. Heave and throw measurements were completed at the Top Pre-Kinematic 2 and 3 (PK-2 & PK-3) horizons in Sections I – VIII (Fig. 5.3 - 5.18). These measurements are used to calculate the displacement profile. Displacement measurements were made on four fault groups; the main thrust fault, forelimb-breakthough-thrust (FBT), backthrust, and fore-thrusts.

The resultant values are plotted along the strike of the fold. The plots include the total displacement (Fig. 5.25), total heave (Fig. 5.27) and total throw (Fig. 5.26) charts. Moreover, detailed displacement values of the individual faults within the fold were plotted along the strike of the fold (Fig. 5.28 & 5.29).

Total Displacement profiles

These displacement profiles provide an overview of the fault displacement. The heave highlights the horizontal displacement along the strike of the fold (Fig. 5.27) whereas the throw or vertical displacement profile shows the vertical uplift in the hanging wall (Fig. 5.26). Finally, the total displacement shows the total distance the different units have moved along the fault plane (Fig. 5.25).

The total displacement profile (Fig. 5.25) shows a PK-2 maxima in the middle of the fold at 14km (Section V; figure 5.11 - 5.12) and a PK-3 maxima at 17.5 km. The SE nose of the fold shows no evidence for fault ramp development and therefore, no displacement. In between the central point and SE edge, the curve follows a near parabolic trajectory.

The Aghar North interferes with the growth of the Main Aghar fold and the exact northern extent of the fold is not fully determined. Furthermore, the northern displacement profile also creates a downward parabolic plot between 3.5 and 14 km; however, it is considerably tighter than the southern part.

The total heave profile (Fig. 5.27) similarly shows a PK-2 maxima in the middle of the fold at the 14 km point (Section V; figure 5.11 - 5.12) and a PK-3 maxima at 17.5 km (Section VI; figure 5.13 - 5.14). The heave profile is less parabolic than the total displacement profile. Between 17.5 - 24.5 km points in the southern part of the fold follow a horizontal path in PK-2 and form a local minimum in the PK-3. Furthermore, the PK-2 and PK-3 intersect at the 3.5 km mark.

The total throw profile (Fig. 5.27) shows a parabolic distribution of PK-2 values and an almost linear PK-3 trend between 0 and 21 km. The PK-3 rapidly increases between 21 and 24.5 km and dips to zero at the edge of the fold. The PK-2 and PK-3 values also intersect at 3.5 km.

Detailed Fault Displacement Analyses

The fault systems associated with the Aghar fold consist of a complex of faults rather than a single uniform thrust fault. In the previous section, the values plotted were the overall sum of fault heaves and throws. For a more detailed analysis, the displacement of the four thrust fault types are plotted separately (Fig. 5.28 & 5.29).

In the middle of the fold, 3.5 to 21 km, PK-2 is only affected by the main thrust fault as well as the FBT (Fig. 5.28). In the southern part, additional displacement occurs on a back-thrust. The northern part has a complex of three fault types (main, fore- and back thrusts) with a small displacement on each fault (Section I; figure 5.3 - 5.4). Some of these faults may be related to the Aghar North, however this structure goes beyond the edge of the 3D survey.

The Top of Pre-Kinematic 3 creates displacement only on three fault types; the main thrust, FBT and back thrust. The main thrust displacement plot shows an oscillating trend, which generally decreases away from the 17.5 km point (Section VI; figure 5.13 - 5.14). The back-thrust is limited to the southern part between 21 and 27.5 km. The rest of the fault displacement is dominated by the

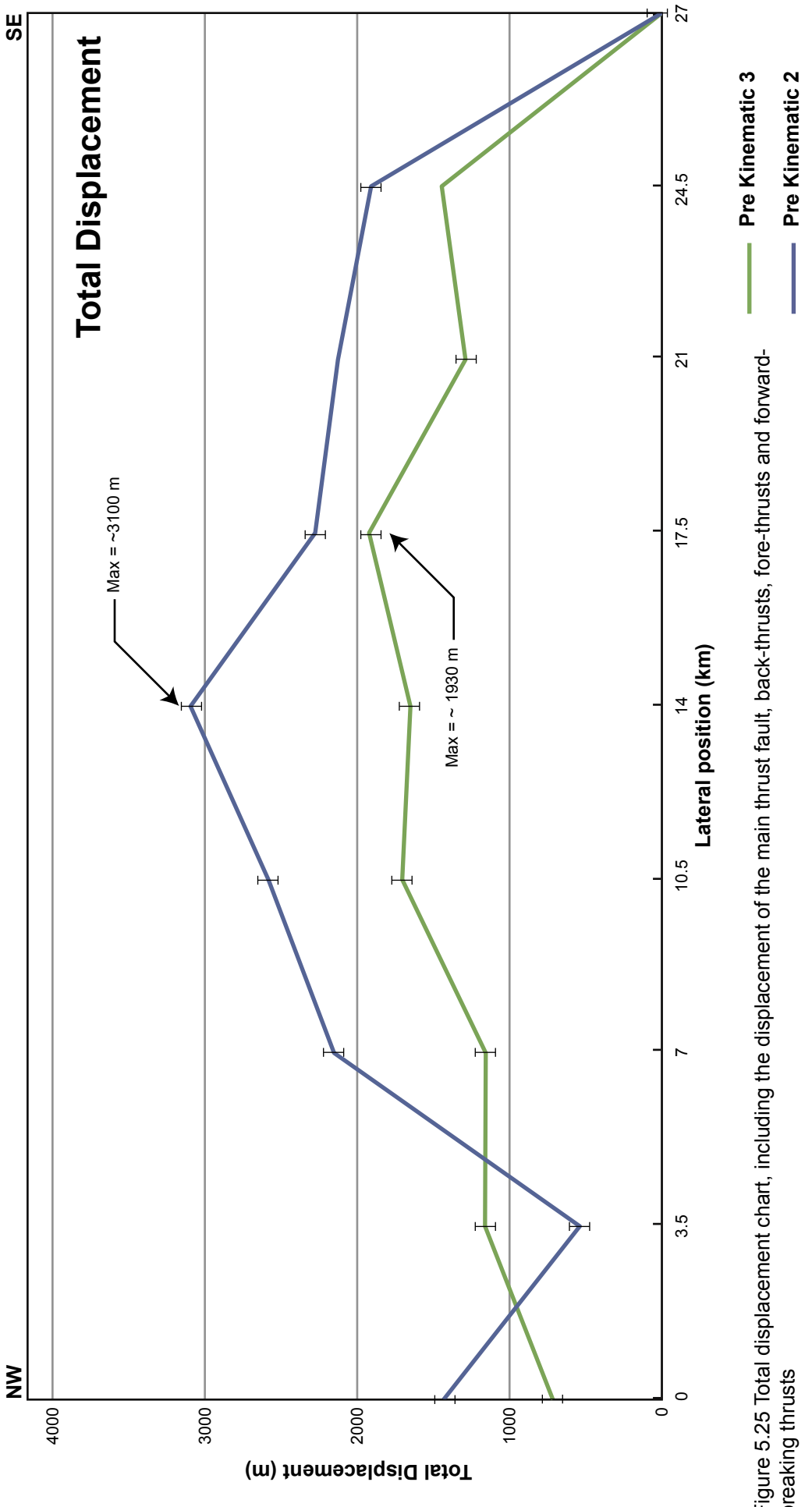

Figure 5.25 Total displacement chart, including the displacement of the main thrust fault, back-thrusts, fore-thrusts and forward-breaking thrusts

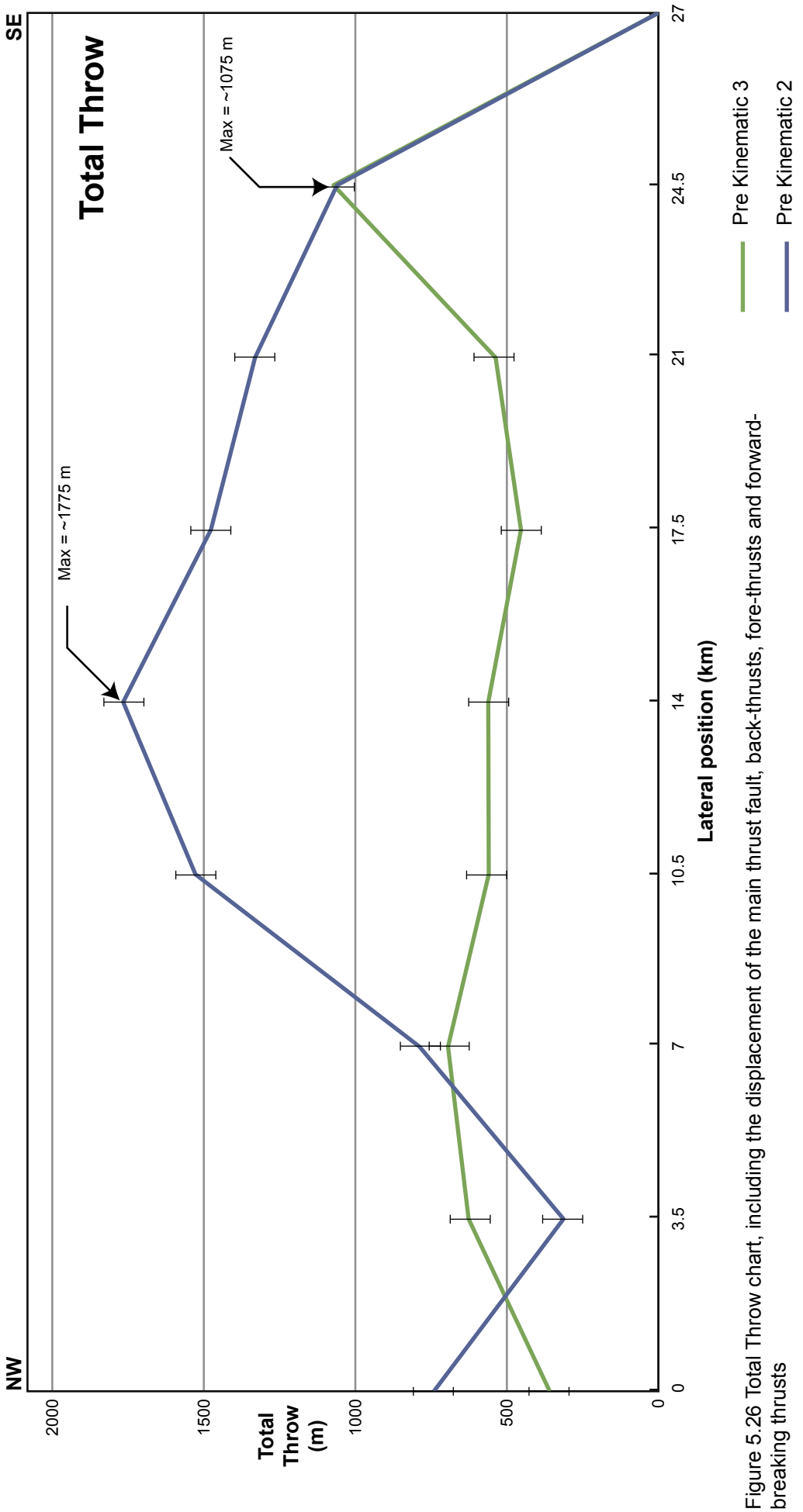

Figure 5.26 Total Throw chart, including the displacement of the main thrust fault, back-thrusts, fore-thrusts and forward-breaking thrusts

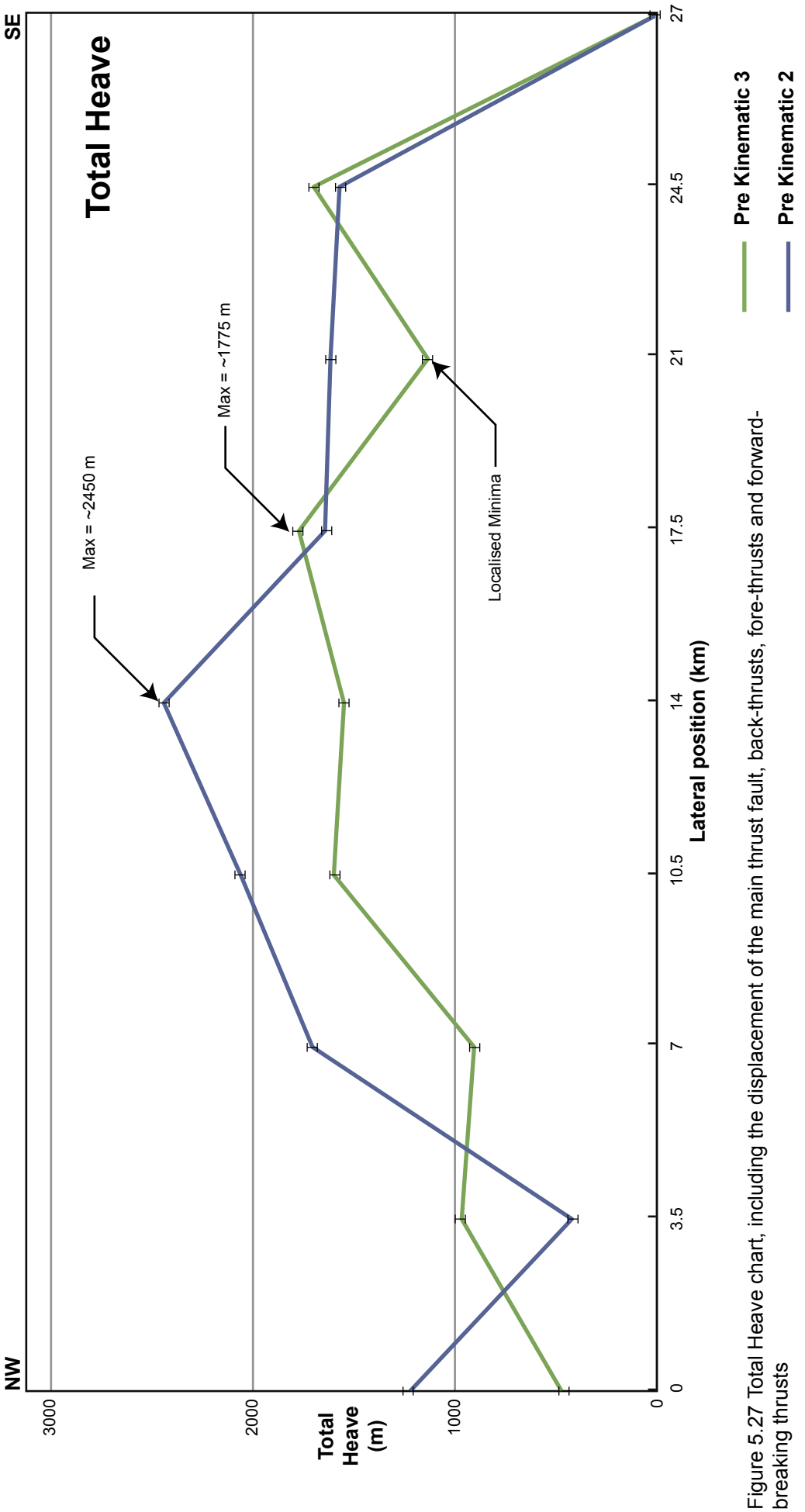

Figure 5.27 Total Heave chart, including the displacement of the main thrust fault, back-thrusts, fore-thrusts and forward-breaking thrusts

main and FBTs. The FBT displacement profile decreases away from the 14 km maxima point, which corresponds to a dip in the main thrust fault displacement.

5.4. Growth Stratal Analyses

To understand the amplification of the Aghar fold, a detailed analysis of the growth strata has been carried out on both isochron maps and cross sections.

5.4.1. Syn-Kinematic 1 Sequence

The isochron of Syn-Kinematic 1 sequence (Fig. 4.34) shows thinning of the sequence towards the middle of both the Aghar and Central Bobo folds. This indicates that the Aghar was mostly active in the middle of the structure (Sections III – VII; figure 5.7 - 5.16). The remainder of the structure shows a homogeneous but smaller amount of growth (Sections I – II and VIII – IX; figure 5.3 - 5.6 and Fig. 5.17 - 5.20). Sections I-III (Fig. 5.3 - 5.8) generally show some thinning but no major truncation of onlapping features.

Sections IV – VII (Fig. 5.9 - 5.16) on the other hand show both onlapping and truncational features. The onlap features occur in the upper parts near the crest of the fold, which indicates that the syn-kinematic unit was deposited when the fold was in early stages of amplification. The truncation of reflectors that occurs in the backlimb indicates that the backlimb was being rotated causing instability and degradation. Similar onlapping features occur against the forelimb of the fold.

In the northern and southern segments of the Aghar Main fold (Section I – II and VIII; figure 5.3 - 5.6 and Fig. 5.17 - 5.18), the syn-kinematic geometries show sub-parallel reflectors particularly in the lower part of the unit. Some onlapping occurs in the middle and upper parts of the unit around the crestal part of the fold (Section I & VIII; figure 5.3 - 5.4 and Fig. 5.17 - 5.18). At these locations the Syn-Kinematic 1 unit was deposited prior to folding, forming beds that are parallel to the pre-kinematic sequences. Subsequently, it was cut by the

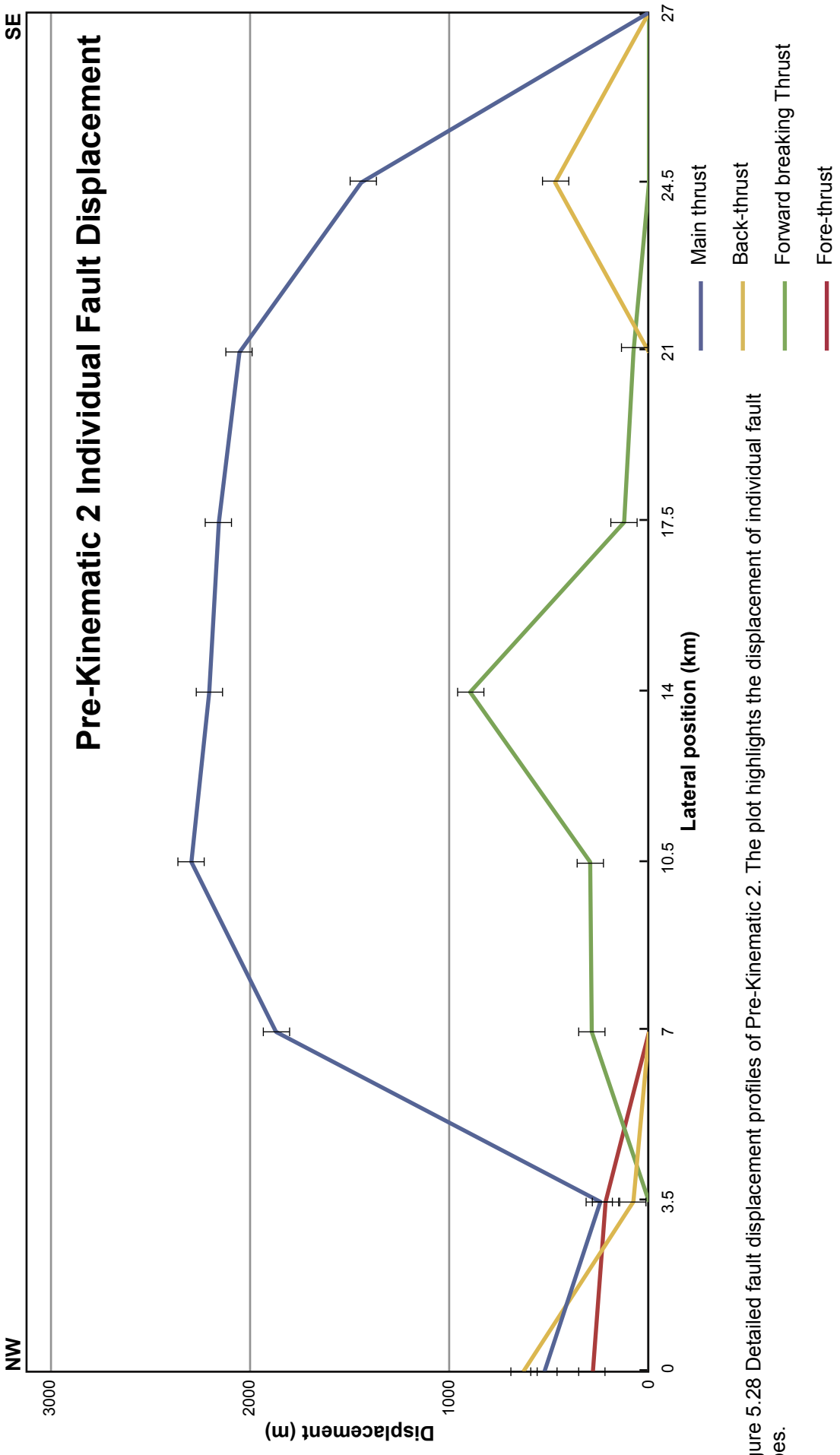

Figure 5.28 Detailed fault displacement profiles of Pre-Kinematic 2. The plot highlights the displacement of individual fault types.

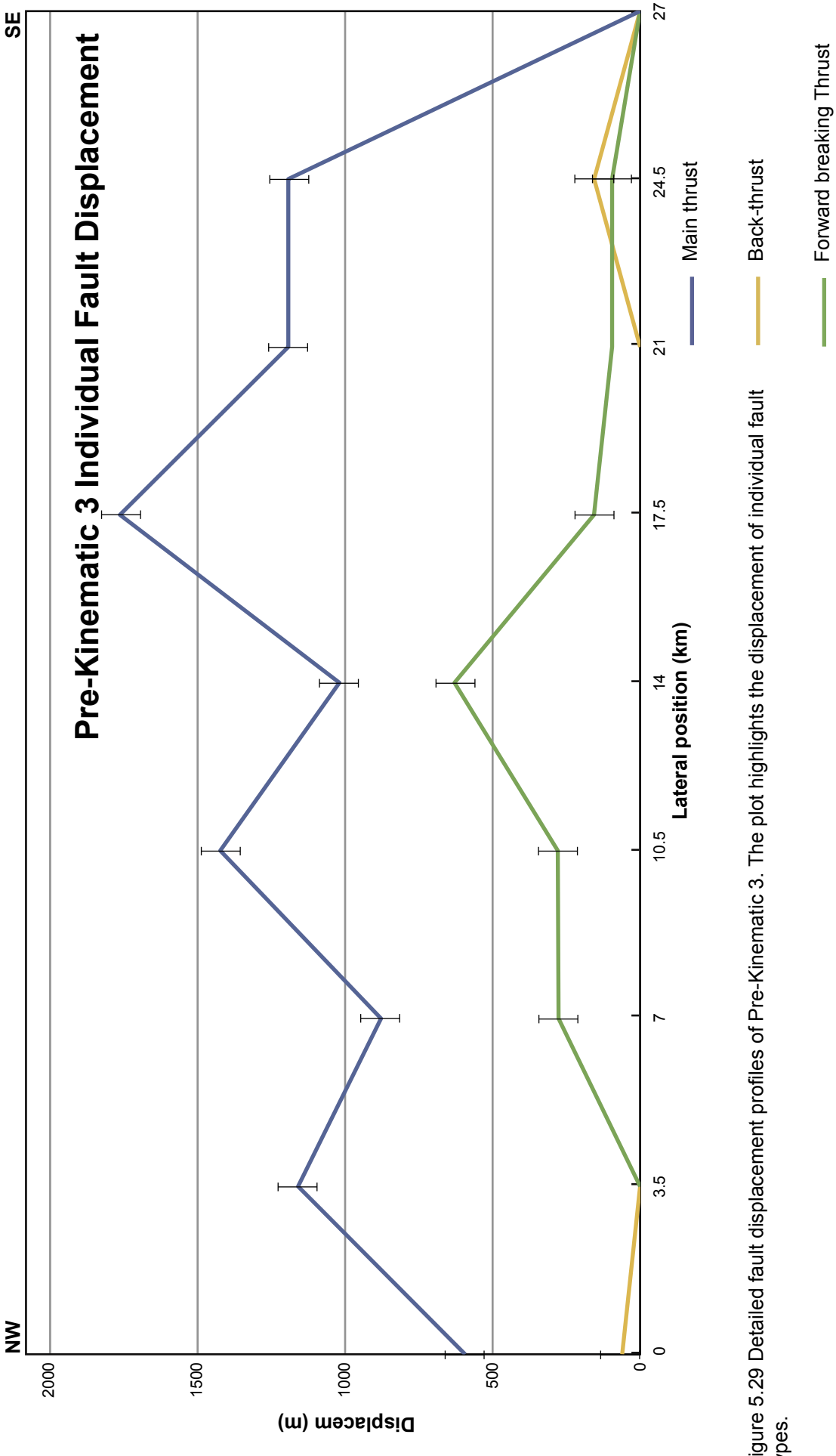

Figure 5.29 Detailed fault displacement profiles of Pre-Kinematic 3. The plot highlights the displacement of individual fault types.

propagating thrust fault and was folded similarly to the pre-kinematic section. Furthermore, Section VIII (Fig. 5.17 - 5.18) shows that the lower part of the unit is cut by backthrusting, and the top of the layer has been folded as a result.

Terminating against the Aghar South to the NE is a thicker part of the sequence. This is probably related to a channel system (Fig. 4.28) that travels NE - SW within the saddle between the Aghar and southern Aghar extension. The channel itself is associated with a thicker section.

Beyond the fold in the footwall area (SW of the fold), the syn-kinematic unit is mostly parallel to sub-parallel. The fault termination of the sequences does not show evidence for synclinal folding.

5.4.2. Syn-Kinematic 2 Sequence

The Syn-Kinematic 2 is missing in the crestal part of the fold (Fig. 4.35). This is caused by a combination of thinning and onlapping against the flanks of the fold, in addition to uplift and erosion. Aghar North and South show some movement during this period.

From the bottom to the top of the sequences, onlapping reflectors in the backlimb progress towards the crest of the fold. Additionally the dip of the reflectors becomes shallower up the section. The shift of onlapping closer to the crest is indicative of sedimentation rates exceeding fold amplification, whereas the shallowing of the reflector dips is indicative of backlimb rotation.

The forelimb part of the fold was faulted by the main thrust and the FBT. The thrusting caused the reflectors to become highly rotated. However, this rotation does not correspond to limb rotation, but is caused by the continuous displacement of the fold forelimb along the thrust during the deposition of the unit. Furthermore, in the forelimb – footwall contact area, an angular unconformity forms, where the reflectors of the Syn-Kinematic 2 onlap against the Syn-Kinematic 1.

In northern and southern segment of the Aghar fold, especially in Section II (Fig. 5.5 - 5.6), backthrusting causes basinward rotation of the backlimb, resulting in the erosion of the backlimb forming a truncation surface. The formation of the FBT in sections III and VI (Fig. 5.7 - 5.8 and Fig. 5.13 - 5.14) caused a change in fold geometry, which also leads to truncation of the unit.

5.4.3. Syn-Kinematic 3 Sequence

During this period, the Aghar fold maintained growth, causing the thinning of the syn-kinematic sequence on the flanks of the fold (Fig. 4.36). The sequence either thins against the limbs of the fold (Sections II and VIII (Fig. 5.5 - 5.6 and Fig. 5.17 - 5.18) and forelimb of Section III (Fig. 5.7 - 5.8)), or has been emplaced and removed by subsequent fold degradation (Sections IV - VII; figure 5.9 - 5.16).

The geometry of this unit varies along strike due to the variation of fault geometry. In the northern part of the fold (Sections I – II; figure 5.3 - 5.6), the unit has a uniform thinning along a flat backlimb, where the top and bottom of the unit are near parallel. This indicates that the growth in this part of the fold was self-similar, where the upper part of the fold was uplifted without much rotation of the limbs, in particular the backlimb.

The reflectors in the middle of the fold (Sections IV – VIII; figure 5.9 - 5.18) have been thinned and rotated in the backlimb. This is indicative of continued limb rotation in the middle of the fold. At the bottom of this sequence, the reflectors onlap in the upper parts of the fold near the crest, and then the onlaps translate away from the crest. This indicates that the fold amplification exceeds sedimentation.

The forelimb section has not been penetrated by the thrust faults; however, the reflectors have been rotated as a result of fault slip. The unit is highly thinned (Section IV – VI; figure 5.9 - 5.14).

In section IX (Fig. 5.19 - 5.20), the termination of the fold, the sequence shows a small amount of thinning over the Aghar fold. Onlap features are not as prominent as other parts of the fold. Reflectors within the unit are sub-parallel to the Present Day seabed.

5.4.4. Syn-Kinematic 4 Sequence

During the last of the syn-kinematic sequences (Fig. 4.37), growth of the Aghar Main and North folds continued. Again, the sequence thins along the fold flanks and is not present above the crest of the Aghar fold.

The reflectors within the unit are parallel to sub-parallel to the Present Day seabed. Onlaps developed along the Pre-Kinematic 3 contact in the backlimb. The onlaps progress toward the fold crest up the section (Sections II – VIII; figure 5.5 - 5.18).

The forelimb only shows deformation related to the movement on the FBT. The onlap features observed vary from simple geometries (Section II – III and Sections VIII – IX; figure 5.5 - 5.8 and Fig. 5.17 - 5.20) to more complicated geometries associated the geometry of underlying substrate (Sections IV – VII; figure 5.9 - 5.16). This correlates with the variation in fault geometries; the northern and southern parts of the fold have a simple main thrust geometry whereas the middle segment is associated with a FBT complex.

Section IX (Fig. 5.19 & 5.20) only shows a subtle relief over the fold structure with some onlapping features.

5.5. Summary and Discussion

5.5.1. Summary of Aghar Fold Observations

- The Aghar fold extends is ~34 km long and ~4.3 – 7.2 km wide that creates a 400m relief on the seabed. The asymmetric geometry of the fold dips 3.5° in the backlimb and 10-12° in the forelimb on the seabed. In the top of Pre-

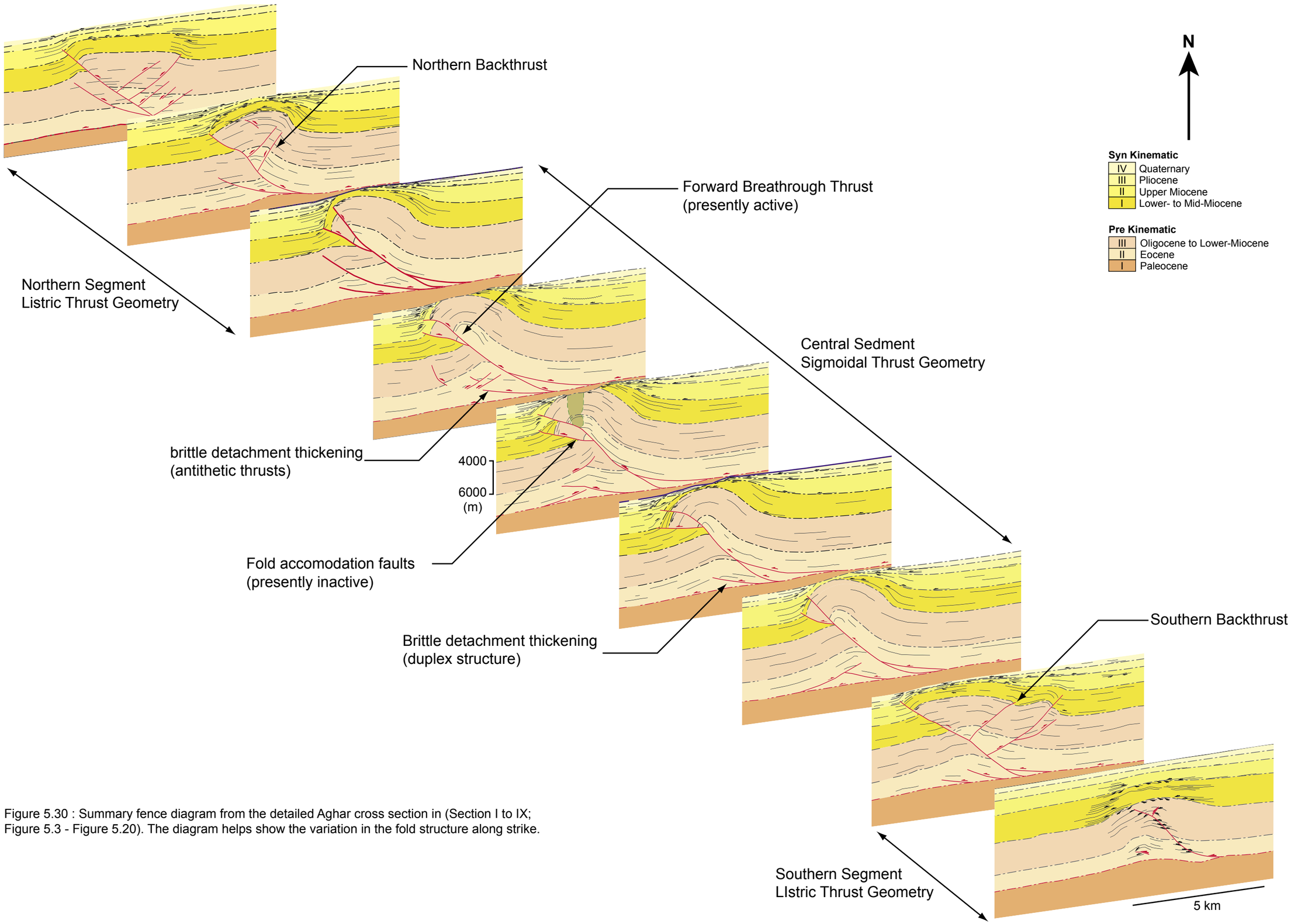

Figure 5.30 : Summary fence diagram from the detailed Aghar cross section in (Section I to IX; Figure 5.3 - Figure 5.20). The diagram helps show the variation in the fold structure along strike.

Kinematic 3, the forelimb dips 61° - 72° and the backlimb dips up to 20° – 40°.

- Two kinks occur along strike of the main Aghar fold in a left-steeping configuration, which indicates that the Aghar fold has formed from as a result of amalgamating three thrust faults. Furthermore, the geometry of each segment differs from the other. The Northern and Southern edge segments show a flat-ramp geometry with back-thrusting where as the central segment shows a flat-ramp-flat geometry with FBT. Additionally, the middle segment has the largest displacement values.

- Various horizons show that the Aghar fold traps multiple flows to the NE of the fold, and as a result, the areas to the SW of the Aghar fold has a different elevation and slope compared other parts of the survey.

- Evidence shows that forelimb scarp has been active since the mid- to upper-Miocene period (Syn-Kinematic 1) and continue to Present Day. The size of the scarp increases upwards in the section with fold growth.

- The decollement ascends by ~227 – 311 m in the middle of the fold, creating a geometry similar to a low-amplitude detachment fold. This is caused by thickening of the of the detachment unit. However, unlike salt that flows like a viscous fluid, shale layers create bourrage and duplex structures that infill the core of the fold, which was not resolved by seismic.

5.5.2. Implications of Fault Analyses

- The shape of the fault varies along strike; the central part is characterised by a flat-ramp-flat geometry, whereas the northern and southern cross sections show a flat-ramp geometry. This coincides with the two kink-points observed in the Pre-Kinematic 2 (PK-2) maps (Fig. 4.24).

- The cutoff angles are consistent between 0 and 1750 ± 250 m above the detachment. Beyond this height, cutoff values begin to deviate in particular

in the centre of the fold, which coincides with the upper inflection point of the flat-ramp-flat fault geometry.

5.5.3. Implications of Fault Displacement Profiles

- PK-2 has larger displacement values than PK-3 (Fig. 5.25), which indicates that the thrust fault initially displaced PK-2, before propagating into PK-3. Thus, the fault probably initiated within the lower layer and propagated upwards in the section.

- The total heave (horizontal displacement) (Fig. 5.27) values are generally greater than the total throw values (vertical displacement) (Fig. 5.26).

- The PK-2 displacement profile creates a parabolic shape. The peak displacement value occurs at 14 km in the middle of the fault and reduces away from the centre. The shape of the profile is nearly symmetric across the maxima, suggesting that fault nucleation probably began in the central part of the fold.

- The total displacement plot of the PK-3 has a low-relief parabolic shape with some variation (Fig. 5.25) whereas the detailed displacement profile shows the main thrust fault to have values with large variations (Fig. 5.29). This implies that the displacement within the PK-3 was distributed along a number of faults during the early periods of fault propagation.

- The detailed displacement plots (Fig. 5.28 & 5.29) of individual faults show that the fold can be divided into three distinct parts; the northern part which shows interference with the Aghar North, a central part that consists of main thrust and FBT, and a southern part that has developed back-thrusts, but is independent from the Aghar South.

5.5.4. Implications of Growth Stratal Geometries

- Growth of the Aghar fold began in the centre of the fold between the Mid- to

Late-Miocene, and then progressed to the north and south.

- The Aghar North and South folds became active in the Late-Miocene – Early-Pleistocene.

- Syn-Kinematic 2 units have onlapping reflectors that progress towards the crest of the fold. This indicates that the sedimentation rate exceeded the rate of fold growth. Conversely, Syn-Kinematic 1, 3 & 4 have onlapping that progresses away from the crest indicating growth exceeding sedimentation rate.

- Along strike the Aghar fold growth style varies from self-similar growth in the northern and southern segments to growth by limb-rotation in the central segment.

- Backthrusts that affect the northern and southern segments of the Aghar fold cause basinward rotation of the backlimb, making the dips of the backlimb reflectors and the cutoff angles shallower.

Chapter 6

Section Restoration and Forward Numerical Modelling

6.1. Introduction

This chapter investigates the feasibility and quality of forward numerical model and cross-sectional restoration using Igeos Dynel2D. The purpose of this modelling is to provide a better understanding of the evolution of the thrust related folds and the distribution of stress and strain during the evolution. The methodology and summary of the software assumptions is discussed in Chapter 3.4.

The first part of the chapter discusses the restoration of Section V from the Aghar Fold (Chapter 6.2). The following section consists of two forward numerical models; one with a sigmoidal flat-ramp-flat fault geometry (Chapter 6.3.1) and the other with a listric flat-ramp thrust geometry (Chapter 6.3.2). In Chapter 6.4, the outcomes of the restoration and models is investigated and discussed, and future recommendations are made in Chapter 6.5.

6.2. Section Restoration

Section restoration using Dynel 2D was carried out on a cross-section through the middle of the Aghar fold (Fig. 5.11 - 5.12), with and without bed slip in the post detachment sequences.

6.2.1. Section V Restoration

Structural restoration of Section V was carried out to understand the evolution of the fault complex in the middle of the fold. As discussed previously, the middle of the Aghar fold has a major basinward-vergent thrust fault with a flat-ramp-flat geometry. A forelimb breakthrough thrust (FBT) formed in the forelimb of the fold which has dominated the fault displacement. The structural restoration is utilized to show the development of this fault complex through time and as a result show the evolution of the fold geometry with time.

The restoration shows that the middle of the Aghar fold has undergone five major phases.

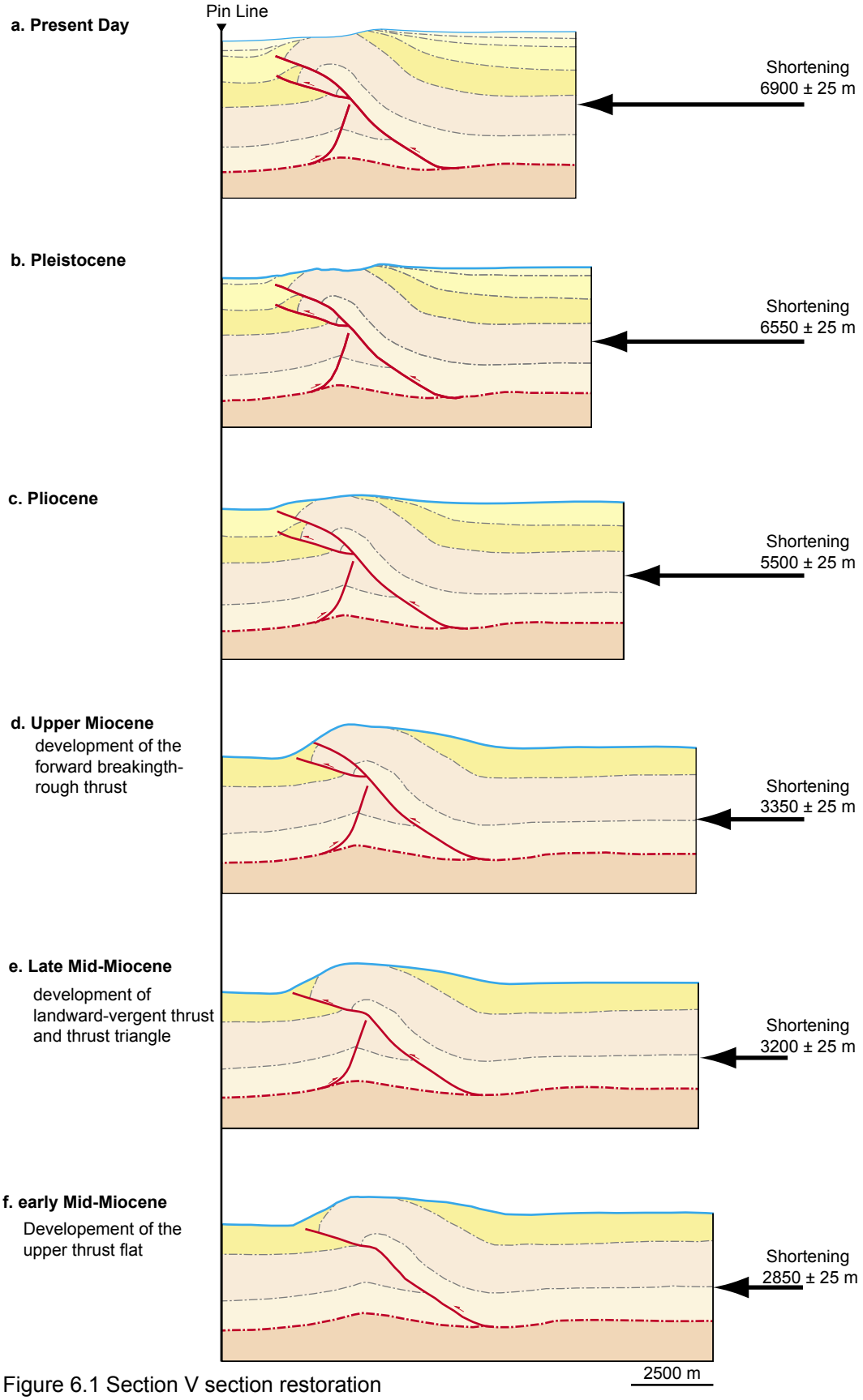

Figure 6.1 Section V section restoration from the late Lower-Miocene to Present Day in five stages. Illustrations h - j show the pre-fault section, non of which restore the section completely. (k) is a plot of uplift vs. shortening.

Continued on next page.

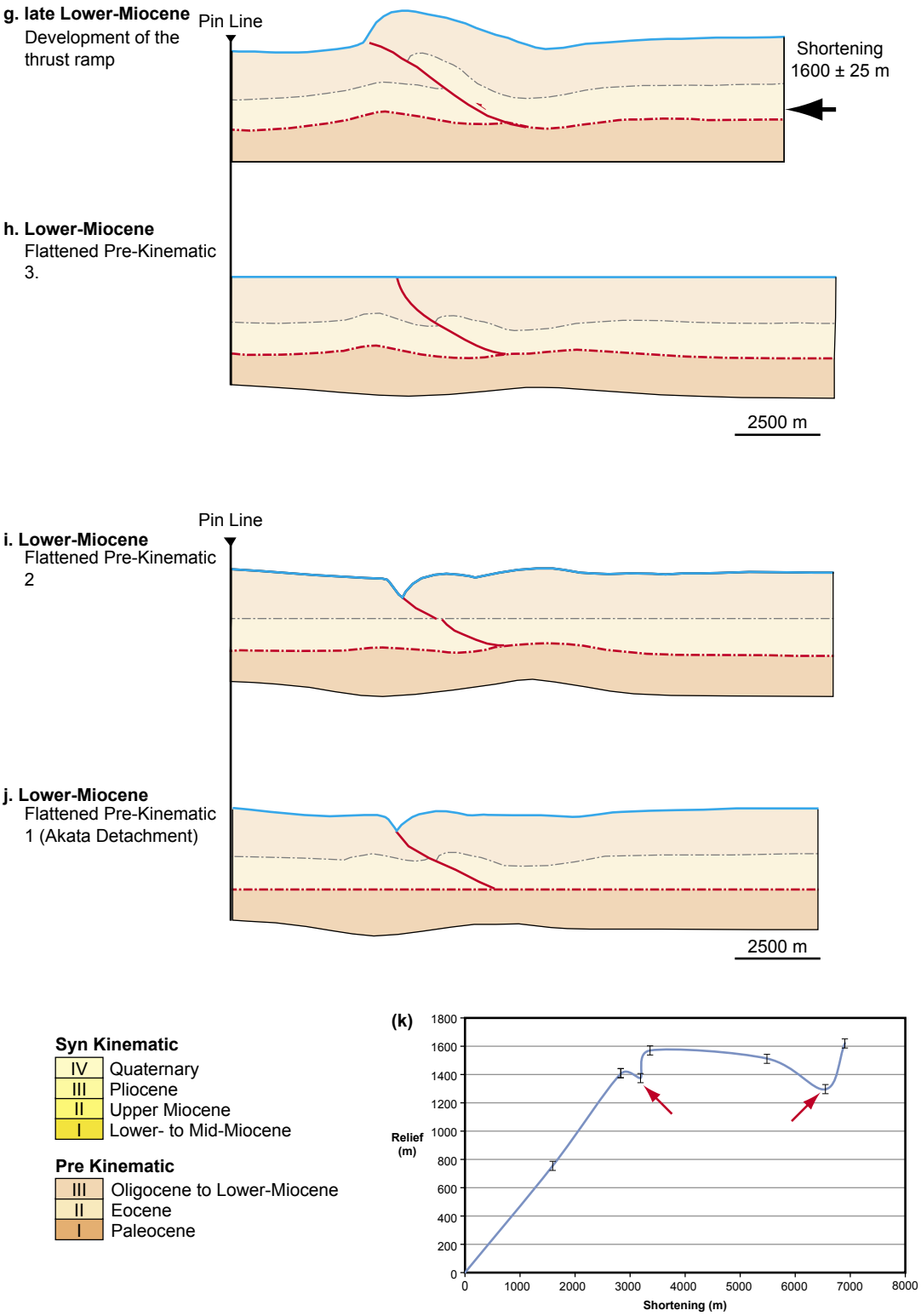

figure 6.1 Section V section restoration from the late Lower-Miocene to Present Day in five stages. Illustrations h - j show the pre-fault section, non of which restore the section completely. (k) is a plot of uplift vs. shortening. The red arrows show variation in relief caused by fold degradation.

1. During the early Lower-Miocene, there was no deformation taking place (Fig. 6.1 h - j). However, this was found to be unlikely. Growth initiated with detachment thickening by means of duplex formation, which was not incorporated into the model.

2. Main ramp development (Fig. 6.1 g): in the late Lower-Miocene, after the development of the detachment fold, the thrust ramp developed from the detachment and propagated upwards through the section.

3. Development of the upper flat (Fig. 6.1 - f): in the early Mid-Miocene, the upper part of the fault propagated at a less steep angle, compared to the 40° ramp.

4. Development of the landward-vergent backthrust (Fig. 6.1 - e): also during the late Mid-Miocene, an antithetic NE-vergent thrust fault developed in the footwall near the detachment and created a small displacement that slightly deforms the main thrust plane. This also resulted in the formation of a thrust triangle localised to the centre of the Aghar fold.

5. The development of the forelimb breakthrough thrust (Fig. 6.1 - a - d): During the Pliocene and to Present Day, the remainder of the displacement is taken-up by the FBT that develops in the forelimb of the fold.

The uplift is plotted against the shortening for the reconstructed section. One of the main feature observed is that the uplift values are significantly smaller than shortening. Furthermore, fold degradation such as forelimb scarps, strip a large amount of material from the fold crest area, which reduces the uplift values of the fold. This is common in poorly consolidated deepmarine fold systems.

6.3. Numerical Modelling

Two numerical models of fault-related-folds have been constructed to further understand the evolution of the Aghar fold. The properties of these folds have

been derived from observations made on the Aghar fold such as the fault complexes and from literature such as the lithological composition. Igeoss Dynel, which is a mechanical modelling package, was used to create models that provide a more accurate simulation of deformation compared to geometric and kinematic modelling packages such as 2DMove and Trishear.

Two models were created; one with a sigmoidal flat-ramp-flat thrust geometry and the other with a listric flat-ramp thrust geometry. The sigmoidal fault model simulates the central segment of the Aghar fold, and the latter backthrusted model simulates the northern and southern segments of the fold.

The numerical models were also independent of scale, and therefore arbitrary length units were used.

6.3.1. Sigmoidal Flat-Ramp-Flat Model with Forelimb Breakthrough Thrust

This three-stage forward model simulates the middle part of the Aghar fold (Sections III to VII) (Fig. 6.2 & Table 6.1). The model consists of a main thrust fault with a sigmoidal flat-ramp-flat geometry. During the second phase of shortening, a FBT fault was introduced to the model.

The initial layer cake model consists of three pre-kinematic units (Fig. 6.2 -a). The lowermost unit, Pre-Kinematic 1, is the detachment sequence with a sliding top surface. The Pre-Kinematic 2 and 3 are 1 length unit thick shale sequences that have a locked interfaces. Each phase of deformation is shown by a representative cross-section and section showing the strain distribution (Fig. 6.2).

Step	Total Shortening	Uplift	Incremental shortening	S:U ratio
1	9.0	6.1	9.0	1:0.7
2	15.0	9.9	6.0	1:0.6
3	23.0	13.4	8.0	1:0.4

Table 6.1 Incremental values of shortening and uplift for each step of model sigmoidal flat-ramp-flat model (Fig. 6.2)

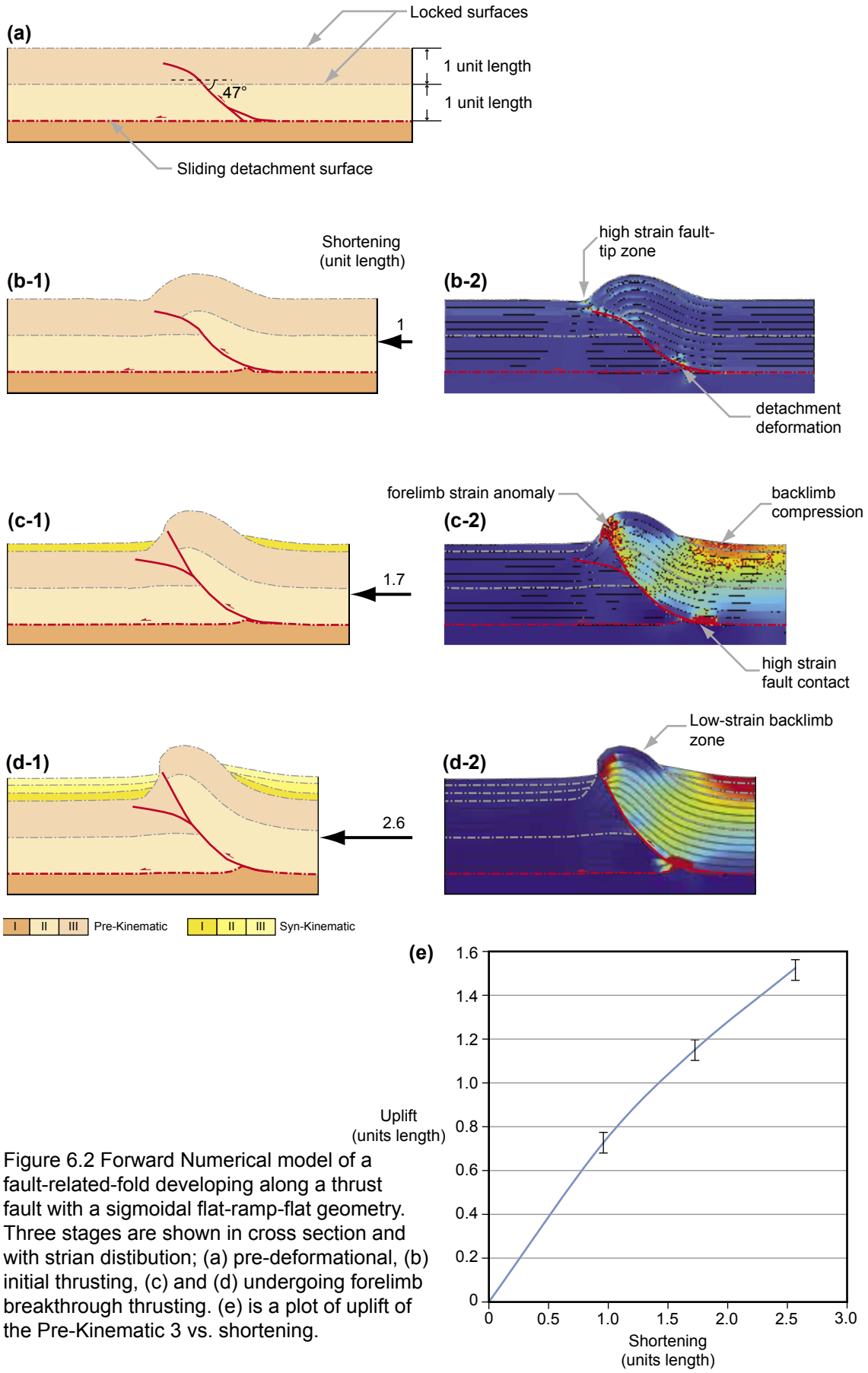

Figure 6.2 Forward Numerical model of a fault-related-fold developing along a thrust fault with a sigmoidal flat-ramp-flat geometry. Three stages are shown in cross section and with strian distibution; (a) pre-deformational, (b) initial thrusting, (c) and (d) undergoing forelimb breakthrough thrusting. (e) is a plot of uplift of the Pre-Kinematic 3 vs. shortening.

The initial thrust setup is a flat-ramp-flat geometry that does not penetrate to the surface. This allowed folding of the two upper pre-kinematic units in the Pre-Kinematic 3, which is observed in the middle sections of the fold. The thrust ramp dips at a maximum of ~47°.

The first shortening phase (shortening = 1units length) (Fig. 6.2 B-1 & B-2) shows only a small amount of deformation taking place in the layers, in particular near the fault contact. Strain is concentrated at the backlimb syncline as well as the upper part of the fold between the crest and the edge of the forelimb.

In the second phase (shortening = 0.7 units length, total shortening = 1.7units length) (Fig. 6.2 C-1 & C-2), a FBT fault is incorporated into the model. The FBT dominates the contractional movement. The steep dip of the main fault (~60°) in the upper parts of the section compared to the previous fault geometry (~14°) causes large variations in strain distribution (Fig. 6.2 C-2). At the tip of the fault, a culmination of strain is observed on the termination of the upper layers. These layers also undergo rotation and thinning near the fault termination. Another strain maximum occurs at the backlimb syncline near the fault plane. This is associated with the strain maximum that occurs in the upper part of the section that also coincides with the axial surface of the backlimb syncline. Some detachment deformation also occurs beneath the thrust ramp.

The third and final phase (shortening = 0.9, total shortening = 2.6) follows a similar trend to the second phase of shortening. The strain focused at the tip of the fault and the backlimb synclinal area. The additional shortening also caused strain to develop near the fault in the bottom two units were folded.

In general, the geometry of the fold continuously tightened and became more asymmetric with increased shortening. The cutoff angle of the pre-kinematic beds increased upwards in the section and the dips of the backlimb beds were near parallel but shallower than the dip of the fault plane.

Step	Total Shortening	Uplift	Incremental shortening	S:U ratio
1	2	1.9	2.0	1:0.9
2	3.5	3.9	1.5	1:1.4
3	5.5	8.6	2.0	1:2.3
4	6.5	9.5	1.0	1:1.0

Table 6.2 Incremental shortening and uplift values of each step in the listric flat-ramp model (Fig. 6.3)

6.3.2. Listric Flat-Ramp Model

This model shows the four-stage in the evolution of a listric flat-ramp thrust-related-fold with a backthrust (Fig. 6.3 & Table 6.2). This simulates the evolution of the northern and southern parts of the Aghar fold. During the first two stages of growth the fold evolved along the main forward-vergent (in the direction of shortening) thrust fault and the backthrust was introduced in the third and fourth stages of growth.

The initial pre-deformational section consists of two pre-kinematic shale units, Pre-Kinematic 2 & 3 on top of a detachment unit, Pre-Kinematic 1. The thrust fault geometry prior to deformation consisted of a listric fault with ~54° ramp dip, similar to that observed in the Aghar fold. Coulomb shear was calculated for each stage of deformation in order to visualize the distribution of shear stresses.

At the first stage, 2 units of shortening (Fig. 6.3 b-1 & b-2) caused the hangingwall propagate along the fault plane. This induced stresses at the bottom of the hangingwall near the fault inflection point and in the front of the crestal part of the fold, which was highly rotated and compressed. High stresses were also developed in the footwall at the tip of the thrust fault and where the fault joined the detachment. A high-strain anomaly occurs beneath the fault in the detachment unit.

During the second stage (Fig. 6.3 c-1 & c-2), the fold continues to grow with a similar fault geometry to the previous stage. This stage accounts for 1.5 units length of shortening to a total shortening of 3.5 units. A sandstone syn-kinematic unit was inserted to the model prior to this stage of deformation. The stress distribution remained the same as the previous stage, where the maximum

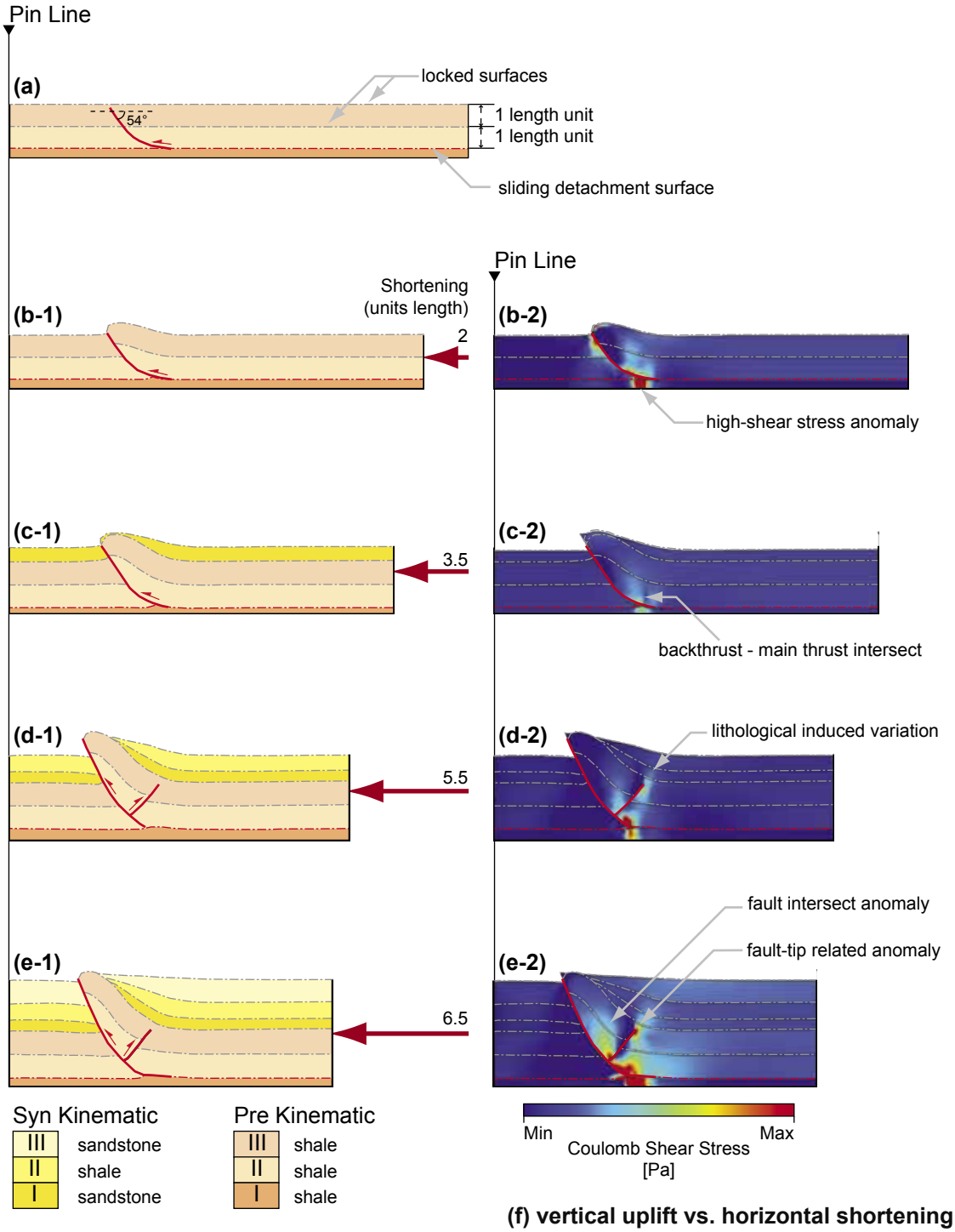

(f) vertical uplift vs. horizontal shortening

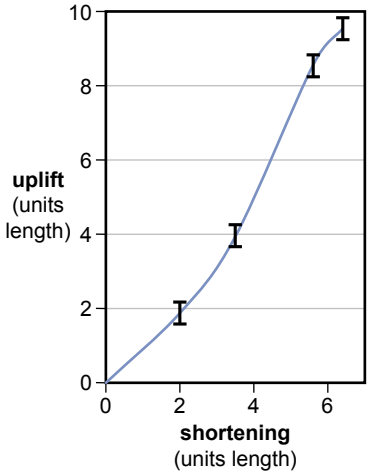

Figure 6.3 Evolution of a fault-related-fold with a listric flat-ramp thrust fault geometry and a backthrust. (a) shows the pre-deformation, (b - c) initial forward vergent thrust and (d - e) have a backward vergent backthrust. (b-2 to e-2) show the maximum Coulomb shear strain (MCSS). (f) shows the vertical uplift vs. horizontal shortening from the model. MCSS is considered an indication of maximum shear strength along conjugate shear faults that are defined by Coulombs failure criterion.

stress was concentrated at the base of the section stage, near the fault inflection point. The footwall and hangingwall fault contact continues to deform, where the hangingwall units were rotated further.

In the third stage of growth (Fig. 6.3 d-1 & d-2), a backthrust was introduced to the model as well as the shale Syn-Kinematic 2 unit. At this stage, the majority of the shortening has taken up by the main thrust fault. Minor displacement occured place on the backthrust, however only Pre-Kinematic 2 is displaced, and the top of Pre-Kinematic 3 does not show associated deformation. The stress distribution was focused in three parts of the model at the base of the main thrust at the point of inflection, at the main-thrust and backthrust intersection, as well as at the tip of the backthrust (Fig. 6.3 – d).

The final stage (Fig. 6.3 e-1 & e-2) accounted for 1 unit of shortening to give a total shortening of 6.5 units. The backthrust became more active during this period and absorbed the majority of the shortening. The Pre-Kinematic 2 showed slip on the backthrust and Pre-Kinematic 3 was folded. Shear stress was concentrated at the tip and base of the backthrust as well as above the point of inflection of the main thrust (Fig. 6.3 – e).

During first two stages the associated relief is comparable to the amount of shortening (Table 6.2). The ratio of shortening-to-uplift (S:U ratio) of the first and second stages are 1:0.9, and 1:1.4 respectively. The maximum S:U ratio is during the third stage, when the back-thrust is introduced to the model, where the ratio was 1:2.3. This rapidly decreases with additional shortening during the fourth stage, when the ratio drops to ~1:1.

The pre-kinematic footwall and hangingwall fault contact geometry also changes with growth. The upper hangingwall sequences tend to thin and narrow, whereas the footwall contacts tend to widen. The bottom part of the footwall also undergoes some uplift, which causes the detachment to create an upward cusp under the fault plane.

The shear stress distribution was affected by lithology (Fig. 6.3 – d-2). Interfaces between shale and sand sequences (such as the Top of Pre-Kinematic III), act like stress barrier because of the difference of their mechanical properties.

6.3.3. Implications of Numerical Modeling

- Stress and strain focuses on fault tips, as well as areas, which undergo folding, such as the hanging wall syncline and crestal area.
- During fold amplification, the crestal area undergoes high-stress, which results in thinning and rotation of the forelimb.
- The pre-kinematic cutoff angles increase with depth.
- In both models, the fault contact in the footwall also undergoes high strain and thickens. This implies the significance of footwall deformation in fault-related-folds, in particular in poorly consolidated sediment.

6.4. Discussion

This section discusses of the previous models and sheds light on the their kinematic implications. Even though the models highlight several features that improve the understanding of the Aghar Fold and similar structures, the models have several shortcomings that need to be addressed for future work discussed at the end of the chapter.

6.4.1. Development of the upper Ramp

The restoration and the sigmoidal model have a fault geometry that has an upper flat. It is apparent that the upper flat is not necessary part of the initial geometry as such, but as the restoration showed, it may have developed at a later stage than the original fault. Correctly modelling this aspect would improve the understanding and even interpretation of the Aghar thrust fault. This upper flat could be associated with a weaker rheology, which can be explained by

the weaker, less compacted (less dewatered) sediments of the upper 1 to 1.5 km of deepmarine clays. Additionally, the propagation of the fault is probably caused by the high shear stress applied on the forelimb as a result of its rotation and folds as observed in the numerical models. The faults may have therefore developed as an accommodation fault (See discussion Chapter 7). This would also explain the complex syn-kinematic geometries that would form as a result.

6.4.2. Development of the Forward Breakthrough Thrust (FBT)

The formation of the FBT in the Aghar fold is an indication of where the minimum work direction would have been. In other words, the hanging wall propagating up the fault would have require less energy or work than to continue to displace along the upper flat. There are two explanation to this; either the deformed strata ahead of the forelimb hardened enough with strain that it prevented the structure form further propagation, or the syn-kinematic strata has built-up a buttress-like body ahead of the forelimb which prevented further propagation in a lateral sense. The latter is more likely, where syn-kinematic sedimentation plays a key role in defining the geometry of fold structures.

After the development of the FBT, the structure becomes significantly asymmetric compared to the previous geometry. The rotation of the forelimb applies a significant amount of shear stress on the limb, which causes shearing. that is observed in the model (Fig. 6.2 c-2).

6.4.3. Uplift vs. Shortening Plots

These plots are commonly used when discussing models and restorations. In this instance they also highlighted some of the shortcomings in the models of this chapter.

In the restoration, two growth patterns can be recognised. The initial phase which consists of most of the vertical uplift. The following phase is associated

with the majority of shortening but without significant uplift, ie the fold began to accommodate shortening laterally more than vertically. This is expected in such a section where the initial growth was along a steep ramp, later shortening phases followed a shallower dipping thrust fault in the upper section.

However, there are two variations in the plot. These were attributed to fold degradation such as crestal collapse and scarp development. It is more likely that these variations in the plot show problem with the restorations as opposed to natural phenomena. Additionally, the full extent of scarp deformation cannot be fully quantifies and therefore the full effect of this degradation on the growth of the fold is unknown. Thus, incorporating it into the model would be difficult and probably inaccurate.

In the Sigmoidal model, the curve is very linear and does not reflect the changes in fault geometry. In this case it is likely to be cause by the small displacements used in the model. The restoration suggests that there is a significant amount of shortening taking place in the section, and in order for the model to better represent the its natural counterparts, it must have a similar amount of shortening.

In the listric fault model, a larger, more representative shortening was employed, however the steep fault geometry caused the uplift of the section to be significantly higher than the elevation achieved in the restoration.

6.4.4. Limitations of the Models

Several aspects of the restoration and the models have to be corrected before carrying out future models.

The geomechanics of the strata, detachment and faults have not been correctly initialized in the models. Petrophysical and rock mechanics should be incorporated into the models to provide better representation of natural structures.

Another aspect is the length of the model and restored sections. Exaggeration of the length of the model is needed to tackle edge effects that are inherited artefacts of finite element modelling.

An additional problem is the models setup. The fold geometry that was used for the restoration has since been updated (Chapter 5). In particular in the footwall area, the updated interpretation suggests the presence of a fault complex that includes a series of basinward and landward thrusts within the upper detachment unit (Pre-Kinematic 2) . This leads to the second problem with the input geometry of the restored section where it does not account for the initial thickening of the detachment unit by means of brittle thrusting. These issues hinder the restoration and do not allow the full restoration of the section (Fig. 6.1-h, -i, & -j).

The forelimb restoration is also a critical point to address. This part of the fold underwent a high amount of shear deformation (discussed further in Chapter 7.6). The software is not fully capable of restoring this kind of deformation. Furthermore, the steep limbs prevent detailed interpretation of the small-scale accommodation faults that form in this highly sheared area. These structures can account a significant amount of deformation, which the model does not account for.

In the forward models, the listric thrust fault model (Chapter 6.3.2) used a fault geometry that is significantly different than what is observed in the Aghar fold. the dip of the thrust fault was ~54°, where as the Aghar fold has a thrust fault dip of ~40°. This aliases the results and causes the fault to grow vertically more than the observed in the Aghar fold and in most natural examples. This shortcoming also affects all the measurements made on the model, such as the uplift vs. shortening and distributions of stress, strain and shear planes. Suffice to say, the outcomes are inaccurate and are not representative of its natural counterpart.

In the sigmoidal fault model, the model does not account for the multi-phase development of the thrust fault. As the restoration shows, the fault probably evolved with the growth of the structure. The structure may have evolved with a simple planar fault geometry in the upper section, and the fault propagated at a shallower angle in the upper, weaker sequences. This may also be the case for the listric fault, where the main thrust main thrust fault may have evolved and propagated with increased stress concentrations on the forelimb.

Furthermore, the elevation of the upper flat is not representative to that in the data. In the data, the upper flat occurs within the syn-kinamtic sequences. This would have important implication for the mechanics of the folded strata. This fault would have developed during the formation of Syn-Kinematic 1. Prior to this period, the deformation would have been focused on the folding and rotating of the forelimb. This would have formed syn-kinematic strata with fanning geometries, however, poor resolution of the syn-kinematic sequences does not resolve this in the seismic volume. With the development of the upper flat, the deformation would follow a more self-similar growth style of a kink-band migration model.

In the sigmoidal model and the restoration there was no emphasis on the crestal collapse structures that alter the Present Day crestal geometry, and is interpreted to have also done so in the past (See amplitude map interpretation Chapter 4).

6.5. Future Recommendations

The purpose of this chapter is to introduce the numerical modelling and restoration capabilities of Dynel2D. The methodology and models were not perfect, and in some cases did not correctly depict its natural counterparts. Nevertheless, the outcomes of this chapter can be the basis for future numerical modeling using this software or other similar packages.

These models need to be improved in order to better simulate their natural

counter parts. The initial geometry, in particular with the listric model above, should be more representative of thrust related folds occurring in nature. Another aspect is to use mechanical parameters that are derived from measurement based on observation in the field or in boreholes rather than using the software defaults. These include the geomechanical parameters and lithology.

This study was only restricted to two forward models and a restoration. In future work flows, several iterations should be carries out. This would allow several different models to be tested, where different parameters, or even alternative interpretation are used. Varying the fault dip and/or geometry would drastically alter the results, and systematic comparison of this variation would improve the understanding of the evolution of these structures. Furthermore, the software allows previewing different stress and strain attributes, which compared and critically discussed. Finally, where possible, these models should incorporate as much detail as possible to mimic real structures. Minor features such as the crestal faulting, scarp development and duplex development in the detachment should be addressed in associated models or treated separately.

The outcomes of such a detailed study would allow better understanding of the evolution of structures and their interpretation. The results would also benefit understanding of hydrocarbon systems in terms of burial and compaction, migration, trapping style, reservoir quality (compartmentalization and mineral vein development, fracturing, creation and depletion of porosity and permeability, as well as stress orientation and anisotropy).

Chapter 7
Discussion

7.1. Introduction

The Niger Delta is a Cenozoic delta that has been continuously active from the Paleogene to Present Day. It has been undergoing thin-skinned deformation due to differential loading, where the proximal parts collapse by extensional faults due to sediment loading, which is translated to the distal parts of the delta and creates contractional structures. This research focuses on the western contractional parts of the delta, studying the geometry and evolution of the Aghar Fold.

In previous chapters, a regional and detailed analysis was carried out for the contractional fold and thrust belt. These chapters provided insight intot he regional setting, as well as detailed analysis of the Aghar Fold geometry and a description of the growth strata. This chapter integrates the findings of the previous chapters to construct a 4D evolutionary model of the Aghar Fold. The findings of this model are then compared to the observation made on the regional lines to understand implications on a broader area. The model and geometry of the Aghar Fold is also compared to other structures from literature on the Niger Delta.

This section will start with a review of the Aghar fold structure (Chapter 7.2). This is followed by a suggested evolutionary model for the Aghar fold (Chapter 7.3). The implications of the Aghar fold geometry and evolution is discussed in a context to the greater 3D seismic area (Chapter 7.4) and the West Niger Delta Fold and Thrust Belt (Chapter 7.5). The outcomes of these discussions is then compared to other published works on the Niger Delta and fold models (Chapter 7.6). Finally, the chapter ends with a discussion of potential hydrocarbon plays in the Niger Delta deepwater fold and thrust belt (Chapter 7.7).

7.2. Structural Geometry and Analysis of the Aghar Fold

7.2.1. Fold Geometry

The Aghar Fold is a basinward vergent (SW) fault-related-fold that formed in a left-stepping en-echelon series of folds. The fold strike is N140°E, following the outline of the outer FTB. The fold is a ~34 km long by ~6 km wide structure that has been active since the Mid Miocene to Present Day. On the present seafloor, the fold creates up to 400 m relief over an area 23 km long by 5 km wide. The forelimb is dominated by a scarp ~17 km long. The Aghar Fold is an asymmetric fold with a steep ~61° – 72° forelimb, and a longer, less steep ~20° – 40° backlimb (measured on the Pre-Kinematic 3 horizon) (Fig. 7.1 & 7.2).

The shape of the fold varies with the variation of the associated fault complex. In the central parts (Fig. 7.2), the fold follows a similar trend to the fault plane. In the northern and southern segments of the fold (Fig. 7.1), back-thrusts cause the backlimb of the fold to have a shallower dip than the main thrust plane.

7.2.2. Associated Thrust Fault Geometry

The fold is associated with a blind basinward vergent, landward dipping thrust complex that cuts the forelimb. The northern and southern segments have listric flat-ramp fault geometries (Fig. 7.1) and the central segment has a sigmoidal flat-ramp-flat geometry (Fig. 7.2). Both geometries have a near horizontal fault dip at the base and ~40° in the middle of the section. The upper part of the sigmoidal faults is ~8° – 19°. Along strike, the fault shows two distinct kink-points with a left-stepping configuration.

Hangingwall forward breakthrough thrusts (FBTs) nucleated from the sigmoidal main thrust upper inflection point in central segment. The northern and southern segments, on the other hand, developed backthrusts.

Forward breakthrough thrust and backthrusts are fold-accommodation faults (Mitra 2002). The FBT accommodates for the excess shearing that occurs as a

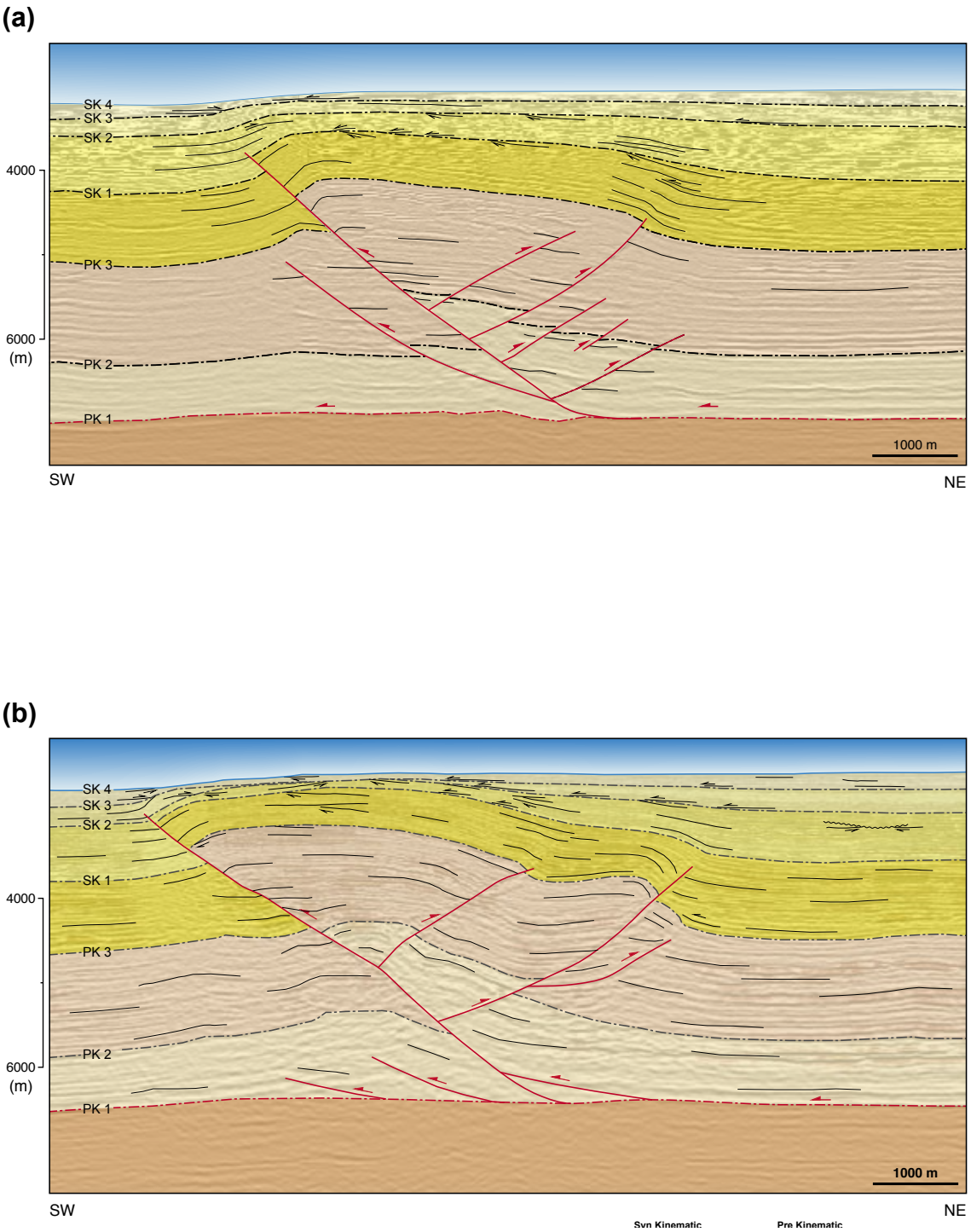

Figure 7.1 Seismic Section I and VIII showing the backthrusted listric fault geometry of the (a) northern and (b) southern segments in the Aghar fold.

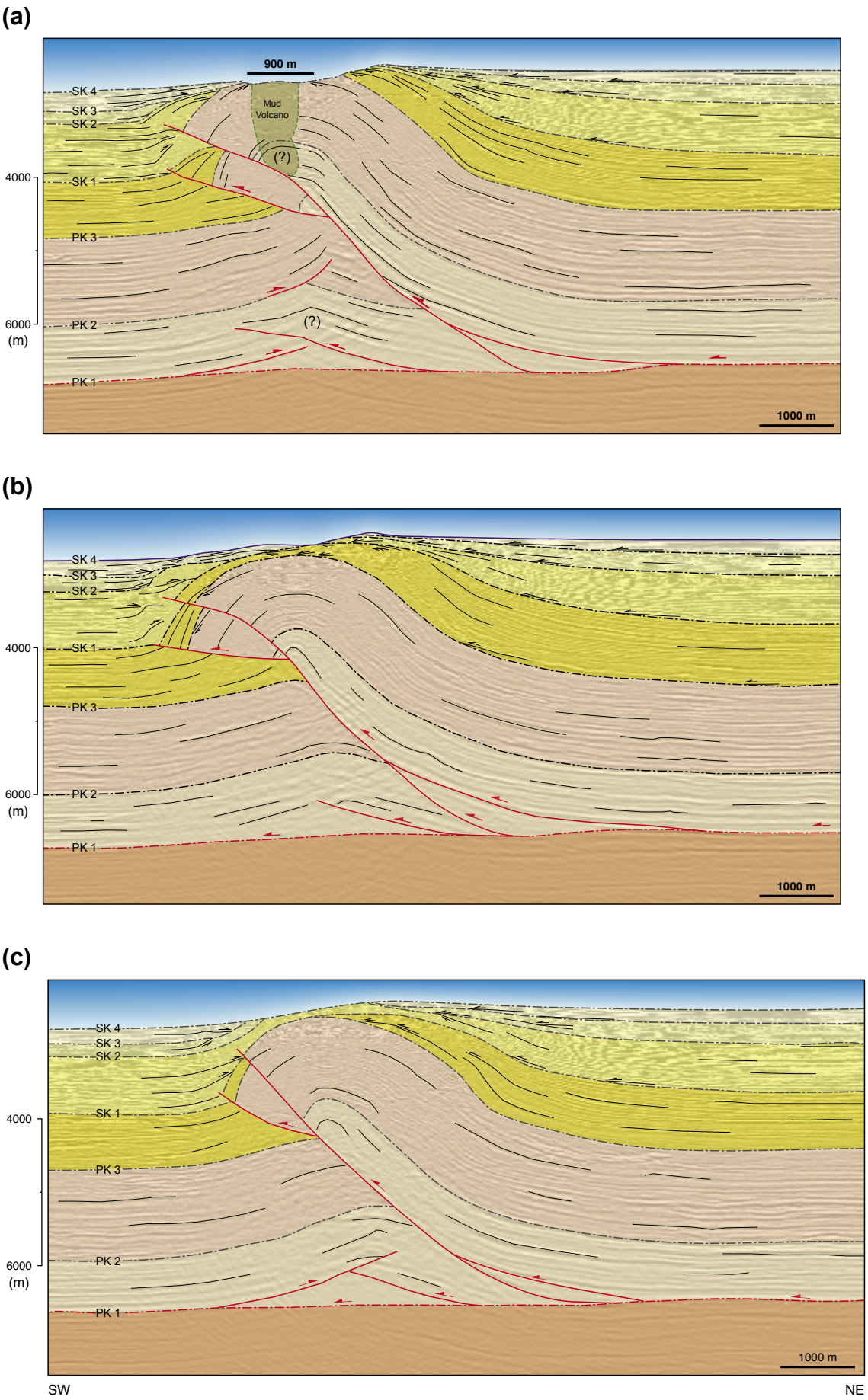

Figure 7.2 Seismic (a) Section V, (b) VI & (c) VII shows the sigmoidal fault geometry from the middle segment in the Aghar fold.

result of the highly rotated to perpendicular forelimb. Backthrusts on the other hand accommodate for the deformation of the units in the hanging wall.

The maximum displacement of ~3100 ± 25m occurs in the middle of the fold (Fig. 7.2), and the minimum displacement occurs in the southern part of the fold, which shows early stages of ramp development.

7.2.3. Aghar Growth Stratal Geometries and Analysis

Syn-Kinematic 1 shows a thickness minima ~14.6 km long by ~3.3 km wide occurs under the Aghar crest, particularly a ~6.7 km segment section at the centre of the Present Day Aghar Fold. Onlap geometries occur near the crestal part suggest fold amplification by limb-rotation.

Syn-Kinematic 2 shows a missing section ~20 km long and ~3.2 km in the central part of the Aghar Fold. Within this sequence onlap geometries progressively shallow in dip and near the crest of the fold. the first indicates limb-rotation, and the latter indicates that rate of sedimentation exceeded the rate of growth.

During the Syn-Kinematic 3 the Aghar creates a thinned section 26.4 km long by 3 km wide. The onlap geometry within this sequence shallows up the section and recedes away from the crest. This indicates growth by limb-rotation and fold growth exceeding sedimentation rate.

Syn-Kinematic 4 shows thinning toward the Aghar crest, at which there is a missing section 24.5 km long by 2.8 km wide. Reflectors within this package are parallel to sub-parallel to Present Day sea bed, indicative of slow fold growth.

The analysis shows that initially in the Mid Miocene only the central Aghar developed. By the Late Miocene – Early Pliocene, the northern and southern segments began to form.

7.3. 4D Evolutionary Model of the Aghar Fold

The Aghar Fold is an amalgamation of three basinward vergent fault-related folds that evolved separately and linked along strike. This section suggests an evolutionary model of the Aghar Fold.

7.3.1. Pre-Kinematic (Pre Lower Miocene)

The pre-deformational configuration was planar with a subtle SW dip (Fig. 7.3 - a). The Top of Pre-Kinematic 3 shows several turbidite flows that have not been deterred by structural growth in the Aghar area.

7.3.2. Syn-Kinematic 1 (late Lower to Mid Miocene)

Initially, the middle segment accommodated shortening by thickening of the detachment unit by duplexing (Fig. 7.3). The brittle character of the shale would not allow ductile flow of material into the core of the fold, but is more likely to have infilled the core by brittle mechanisms such duplex deformation.

Following the formation of the detachment fold, a blind listric thrust fault developed at the base of the section. Shortening was accommodated by fault slip and folding of the trishear zone ahead of the tip of the fault.

By the end of this period, the fault began to propagate upwards through the section at a shallower dip than the ramp. This gives the fault plane the characteristic sigmoidal geometry observed in Sections IV – VII (Fig. 7.3 - b).

7.3.3. Syn-Kinematic 2 (Upper-Miocene)

The growth strata analysis shows that all three fold segments were active during this period (Fig. 7.3 - c). During the Early Upper-Miocene, the northern and southern segments nucleated as separate folds. Both folds rapidly formed listric thrust faults that linked with the detachment.

During the Late Upper-Miocene, the folds began to interact and link along strike.

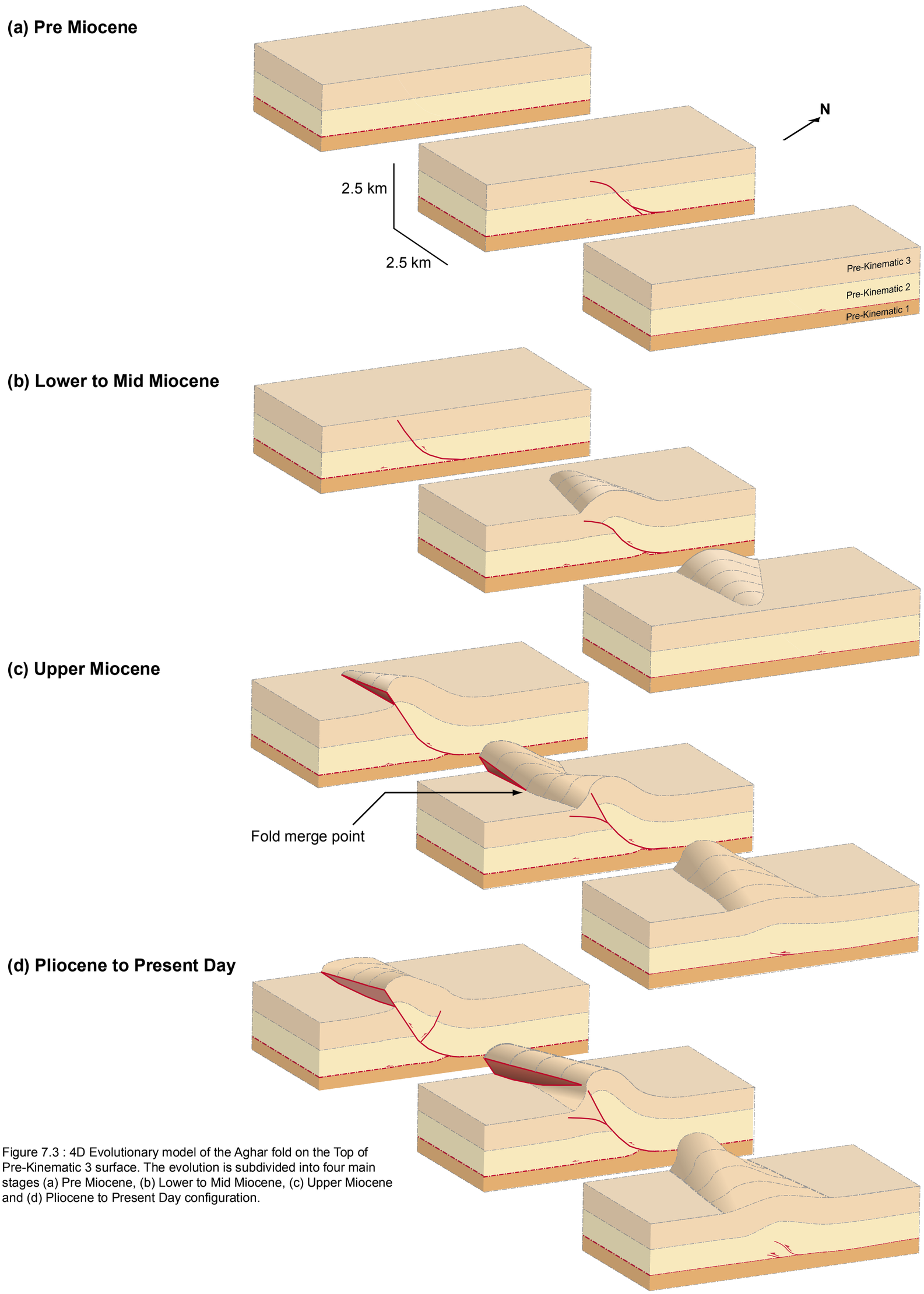

Figure 7.3 : 4D Evolutionary model of the Aghar fold on the Top of Pre-Kinematic 3 surface. The evolution is subdivided into four main stages (a) Pre Miocene, (b) Lower to Mid Miocene, (c) Upper Miocene and (d) Pliocene to Present Day configuration.

By the end of this period, the thrust faults of the three segments were hard-linked.

In the middle segment, a FBT formed in the hangingwall following a similar dip to the main thrust ramp. The upper flat of the main thrust became inactive and all shortening was taken up by the newly formed thrust. The formation of the FBT may be attributed to interaction between the fold segments, where the listric geometry of the northern and southern segments influenced the stress distribution of the middle segment, causing failure to occur in the hangingwall.

7.3.4. Syn-Kinematic 3 – 4 (Pliocene – Present)

By the Pleistocene, the main thrust faults of the three segments were completely linked and shortening was evenly distributed along the fold (Fig. 7.3 - d). This is observed in the Syn-Kinematic 4 sequence, where the thinning is homogenous along the length of the fold.

7.4. Implication for the 3D Seismic Area

7.4.1. Geometry and Structure

The structural strike in the 3D area is oriented N140°E, which follows the outer edge of the delta. There are three main contractional features that dominate the 3D seismic area, from NE to SW, are the Bobo Fold, the Aghar Fold and the Southern Imbricates. The Bobo consists of three opposite vergent thrust faults that linked along strike. The Aghar Fold is associated with a thrust fault that amalgamated from several smaller basinward vergent thrusts. The Southern Imbricates are at least imbricated landward vergent thrust related folds. A common feature among all the thrusts in the 3D area is the trajectory of the thrust faults; the faults have a steep ramp (~40°) that soles along the detachment at a shallow to near horizontal angle.

The distinct geometry of the Bobo Fold is directly associated with the thrust complex, where the northern and southern faults are basinward vergent,

(a)

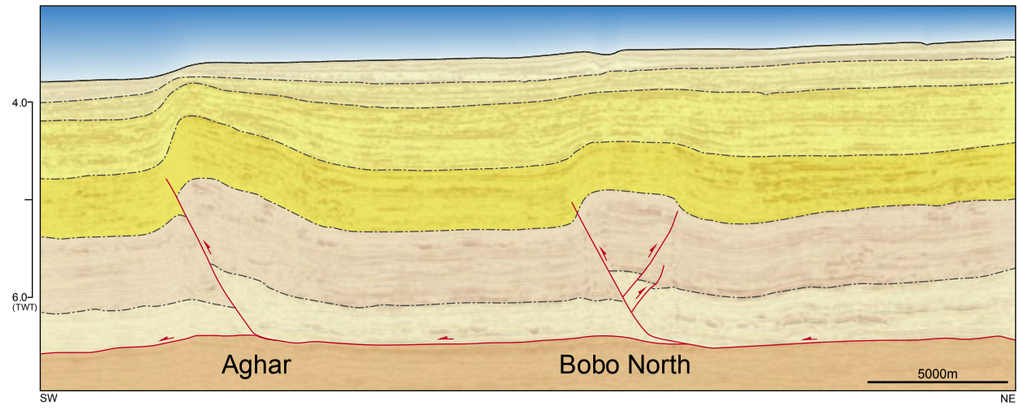

(b)

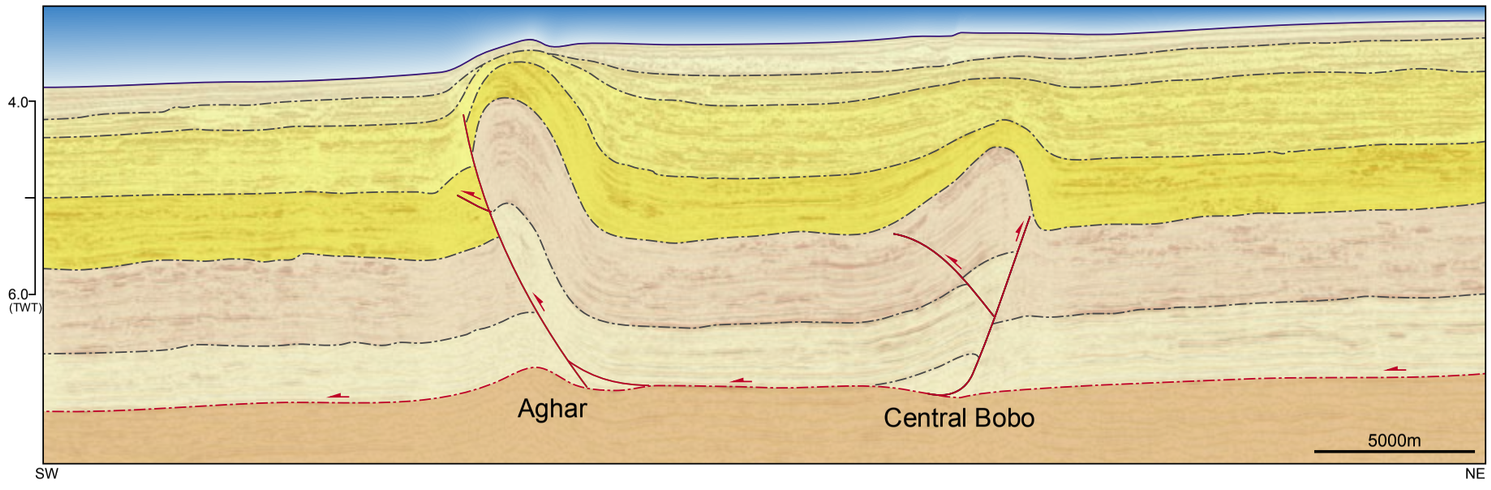

(c)

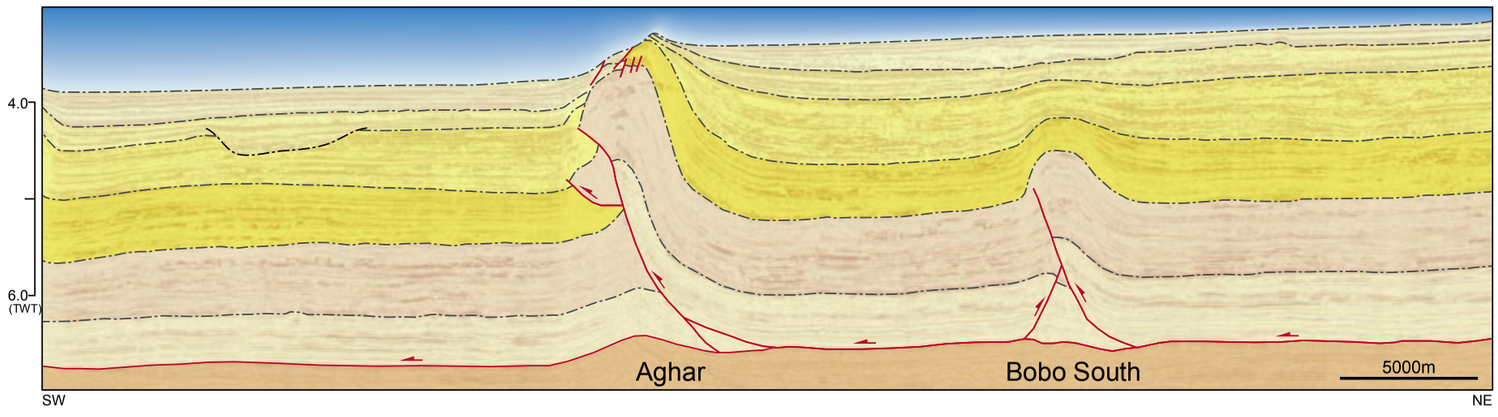

(d)

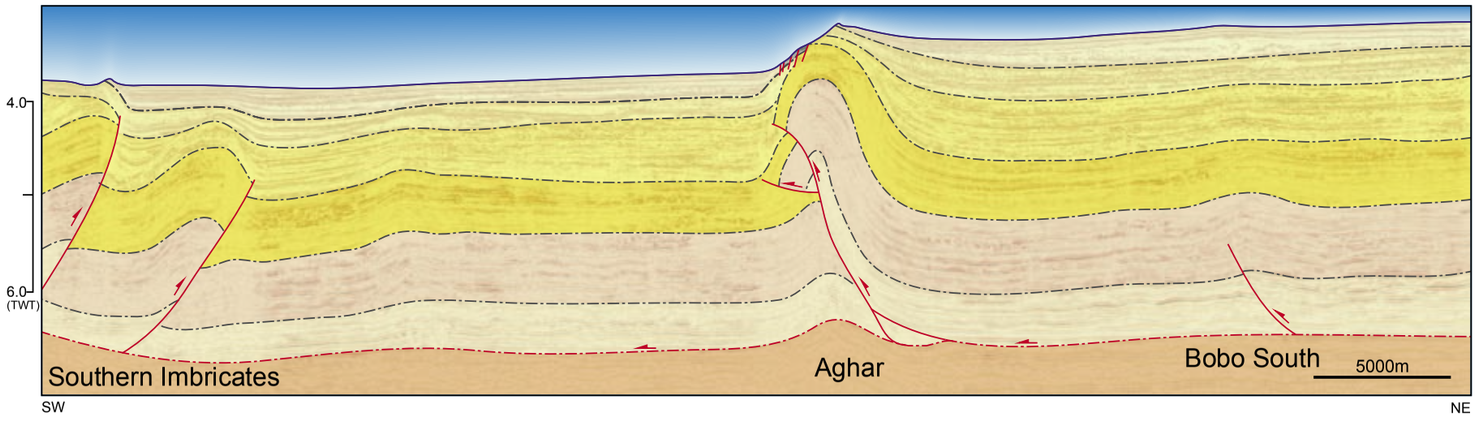

Figure 7.4 : Two-Way-Time 3D Seismic transects A - D. Vertical Exaggeration ×2

and the central fault is landward vergent. The fold geometry follows these orientations, in particular at the middle of each fault. The joining points between the northern-central and central-southern folds follow a more symmetrical geometry and have fault and fracture complexes associated with the along strike linkage of opposite verging faults.

The full geometry of the Southern Imbricates cannot be resolved because of lack of data, however, the imbricate faults link in the bottom of the section along the detachment unit. The folds to the SW have been thrusted over the folds in the NE of the imbricates.

A heave plot was concocted to study the variation in the amount of shortening throughout the section (Fig. 7.5 -b). The data was derived from the 3D transects and compares the total heave to the independent heave of the Aghar Fold and Bobo Fold. The Souther imbricates only occur in one section, but were incorporated into the Total Heave plot at Section D.

The plot show that the majority of the shortening throughout the section is concentrated on the Aghar fold and probably the Southern Imbricates. The amount of heave taken up by the Aghar fold is significantly larger than that of the Bobo fold where the latter may only account a maximum of ~900m or ~ 50% of the total shortening (Fig. 7.5 -b; Section A). The Aghar fold may dominate the shortening as observed in Sections B, C, & D, (Fig. 7.5 -b) and accounts for a significant amount of shortening in the area. The Southern Imbricates also shows a large amount of shortening (~2000m in Section E) similar to that of the Aghar fold, however, due to the lack of data the NW and SE extension of this structural feature is not present for this study. Nonetheless, the southern imbricates are likely to be a series of closely spaced (laterally) fault-related folds with almost uniform shortening taking place. These folds are likely to represent the outer fold and thrust belt, which are characterised to have lateral continuity for the majority of the western lobe of the Niger Delta.

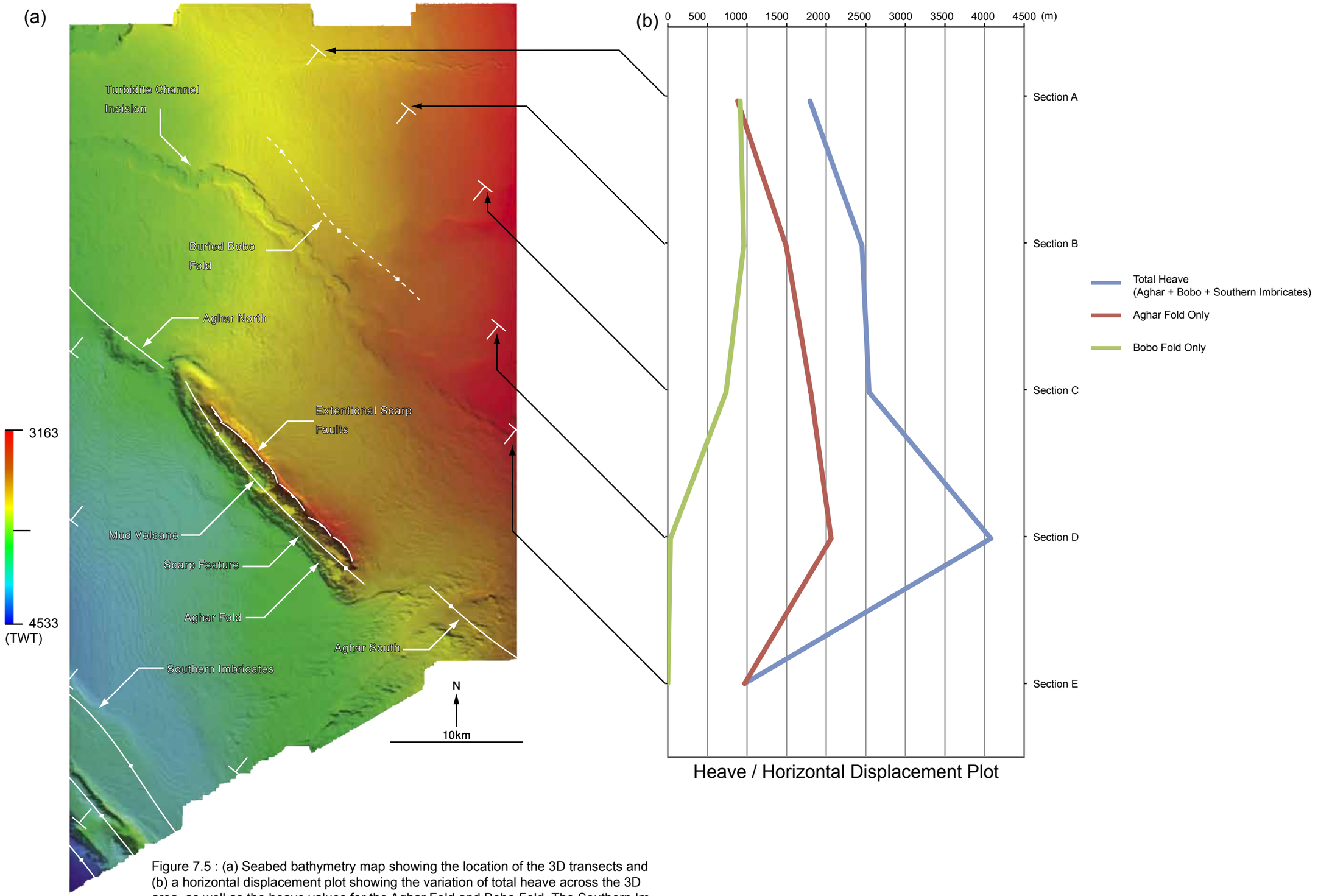

Figure 7.5 : (a) Seabed bathymetry map showing the location of the 3D transects and (b) a horizontal displacement plot showing the variation of total heave across the 3D area, as well as the heave values for the Aghar Fold and Bobo Fold. The Southern Imbricates have been incorporated into the Total heave plot.

7.4.2. Evolution and Age Relations

From the 3D transects and thickness maps, a wider evolutionary history can be derived. The purpose of this section is to compare the growth of the Aghar structure to the other structures within the 3D seismic area, and to understand the distribution of shortening over time.

During Syn-Kinematic 1 period (Lower- to Mid-Miocene), both the central segments in the Bobo and Aghar Folds were dominantly active. The Bobo South segment shows some growth in cross section (Fig. 7.4 - c) but this would have occurred at a late part of this period.

During the Syn Kinematic 2 (Upper Miocene), growth occurred along all three segments of the Aghar and Bobo Fold, and one of the Southern Imbricates began to grow. The growth is characterised to occur along most of the Present Day folds.

During Syn Kinematic 3 (Pliocene), the Aghar and Southern Imbricates continue to grow, and the Bobo Fold growth begins to slow down and only occurs within the North and Central segments.

During Syn Kinematic 4 and to Present Day (Quaternary), the Aghar Fold and the Southern imbricates continue to grow except for the foremost (NE) fold, which has ceased growth.

During the Syn-Kinematic 3 and 4 (Pliocene to Present Day) Shortening was dominated by the Aghar Fold and Southern Imbricates. The foremost fold in of the Southern Imbricates, has creased growth during the end of this period. The growth of the Bobo Fold also began to slow down, and completely ceased by the Quaternary.

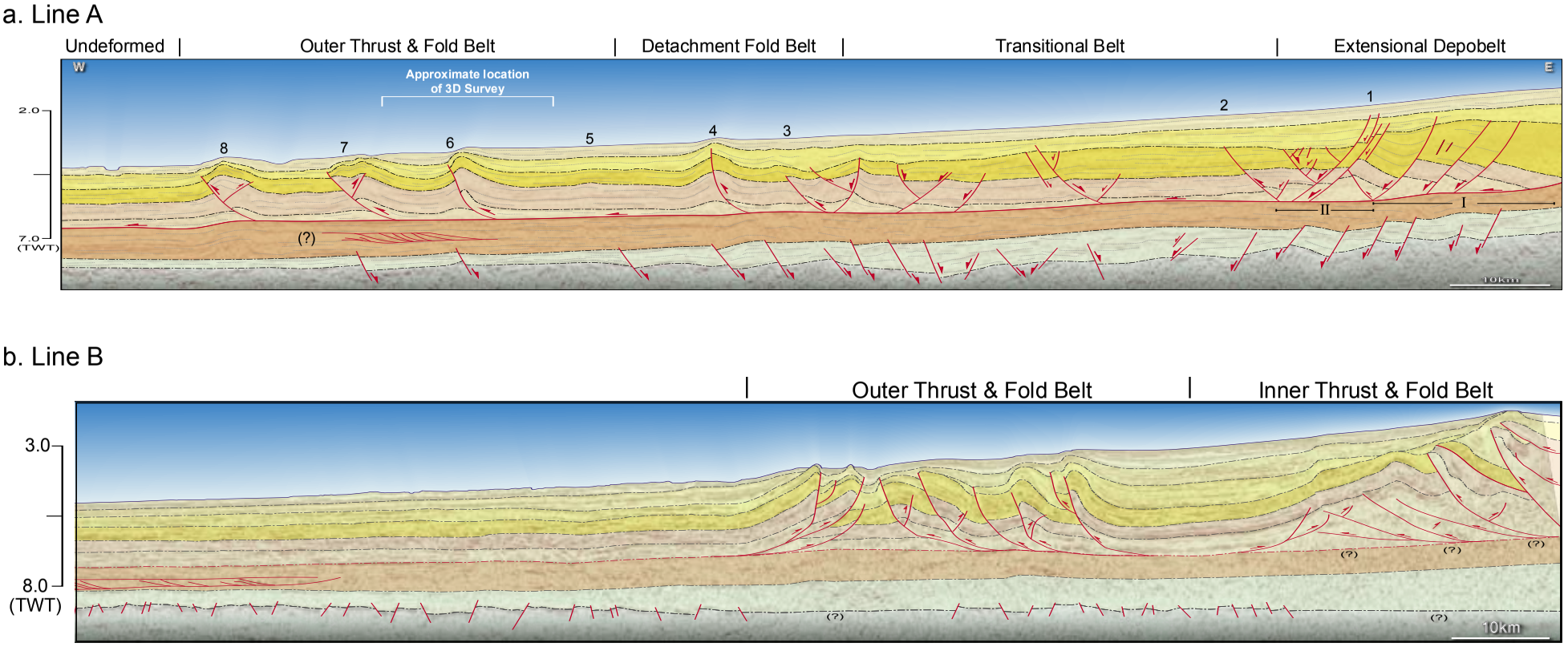

Figure 7.6 2D regional lines. (a) shows Line A with extensional depobelts in the proximal part and contractional belts in the distal parts. (b) shows Line B that intersects the inner and outer FTB.

Syn Kinematic	
I	Quaternary - Pliocene
II	Upper - Miocene
III	Mid - Miocene

Pre Kinematic	
I	Lower - Miocene
II	Oligocene
III	Paleo-Eocene

Pre Niger Delta	
	Late Cretacrous (?)
	Oceanic Crust

7.5. Implications for the West Niger Delta Fold and Thrust Belt

7.5.1. Geometry and Structure

The Fault related Folds (FRF) in the 3D area are a mix of both basinward and landward vergent structures. The structures are characterised to be widely spaced, with the exception of the southern imbricates. These characteristics are observed in the outer fold and thrust belt (FBT) in both regional lines.

Regional Line A shows a set of basinward vergent, widely spaced FRF that have listric thrust fault geometries (Fig. 7.6 - a). The outer fold and thrust belt in Regional Line B (Fig. 7.6 – b), which is also less widely spaced, but has both basinward and landward vergent folds. The latter are located to the basinward part of the delta and are considered to delineate the lateral extent of the main Akata detachment. Knowing that the location of the 3D dataset is near the edge of the delta deformation domain would similarly suggest that the southern imbricates may represent the lateral extent of the main Akata detachment.

The majority of the folds that occur on both the regional lines are associated with a thrust fault, which commonly develop back thrusts (Fig. 7.6 – a & b). This creates a more gentle backlimb dip that is observed in the northern and southern segments of the Aghar Fold. Furthermore, some thrust faults developed Forelimb breakthrough thrusts in Line B (Fig. 7.6 - b), also similar to the Aghar Fold.

Syn Kinematic units in Regional Line A have a geometry that is thick at the proximal part and thin at the distal parts. This is not only associated with growth but is also attributed to differential loading, where a larger amount of sediments is deposited at the proximal parts.

7.5.2. Evolution of the West Niger Delta Fold and Thrust Belt

The 2D lines show a multi phase evolution of the delta deformation domain. The overprinting of contractional fault by extensional faults is an indication of

migration of deformation basinwards.

In Regional Line A (Fig. 7.6 - a), during the early stages of Syn Kinematic 1, thrust fault 1 and 2 were active. By the middle of this period, these faults were superimposed by extensional faults, and the contractional domain migrated basinwards. In literature, escalator regression is an accepted model of basinward migration of extentional fault bound depobelts (Knox & Omatsola 1989). The theory, however, does not correctly address the lateral migration of the thrust front which is discussed further in Chapter 7.6.4.

Not all the extension that occurs in the landward part of the Line A is accommodated by folding in the distal parts. Lateral compaction of weakly lithified strata also contribute by 18-25% of volume loss (de Vera, Grando & McClay 2010; Butler & Paton 2010). The volumetric compaction is related to the loss of pore-fluid, therefore fluid expulsion mechanisms such as mud volcanoes are observed in the Niger Delta. Therefore, even the transitional zone between the extensional and contractional belts accounts for some of the shortening that occurs in the delta. The Mud volcanoes are not likely to originate from the deep section, they are limited to the Pliocene section (Graue 2000) ~1 km below the seabed. This depth also coincides with the main dewatering zone of clays, where mudrocks reduce water content from 70-90% to ~30% (Tucker 2001).

However, large-scale structures, such as contractional fold and roll-over folds associated with extensional faulting, are also associate with mud volcanoes as is observed in the Aghar Fold. This would allow the older section (pre-Pliocene section) to also release additional pore fluid such as hydrocarbons in crestal reservoirs (discussed further in **7.7** Implications for Hydrocarbons).

7.6. Comparative Examples

7.6.1. Introduction

In This section, the geometric and evolutionary finding of this research are

compared to other works done on the Niger Delta and fold evolutionary models. This comparison not only compares the fold structure in the west Niger Delta, but also compares the observations to those made in the southern lobe of the Niger Delta.

7.6.2. Shear Fault-Related Folding

Fold and thrust belts fold growth models have been a topic of study and controversy for many years. Simple geometric models such as fault-bend folds, fault-propagation fold, and detachment folds were used to describe contractional folds (Suppe 1983; 1985; Suppe & Medwedeff 1984; 1990). The basic assumption in these models is to conserve the pre-kinematic layer thickness (Shaw et al. 2005). These simple geometric theories have been refined by several workers to address several observation made in nature. Trishear Fault propagation folding was introduced to explain the deformation associated with the tip of a propagating thrust (Erslev, 1991; Hardy and Ford, 1997).

However, these geometric models were over simplified. They were conceptualized base on 2D geometries and restorations that do not account for the 3D evolution of the fold structures and they do not account for the mechanical properties that occur in the nature.

Suppe et al. (2004) suggested that shearing plays an important role in the deformation that takes place in distal fold and thrust belts. Shear fault related fold models are characterised to have a long back limb that has a shallower dip than the fault plane, and a short forelimb that is highly rotated (Shaw et al. 2005) (Fig. 7.7). The growth strata associated with this structure typically shows shallowing dip with younger sequences similar to limb-rotational models, and forelimb syn-kinematic strata that has a similar dip to the pre-kinematic strata, akin kink-band migration models (Suppe et al. 2004; Shaw et al. 2005). Both the fold and growth stratal geometries are observed in the Aghar fold and are likely

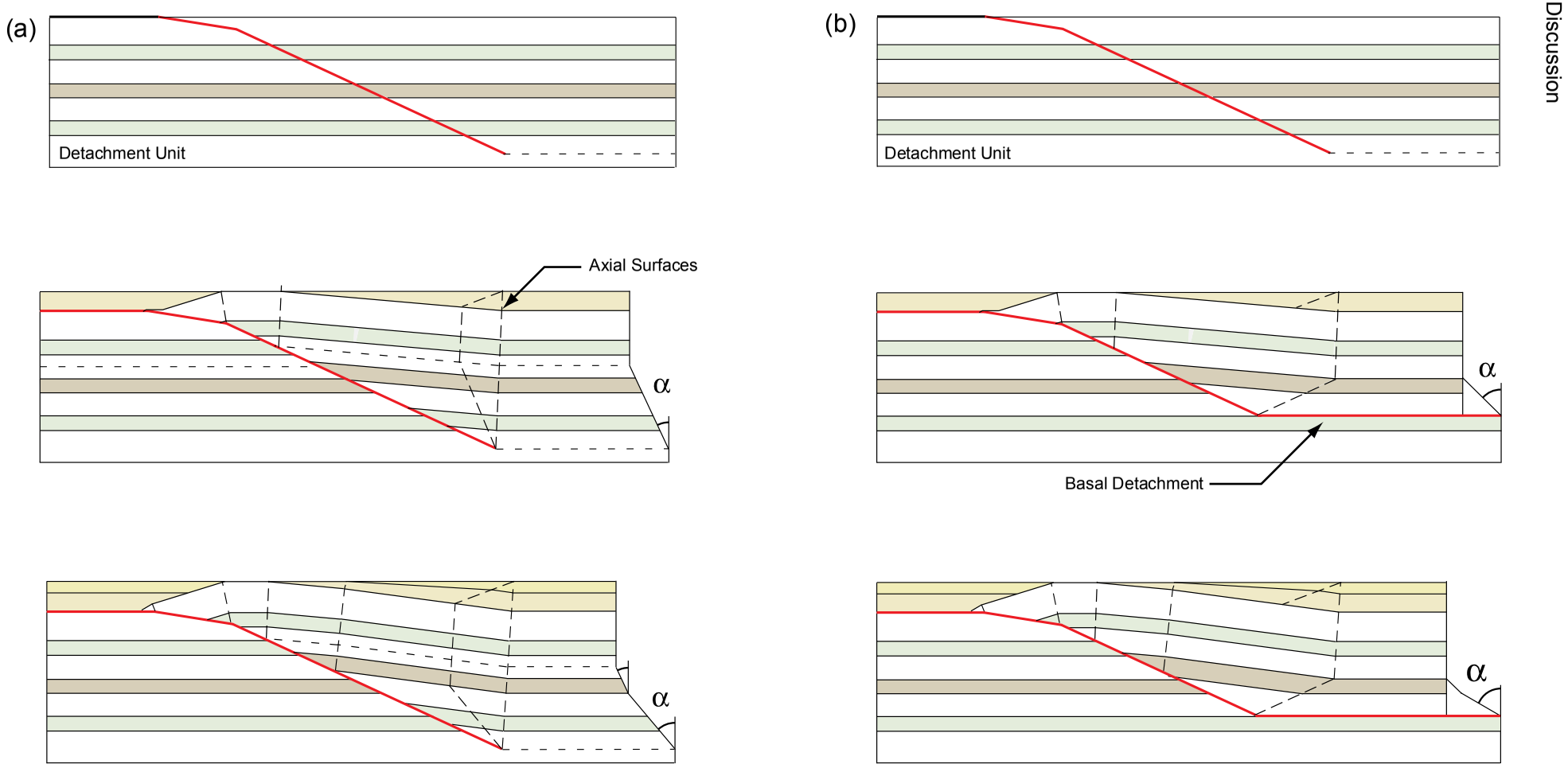

Figure 7.7 Schematic evolutionary model of (a) simple-shear fault-bend folds and (b) pure-shear fault bend folds. Both fold have a backlimb that has a shallower dip than the associated thrust fault, and a steeper forelimb. Fanning growth stratal geometries occur at the backlimb that is not observed in the forelimb. Simple-shear fault bend fold (a) grow due an external force that is applied to the whole section with zero offset at the base of the thrust, where as the pure-shear model has most the strain focused on the bottom of the section along the detachment surface (Modified after Suppe et al. 2004; Corredor et al. 2005; Shaw et al. 2005).

to also apply to other folds in other parts of the Niger Delta (eg. Corredor et al. 2005).

Two end member models were devised, the pure-shear and simple-shear models. Simple shear-folding occurs when the layers undergo external simple-shearing that is parallel to the beds with no defined basal detachment. The Pure-shear model, on the other hand, has a well defined basal detachment of which shortens and thickens above the ramp with no external inter-layer shearing (Suppe et al. 2004). Although these models conveniently subdivide fault related folding into distinct end members, it is more likely that in nature structures would be a combination of both (Suppe et al. 2004; Corredor et al. 2005) with external complexities such as back-thrusts and variable lithology.

The limb and growth stratal geometries of the Aghar Fold are similar to those that describe shear fault-bend fold, with the limb and growth stratal geometries. However, the Aghar fold accumulated a significant amount of displacement since its conception, which would make the fold appear more like the classic fault-bend fold. To determine if the Aghar fold underwent simple- or pure shear deformation, one must know the trajectory of the axial surface that goes through the hanging-wall syncline, which has been altered significantly due to the large displacement and secondary faulting that occurred near the bottom part of the thrust.

However, the large amount of displacement that occurred along the detachment is observed in the bottom part of the fold would at least indicate that the fold is not following a simple-shear fold-bend fold deformation model. This may have been the case since the nucleation of the fold, where the fault may have originally began to deform by means of simple-shear, and with accumulated shortening, shear-strain began to focused on the lower part of the section and the detachment causing the structure to deform in a pure-shear manner. Such a model would support the formation of a wedge shaped thickened detachment in the at the bottom of the main thrust fault on hanging-wall side (Fig. 7.1-b and

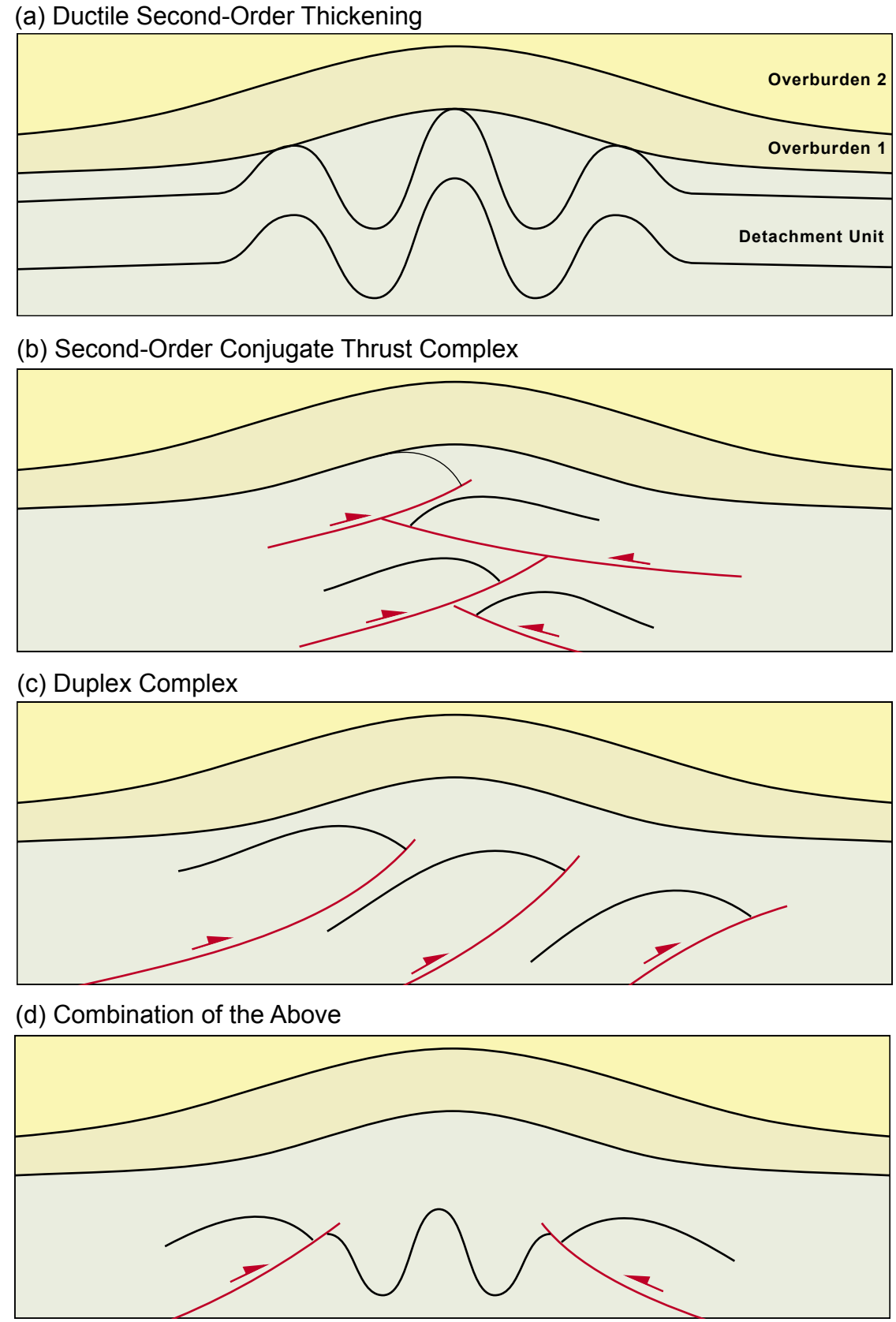

Figure 7.8 Brittle thickening of fold cores in shale detached systems (modified after Epard & Groshong 1995; Plesch et al. 2007; Maloney et al. 2010).

Fig. 7.2-a to c).

7.6.3. Detachment Thickening by Brittle Mechanisms

It is now accepted that the core of detachment folds in overpressured shale complexes are not infilled by viscous flow (eg. Morley 2003; Bilotti et al. 2005; Ings & Beaumont 2010) of shale but is thickened by brittle means. Several workers (Epard & Groshong 1995; Maloney et al. 2010) have suggested four major mechanism: ductile second-order folding, second-order conjugate thrusting, duplexing or a combination of the previous (Fig. 7.8).

It is apparent that detachment thickening occurred in the below the Pre-Kinematic 3 (upper detachment unit). The thickening varies along the length of the fold where the central segments shows conjugate thrusts and the northern and southern segment shows duplexing similar to that suggested by Plesch et al. (2007) (Fig. 7.8-c). Therefore, along strike the geometry of the detachment thrusting system must vary as well. The extent of the interaction is not fully understood due to poor imaging in the lower of the section. Numerical modelling would assist in further understanding this contractional feature.

7.6.4. Escalator Regression

The translation of fault bound depobelts was explained by the escalator regression theory, which suggested that extensional depobelts are infilled with sediments until it can no longer accommodate the sediments, and deposition bypasses the old depobelt to begin deposition in a new belt. Magbagbeola & Wilis (2007) and Doust & Omatsola (1990) suggested that the subsidence that occurs in the depobelts causes the shale detachment unit to withdraw and extrudes it further into the basin (Fig. 7.9).

This is now appreciated not to be true since shale behaves in a brittle manner as opposed to a ductile or viscous manner. Alternatively, stress is translated along the detachment surface. The lateral extent of the detachment begins

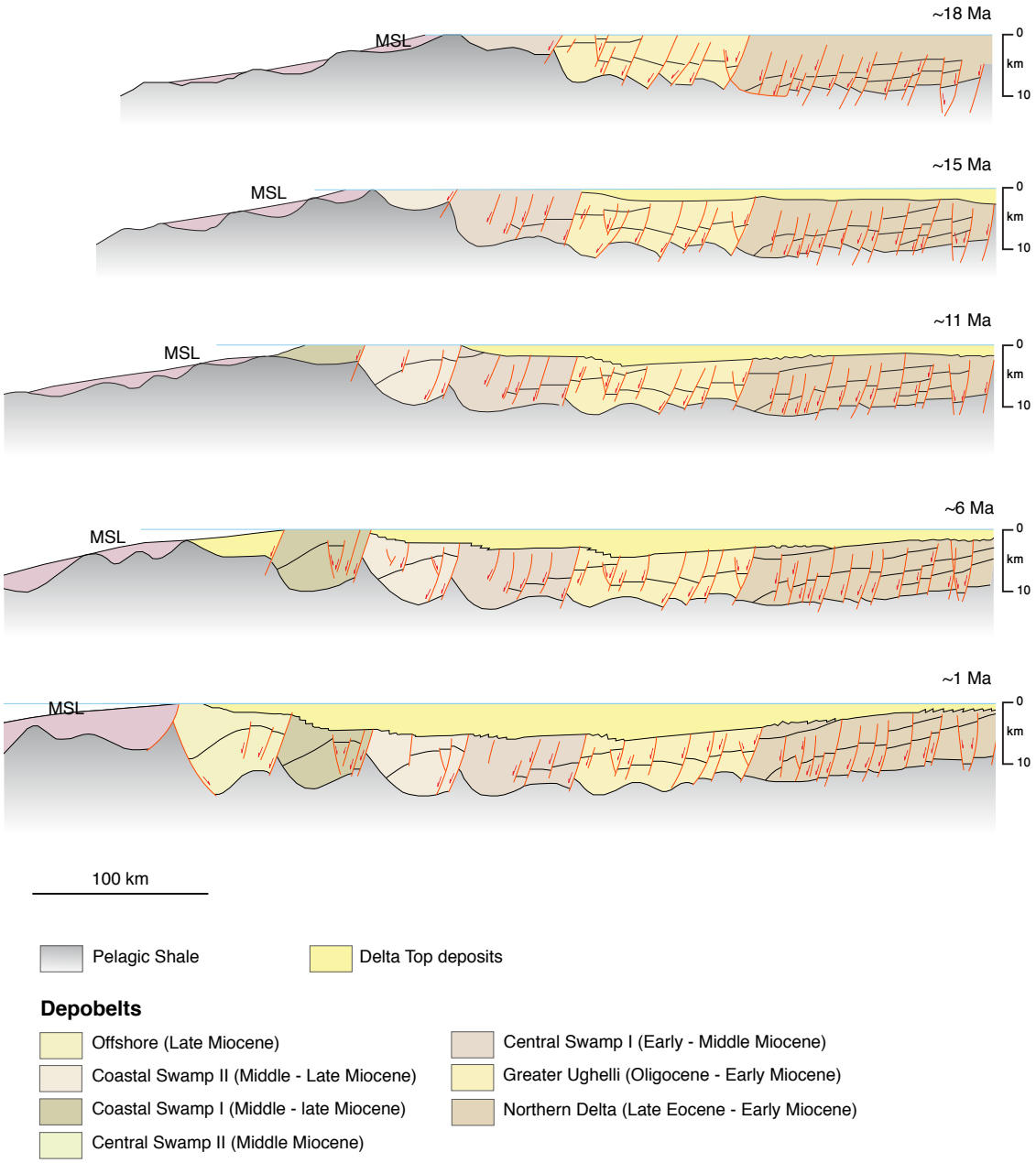

Figure 7.9 Escalator regression and deltaic structural evolution as explained by ductile shale extrusion (Magbagbeola & Wilis, 2007; Doust & Omatsola, 1990).

to accumulate stress which is accommodated by contractional features. The limit of the detachment is determined by the ability of the of the unit to produce overpressure, which in this case is the ability to generate hydrocarbons and retain the overpressure. Therefore, the thickness of the overburden must be ~4km for hydrocarbon generation to take place. Extending the detachment would cause the contraction to translate further into the basin.

One of the features observed in the 3D seismic area as well the regional lines the dip of the seabed behind and ahead of the major folding features. Ponding of syn-kinematic strata prevents sediments from depositing further into the basin. This would hinder the thickening of the overburden, and thus hydrocarbon generation and translation of the detachment further. The sediments would have overcome the fold structures by means of mass transport complexes and incision mechanisms to by pass the active structrues and begin to deposit beyond them.

As observed in Regional Line A, extensional features overprint older contractional features. Knowing the history of depobelt progression into the basin would indicate the contraction and thus the lateral extent of the deformation has progressed further into the basin in a similar manner to the progression of the depobelts.

7.7. Implications for Hydrocarbons

From the evolutionary model, several petroleum plays were inferred. This section investigates the potential plays in the deepwater Niger Delta and their associated risks.

7.7.1. Source Rock Potential and Generation

The active production taking place from the Bobo Fold is indication of an active source rock in the area. This minimises the risk associated with source potential. Although most information remains confidential, the source

rock is likely to be the Akata formation, which causes the overpressure and detachment.

7.7.2. Migration

As several authors have suggested the primary migration path is thought to be vertical from a source rock below the trap (Samuel et al. 2009; Morgan 2003; Løseth et al. 2009). However, the Akata acts as a barrier between sub-detachment source rocks and reservoirs above (Morgan 2003). Therefore, either the source rock is above the detachment or the Akata seal has to be breached to allow migration. Faulting and fracturing within the Akata and especially faulting that extends into the Agbada allows hydrocarbons to migrate upwards (Morgan 2003). However, there is moderate risk associated with shale rich units in the deepwater fold belt. This may create sealing faults that do not allow migration into reservoir intervals.

Lateral migration may also be present especially in locations where the source rock has not reached the hydrocarbon generation window. This would require the petroleum to be generated at a different location that is already producing hydrocarbons and migrate laterally.

Moreover, the constant deformation taking place in the delta may cause the traps to move and deform. Such activity may cause a second phase of migration form one reservoir trap to another. This in particular is suggested for hydrocarbons that may have been generated in Late Cretaceous sequences, which began petroleum generation in the Paleogene before trap development. The hydrocarbons were probably stored in a pre-Niger Delta reservoir before being migrated into the Present Day traps in the Miocene reservoirs.

7.7.3. Reservoir Potential

The Niger Delta is predominantly shale with some ~10% sand content that has been carried by various deepwater processes such as turbitide flows and mass

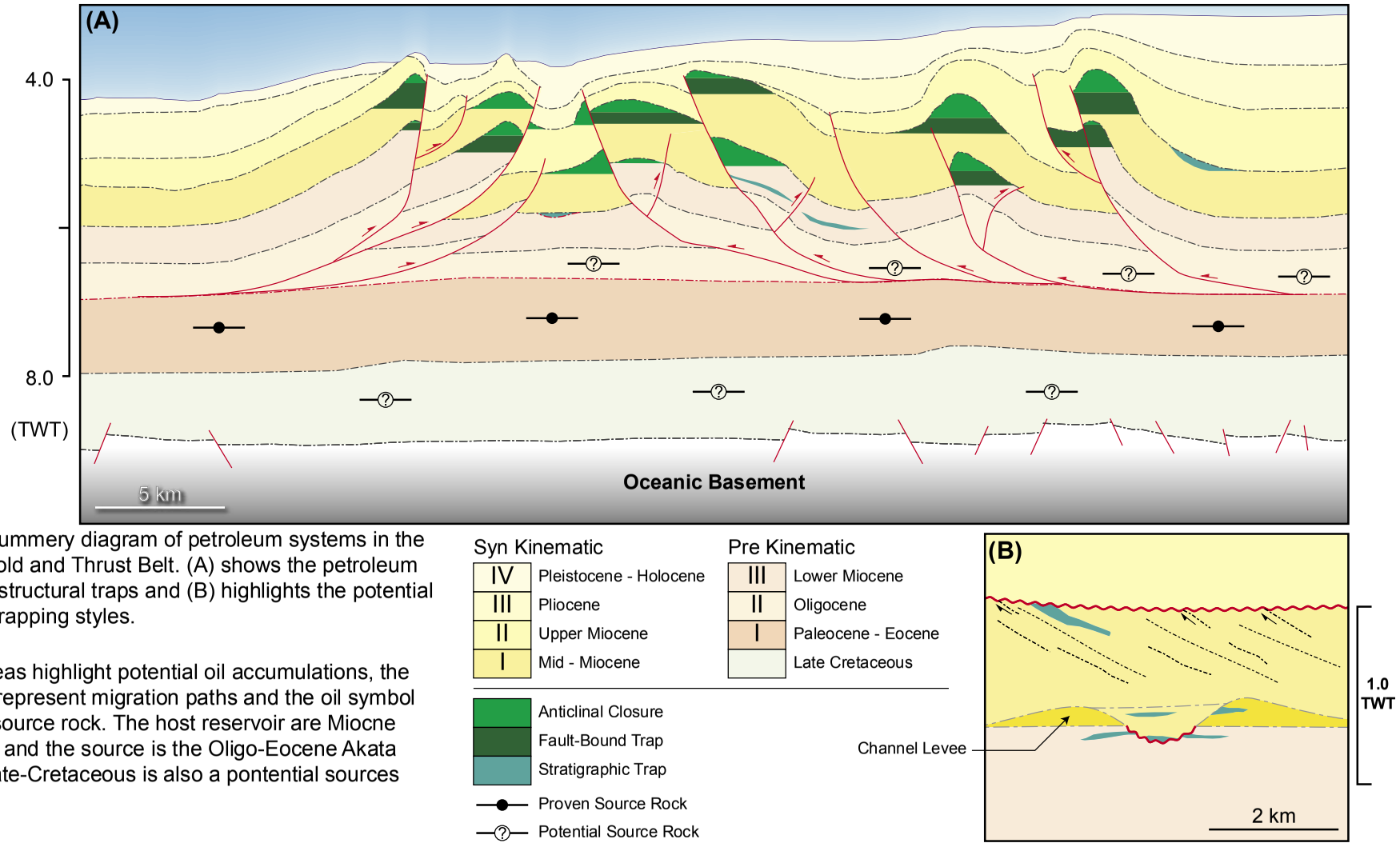

Figure 7.10 Summery diagram of petroleum systems in the Niger Delta Fold and Thrust Belt. (A) shows the petroleum systems with structural traps and (B) highlights the potential stratigraphic trapping styles.

The green areas highlight potential oil accumulations, the black arrows represent migration paths and the oil symbol highlight the source rock. The host reservoir are Miocne turbidite sand and the source is the Oligo-Eocene Akata shales. The late-Cretaceous is also a pontential sources rock.

transport complexes (MTC) (Morgan 2003; Weimer & Slatt 2007). Seismic data shows the extensive channel incision and levee building processes taking place in the study area, Morgan (2003) noted similar features as well as channel-stacking in deepwater 2D seismic data. Therefore, reservoirs are not laterally continuous and are limited to the geometry of the sedimentary complex. Hence, reservoir acts as a high risk when drilling in the Niger Delta.

Numberical modelling may also be used in to assess the amount of lost porosity due to thinning at the fold crest. Although the technique was not thoroughly tested in this research. Future works can incorporate numerical modelling to better understand porosity and fracture distribution in reservoir intervals.œ

7.7.4. Trap Style and Formation

The trapping styles have been divided into three types (Fig. 7.10): Four-way anticlinal closures (Class I), fault traps (Class I) and stratigraphic traps (Class III).

- The four-way closure style of traps is a simple anticlinal structure that forms at fold crests but has not been breached by thrust faulting. The Bobo Fold is an example of this sort of structure. 25% of giant deepwater field produce from this kind of trap (Bouroullec & Tari 2006).

- Fault traps also have potential to trap hydrocarbons, as major thrust faults juxtapose the thin sand sequences against impermeable shale sequences significantly reducing leakage risk (Kostenko et al. 2008). These traps may occur on both sides of the thrust fault, in the hanging-wall and foot-wall. There is risk associated with fault leakage. Therefore, these would be of higher risk than the previous if a top seal is present.

- Stratigraphic traps are also important in delta petroleum plays (Fig. 7.10 - b) (Matava et al. 2003) and account for 9% of deepwater production (Bouroullec & Tari 2006). The different bedding geometries introduced by pinched-out

growth strata against folds and truncated sand beds in fold backlimbs that are superimposed by impermeable strata are characteristic of these traps. Channels and fan complexes also create potential pinch-out style traps. Infilling these sedimetological features with sand poses a risk. With advanced seismic imaging and amplitude analysis, in particular if the target was gas, this risk can be reduced but not completely eliminated.

- Combination traps, which have structural and stratigraphic trapping also play a very large role in deepwater exploration and account for 66% of production in the deepwater settings (Bouroullec & Tari 2006). These are higher risk than the four-way anticlines but are less risky than pure stratigraphic plays. These typically occur in the onlapping syn-kinematic strata on fold limbs.

7.7.5. Seal Potential

Sedimentation in the delta is dominantly low-permeability shale, which is creates a seal that can handle a thick hydrocarbon column (Kostenko et al. 2008). However, the sealing units may be breached by mud volcano activity or crestal degradational faults. The latter is not uncommon in deepwater FBT belts, including those in the Niger Delta (Heinio & Davies 2006) and was observed in the upper part of the Aghar Fold. Buried dormant folds, like the Bobo, are less likely to have breached seals, however folds that continue growth to Present Day are more like to be breached by degradational features. Fluid pipes, such as the mud volcano that occurs in the Aghar Fold, would also cause hydrcarbon leakage in the upper anticlinal closure as suggested by Morley et al. 2011.

7.7.6. Prospectivity of the Aghar Fold and Similar Structures

The Aghar Fold is located to the SW of the producing Bobo Fold, which significantly reduces the source potential risk. It both indicates the presence of an active source rock with a working migration path. The structural similarities between the two folds would promote a similar migration system.

However, unlike the Bobo Fold, the Aghar Fold is an active fold at Present Day with significant crestal degradation that would compromise the top seal. Furthermore, the Bobo was drilled after identifying an amplitude anomaly, which is not present in the Aghar Fold. The presence of reservoir is also questionable in this environment.

Targeting the Aghar Fold would require a more detailed interpretation of sand distribution and crestal fracturing. The present seismic does not allow the imaging of the crestal faults, although they are most probably present. Better understanding of the sand distribution would allow the drilling of more complicated non-crestal fold limb plays or hybrid closure (a mix of structural and stratigraphic trapping). Finding potential sand reservoirs that terminate against the fault or a sedimentary pinch out would open new opportunities.

In conclusion, in the presence of active hydrocarbon charge, targeting conventional four-way anticlinal closures in folds similar to the Aghar Fold is very risky, and is unlikely to succeed due to seal breaching in the upper parts of the fold. Fault related closures, and sedimentological pinch-outs are more likely to be hydrocarbon bearing.

The outcomes of this research do not provide enough information regarding the migration pathways from source to reservoir, but should be considered. The seal potential of faults is high, making them a good lateral seal, but also increases risk.

Chapter 8

Conclusions

8.1. Summary of Regional Structures and Stratigraphy

8.1.1. Regional Structure of the Western Lobe in the Niger Delta

- Basinward-vergent listric extensional faults dominate the proximal parts of the delta and. The largest displacement occurs on the eastern faults and are likely to be older than the younger more distal fault that show smaller displacements. Distal extensional fault superimpose older thrust faults.

- The inner FTB is dominated by basinward-vergent imbricate thrust system that is highly shortened. The Outer FTB has both basinward and landward-vergent FRFs, which develop a thrust triangle.

- Syn Kinematic sequences show that the deformation migrates basinwards, causing the extensional domains to overprint older contractional zones.

8.1.2. Structures of the 3D Seismic Survey

- Deformation began within the 3D survey area in the Mid-Miocene and continues to Present Day, similar to the outer FTB.

- The detachment is interpreted as an overpressured shale detachment that dips to the SW 0° - 1°.

- The Aghar and Bobo are fold structures oriented NW-SE and separated by 12.5 km. The Bobo formed from three opposite vergent fault-related folds and was only active between the Mid-Miocene and Early Pleistocene.

- The Aghar fold is located within a left-stepping en-echelon series of fault-related folds. The main Aghar and Aghar North overlap and creates a complex thrust fault geometry, whereas the main Aghar and Aghar South are laterally spaced by ~5.4 km and create a series of near-surface extensional en-echelon faults.

8.2. Summary of the Aghar Fold Geometry

8.2.1. Summary of Aghar Fold Observations

- The Aghar fold extends ~34 km long and ~4.3 – 7.2 km wide and creates a 400m relief on the seabed. The asymmetric geometry of the fold dips 3.5° in the backlimb and 10-12° in the forelimb on the seabed. In the top of Pre-Kinematic 3, the forelimb dips 61° - 72° and the backlimb dips 20° – 40°.

- Two kinks occur along strike of the main Aghar fold in a left-steeping configuration, which indicates that the Aghar fold has formed from as a result of amalgamating three thrust faults.

- Evidence shows that a forelimb scarp have been active since the mid- to upper-Miocene period (Syn-Kinematic 1) and continue to Present Day. The size of the scarp increases in younger sequences.

- The decollement ascends by ~227 – 311 m in the middle of the fold, creating a geometry similar to a low-amplitude detachment fold. This is caused by thickening of the of the detachment unit. However, unlike salt that flows like a viscous fluid, shale layers create bourrage and duplex structures that infill the core of the fold.

8.2.2. Implications of Fault Analyses

- The shape of the fault varies along strike; the central part is characterised by a sigmoidal flat-ramp-flat geometry, whereas the northern and southern cross sections show a listric flat-ramp geometry. This coincides with the two kink-points observed in the Pre-Kinematic 2 (PK-2) maps.

8.2.3. Implications of Fault Displacement Profiles

- PK-2 has larger displacement values than PK-3, which indicates that the thrust fault initially displaced PK-2, before propagating into PK-3. Thus, the fault probably initiated within the lower layer and propagated upwards in the

section.

- The total heave (horizontal displacement) values are generally greater than the total throw values (vertical displacement).

- The peak displacement value (~3100 m) occurs at 14 km in the middle of the fault and reduces away from the centre. The fault nucleation probably began in the central part of the fold.

8.2.4. Implications of Growth Stratal Geometries

- Growth of the Aghar fold began in the centre of the fold between the Mid- to Late-Miocene, and then progressed to the north and south.

- The Aghar North and South folds became active in the Late-Miocene – Early-Pleistocene.

- Syn-Kinematic 2 units have onlapping reflectors that progress towards the crest of the fold. This indicates that the sedimentation rate exceeded the rate of fold growth. Conversely, Syn-Kinematic 1, 3 & 4 have onlapping that progresses away from the crest indicating growth exceeding sedimentation rate.

- Along strike the Aghar fold growth style varies from self-similar growth in the northern and southern segments to growth by limb-rotation in the central segment.

8.3. Summary of Section Restoration and Forward Numerical Modelling

8.3.1. Restoration of Section V

- During the early stages of fold amplification in the Lower-Miocene, the detachment began to thicken beneath the fold, accounting for ~150 – 200 ± 25 m of shortening. However, more shortening is likely to be accommodated

during this period.

- During the second stage during in Lower to Mid-Miocene, the main thrust fault developed and accounted for 1400 ± 25 m shortening. In the pre-kinematic sequences the fault has a listric flat-ramp geometry.

- In the third stage during the Mid-Miocene, the fault propagates at a shallower angle in the syn-kinematic units developing the upper fault flat, which can be associated with higher growth vs. sedimentation rates. This stage accounts for 1250 ± 25 m.

- During the fourth stage in the Upper-Miocene, a landward-vergent thrust fault develops in the footwall, and deforms the main thrust ramp, accounting for 350 ± 25 m.

- In fifth and final stage of development (Pliocene to Present Day) a forelimb breakthrough thrust (FBT) developed. The FBT took up all the displacement, and the upper flat of the previous fault geometry became inactive. To Present Day, this stage accounts for 3700 ± 25 m, bringing the total shortening to 6900 ± 25 m.

8.3.2. Implications of Numerical Modeling

- Further work is required to attain plausible results from this section.

- Stress and strain focuses on fault tips, as well as areas that undergo folding, such as the hanging wall syncline and crestal area.

- During fold amplification, the crestal area undergoes high-stress, which results in thinning and rotation of the forelimb.

- The pre-kinematic cutoff angles increase with depth.

- In both models, the fault contact in the footwall also undergoes high strain and thickens.

8.4. 4D Evolutionary Model of the Aghar Fold

The Aghar fault-related-fold has been active since the Mid Miocene to Present Day. It evolved from three basinward vergent, left-stepping en-echelon fault-related-folds (northern, central and southern segments) that amalgamated during the Mid- to Upper-Miocene. The evolution of the Aghar fold can be summarised in the following (Fig. 7.3):

- Lower to Mid-Miocene: initial growth only took place in the middle segment and was dominated by thickening of the pre-kinematic units. The forelimb began to fail forming a blind sigmoidal thrust fault.

- Upper Miocene: two main events occur during this period; the activation of the northern and southern segments, and the formation of the forelimb breakthrough thrust (FBT). The three segments initially grew independently, but soft-linkage occurred during the Late Pliocene.

- Pliocene to Present Day: all three segments become hard-linked.

8.5. Implications for Fault-Related-Folds

- Fault-related fold in shale-detached systems initially form as asymmetric low-amplitude detachment folds. Thrust faults develop in the steep limb of the detachment with small amounts of shortening.

- Unlike ductile salt, the shale deforms by brittle mechanisms. In the case of the Aghar Fold, deforms by means of duplexing and antithetic thrusting. Therefore, thickening detachment occurs by second-order folding or imbrication. This also hinders the formation of high-amplitude detachment folds with symmetrical geometries.

- Poorly lithified sediments that occur in the deepwater environment accommodate initial shortening by thickening and sub-seismic resolution deformation in the detachment unit.

8.6. Future Work and Recommendation

This research focused on the evolution of the Aghar fault-related-fold. Future research should focus on similar structures in other regions around the world. The following are some recommendations for future works.

- Integrate well and biostratigraphic markers into study to enhance timing and lithological properties used in models and restoration.
- More detailed interpretation of syn-kinematic sequences to better constrain the timing of growth.
- More detailed interpretation of pre-kinematic sequences to improve understanding of the folding mechanism.
- Section restoration of sections in the northern and southern segments in the Aghar fold and calculating the associated shortening and vertical uplift in those areas.
- Forward numerical model should accommodate for unconsolidated sediments rather than using lithified shale sequences.
- Conducting forward numerical models to simulate brittle thickening mechanisms such as duplexes, second-order folding and conjugate-folding (Epard & Groshong 1995; Mitra 2002). This is to understand the stress and strain distributions in the detachment during the evolution of the fold, as well as the transmission of strain into the overburden.
- 3D forward numerical models to simulate lateral fault linkage of thrust faults and folds in deepwater setting.

References

Akpabio, I. & Ejedawe, J. 2010. Thermal conductivity estimates in the Niger Delta using lithologic data and geophysical well logs. *Current Science, India,* **3**, 6/10/2010-411.

Amante, C. & Eakins, B. W. 2009. ETOPO1 1 Arc-Minute Global Relief Model: Procedures, Data Sources and Analysis. , 19 pp, *NOAA Technical Memorandum NESDIS NGDC,* **24**, 21/jun/2010-19.

Benkhelil, J. 1982. Benue Trough and Benue Chain. *Geological Magazine,* **119**, 155.

Benkhelil, J. 1989. The origin and evolution of the Cretaceous Benue Trough (Nigeria). Journal of African Earth Sciences, 8, 251-282.

Bilotti, F. & Shaw, J. H. 2005. Deep-water Niger Delta fold and thrust belt modeled as a critical-taper wedge: The influence of elevated basal fluid pressure on structural styles. *AAPG Bulletin,* **89**, 1475-1491.

Bilotti, F., Shaw, J., Cupich, R. M. & Lakings, R. M. 2005. Detachment fold, Niger Delta. *In:* Shaw, J. H., Connors, C. & Suppe, J. (eds) *Seismic interpretation of contractional fault-related folds: An AAPG seismic atlas Studies in Geology #53.* AAPG, Tulsa, Okla., USA, 103-104.

Bortolotti, V. & Principi, G. 2005. Tethyan ophiolites and Pangea break-up. *Island Arc,* **14**, 442-470.

Bouroullec, R. & Tari, G. 2006. Petroleum Traps in Deepwater Settings. *In*: Weimer P. & Slatt, R. (eds) *Introduction to the Petroleum Geology of Deepwater Settings: AAPG Special Studies in Geology 57, AAPG/Datapage Discovery Series 8.* AAPG, Okla., USA, 683-777.

Briggs, S. E., Davies, R. J., Cartwright, J. A. & Morgan, R. 2006. Multiple detachment levels and their control on fold styles in the compressional domain of the deepwater west Niger Delta. *Basin Research,* **18**, 435-450.

Briggs, S. E., Davies, R. J., Cartwright, J. A. & Morgan, R. 2009. Thrusting in oceanic crust during continental drift offshore Niger Delta, equatorial Africa. *Tectonics,* **1**.

Bustin, R. M. 1988. Sedimentology and characteristics of dispersed organic matter in Tertiary Niger Delta; origin of source rocks in a deltaic environment. *AAPG Bulletin,* **72**, 277-298.

Butler, R. & Paton, D. 2010. Evaluating lateral compaction in deepwater fold and thrust belts: How much are we missing from “nature’s sandbox”?. *GSA Today*, **20**, 4-10.

Cobbold, P. R., Clarke, B. J. & Loseth, H. 2009. Structural consequences of fluid overpressure and seepage forces in the outer thrust belt of the Niger Delta. *Petroleum Geoscience,* **15**, 3-15.

Cobbold, P. R., Durand, S. & Mourgues, R. 2001. Sandbox modelling of thrust wedges with fluid-assisted detachments. *Tectonophysics,* **334**, 245-258.

Cobbold, P. R., Mourgues, R. & Boyd, K. 2004. Mechanism of thin-skinned detachment in the Amazon Fan: assessing the importance of fluid overpressure and hydrocarbon generation. *Marine and Petroleum Geology,* **21**, 1013-1025.

Cohen, H. A. & McClay, K. 1996. Sedimentation and shale tectonics of the northwestern Niger Delta front. *Marine and Petroleum Geology,* **13**, 313-328.

Corredor, F., Shaw, J. H. & Bilotti, F. 2005. Structural styles in the deep-water fold and thrust belts of the Niger Delta. *AAPG Bulletin,* **89**, 753-780.

Coward, M. P., Purdy, E. G., Ries, A. C. & Smith, D. G. 1999. The distribution of petroleum reserves in basins of the South Atlantic margins. *Geological Society, London, Special Publications,* **153**, 101-131.

Dahlen, F. A. 1990. Critical Taper Model of Fold-and-Thrust Belt and Accretionary Wedges. *Annual Review of Earth and Planetary Sciences,* **18**, 55-99.

Daly, M. C., Chorowicz, J. & Fairhead, J. D. 1989. Rift basin evolution in Africa: the influence of reactivated steep basement shear zones. *Geological Society, London, Special Publications,* **44**, 309-334.

Damuth, J. E. 1994. Neogene gravity tectonics and depositional processes on the deep Niger Delta continental margin. *Marine and Petroleum Geology,* **11**, 320, IN1-IN10, 321-346.

Darros de Matos, R. M. 1999. History of the northeast Brazilian rift system: kinematic implications for the break-up between Brazil and West Africa. *Geological Society, London, Special Publications,* **153**, 55-73.

de Vera, J., Granado, P. & McClay, K. 2010. Structural evolution of the Orange Basin gravity-driven system, offshore Namibia. *Marine and Petroleum Geology,* **27**, 223-237.

Deville, E., Guerlais, S., Callec, Y., Griboulard, R., Huyghe, P., Lallemant, S., Mascle, A., Noble, M. & Schmitz, J. 2006. Liquefied vs stratified sediment mobilization processes: Insight from the South of the Barbados accretionary prism. *Tectonophysics,* **428**, 33-47.

Diegel, F. A., Karlo, J. F., Schuster, D. C., Shoup, R. C. & Tauver, P. R. 1995. Cenozoic structural evolution and tectono-stratigraphic framework of the northern Gulf Coast continental margin. *In:* Jackson, M. P. A., Roberts, D. G., et al (eds) *Salt tectonics; a global perspective.* AAPG, Tulsa, OK, USA, 109-151.

Doust, H. & Omatsola, E. 1990. Niger Delta. *In:* Edwards, J. D. &Santogrossi, P. A. (eds) *Divergent/passive margin basins.* AAPG, Tulsa, Okla., 201-238.

Eagles, G. 2007. New angles on South Atlantic opening. *Geophysical Journal International,* **168**, 353-361.

Ejedawe, J. E. 1986. The Expulsion Criterion in the Evaluation of the Petroleum Source Beds of the Tertiary Niger Delta. *Journal of Petroleum Geology,* **9**, 439-450.

Ekweozor, C. M. & Okoye, N. V. 1980. Petroleum source-bed evaluation of Tertiary Niger Delta. *AAPG Bulletin,* **64**, 1251-1259.

Emery, K. O., Uchupi, E., et al. 1975. Continental margin off western Africa; Angola to Sierra Leone. AAPG Bulletin, 59, 2209-2265.

Epard, J. . & Groshong, R. H. 1995. Kinematic model of detachment folding including limb rotation, fixed hinges and layer-parallel strain. *Tectonophysics,* **247**, 85-103.

Erickson, S. G. 1996. Influence of mechanical stratigraphy on folding vs faulting. *Journal of Structural Geology,* **18**, 443-450.

Erslev, E. A. 1991. Trishear fault propagation folding. *Geology*, **19**, 617–620.

Ghassemi, M. R., Schmalholz, S. M., Ghassemi, Ali R. 2010. Kinematics of constant arc length folding for different fold shapes. Journal of Structural Geology, 32, 755-765.

Gonzalez-Mieres, R. & Suppe, J. 2006. Relief and shortening in detachment folds. *Journal of Structural Geology,* **28**, 1785-1807.

Grando, G. 2005. *Growth Fold Systems in Deepwater Compressional Fold and Thrust Belts.* PhD, Royal Holloway, University of London, Egham, Surrey, UK.

Graue, K. 2000. Mud volcanoes in deepwater Nigeria. *Marine and Petroleum Geology*, **17**, 959-974.

Guiraud, R., Bellion, Y., Benkhelil, J. & Moreau, C. 1987. Post-Hercynian tectonics in Northern and Western Africa. *Geological Journal,* **22**, 433-466.

Guiraud, R., Bosworth, W., Thierry, J. & Delplanque, A. 2005. Phanerozoic geological evolution of Northern and Central Africa: An overview. *Journal of African Earth Sciences,* **43**, 83-143.

Haack, R. C., Sundararaman, P., Diedjomahor, J. O., Xiao, H., Gant, N. J., May,

E. D. & Kelsch, K. 2000. Niger Delta Petroleum Systems, Nigeria. *In:* Mello, M. R. &Katz, B. J. (eds) *Petroleum systems of South Atlantic margins - AAPG Memoir 73.* AAPG, Tulsa, OK, USA, 213-231.

Hall, S. H. 2002. The role of autochthonous salt inflation and deflation in the northern Gulf of Mexico. *Marine and Petroleum Geology,* **19**, 649-682.

Heinio, P. & Davies, R. J. 2006. Degradation of compressional fold belts: Deep-water Niger Delta. *AAPG Bulletin,* **90**, 753-770.

Hardy, S. & M. Ford 1997. Numerical modeling of trishear fault- propagation folding and associated growth strata. *Tectonics*, **16**, 841–854.

Heiniö, P. & Davies, R. J. 2007. Knickpoint migration in submarine channels in response to fold growth, western Niger Delta. *Marine and Petroleum Geology,* **24**, 434-449.

Hesse, S., Back, S. & Franke, D. 2010a. Deepwater folding and thrusting offshore NW Borneo, SE Asia. *Geological Society, London, Special Publications,* **348**, 169-185.

Hesse, S., Back, S. & Franke, D. 2010b. The structural evolution of folds in a deepwater fold and thrust belt – a case study from the Sabah continental margin offshore NW Borneo, SE Asia. *Marine and Petroleum Geology,* **27**, 442-454.

Higgins, S., Davies, R. J. & Clarke, B. 2007. Antithetic fault linkages in a deep water fold and thrust belt. *Journal of Structural Geology,* **29**, 1900-1914.

Hooper, R. J., Fitzsimmons, R. J., Grant, N. & Vendeville, B. C. 2002. The role of deformation in controlling depositional patterns in the south-central Niger Delta, West Africa. *Journal of Structural Geology,* **24**, 847-859.

Ingram, G. M., Chisholm, T. J., Grant, C. J., Hedlund, C. A., Stuart-Smith, P. & Teasdale, J. 2004. Deepwater North West Borneo: hydrocarbon accumulation in an active fold and thrust belt. *Marine and Petroleum Geology,* **21**, 879-887.

Ings, S. J. & Beaumont C. 2010. Continental margin shale tectonics: preliminary results from coupled fluid-mechanical models of large-scale delta instability. *Journal of the Geological Society, London,* **167**, 571-582.

Jermannaud, P., Rouby, D., Robin, C., Nalpas, T., Guillocheau, F. & Raillard, S. Plio-Pleistocene sequence stratigraphic architecture of the eastern Niger Delta: A record of eustasy and aridification of Africa. *Marine and Petroleum Geology,* **In Press, Corrected Proof**.

Katz, B. J. 2006. Significance of ODP results on deepwater hydrocarbon exploration – Eastern equatorial Atlantic region. *Journal of African Earth Sciences,* **46**, 331-345.

King, R. C., Backé, G., Morley, C. K., Hillis, R. R. & Tingay, M. R. P. 2010. Balancing deformation in NW Borneo: Quantifying plate-scale vs. gravitational tectonics in a delta and deepwater fold-thrust belt system. *Marine and Petroleum Geology,* **27**, 238-246.

King, R. C., Hillis, R. R., Tingay, M. R. P. & Morley, C. K. 2009. Present-day stress and neotectonic provinces of the Baram Delta and deep-water fold-thrust belt. *Journal of the Geological Society, London,* **166**, 197-200.

Knox, G. & Omatsola, E. 1989. Development of the Cenozoic Niger Delta in terms of the" Escalator Regression" model and impact on hydrocarbon distribution. , 181-202.

Konate, M., Guiraud, M., Lang, J. & Yahaya, M. 2003. Sedimentation in the Kandi extensional basin (Benin and Niger): fluvial and marine deposits related to the Late Ordovician deglaciation in West Africa. *Journal of African Earth Sciences,* **36**, 185-206.

Kostenko, O. V., Naruk, S. J., Hack, W., Poupon, M., Meyer, H., Mora-Glukstad, M., Anowai, C. & Mordi, M. 2008. Structural evaluation of column-height controls at a toe-thrust discovery, deep-water Niger Delta. *AAPG Bulletin,* **92**, 1615-1638.

Krueger, S. W. & Grant, N. T. 2010. The Growth History of Toe Thrusts of the Niger Delta and the Role of Pore Pressure. *In:* McClay, K. R., Shaw, J., et al (eds) *Thrust fault-related folding: AAPG Memoir 94.* AAPG, .

Lambert-Aikhionbare, D. O., Ibe, A. C., Ekweozor, C. M. & Daukoru, E. M. 1984. Petroleum source-bed evaluation of Tertiary Niger Delta; discussion and reply. *AAPG Bulletin,* **68**, 387-394.

Lawrence, S. R., Munday, S. & Bray, R. 2002. Regional geology and geophysics of the eastern Gulf of Guinea (Niger Delta to Rio Muni). *The Leading Edge,* **21**, 1112-1117.

Løseth, H., Gading, M. & Wensaas, L. 2009. Hydrocarbon leakage interpreted on seismic data. *Marine and Petroleum Geology,* **26**, 1304-1319.

Magbagbeola, O. A. & Willis, B. J. 2007. Sequence stratigraphy and syndepositional deformation of the Agbada Formation, Robertkiri field, Niger Delta, Nigeria. *AAPG Bulletin,* **91**, 945-958.

Maloney, D., Davies, R., Imber, J., Higgins, S. & King, S. 2010. New insights into deformation mechanisms in the gravitationally driven Niger Delta deepwater fold and thrust belt. *AAPG Bulletin,* **94**, 1401-1424.

Matava, T., Rooney, M. A., Chung, H. M., Nwankwo, B. C. & Unomah, G. I. 2003. Migration effects on the composition of hydrocarbon accumulations in the OML 67-70 areas of the Niger Delta. *AAPG Bulletin,* **87**, 1193-1206.

McClay, K. R., Dooley, T. & Lewis, G. 1998. Analog modeling of progradational delta systems. *Geology,* **26**, 771-774.

McClay, K. R., Dooley, T. & Zamora, G. 2003. Analogue models of delta systems above ductile substrates. *Geological Society, London, Special Publications,* **216**, 411-428.

McCurry, P. 1971. Pan-African Orogeny in Northern Nigeria. *Geological Society of America Bulletin,* **82**, 3251-3262.

Meyers, J. B., Rosendahl, B. R., Harrison, C. G. A. & Ding, Z. 1998. Deep-imaging seismic and gravity results from the offshore Cameroon Volcanic Line, and speculation of African hotlines. *Tectonophysics,* **284**, 31-63.

Mitra, S. 2002. Fold-accommodation faults. *AAPG Bulletin,* **86**, 671-693.

Mitra, S. 2002. Structural Models of Faulted Detachment Folds. *AAPG Bulletin,* **86**, 1673-1694.

Morgan, R. 2003. Prospectivity in ultradeep water: the case for petroleum generation and migration within the outer parts of the Niger Delta apron. *Geological Society, London, Special Publications,* **207**, 151-164.

Morley, C. K. 2009. Geometry of an oblique thrust fault zone in a deepwater fold belt from 3D seismic data. *Journal of Structural Geology,* **31**, 1540-1555.

Morley, C. K. & Leong, L. C. 2008. Evolution of deep-water synkinematic sedimentation in a piggyback basin, determined from three-dimensional seismic reflection data. *Geosphere,* **4**, 939-962.

Morley, C. K. 2003. Mobile shale related deformation in large deltas developed on passive and active margins. *Geological Society, London, Special Publications,* **216**, 335-357.

Morley, C. K. 2007. Development of crestal normal faults associated with deepwater fold growth. *Journal of Structural Geology,* **29**, 1148-1163.

Morley, C. K. 2009. Growth of folds in a deep-water setting. *Geosphere,* **5**, 59-89.

Morley, C. K., King, R., Hillis, R., Tingay, M. & Backe, G. 2010. Deepwater fold and thrust belt classification, tectonics, structure and hydrocarbon prospectivity: A review. *Earth-Science Reviews,* **In Press, Accepted Manuscript**.

Moulin, M., Aslanian, D. & Unternehr, P. 2010. A new starting point for the South

and Equatorial Atlantic Ocean. *Earth-Science Reviews,* **98**, 1-37.

Mourgues, R., Lecomte, E., Vendeville, B. & Raillard, S. 2009. An experimental investigation of gravity-driven shale tectonics in progradational delta. *Tectonophysics,* **474**, 643-656.

Müller, R. D., Sdrolias, M., Gaina, C. & Roest, W. R. 2008. Age, spreading rates, and spreading asymmetry of the world's ocean crust. *Geochemestry Geophysics Geosystems,* **9**, 21/jun/2010-Q04006.

Oboh, F. E. & Salami, M. B. 1989. Lithostraigraphical and palynostratigraphical studies of Igbomotoru-1 Well, Niger Delta. *Journal of African Earth Sciences,* **9**, 531-540.

Plesch, A., Shaw, J.H. & Kronman, D. 2007. Mechanics of low-relief detachment folding in the Bajiaochang field, Sichuan Basin, China. *AAPG Bulletin*, **91**, 1559-1575.

Pochat, S., Castelltort, S., Van Den Driessche, J., Besnard, K. & Gumiaux, C. 2004. A simple method of determining sand/shale ratios from seismic analysis of growth faults: An example from upper Oligocene to lower Miocene Niger Delta deposits. *AAPG Bulletin,* **88**, 1357-1367.

Reijers, T. J. A., Petters, S. W. & Nwajide, C. S. 1997. Chapter 7 The niger delta basin. *In:* R.C. Selley (ed) *Sedimentary Basins of the World.* Elsevier, 151-172.

Rowan, M. G., Peel, F. J. & Vendeville, B. C. 2004. Gravity-driven fold belts on passive margins. *In:* McClay, K. (ed) *Thrust tectonics and hydrocarbon systems.* Tulsa, .

Samuel, O. J., Cornford, C., Jones, M., Adekeye, O. A. & Akande, S. O. 2009. Improved understanding of the petroleum systems of the Niger Delta Basin, Nigeria. *Organic Geochemistry,* **40**, 461-483.

Saugy, L. & Eyer, J. A. 2003. Fifty Years of Exploration in the Niger Delta (West Africa). *In:* Halbouty, M. T. (ed) *Giant Oil and Gas Fields of the Decade 1990 -*

1999, AAPG Memoir 78. AAPG, Tulsa, Oaklahoma, U.S.A., 211-226.

Schiefelbein, C. F., Zumberge, J. E., Cameron, N. R. & Brown, S. W. 1999. Petroleum systems in the South Atlantic margins. *Geological Society, London, Special Publications,* **153**, 169-179.

Selley, R. C. 1998. Elements of Petroleum Geology. Academic Press, San Diego, California, USA, 470-189.

Short, K. C. & Staeuble, A. J. 1967. Outline of geology of Niger delta. *AAPG Bulletin,* **51**, 761-799.

by Editors 2005. Shear Fault-bend Folding. *In:* Shaw, J.H., Connors C. & Suppe J. (ed) *Seismic interpretation of contractional fault-related folds: AAPG Studies in Geology 53.* AAPG, Tulsa, Okla.

Sonibare, O., Alimi, H., Jarvie, D. & Ehinola, O. A. 2008. Origin and occurrence of crude oil in the Niger delta, Nigeria. *Journal of Petroleum Science and Engineering,* **61**, 99-107.

Spratt, D. A., Dixon, J. M. & Beattie, E. T. 2004. Changes in Structural Style Controlled by Lithofacies Contrast Across Transverse Carbonate Bank Margins—Canadian Rocky Mountains and Scaled Physical Models. *In:* McClay, K. R. (ed) AAPG, Tulsa, OK, USA, 259-275.

Suppe, J. 1983. Geometry and kinematics of fault-bend folding. *American Journal of Science,* **283**, 684-721.

Suppe, J. 1985. Principles of structural geology. Englewood Cliffs, New Jersey, Prentice Hall, 537.

Suppe, J. & D. A. Medwedeff 1984. Fault-propagation folding (abs.). *Geological Society of America Abstracts with Programs*, **16**, 670.

Suppe J. & Medwedeff, D. 1990. Geometry and kinematics of fault-propagation folding, *Eclogae Geologicae Helvetiae*, **83**, 409–454.

Suppe, J., Connors, C. & Zhang, Y. 2004. Shear Fault-bend Folding. *In:* McClay, K. (ed) *Thrust tectonics and hydrocarbon systems.* AAPG, Tulsa, Okla.

Tucker, M. E. 2001. Sedimentary Petrology: an introduction to the origin of sedimentary rocks, 3rd ed.. Blackwell Science. Oxford, United Kingdom.

Tuttle, M. L. W., Charpentier, R. R. & Brownfield, M. E. 1999. The Niger Delta Petroleum System: Niger Delta Province, Nigeria, Cameroon, and Equatorial Guinea, Africa. *USGS Open File Report, Denver, Colorado, USA,* .

van Heijst, M. W. I. M., Postma, G., van Kesteren, W. P. & de Jongh, R. G. 2002. Control of Syndepositional Faulting on Systems Tract Evolution Across Growth-Faulted Shelf Margins: An Analog Experimental Model of the Miocene Imo River Field, Nigeria. *AAPG Bulletin,* **86**, 1335-1366.

Van Rensbergen, P., Morley, C. K., Ang, D. W., Hoan, T. Q. & Lam, N. T. 1999. Structural evolution of shale diapirs from reactive rise to mud volcanism: 3D seismic data from the Baram delta, offshore Brunei Darussalam. *Journal of the Geological Society, London,* **156**, 633-650.

Weber, K. J. 1987. Hydrocarbon distribution patterns in Nigerian growth fault structures controlled by structural style and stratigraphy. *Journal of Petroleum Science and Engineering,* **1**, 91-104.

Weimer, P. & Slatt, R. M. 2007. Petroleum Systems of Deepwater Settings. *In:* Anonymous *Introductions to the Petroleum Geology of Deepwater Settings; AAPG Studies in Geology 57 AAPG/Datapages Discovery series 8.* AAPG/ Datapages, Tulsa, OK, USA, .

Whiteman, A. 1982. Nigeria: Its Petroleum Geology, Resources and Potential. Graham & Trotman Ltd., London, 166.

Appendix A

Structural Maps and Amplitude Extractions

List of Figures

Page

Seabed Structures and Morphology

Figure A.1 Seabed coherency map.

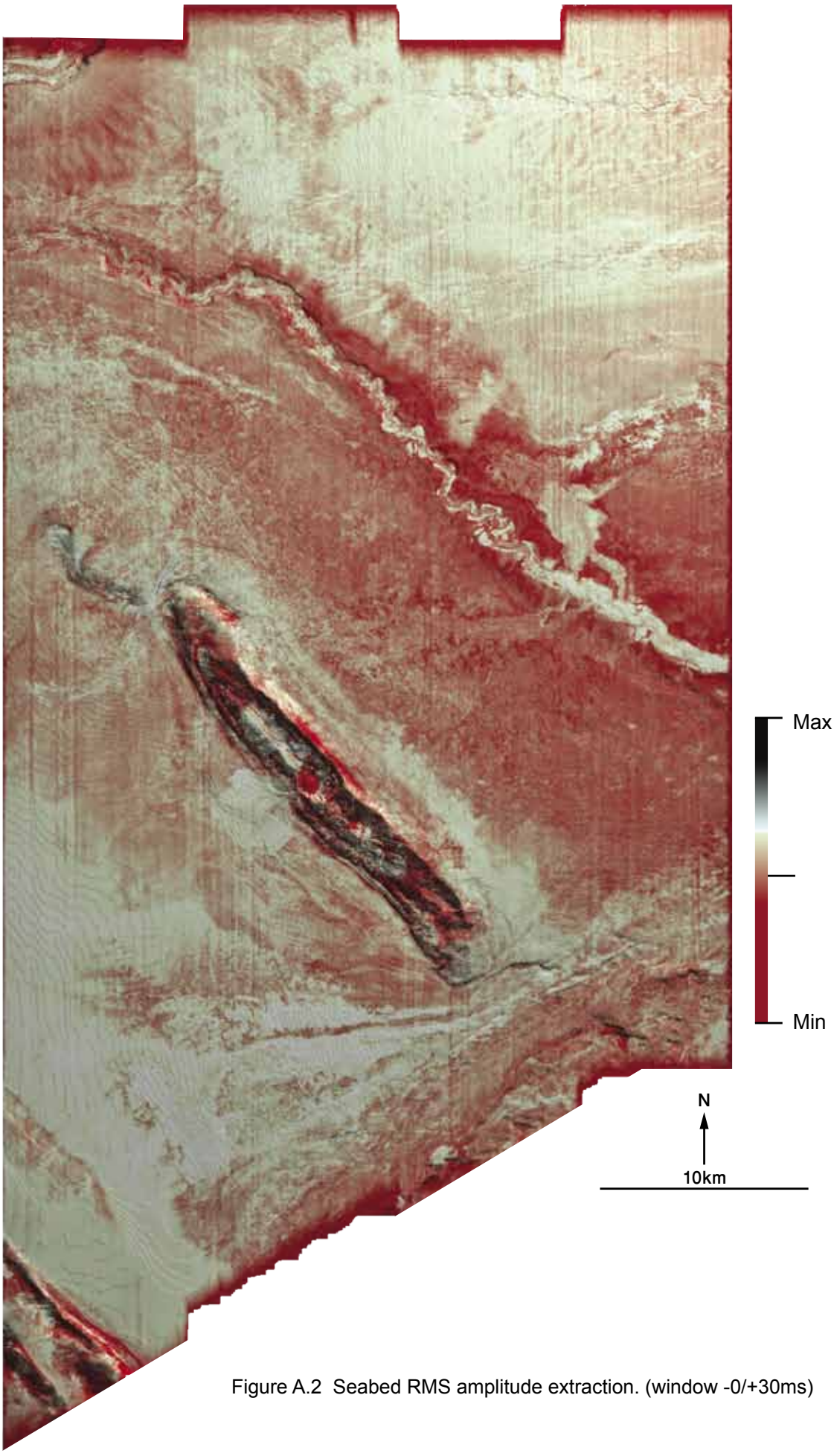

Figure A.2 Seabed RMS amplitude extraction. (window -0/+30ms)

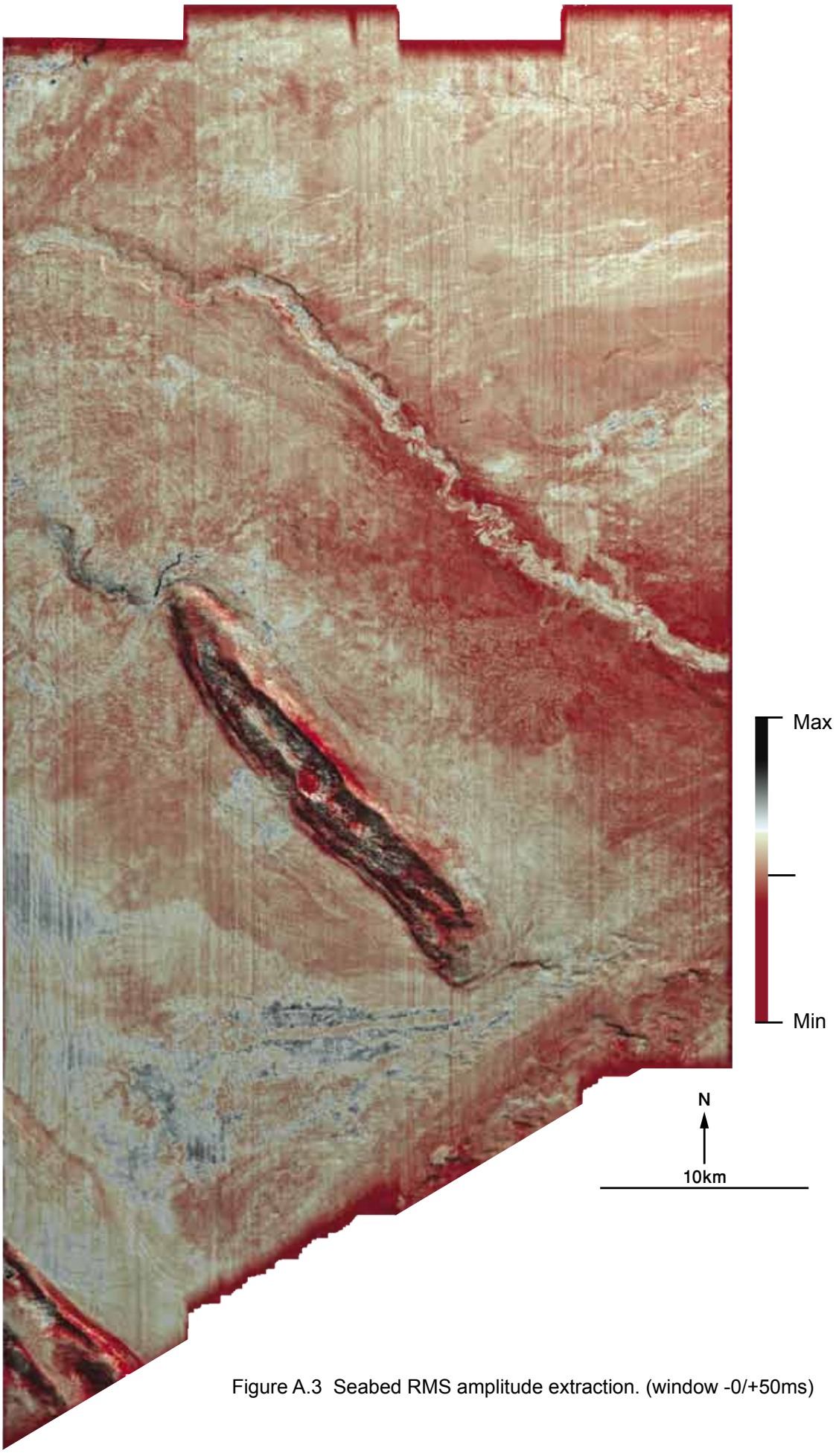

Figure A.3 Seabed RMS amplitude extraction. (window -0/+50ms)

Pre-Kinematic Structures and Geomorphologies

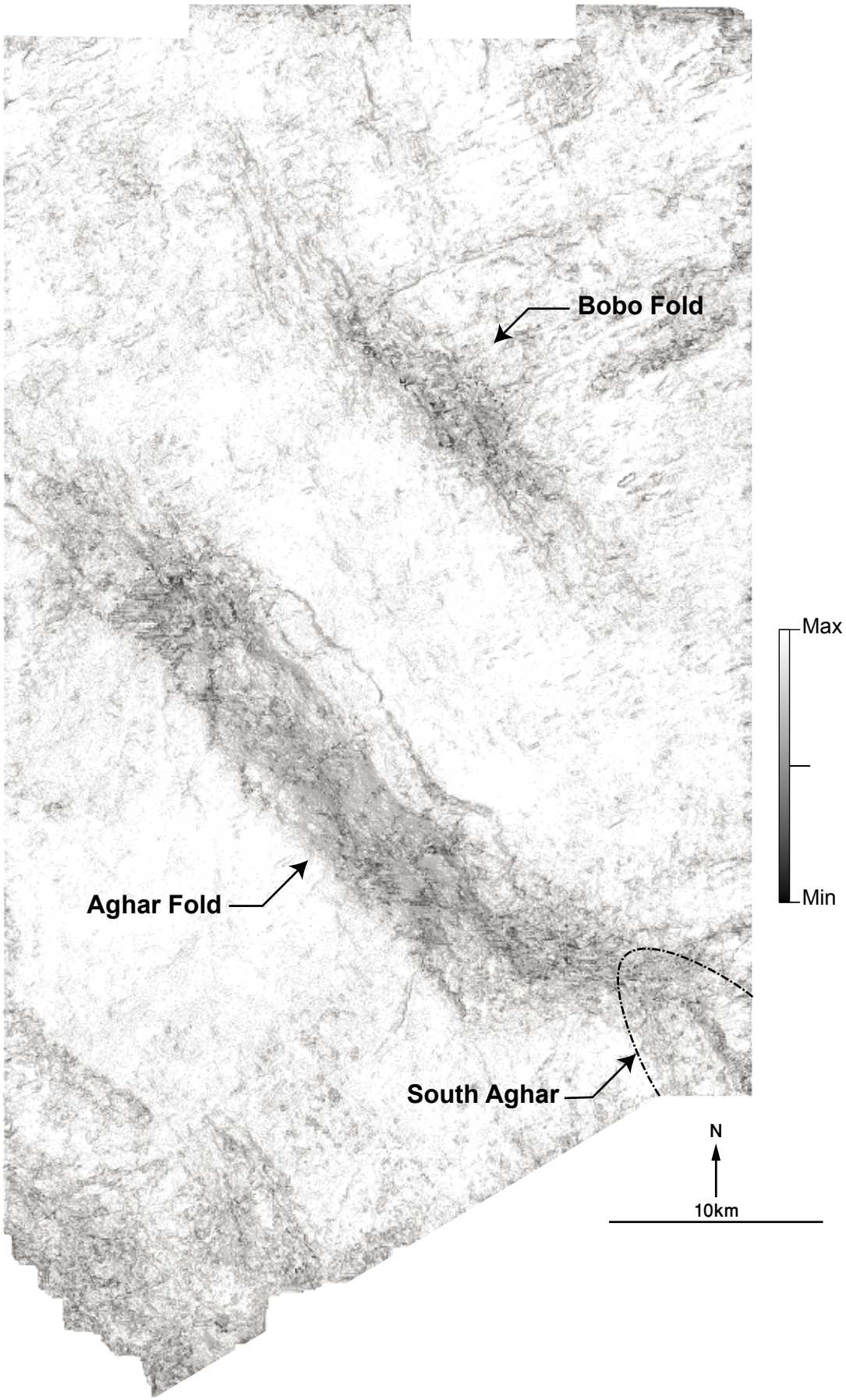

Figure A.4 Pre Kinematic 1 coherency map

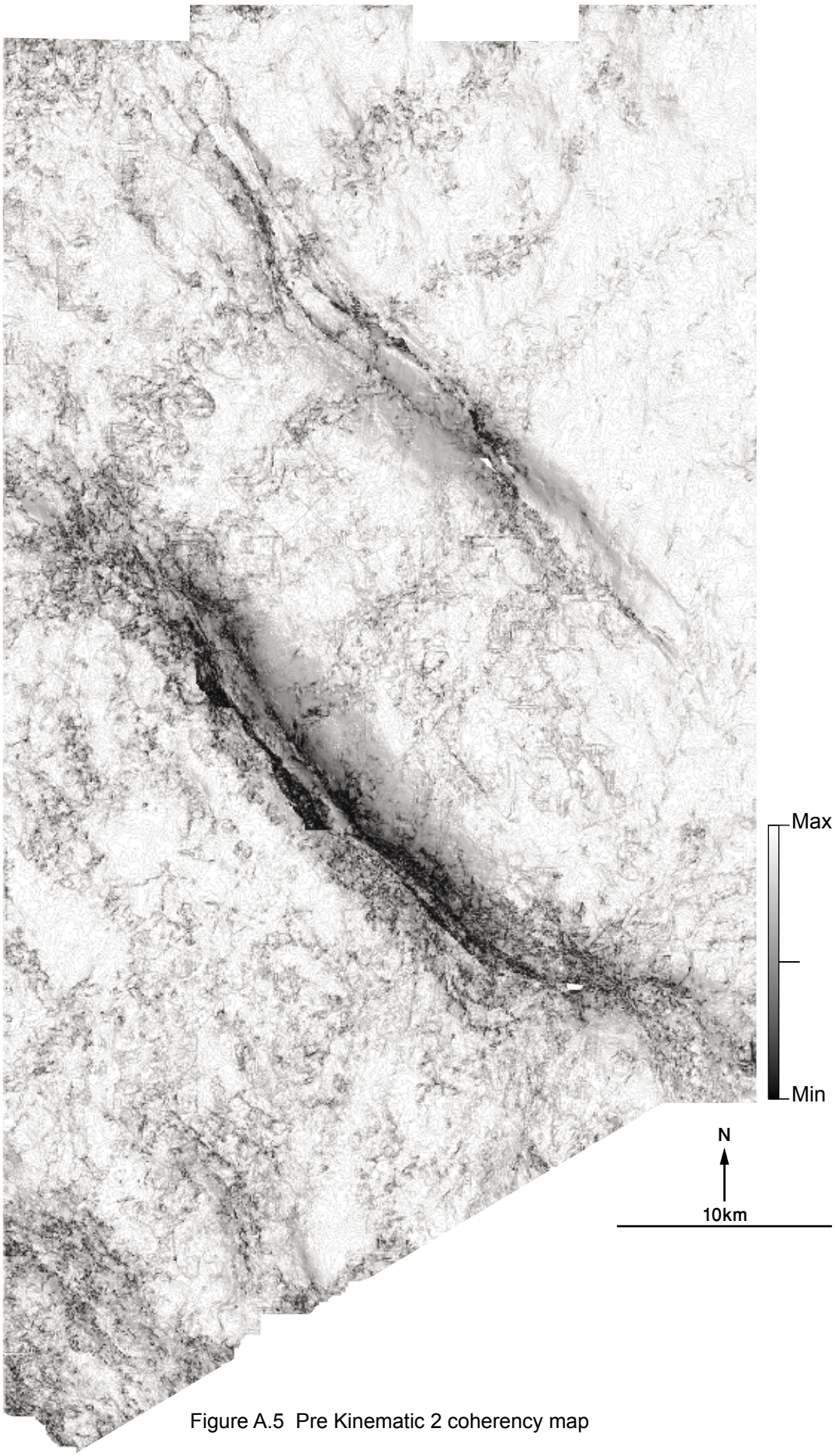

Figure A.5 Pre Kinematic 2 coherency map

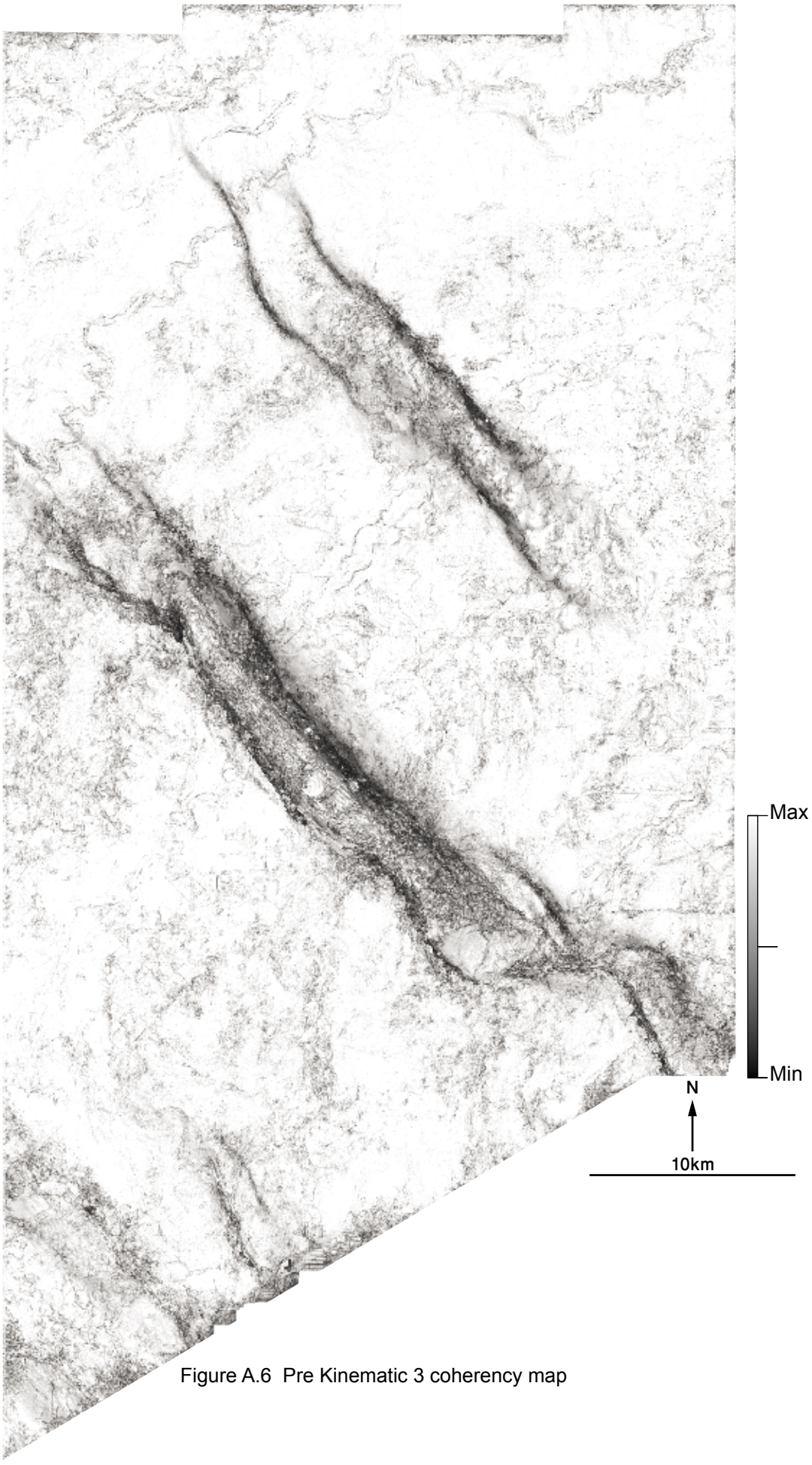

Figure A.6 Pre Kinematic 3 coherency map

Syn-Kinematic Structures and Geomorphologies

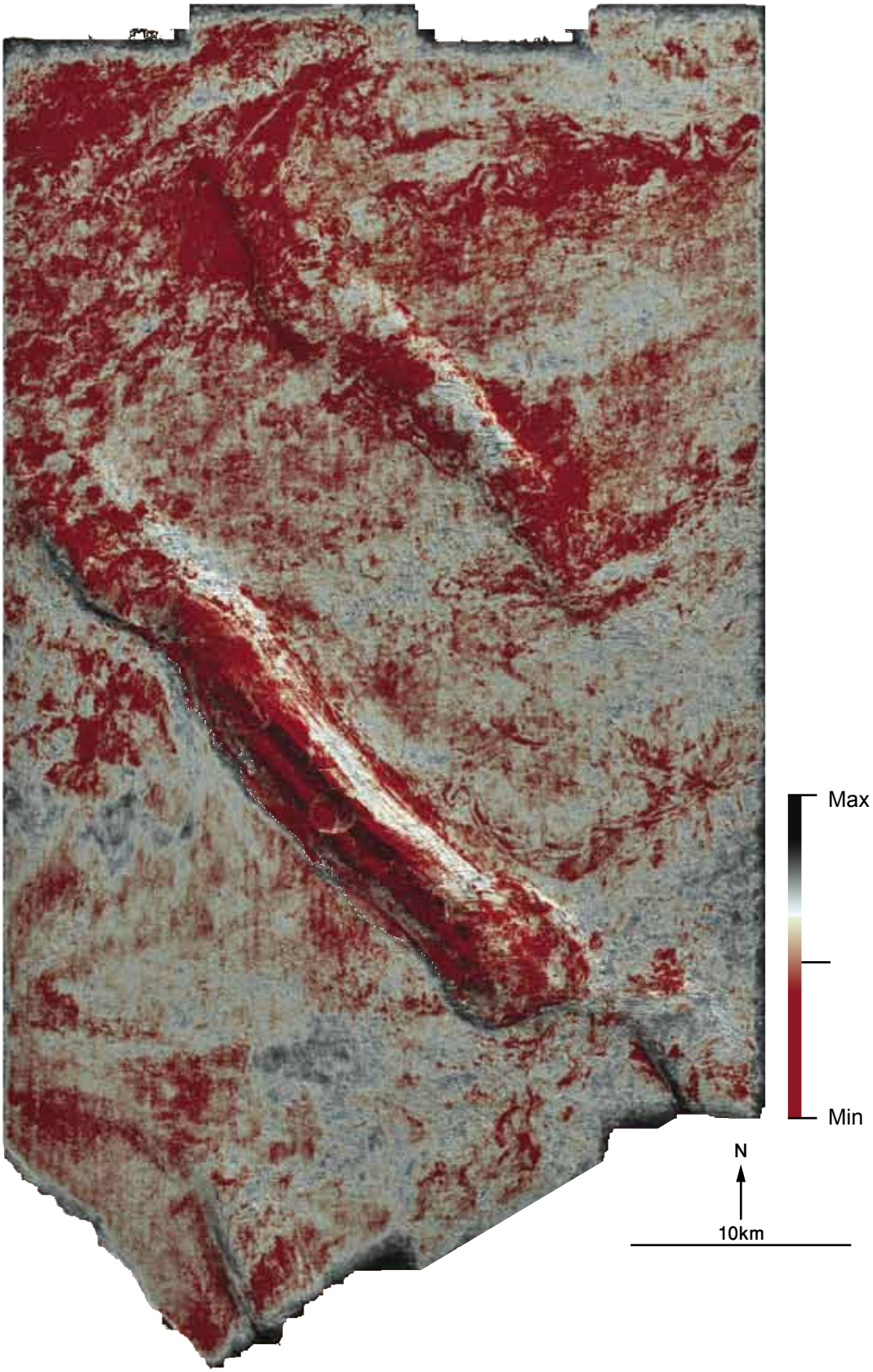

Figure A.7 Top Syn Kinematic 1 RMS amplitude extraction map. (window ±5ms)

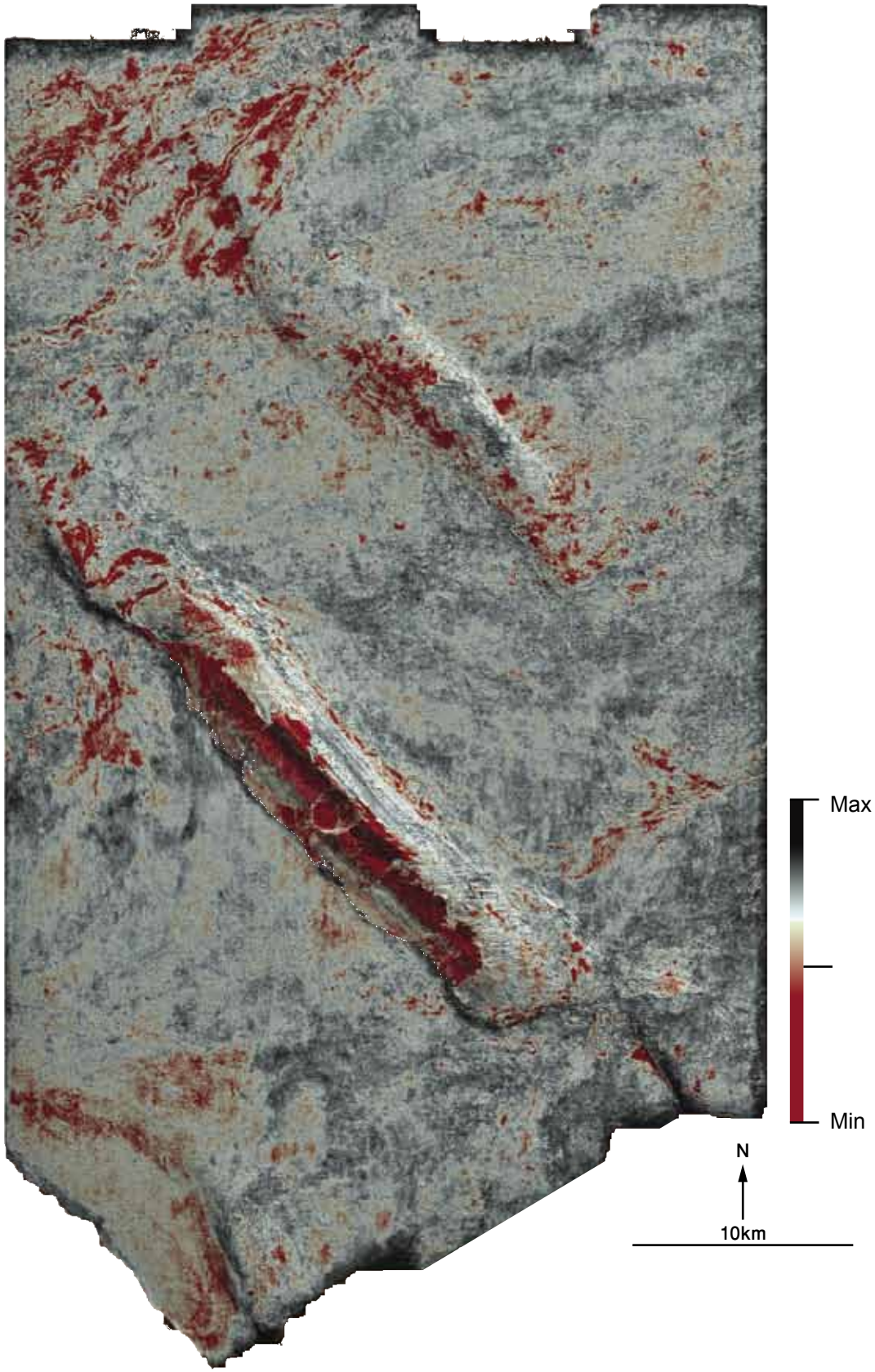

Figure A.8 Top Syn-Kinematic 1 RMS amplitude extraction map. (window ±10ms)

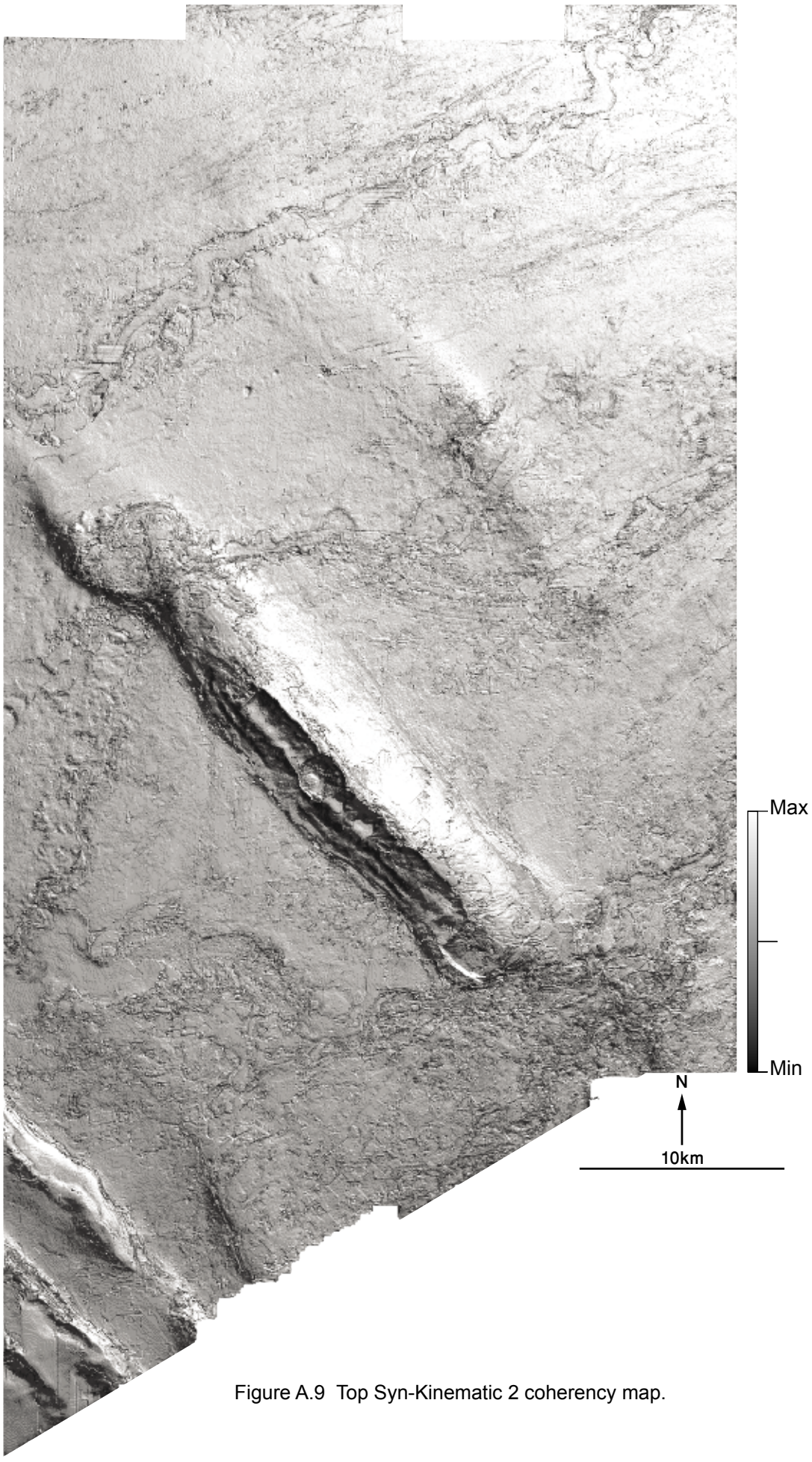

Figure A.9 Top Syn-Kinematic 2 coherency map.

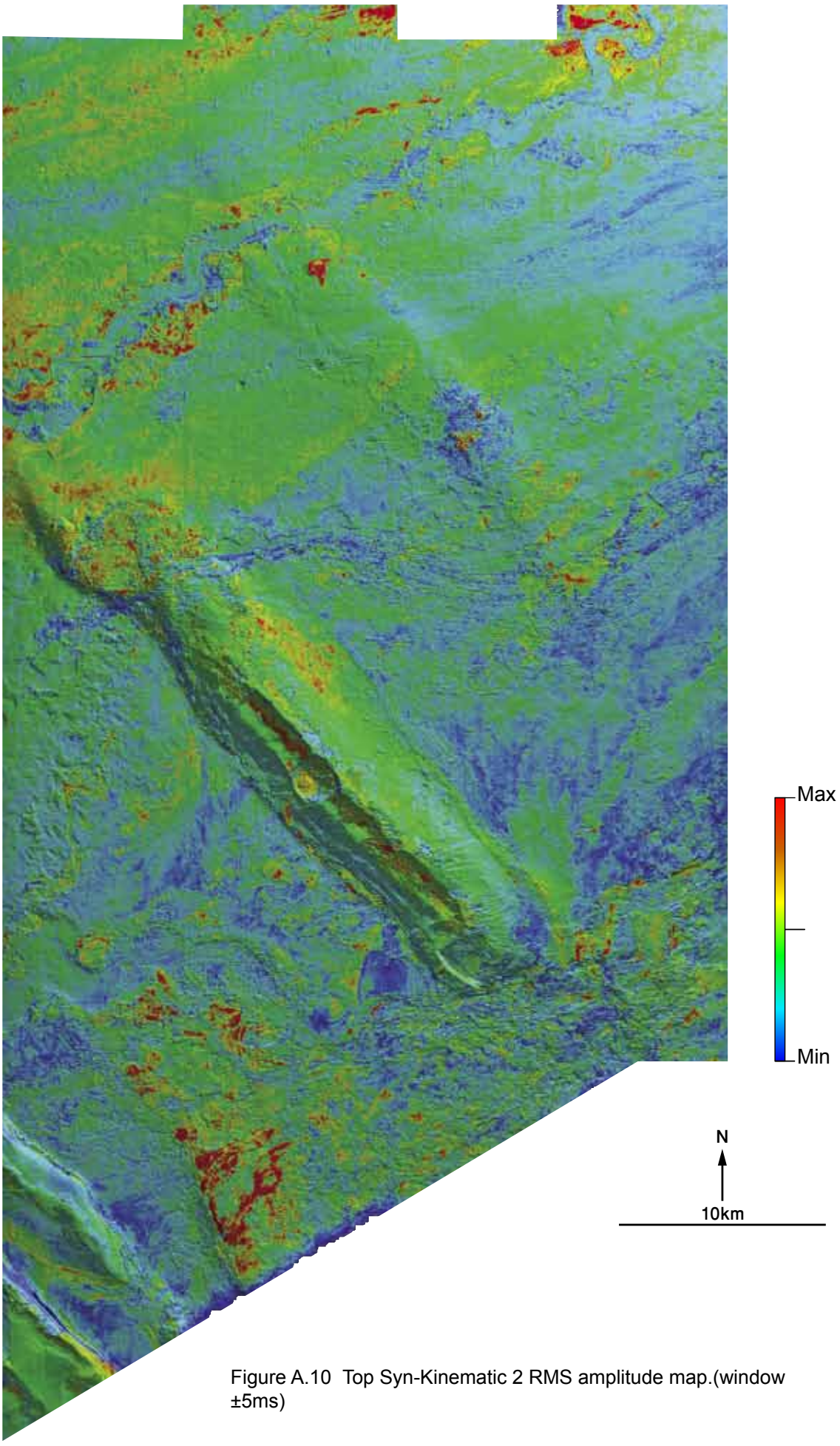

Figure A.10 Top Syn-Kinematic 2 RMS amplitude map.(window ±5ms)

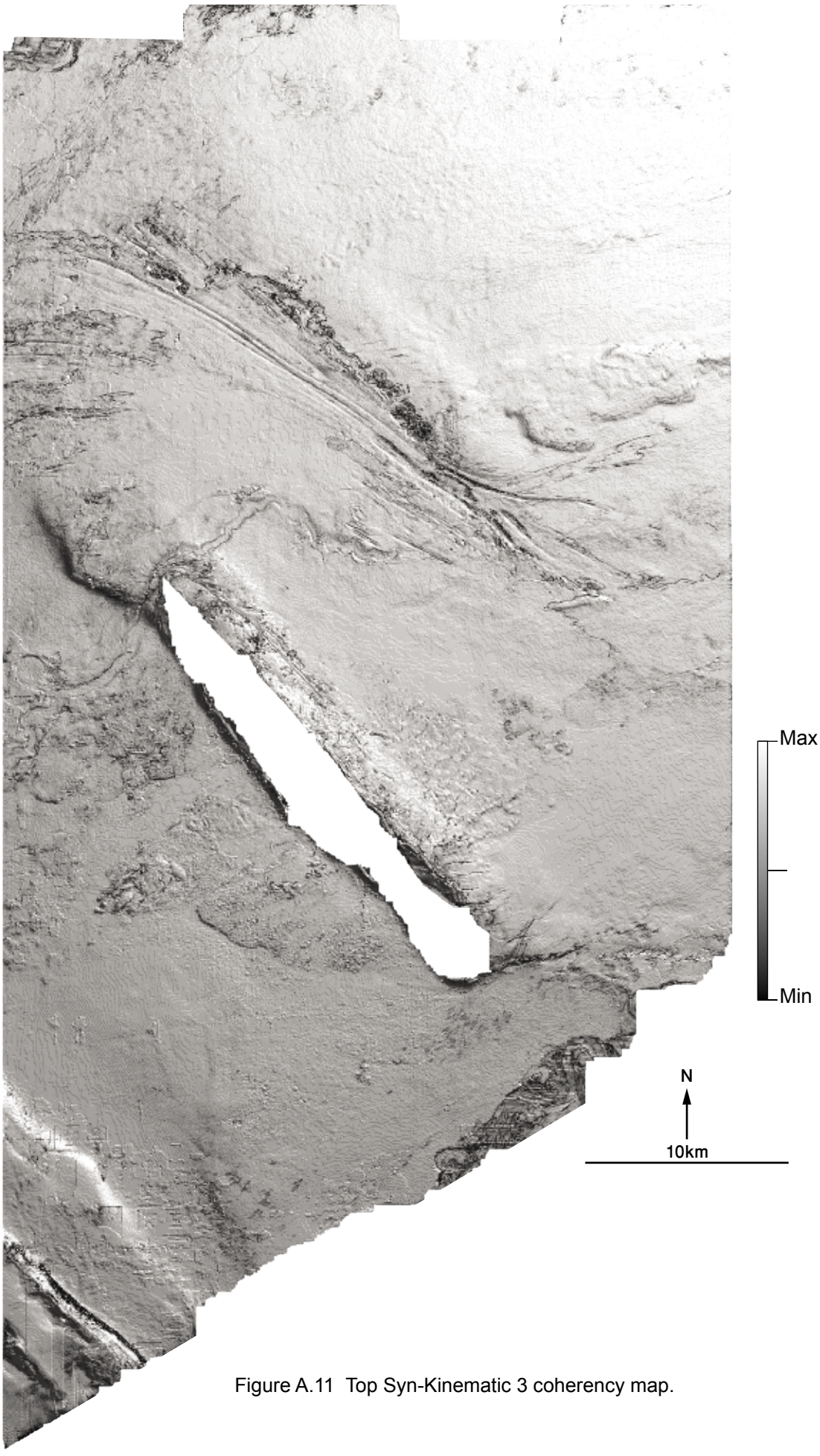

Figure A.11 Top Syn-Kinematic 3 coherency map.

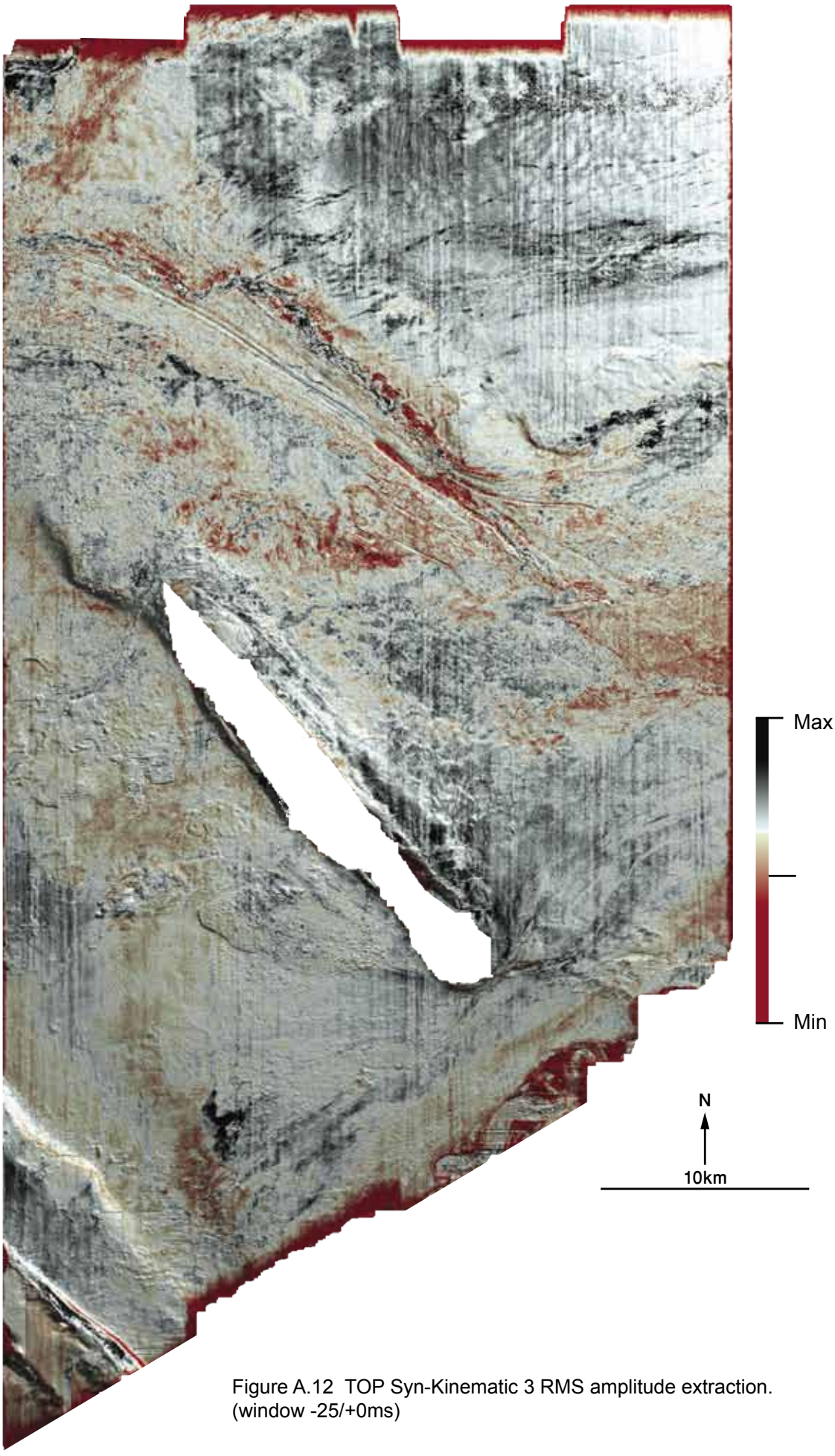

Figure A.12 TOP Syn-Kinematic 3 RMS amplitude extraction. (window -25/+0ms)

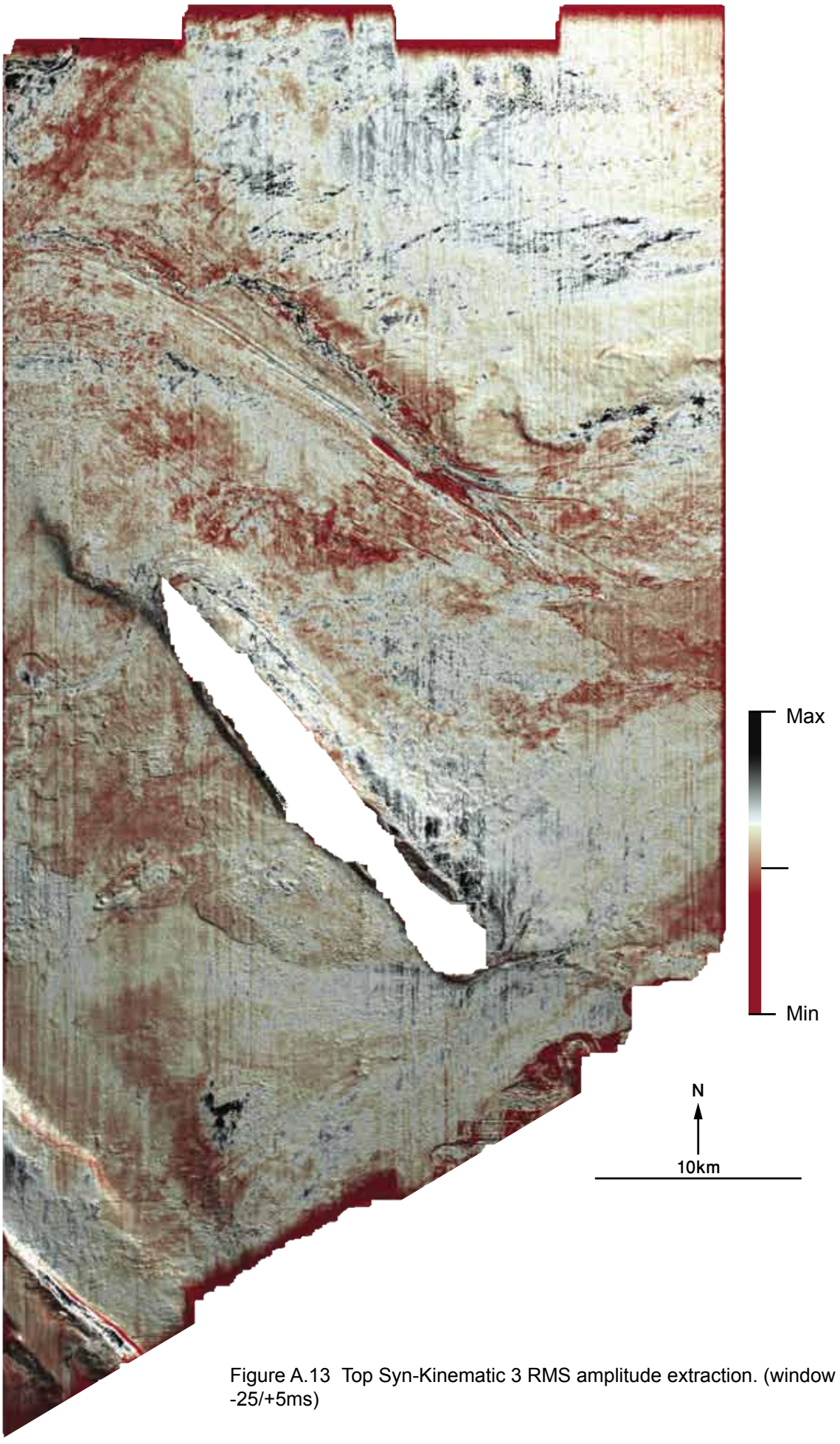

Figure A.13 Top Syn-Kinematic 3 RMS amplitude extraction. (window -25/+5ms)

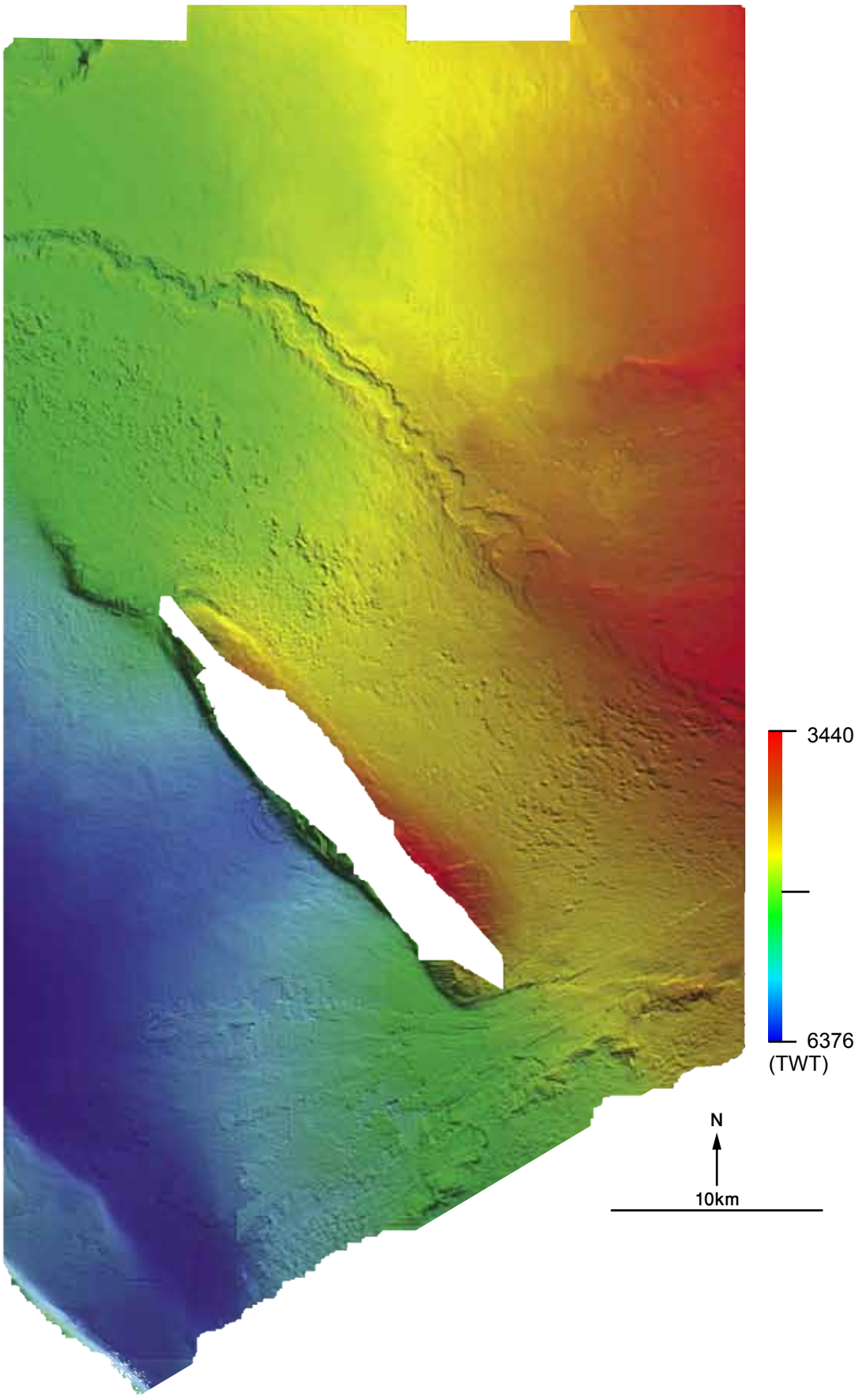

Figure A.14 TOP Syn-Kinematic 4 TWT structural map.

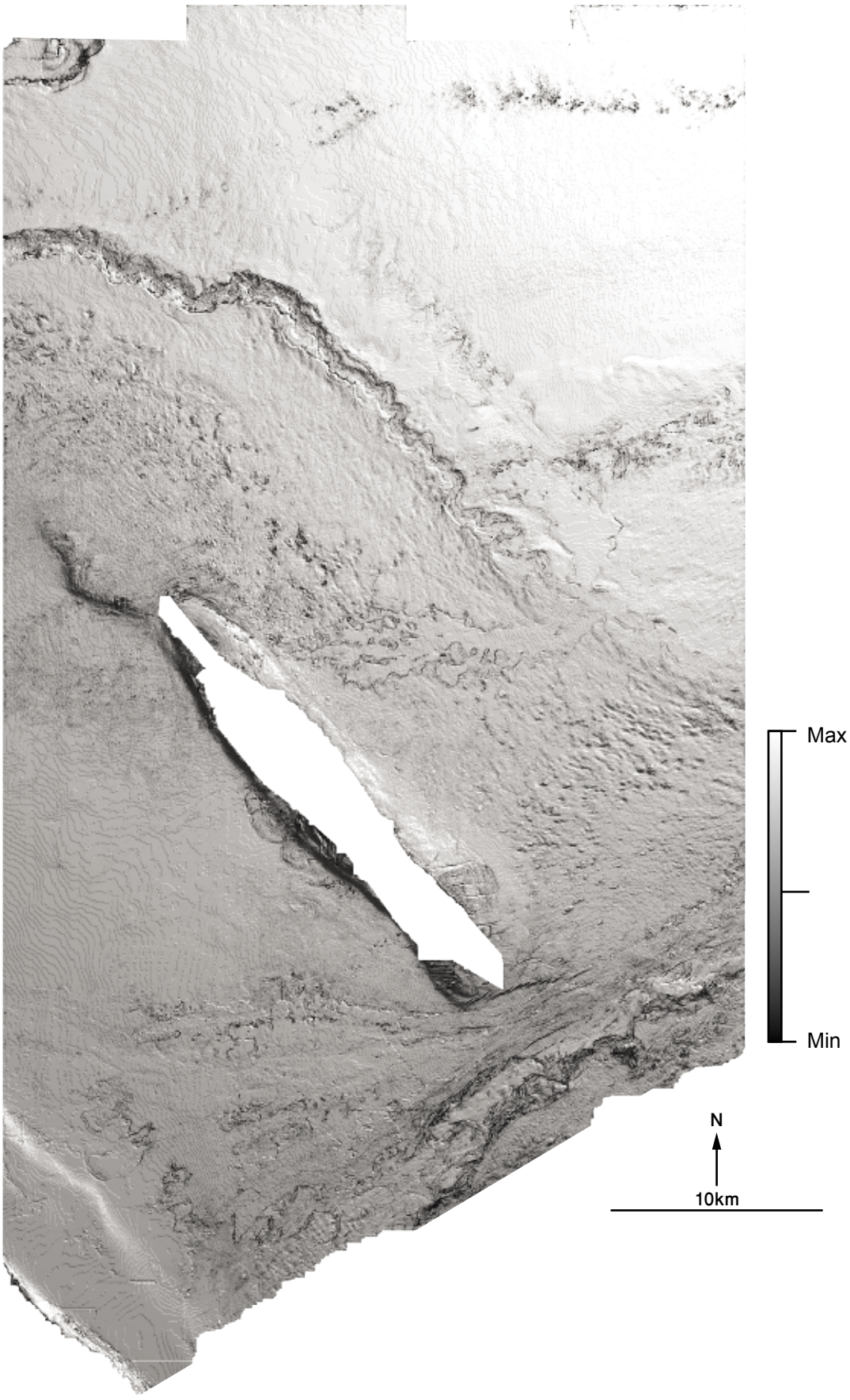

Figure A.15 TOP Syn-Kinematic 4 RMS coherency map

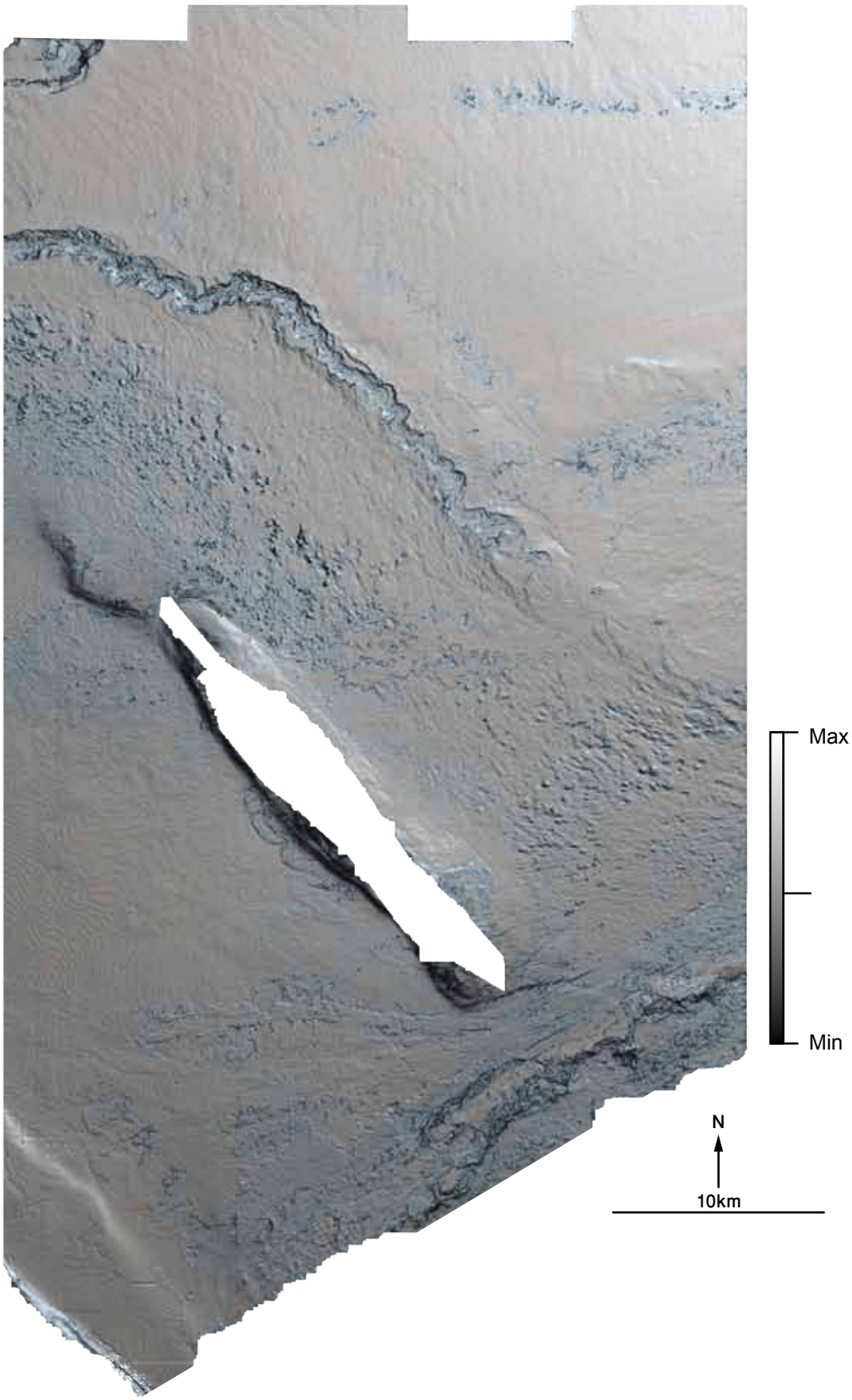

Figure A.16 TOP Syn-Kinematic 4 Dip corrected coherency map

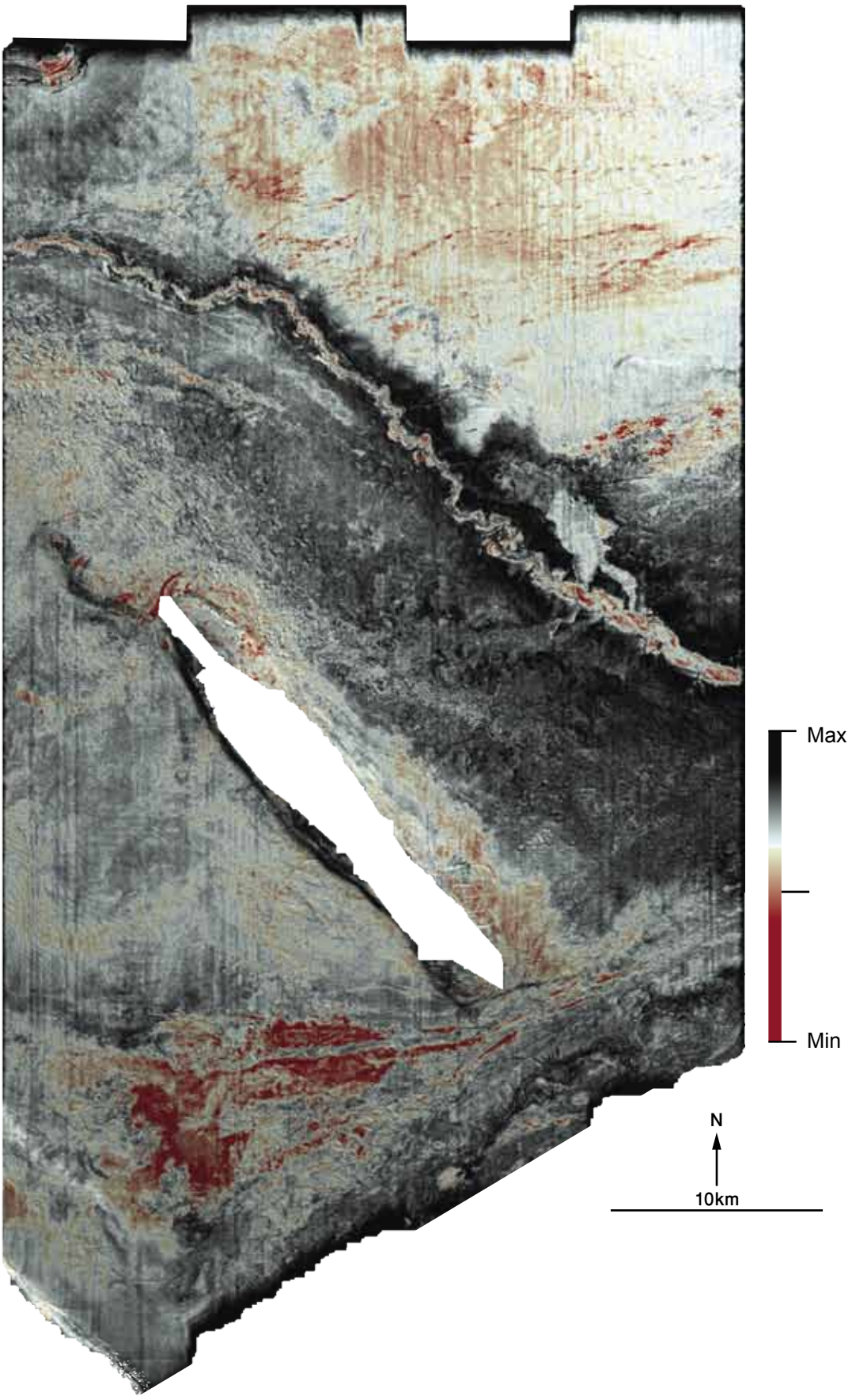

Figure A.17 TOP Syn-Kinematic 4 RMS amplitude extraction. (window -0/+25ms)

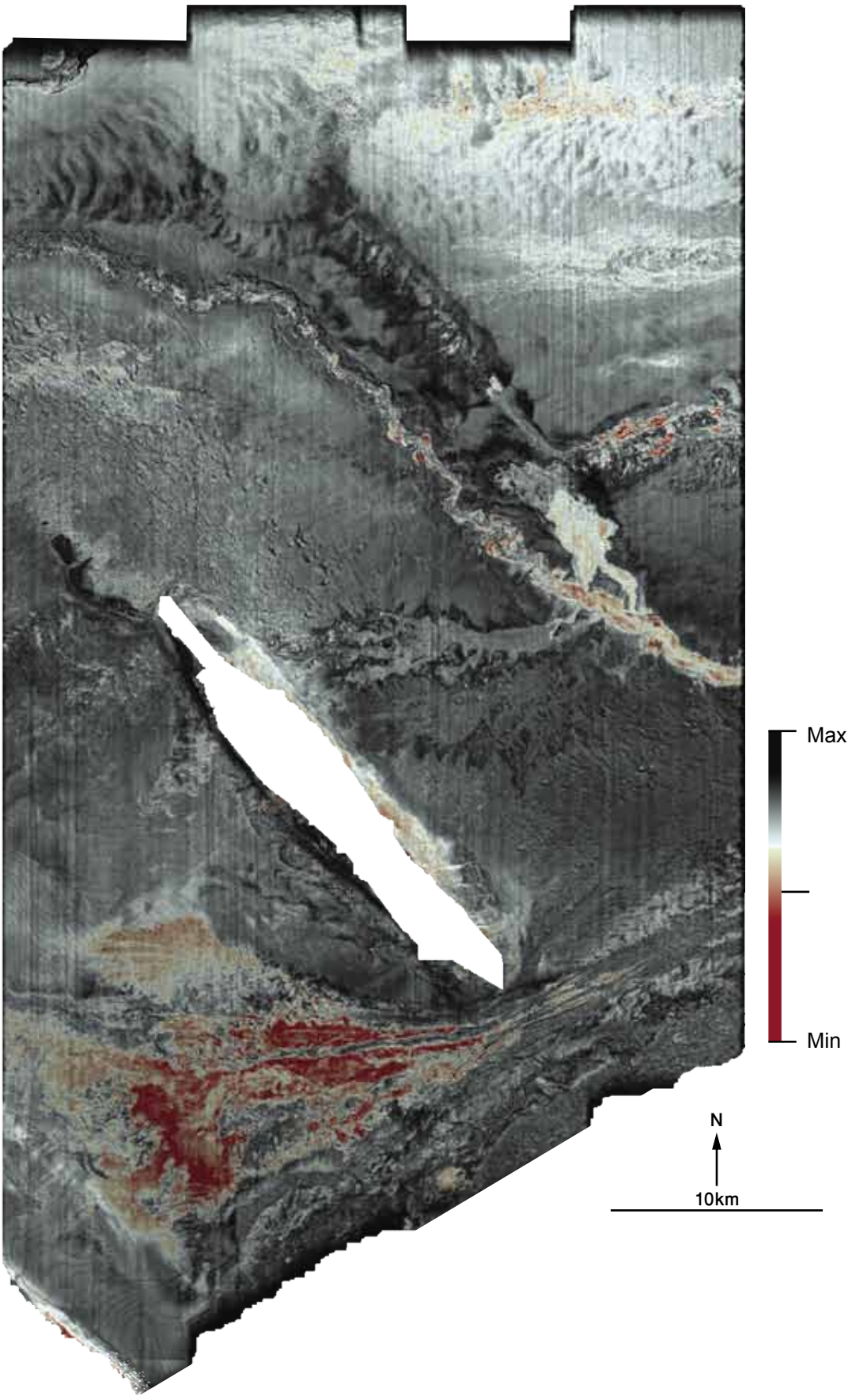

Figure A.18 TOP Syn-Kinematic 3 RMS amplitude extraction. (window ±5ms)

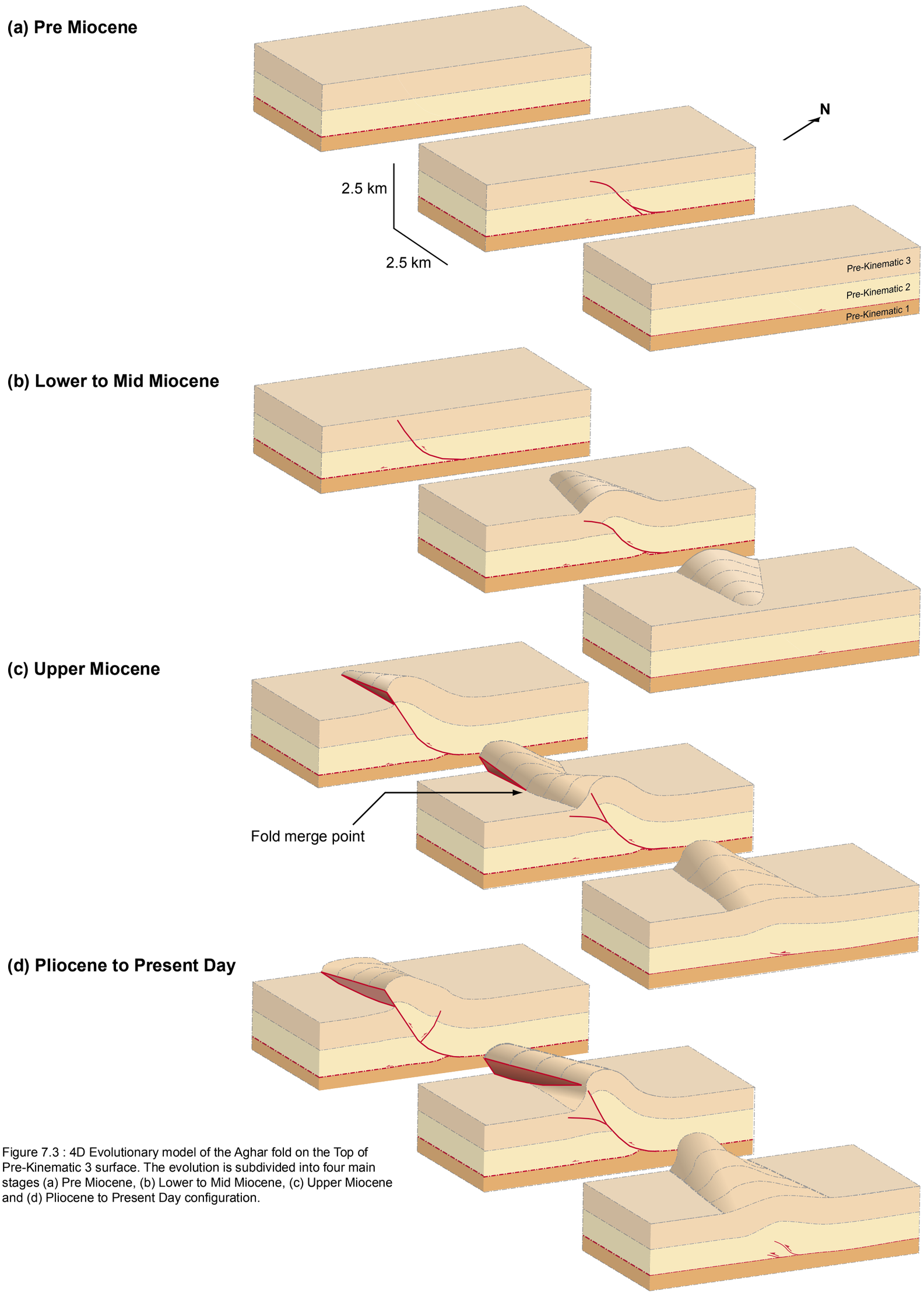

Figure 7.3 : 4D Evolutionary model of the Aghar fold on the Top of Pre-Kinematic 3 surface. The evolution is subdivided into four main stages (a) Pre Miocene, (b) Lower to Mid Miocene, (c) Upper Miocene and (d) Pliocene to Present Day configuration.

(a)

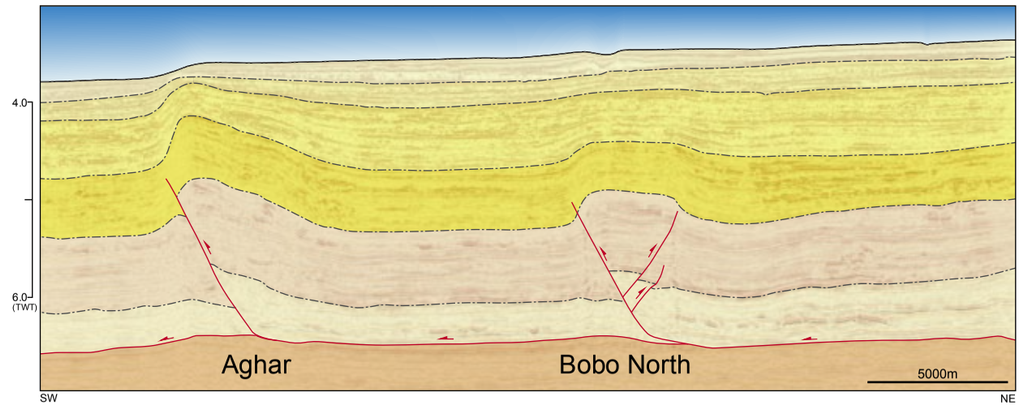

(b)

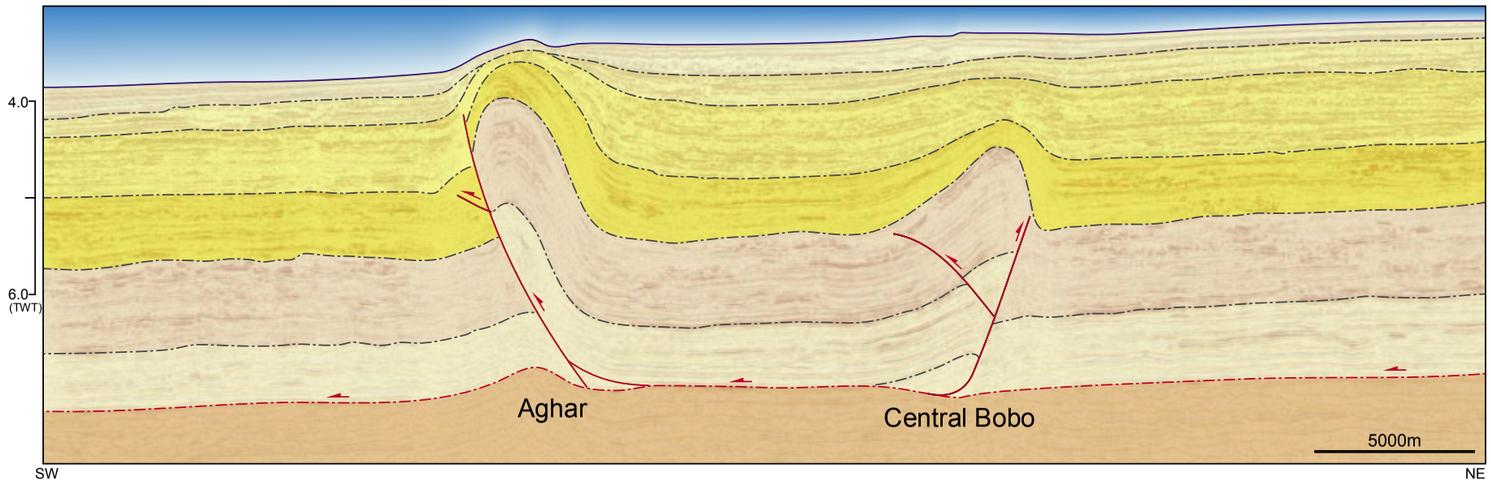

(c)

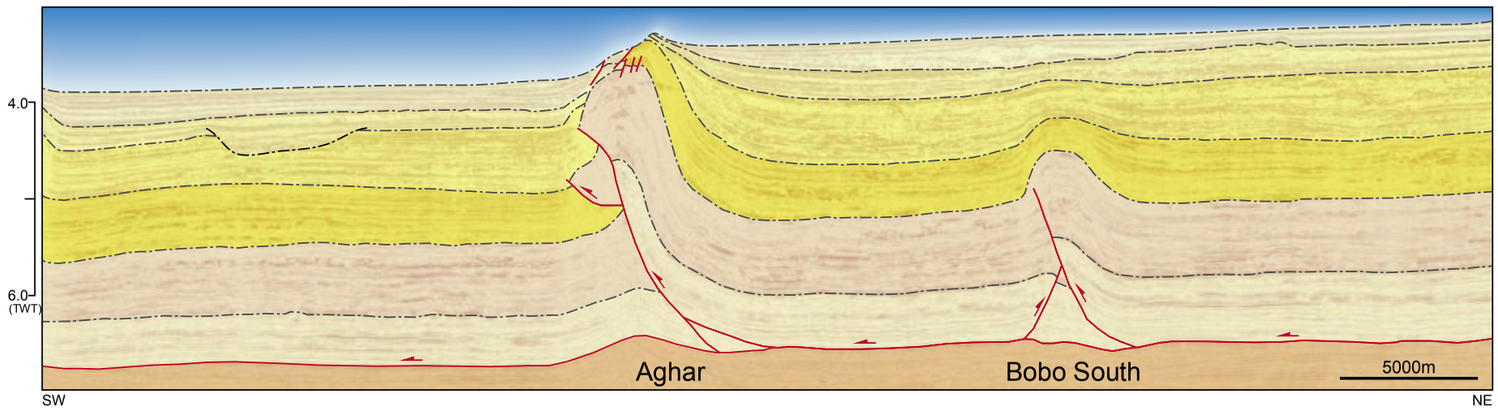

(d)

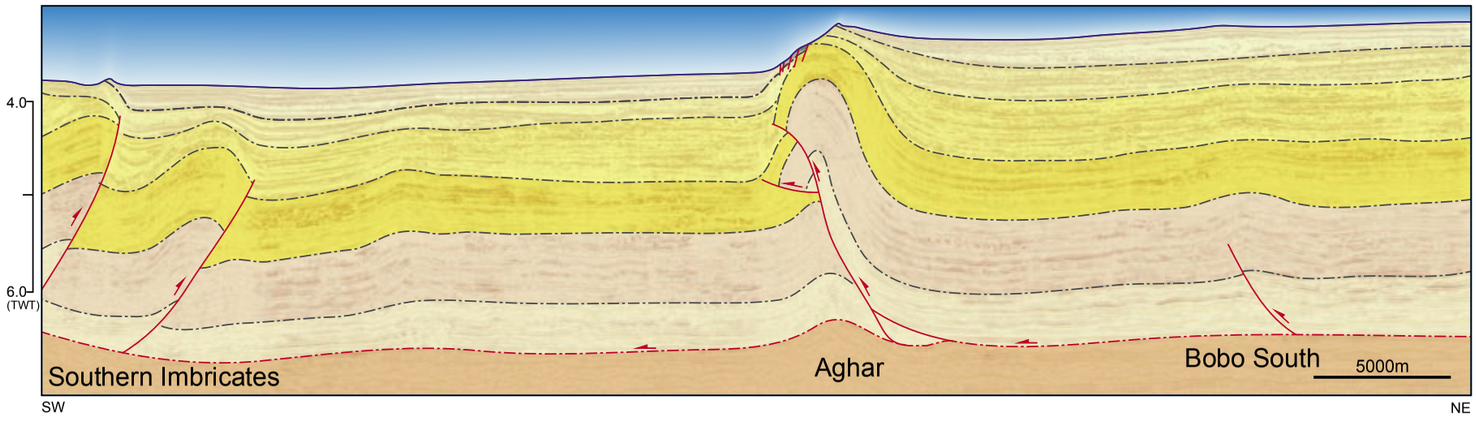

Figure 7.4 : Two-Way-Time 3D Seismic transects A - D. Vertical Exaggeration ×2